Freezing Characteristics of Mine Waste Tailings and their Relation to Unsaturated Soil Properties

by

Haley Schafer

A thesis submitted in partial fulfillment of the requirements for the degree of

Master of Science

in

Geoenvironmental Engineering

Department of Civil and Environmental Engineering
University of Alberta

ABSTRACT

The study investigated the feasibility of using the soil freezing characteristic curve (SFCC) to estimate the soil water characteristic curve (SWCC) in mine waste tailings as an alternative to traditional SWCC testing. Traditional SWCC tests are challenging and time-consuming to conduct, taking anywhere from weeks to months to complete a single test. In contrast, a SFCC tests takes days to complete, which is a huge advantage over a traditional SWCC. An experimental method and apparatus was developed to measure the SFCC. The experimental method involved using a resistance temperature detector (RTD) to measure the temperature and time domain reflectometry (TDR) to determine the unfrozen water content of the soil. SFCC testing was performed on a variety of materials with different GSDs, including Devon silt, copper tailings, sand tailings, gold tailings, and oil sands tailings. The SFCC was used to estimate the SWCC and the results were compared to SWCCs measured using traditional methods.

The experimental method produced repeatable and reliable results. The results showed that the SWCC could be estimated from the SFCC for tailings from metal mines (gold tailings and copper tailings) with a high portion of sand and a small amount of clay. The SFCC was not able to estimate the SWCC for oil sands tailings. This is attributed to the high clay content, adsorbed water, and the high initial water content of the tailings. It is recommended that the SWCC be conducted in conjunction with a shrinkage test to determine the shrinkage curve, or that the shrinkage curve be estimated. This method is highly promising as a screening tool to rapidly test a wide variety of tailings to determine which should have additional traditional SWCC testing. Issues were encountered with the TDR calibration as it was conducted under unfrozen conditions

and applied to frozen conditions. As a result, it is recommended that the TDR calibration be conducted under frozen conditions using a secondary method such as Nuclear Magnetic Resonance (NMR).

John 14:27

"Peace I leave with you; my peace I give to you.

Not as the world gives do I give to you.

Let not your hearts be troubled, neither let them be afraid."

ACKNOWLEDGEMENTS

I am so grateful to so many individuals who have supported and encouraged me during my program. This research would not have been possible without the guidance of Dr. Beier and Dr. Wilson who have provided insight, direction, and advice at every single stage of this process. I am grateful for their patience, kindness, and enthusiasm for research. I would also like to thank Christine Hereygers and Louis Kabwe for their technical help with the laboratory component of this research project, which was instrumental to the success of the project. I cannot thank Vivian Giang enough for her constant encouragement and assistance with scholarships.

I would also to thank the Natural Sciences and Engineering Research Council of Canada (NSERC), Alberta Innovates Technology Futures (AITF), Canada's Oil Sands Innovation Alliance (COSIA), Alberta Innovates Energy and Environmental Solutions (AIEES), and the University of Alberta for financial support, which made this research possible.

I have been blessed with great friends and colleagues during this program. James Bartz, Stephen Lanyi, Hugh Gillen, and Courtney Mulhall made this experience enjoyable by providing support through coursework, graduate labs, and research.

I would not have made it this point in my career without the love of my parents, Sandy and Leroy, who have strived to give me every opportunity possible and have been my biggest supporters since the day I was born. Thank you for blessing me with an incredible family. Thank you to Kerry and Jack Schafer who have always made me feel like part of the family. I am so grateful for my brothers, my sister-in-laws, my brother-in-law, and all of my nieces and nephews (Lucas, Noah, Adaleigh, Tristan, and Eleanor) who make life joyful. I cannot begin to express how much I appreciate my husband, Matt. Thank you for always laughing with me, loving me, adventuring with me, and encouraging me to pursue my dreams.

TABLE OF CONTENTS

LIST OF TABLES

LIST OF FIGURES

LIST OF SYMBOLS AND ACRONYMS

AE	Actual Evaporation
AER	Alberta Energy Regulator
AEV	Air Entry Value
CHWE	Clark Hot Water Extraction
CT	Composite Tailings
FFT	Fluid Fine Tailings
GSD	Grain Size Distribution
IEV	Ice Entry Value
ILTT	In-line thickened tailings
K_a	Apparent Dielectric Constant
MFT	Mature Fine Tailings
NMM	Neutron Moisture Meter
NMR	Nuclear Magnetic Resonance
NST	Nonsegregating Tailings
PE	Potential Evaporation
PTF	Pedo-transfer Function
RTD	Resistance Temperature Detectors
SFCC	Soil Freezing Characteristic Curve
SSA	Specific Surface Area
SWCC	Soil Water Characteristic Curve
TDR	Time Domain Reflectometry
TFT	Thin Fine Tailings
TMF	Tailings Management Framework
TT	Thickened Tailings
WT	Whole Tailings
w_u	Unfrozen Gravimetric Water Content
θ	Volumetric Water Content
θ_u	Unfrozen Volumetric Water Content
θ_i	Instantaneous Volumetric Water Content

1 INTRODUCTION

1.1 Background

The research performed in this study investigated the feasibility of using the soil freezing characteristic curve (SFCC) to determine the soil water characteristic curve (SWCC) in mine waste tailings including copper tailings, gold tailings, and oil sands tailings such as fluid fine tailings (FFT). A literature review demonstrated that SFCCs have been used to determine the SWCC for various soils. However, this method has not been studied for tailings like FFT. To explore this concept, a laboratory testing program was conducted to determine the SFCC and SWCC for various mine waste materials**.** The work conducted in this study is introduced in the following sections.

The oil sands in Alberta are considered to be the third-largest proven reserve in the world and are estimated to cover an area of approximately 142,200 km^2 (Government of Alberta. 2017a)**.** These deposits contain about 293 billion m^3 (1.8 trillion barrels) of in-place reserves of in situ crude bitumen and approximately 28 billion m^3 (177 billion barrels) are established reserves that can be recovered using current technology (AER 2016a). Approximately 20 percent of the established reserves have an overburden of less than 65 m and can be mined using surface mining techniques (AER 2016a). In order to produce oil, bitumen is extracted from mined oil sands ore through water-based processes, which results in waste production. The waste from these processes is managed using tailings impoundments (Scott et al. 2013). The total area covered by active tailings ponds and associated structures in 2014 was estimated to be 234 km^2 (Government of Alberta 2017b) and is expected to continue to grow. As a result, the environmental impact of Alberta's oil sands industry is also increasing.

The processed oil sands ore yields a tailings slurry, which is composed of process-affected water, sand, fines, and a small amount of residual bitumen (Sorta et al. 2013). The tailings are discharged to a settling basin, which allows the sand fraction to settle quickly near the discharge points with the remaining FFT settling in the center (Kabwe et al. 2014). After settling has occurred, clarified water near the surface of the pond is recycled for the extraction process. FFT

is considered non-trafficable as it is essentially in the liquid state with minimal shear strength (Sorta et al. 2012). The FFT must be sufficiently dewatered in order to develop shear strength for the creation of trafficable land that would support equipment and allow reclamation activities to progress (McKenna et al. 2016). Many methods are currently being employed to dewater the FFT and promote the development of shear strength, which often involves desiccation.

Desiccation requires the unsaturated soil properties to be known in order to predict the rate of dewatering and magnitude of strength gain. These properties can be estimated using the SWCC. The current methods for determining the SWCC in the laboratory are time-consuming and challenging (Liu et al. 2012). As a result, it would be beneficial to develop alternative methods to estimate and measure the SWCC of fine, cohesive soils like FFT. One such method is to estimate the SWCC based on the SFCC, which is possible because the forces that prevent water from draining also prevent it from freezing (Spaans and Baker 1996). This is due to the fact that the process of wetting and drying in unfrozen soils is similar to the process of freezing and thawing in frozen soils (Liu et al. 2012). When a soil dries, water is removed and replaced by air, which decreases the matric potential of the remaining water (Azmatch et al. 2012a). This process also occurs when a soil freezes where the water changes phase and becomes ice (Azmatch et al. 2012a).

1.2 Scope and Objectives

The objective of this research was to assess the validity of using SFCCs to estimate the SWCC for fine grained tailings like oil sands FFT and then define the range of slurry tailings for which this method may be applicable. The research included a laboratory testing program where the SFCC was determined using time domain reflectometry (TDR) probes and resistance temperature detectors (RTDs). The TDR probes were used to determine the unfrozen volumetric water content and the RTDs were used to determine the temperature (Azmatch et al. 2012a). The temperature measurement was used to estimate the suction in the tailings at various unfrozen volumetric water contents using the Clapeyron equation (Azmatch et al. 2012a). To determine the validity of the SFCC to estimate the SWCC, conventional SWCC measurements were also conducted on samples of tailings.

1.3 Organization of Thesis

Chapter 1 provides an overview of the background, objectives and scope of this research. Chapter 2 summarizes a review of literature related to the importance of SWCC for oil sands tailings, the similarity between SWCCs and SFCCs, and the use of time domain reflectometry to measure the unfrozen volumetric water content of a soil. Chapter 3 presents the methodology for the laboratory testing program and Chapter 4 presents the experimental results. Chapter 5 presents a comparison between the SWCCs estimated from the SFCC and the SWCCs measured using traditional methods. The results of the laboratory testing program are analyzed and discussed in Chapter 6. Finally, Chapter 7 summarizes the conclusions from this research and provides recommendations for further research.

2 LITERATURE REVIEW

2.1 General

This chapter begins with a description of the oil sands industry including the geological background, bitumen extraction methods, types of tailings, and deposition methods. The importance of soil water characteristic curves in optimizing the performance of sub-aerial deposition methods is reviewed and the theory is discussed. The principles of frozen soil are reviewed, including the influence of salinity and supercooling on freezing characteristics. The similarity between the soil freezing characteristic curve and soil water characteristic curve is explored. Finally, the theory and limitations of time domain reflectometry are reviewed.

2.2 Oil Sands

2.2.1 Introduction

The oil sands deposit in northern Alberta, Canada covers an area of approximately 142,200 km^2 and is considered to be the third-largest proven reserve (Government of Alberta. 2017a). The majority of the Albertan oil sands are located in three regions: Athabasca, Cold Lake, and Peace River. These deposits contain about 293 billion m^3 (1.8 trillion barrels) of in-place reserves of in situ crude bitumen and approximately 28 billion m^3 (177 billion barrels) are established reserves that can be recovered using current technology (AER 2016a). The oil sands can be extracted using surface mining or in situ techniques. Approximately 20 percent of the established reserves have an overburden of less than 65 m and can be mined using surface mining techniques (AER 2016a). The remaining 80 percent is mined using in situ methods. The majority of surface mining occurs in the Athabasca region, which is the largest of the three regions.

2.2.2 Geology and Mineralogy

This section will focus on the geological background of the Athabasca region as it contains the majority of surface mineable oil sands deposits. The majority of the crude bitumen in this region is contained in the lower Cretaceous Wabiskaw-McMurrary formation that was deposited about 110 million years ago (Mossop 1980) and is overlain by the Clearwater Formation that consists of marine shales and siltstones (McLaws 1980). The Clearwater Formation is divided into three

members: Lower, Middle, Upper. Oil sands generally consists of about 85 percent by mass of sand, silt, and clay, about 12 percent by mass of bitumen, and about 3 percent to 6 percent of water by mass (Chalaturnyk et al. 2002). Furthermore, the sand fraction consists of up to 95 percent quartz with the remaining 5 percent being feldspar grains, mica flakes and clay minerals (Mossop 1980) and has a microscopic layer of water surrounding the sand grains with bitumen filling the pores (Jeeravipoolvarn 2010). The mineralogy of the clay fraction in the oil sands varies, but the predominate clay minerals are kaolinite and illite with minor amounts of chlorite and montmorillonite.

2.2.3 Bitumen Extraction Method in Surface Mining

In surface mining, large shovels dig up the oil sands ore and transfer the material to trucks that move the ore to feeders/crushers (Birn and Khanna 2010). At this point, the ore is crushed and mixed with hot water to allow transportation to an extraction plant via pipelines (Birn and Khanna 2010). At the extraction plant, the bitumen is then extracted from the ore using a process based on the Clark Hot Water Extraction Process (CHWE). The first stage of the process is called conditioning where hot water, steam, and sodium hydroxide (NaOH) are slurried with the oil sands ore to promote separation of the bitumen from the ore (Chalaturnyk et al. 2002). Following this process, the material is transferred from the conditioning drum to primary separation vessels (Chalaturnyk et al. 2002). In the separation vessels, hot water is added to promote further separation of the sand particles (Chalaturnyk et al. 2002). At this point, the bitumen micelles will merge and floatation will occur (Chalaturnyk et al. 2002). The bitumen froth can then be skimmed off the surface of the separation vessel. The center part of the slurry, referred to as middlings, is removed from the primary separation vessel and processed again to recover additional fine bitumen droplets using scavenging cells (Chalaturnyk et al. 2002). The extraction process is capable of recovering from 88 percent to 95 percent of the bitumen present in the ore depending on the oil sands grade and origin (Masliyah et al. 2004).

2.2.4 Tailings Streams

The bitumen extraction process may result in the production of different tailings streams that consist of aqueous slurries with varying proportions of minerals, water, dissolved organic salts,

and residual organics (Kasperski and Mikula 2011). The first tailings stream is produced from the underflow of the Primary Separation Vessels and is referred to as whole tailings (WT). The WT contain sand and fines in proportions that reflect the original ore body (OSTC 2012). The WT stream may then be run through a hydro-cyclone, which results in a coarse tailings stream from the underflow and a fines dominated tailings stream from the overflow (CTMC 2012)

The coarse tailings stream is composed primarily of sand with an average particle size greater then 44 μm (Kasperski and Mikula 2011). This tailings stream is often used as a construction material for dykes and beaches or may be used for the production of composite tailings (CT) or non-segregating tailings (NST). The fine tailings stream consists of process-affected water, sand, fines (particle size of less than 44 μm), and a small amount of residual bitumen (Sorta et al. 2013).

The WT or the fine tailings stream may then be discharged to a tailings impoundment where the sand fraction settles rapidly forming dykes and beaches and the remaining fines and bitumen flow into the center of the pond (Jeeravipoolvarn 2010, Kabwe et al. 2014). This results in the formation of a low solids content material referred to as thin fine tailings (TFT) (CTMC 2012, OSTC 2012). TFT typically have a sand to fines ratio (SFR) less than 0.3 and a solids content of approximately 15 percent to 30 percent by mass (CTMC 2012, OSTC 2012). Over a period of about 3 years to 5 years, the fine tailings will settle to a solids content of about 30 percent to 40 percent by mass at which point it is referred to as mature fine tailings (MFT) (Spence et al. 2015). Tailings streams that behave as fluids (TFT, MFT) are collectively referred to as fluid fine tailings (CTMC 2012, OSTC 2012). OSTC (2012) defines FFT as a liquid suspension of fines and water with a solids content greater than 2 percent, but less than the solids content that corresponds to the liquid limit of the material.

As the tailings settle in the impoundment, clarified water near the surface of the pond is recycled for extraction. After the tailings reaches a solids content of about 30 percent to 35 percent, settling and consolidation will proceed very slowly and it may take hundreds of years before the tailings are deemed suitable for reclamation. Due to this, many methods are currently being employed or researched to dewater the tailings and promote reclamation through the development of shear

strength as described in Section 2.3. This was an attempt to satisfy the requirements of Directive 074, which specified that oil sands deposits should have a minimum undrained shear strength of 5 kPa one year after deposition and an undrained shear strength of 10 kPa five years after deposition (AER 2009). In March 2015, Directive 074 was suspended and replaced by Directive 085, which allows for the implementation of the Tailings Management Framework (TMF). The TMF specifies site-specific thresholds for FFT volumes over the lifespan of an oil sands mine (Dompierre et al. 2016). Each oil sands operator is required to submit an application to the Alberta Energy Regulator (AER) that includes fluid tailings volume profiles and a tailings management plan for new and legacy tailings (AER 2016b). Operators are then required to report their actual fluid tailings volumes on an annual basis (AER 2016b). If fluid tailings volumes exceed the threshold values or are not meeting performance criteria, operators are required to take action to resolve the issues (AER 2016b).

The final tailings stream is referred to as froth-treatment tailings, which is a relatively small stream that results from the addition of solvent to the bitumen froth and consists of process-affected water, sand, fines, and residual bitumen solvent (Kasperski and Mikula 2011). This tailings stream may be discharged to tailings impoundments with the WT or the fine tailings stream.

Due to a zero-effluent discharge policy, oil sands operators cannot release any process-affected water to the environment and must store the inventory in large settling ponds that are often referred to as tailings impoundments (Holden et al. 2011). In order to produce one barrel of bitumen, 12 to 14 barrels of water are required (Birn and Khanna 2010). Approximately 75 percent of the process-affected water can be recycled while the remaining 25 percent becomes suspended in the tailings (Birn and Khanna 2010). This is resulting in a growing volume of process-affected water. As this water is continually recycled, there is a buildup of dissolved ions and organic chemicals in the recycle water and thus the tailings (Beier 2015).

2.3 Tailings Management

As the oil sands industry continues to grow, the inventory of tailings ponds continues to grow. In 2014, the total area of Alberta covered by active tailings ponds was estimated to be about 234 km^2 (Government of Alberta 2017b) and is expected to continue to grow. The FFT deposited in active tailings ponds is considered non-trafficable as it is essentially in the liquid state with minimal shear strength (Sorta et al. 2012). This is problematic as oil sands operators are required to reclaim tailings ponds, mining sites, and other disturbed land to stable, resilient, functional ecosystems with a land use equivalent to the original landscape (although it may differ) as specified in the TMF (Government of Alberta 2015). In order to do so, the FFT must be sufficiently dewatered to develop shear strength for the creation of trafficable land that will support equipment and allow reclamation to occur (McKenna et al. 2016).

Management of oil sands tailings occurs through chemical, physical, or environmental processes, or a combination of these processes. There are three general stages that are important to tailings management. The first stage involves mechanical classification using hydro-cyclones or natural classification during deposition to segregate the tailings stream into a coarser and a finer grained stream (Beier 2015). This concept has been discussed in Section 2.2.4.

The second stage involves mechanical, chemical, and electrical methods including thickeners, centrifuges, and filters that may employ chemical amendments like flocculants (Beier 2015). This stage will result in the formation of different types of tailings: thickened tailings (TT), composite tailings (CT) or nonsegregating tailings (NST), in-line thickened tailings (ILTT), and centrifuge cake. The primary goal of this stage is to change the properties of the tailings to promote consolidation (accelerate dewatering) and the development of strength compared with MFT. This stage is discussed further in Section 2.3.1.

The third stage involves time dependent and environmental dewatering processes such as sedimentation/consolidation, freeze/thaw dewatering, desiccation, and evapotranspiration (Beier 2015). The effectiveness of this stage is influenced by the depositional method and will determine if a wet or dry landscape can be achieved. This stage is discussed further in Section 2.3.2.

2.3.1 Tailings Dewatering

There are currently four dewatering methods being employed to promote the acceleration of dewatering of tailings. The first method involves a combination of flocculation and centrifugation. In this method, a flocculant is added to the FFT and processed using a centrifuge (OSTC 2012). In this method, the solids and water are separated using a centrifugal force resulting in the production of a centrifuge cake that a solids content of about 50 percent to 55 percent (OSTC 2012). The separated water is collected and recycled, and the centrifuge cake can then be deposited in thin lifts or in deep in-pit deposits. Thin lift deposition will take place at a slower rate and will rely on environmental processes primarily to facilitate consolidation. In contrast, the centrifuge cake can be deposited continuously in deep deposits at a higher rate. In this depositional method, consolidation of the centrifuge cake will occur through self-weight consolidation.

The second method involves in-line flocculation of FFT resulting in the production of in-line thickened tailings (ILTT). The ILTT can be deposited in the following ways:

- Thin lifts into cells. In this depositional method, the solids content can be increased to about 60 percent from initial dewatering due to flocculation and drainage (OSTC 2012). There will be an initial release of water when the material is released in the cell. This is a result of maturing of the flocculation process and shearing/draining on the beach (OSTC 2012). This is followed by environmental processes to facilitate dewatering.
- Formation of deep deposits. This method also relies on self-weight consolidation for the development of strength.

The third process is to flocculate FFT from the extraction process and thicken the material in a mechanical thickener creating thickened tailings (TT) (OSTC 2012). The TT can be deposited in thin lifts or into deep deposits. This process is often used to recover energy, but is also useful for dewatering the FFT (OSTC 2012). This method can also be used to increase the density of froth-treatment tailings (OSTC 2012).

The fourth method involves blending FFT with sand slurry using flocculants or coagulants to prevent segregation resulting in the formation of CT or NST (OSTC 2012). CT is formed when MFT is mixed with the sand slurry and NST is formed when TT is mixed with the sand slurry (OSTC 2012). The CT and the NST are then discharged into deep deposits. The goal of this method is to produce a sand-dominated mix with a lower water content. One of the largest issues encountered in this method is minimizing segregation. Additionally, this method requires large volumes of sand which can be challenging as sand is also needed as a capping material and for constructing containment structures.

2.3.2 Tailings Deposition

In general, tailings can be discharged in two ways. The first method involves discharging the tailings in thin lifts on gently sloped beaches. In this method, dewatering is accomplished through a combination of settlement, seepage, and environmental dewatering (Beier 2015). The second method involves discharging the tailings in thick lifts into large cells that are greater than 10 m deep where dewatering will occur primarily through self-weight consolidation and seepage (Beier 2015). Evaporation will only occur at the surface of the deposit.

The dewatering methods discussed in Section 2.3.1 result in the formation of four different types of deposits, as follows (OSTC 2012):

1. Thin layered deposits that are dominated by fines – This type of deposition relies on atmospheric evaporation and free-thaw as the primary mechanisms for dewatering. In order to be used on a commercial scale, there must be sufficient space for adequate surface drying. The desiccated tailings can then be transported to a different location as overburden or left in place to form a multi-layer deposit (OSTC 2012).
2. Deep deposits that are dominated by fines – These deposits rely primarily on self-weight consolidation for consolidation and dewatering.
3. Fines-enriched sand deposits – These deposits rely on self-weight consolidation and are expected to dewater more quickly than deep deposits that are dominated by fines.

4. Water capped fines deposits – MFT or other densified FFT are discharged to a mined out pit and capped with water forming end pit lakes. This type of deposition results in a wet landscape.

2.3.3 Environmental Dewatering Post Deposition

After deposition, tailings will undergo additional dewatering through a combination of the following processes:

- Particulate settling;
- Sedimentation;
- Consolidation;
- Evaporation;
- Freeze-thaw; and,
- Evapotranspiration.

This section will focus on environmental dewatering practices as this research aims to help with the design of these dewatering techniques. These methods can be very effective in over-consolidating the material, which has the potential to lead to a reclaimable deposit. Evaporation is dependent on the material properties of the tailings and the top and bottom boundary conditions (Newson and Fahey 2003, Simms and Grabinsky 2004). The material properties that may impact evaporation are the GSD, saturated/unsaturated hydraulic conductivity, and the SWCC. Evaporation will lead to surface desiccation, which is the process of drying and cracking (Jeeravipoolvarn 2010). This will affect consolidation by changing the stress, degree of saturation, and drainage path, which impacts the availability and flow of water to the evaporation surface (Beier 2015, Jeeravipoolvarn 2010). In order to assess the water balance from the surface of a tailings pond, the potential evaporation (PE) rate and actual evaporation (AE) rate are required. The AE rate of the deposited tailings will decrease with time as the drying occurs (Qiu and Sego 2006).

Freeze-thaw is also effective in dewatering tailings as it changes the macro and micro-fabric, which improves the release of water (Proskin et al. 2012). This allows for subsequent consolidation through self-weight consolidation and by effective stress caused by freezing action (Proskin et al. 2012). The freeze-thaw process results in a three dimensional reticulate ice network surrounding blocks of overconsolidated tailings (Proskin et al. 2012). When thaw occurs, remnant ice fissures leave channels that allow for fluid flow, which increases the hydraulic conductivity at low stresses (Proskin et al. 2012). Freeze-thaw will also result in a change in the micro-fabric from an edge to face flocculated, disaggregated cardhouse fabric to a compact, aggregated fabric (Proskin 1998). This is an effective dewatering method as the compact, aggregated fabric will retain less water resulting in an increase in solids content as the material is able to consolidate rapidly under self-weight (Proskin 1998).

Desiccation can also happen through evapotranspiration where plants transfer water from their roots in the tailings and transpire it through their leaves (Silva 1999). The rate of evapotranspiration is impacted by the soil properties, the plant properties, and the atmospheric conditions (Silva 1999).

2.4 Soil Water Characteristic Curve

2.4.1 General

Soil water characteristic curves (SWCCs) define the relationship between soil water content and soil water suction (or potential) for a soil (Fredlund et al. 2012). This is a measure of the ability of the soil to hold water within its pores (Qiu 2000) due to the matric suction of the soil where matric suction is the affinity of the soil for water (Koopmans and Miller 1966). It should be noted that SWCCs may also be referred to as soil moisture characteristic curves or water retention curves in other literature sources. The SWCC allows for the construction of constitutive equations to assess the mechanical behavior of unsaturated soil (Fredlund and Rahardjo 1993). This soil property is fundamental in assessing the behavior of a soil as it transitions from a saturated state to an unsaturated state and vice versa. The SWCC can then be used to estimate other unsaturated soil property functions, including:

- the unsaturated hydraulic conductivity function;
- the water storage function, and;
- the shear strength function.

As a result, the SWCC is important to oil sands reclamation methods that rely on desiccation to aid in strength gain. In order to predict the behavior during drying, the SWCC is needed as it enables designers to determine the unsaturated hydraulic conductivity function and the volume change properties (Qiu and Sego 2006, Simms and Grabinsky 2004, Vardon et al. 2014). Ultimately, the SWCC is needed to optimize the deposition and performance of methods that rely on desiccation as it influences the availability and flow of water to the evaporation surface (Beier 2015).

The water content of a soil defines the amount of water in the pore space of the soil (Fredlund and Xing 1994). The SWCC may be expressed in terms of (Fredlund et al. 2011):

i. total volumetric water content, θ, defined as the ratio of the volume of water to the original total volume of the sample as defined in Equation 2-1.
ii. gravimetric water content, w, defined as the mass of water to the mass of solids as shown in Equation 2-2. The gravimetric water content can be related to the total volumetric water content using Equation 2-3 and the original dry density.
iii. instantaneous volumetric water content, θ_i, defined as the ratio of the volume of water to the instantaneous total volume of the sample.
iv. degree of saturation, S.

$$\theta = \frac{V_w}{V_{tot}} \quad \textbf{2-1}$$

$$w = \frac{W_w}{W_s} \quad \textbf{2-2}$$

$$w = \frac{\rho_w}{\rho_d}\theta_v \qquad \text{2-3}$$

Where θ is the volumetric water content, V_w is the volume of water in the total volume V_{tot}, w is the gravimetric water content, W_w is the weight of water, W_s is the weight of dry solids, ρ_w is the density of water, and ρ_d is the dry density. This yields four different SWCCs, namely the θ-SWCC, w-SWCC, θ_i-SWCC, and S-SWCC. These SWCCs will provide similar information for a soil that does not undergo volume change. The implications of volume change on the resulting SWCCs is discussed in Section 2.4.3.

The suction used in the SWCC is generally the matric suction or the total suction, which includes the matric and osmotic suction. The matric suction and total suction are generally assumed to be equal at suctions that are greater than about 1500 kPa (Fredlund and Xing 1994). Figure 2-1 shows a typical SWCC for a silty soil and highlights important zones of transition. The air entry value (AEV) is the matric suction at which air starts to enter the largest pores of the soil (Fredlund and Xing 1994). The residual water content is the water content at which large suction changes are required to remove any additional water from the soil (Fredlund and Xing 1994). Figure 2-1 also shows that the desorption curve and adsorption curve can differ substantially from one another due to hysteresis. The stress history of the soil can also affect the shape of the SWCC (Fredlund and Xing 1994).

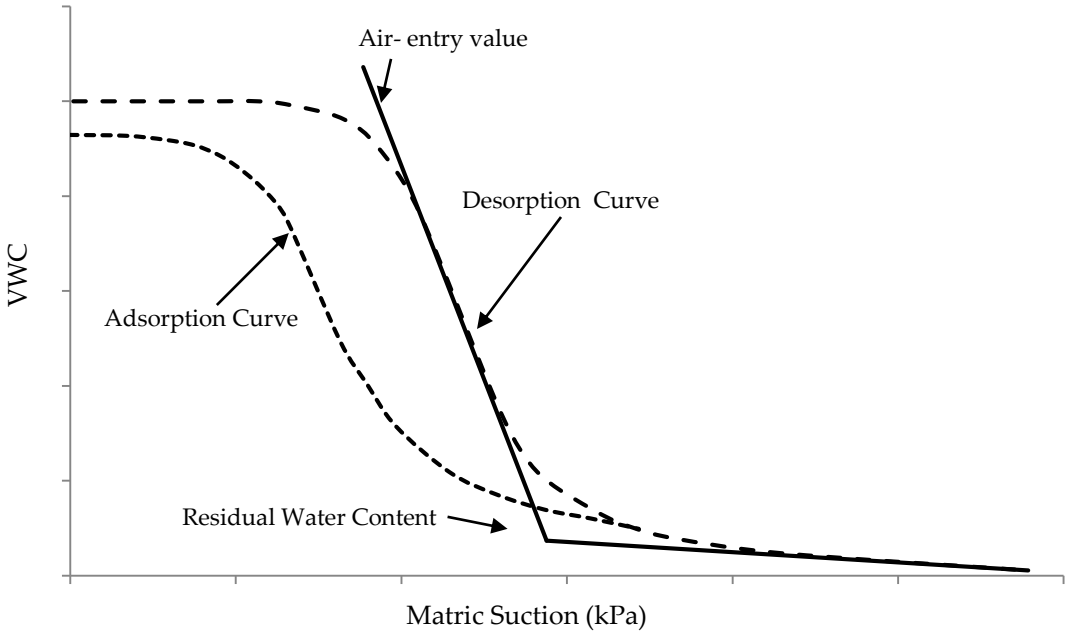

Figure 2-1: Example of a SWCC (after Fredlund and Xing 1994)

Unsaturated soil parameters can be determined from the SWCC using empirical equations (Leong and Rahardjo 1997). Over the years, a number of equations have been proposed by different authors that vary based on the number and type of variables. The success of the majority of the proposed equations is impacted by the soil type (Leong and Rahardjo 1997). As a result, there is not an equation that is considered universal to determine unsaturated soil parameters from the SWCC. Leong and Rahardjo (1997) provide a comprehensive overview of many different sigmoidal equations. They suggest that almost all of the equations can be derived from a single generic form. Their assessment of the various available equations indicates that the equation suggested by Fredlund and Xing (1994) provides the best fit and should be used for the SWCC (Equation 2-4).

$$w(\psi) = \frac{w_s(1 - \ln(1 + \psi/\psi_r)/\ln(1 + 10^6/\psi_r))}{\left(\ln(\exp(1) + (\psi/a_f)^{n_f})\right)^{m_f}} \qquad \textbf{2-4}$$

Where $w(\psi)$ is the water content at any soil suction ψ, a_f is a curve fitting parameter, n_f is a curve fitting parameter, m_f is a curve fitting parameter, ψ_r is a curve fitting parameter, and w_s is the initial saturated gravimetric water content.

The sigmoidal equations investigated by Leong and Rajardjo (1997) should be used for unimodal SWCCs for well-graded soils that have one governing pore size. If the soil has two or more pore series, the SWCC of the soil will tend to be bimodal or multimodal and the fitting equation will require modification to properly represent this behavior (Zhang and Chen 2005). Zhang and Chen (2005) proposed a simplified bimodal equation as shown in Equation 2-5.

$$w(\psi) = w_s\left(1 - \frac{\ln\left(1+\frac{\psi}{\psi_{rb}}\right)}{\ln\left(1+\frac{10^6}{\psi_{rb}}\right)}\right)\left(\frac{p}{\left(\ln\left(\exp(1)+\left(\frac{\psi}{a_{f1}}\right)^{n_{f1}}\right)\right)^{m_{f1}}} + \frac{1-p}{\left(\ln\left(\exp(1)+\left(\frac{\psi}{a_{f2}}\right)^{n_{f2}}\right)\right)^{m_{f2}}}\right) \quad \textbf{2-5}$$

Where $w(\psi)$ is the water content at any soil suction ψ, w_s is the initial saturated gravimetric water content, p is a weighting factor between 0 to 1.0 used to divide the bimodal behavior, and a_{f1}, n_{f1}, m_{f1}, a_{f2}, n_{f2}, m_{f2}, ψ_{rb} are curve fitting parameters.

The SWCC is a fundamental soil property that is essential to understanding unsaturated soil mechanics, but it is difficult and time-consuming to measure (Flerchinger et al. 2006, Liu et al. 2012). The laboratory techniques require delicate experimental controls and the accuracy of the measurement is highly impacted by the operational procedures used to determine the soil suction and the water content (Liu et al. 2012). Laboratory methods of measuring the SWCC are discussed further in Section 2.4.2.

2.4.2 Laboratory Measurement of the SWCC

To attain the full SWCC, multiple laboratory techniques may be needed. These laboratory techniques can be divided into two categories: methods that rely on the application of matric suction and methods that rely on the application of a controlled total suction (Fredlund et al.

2012). In industry, it is common practice to measure the matric suction below a suction of 1500 kPa and the total suction above 1500 kPa (Fredlund et al. 2012). It should be noted that the drying SWCC is generally measured in the laboratory as opposed to the wetting curve for two reasons (Fredlund et al. 2012):

- The drying curve is easier to measure than the wetting curve; and,
- The drying curve has become the primary curve used in estimating unsaturated soil property functions.

The first category of methods typically use high-air entry disks that can have a maximum matric suction of 1500 kPa (Fredlund et al. 2012). Pressure regulators can be used for matric suctions greater than 5 kPa, but inverted columns of water must be used for matric suctions less than 5 kPa (Fredlund et al. 2012). By using a pressure regulator or an inverted column of water, water will drain against atmospheric pressure conditions until the equilibrium water content is reached for a given applied matric suction (Fredlund et al. 2012). As successive matric suctions are applied, the water mass or water volume is monitored so that the equilibrium water content can be determined (Fredlund et al. 2012). Many different types of pressure plate devices with high-air entry disks have been developed over time, including: Tempe cells, volumetric pressure plates, and large pressure plate apparatuses.

The second category of methods involves the application of a controlled total suction, which is accomplished by using a controlled relative humidity environment (Fredlund et al. 2012). In these methods, small soil samples will come to equilibrium with the surrounding vapor pressure (Fredlund et al. 2012). The relative humidity environment may be established using salt solutions and the total suction is then calculated using the Lord Kelvin equation (Fredlund et al. 2012).

2.4.3 SWCC for High Volume Change Materials

The unsaturated soil properties of soils generally assume that the soil will undergo a small amount of volume change as the soil suction is increased (Fredlund et al. 2011). Consequently, there will be minimal differences between the θ-SWCC, w-SWCC, θ_i-SWCC, and S-SWCC for a

soil that does not undergo volume change. However, when the soil is a high volume change material, these three curves will vary substantially yielding different apparent AEVs. As a result, it is important that all of the different SWCCs are plotted and used in the appropriate manner to determine the unsaturated soil property functions. For example, the water storage function of a soil is defined by the volumetric water content of the soil. If the soil is a high volume change material, the θ_i-SWCC must be used to estimate the water storage function (Fredlund et al. 2011). If the θ-SWCC is used, there may be substantial errors in the estimated water storage function. Furthermore, the S-SWCC must be used to define the AEV and to estimate the unsaturated hydraulic conductivity function (Fredlund et al. 2011). Examples of high volume change materials include oil sands tailings and soils with a high percentage of clay. In general, a soil should be treated as a high volume change material unless there is sufficient information to support that it will not undergo volume change.

In order to attain the different SWCCs for a high volume change material, the shrinkage curve of the soil must be estimated or measured. The shrinkage curve describes how the void ratio of the soil changes with changes in the gravimetric water content during drying. The shrinkage curve can be described using a hyperbolic curve proposed by Fredlund (2000) as shown in Equation 2-6.

$$e(w) = a_{sh}\left[\left(\frac{w}{b_{sh}}\right)^{c_{sh}} + 1\right]^{\frac{1}{c_{sh}}} \quad \textbf{2-6}$$

Where $e(w)$ is the void ratio at any gravimetric water content w, a_{sh} is the minimum void ratio, b_{sh} is the slope of the line of tangency, and c_{sh} is the curvature of the shrinkage curve. Equation 2-7 relates the fitting parameters of the hyperbolic function to the volume mass properties of the soil (Fredlund 2000).

$$\frac{a_{sh}}{b_{sh}} = \frac{G_s}{S} \quad \textbf{2-7}$$

Where G_s is the specific gravity of the soil and S is the degree of saturation of the soil. Equation 2-6 can then be combined with the best-fitted w-SWCC equation (such as Equation 2-4 or

Equation 2-5) to determine the void ratio as a function of the suction of the soil as shown in Equation 2-8. It should be noted that this equation will vary depending on the $w(\psi)$ function.

$$e(w(\psi)) = a_{sh}\left[\left(\frac{w(\psi)}{b_{sh}}\right)^{c_{sh}} + 1\right]^{\frac{1}{c_{sh}}} \quad \textbf{2-8}$$

The best-fitting equation for the S-SWCC can then be attained using Equation 2-9 and the best-fitting equation for the θ_i-SWCC can be attained using Equation 2-10.

$$S(\psi) = \frac{G_s w(\psi)}{e(w(\psi))} \quad \textbf{2-9}$$

$$\theta_i(\psi) = \frac{G_s w(\psi)}{1 + e(w(\psi))} \quad \textbf{2-10}$$

2.5 Soil Freezing Characteristic Curve

2.5.1 General

When the temperature of the soil drops below the freezing point, a portion of the pore water freezes forming ice and the remaining water does not freeze (Banin and Anderson 1974, Spaans and Baker 1996). This water is referred to as unfrozen water and is generally present in adsorbed films around soil particles and in pores between soil particles (Spaans and Baker 1996). This water is able to stay unfrozen below the freezing point as the matric forces exerted by the soil on the water decrease the energy status of the water and consequently decreases the freezing point of the water (Spaans and Baker 1996). This decrease in the energy status results in a decrease in the freezing point of the soil, which is induced by the adsorption forces and curvature at the particle surfaces (Watanabe and Mizoguchi 2002). As shown by Watanabe and Mizoguchi (2002), the amount of unfrozen water is strongly influenced by the pore distribution and the specific surface area. Frozen soil is composed of four phases: soil particles, ice, unfrozen water, and air or gas (Andersland and Ladanyi 2004). The overall phase composition of frozen soil is influenced by (Anderson and Tice 1972, Hivon 1991):

- Temperature;
- Pressure;
- Specific surface area of the solid phases;
- Chemical and mineralogical composition of the soil;
- Density and arrangement of soil particles;
- Other physiochemical characteristics, including the nature of the exchangeable cations; and,
- Pore fluid solute content and composition.

The dominant factor that influences the phase composition is the temperature (Anderson and Tice 1972). The unfrozen water content in soil can be measured using a variety of techniques, including dilatometry, adiabatic calorimetry, X-ray diffraction, heat capacity, NMR, and TDR (Anderson and Morgenstern 1973). Each of these methods involves its own set of assumptions and limitations, but have proven to yield consistent results (Anderson and Morgenstern 1973).

Soil freezing characteristic curves (SFCCs) define the relationship between unfrozen water content and subzero temperatures in frozen soil (Zhou et al. 2014). The SFCC represents the variation of the unfrozen water phase and its energy status during the freezing/thawing process (Liu et al. 2012). A typical SFCC is shown in Figure 2-2. Due to the complexity of the structure and the chemistry of the soil, it is not possible to calculate the SFCC of a soil from fundamental properties (Dash et al. 1995). The SFCC can be determined by measuring the unfrozen water content and the temperature. As with the SWCC, the SFCC may be expressed in terms of:

i. total unfrozen volumetric water content, θ_u, defined as the ratio of the volume of unfrozen water to the original total volume of the sample.
ii. unfrozen gravimetric water content, w_u, defined as the mass of unfrozen water to the mass of solids.

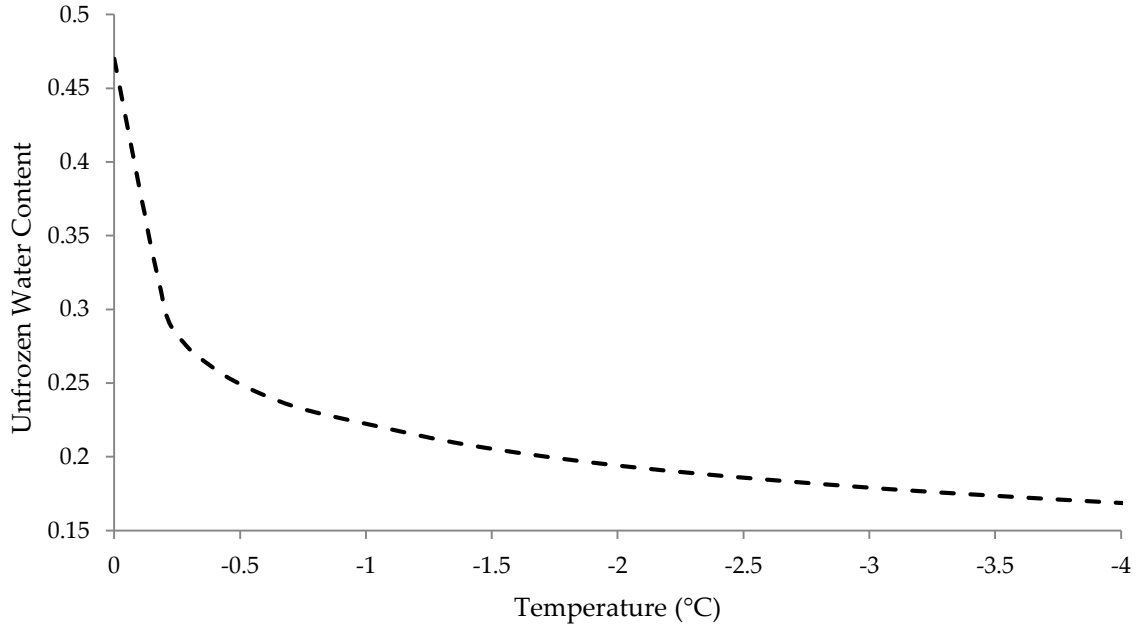

Figure 2-2: Example of a SFCC

An empirical relationship was proposed by Xu et al. (2001) to describe the unfrozen water content in terms of the temperature and the unfrozen water content as shown in Equations 2-11 to 2-13.

$$\theta_u = aT^{-b} \quad \textbf{2-11}$$

$$b = \frac{\ln \theta_i - \ln \theta_u}{\ln T - \ln T_f} \quad \textbf{2-12}$$

$$a = \theta_i T_f^b \quad \textbf{2-13}$$

Where θ_u is the unfrozen water content, a and b are fitting parameters, θ_i is the initial water content, T is the absolute value of the temperature in °C, and T_f is the absolute value of the freezing point in °C.

2.5.2 SFCC and SWCC

The process of wetting and drying in unfrozen soils is similar to the process of freezing and thawing in frozen soils (Lui et al. 2012). When a soil dries, water is removed and replaced by air, which decreases the matric potential of the remaining water (Azmatch et al. 2012). This process

also occurs when a soil freezes where the water changes phase and becomes ice (Azmatch et al. 2012). Additionally, the forces that prevent water from draining also prevent it from freezing (Spaans and Baker 1996). Due to these similarities between wetting and drying and freezing and thawing, many authors are advocating the using the SFCC to estimate the SWCC (Liu et al. 2012). This is advantageous due to how difficult and time-consuming it is to measure the SWCC (Liu et al. 2012).

Koopmans and Miller (1966) suggest that the SFCC can only be used as an analogue for the SWCC provided that the soil is known to be one of two extreme types of soil; however, the majority of natural soils are a mixture between the two extreme types. It should be noted that the difference between the two extreme types is largely due to the difference in adsorption space and capillary space. Adsorption space is defined as the zone where pore water is strongly affected by soil surface forces, and capillary space is the remaining area where the pore water is not affected by surface forces (Black and Tice 1989). The extreme types of soils identified by Koopmans and Miller (1966) are:

- Colloid-free soils such as sand, silt, or coarse clay fractions – these soils are designated as "SS soils" and are described as having direct solid-to-solid contacts between particles where the capillary space is much greater than the adsorption space; and,
- Colloidal soils such as clays – these soils are designated as "SLS soils" where the particles are always separated by water and the adsorption space is much greater than the capillary space.

Soils that are a mixture of two extreme types of soils are designated as SSLS. Koopmans and Miller (1966) present the assumptions required for the analogy between the SWCC and the SFCC to be valid for the two different extreme soils. Based on these assumptions, there is a soil dependent constant that can be used to relate the SWCC and SFCC. The purpose of the constant is to account for the specific surface energies of the air-water and the ice-water interfaces (σ_{aw}/σ_{iw}). Koopmans and Miller (1966) determined that the constant for an SS soils was about 2.2 and was about 1.0 for an SLS type soil. For SSLS soil, the value of the constant is somewhere in between

but can only be determined by measuring the SFCC and SWCC and determining the value (Azmatch et al. 2012a). These values also assume that the soils are ice-free when drying and air-free when freezing (fully saturated) (Spaans and Baker 1996, Zhou et al. 2014). This may result in substantial error as many soils are partially saturated when freezing occurs. It should be noted that the determination of the SWCC is reliable at high matric potentials (low matric suction) and becomes increasingly inaccurate and time-consuming as the soil dries due to long equilibration times (Spaans and Baker 1996). In contrast, the determination of the SFCC is more accurate and rapid at lower matric potentials (higher matric suction) (Spaans and Baker 1996).

In order to compare the SFCC to the SWCC, the temperature measurements must be converted to matric potential or suction. This is achieved using the Clapeyron equation, which involves analysis of the Gibbs free energy for any two phases in equilibrium (Newman and Wilson 1997). The general Clapeyron equation is provided in Equation 2-14 and describes the pressure difference between two phases in response to temperature changes (Newman and Wilson 1997). This equation can be expanded to describe the water potential in frozen soil as shown in Equation 2-15 (Spaans and Baker 1996).

$$\frac{\mathrm{d}P}{\mathrm{d}T} = \frac{\Delta h}{T\Delta V} \qquad \textbf{2-14}$$

$$\mathrm{d}\phi = (L_f/T)\mathrm{d}T + \mathrm{d}\phi_i \qquad \textbf{2-15}$$

Where P is the pressure in kPa, h is the specific enthalpy difference between phases in kJ/kg, V is the specific volume difference between phases in m^3/kg, ϕ is the equilibrium total water potential in J/kg, L_f is the latent heat of fusion of water (333.7 kJ/kg at 273.15 K), ϕ_i is the total ice potential in J/kg, and T is the temperature in degree Kelvin. It is generally assumed that the ice phase pressure is approximately equal to zero gauge pressure or the overburden loading, but this may be inconsistent with the real freezing process (Ma et al. 2015b). Equation 2-15 assumes that the water potential is determined only by temperature and ice pressure when water and ice are both present in the soil. Spaans and Baker (1996) provided an integrated form of Equation 2-15, which

included the temperature dependency of the latent heat of fusion and assumed zero gauge pressure in ice as shown in Equation 2-16.

$$\phi = \psi + \pi = -712.38\ln(T/T_0) + 5.545(T - T_0) - 3.14 \times 10^{-3}(T^2 - T_0^2) \quad \textbf{2-16}$$

Where ψ is the soil matric potential in kJ/kg, π is the soil osmotic potential in kJ/kg, and T_0 is a reference temperature (273.15 K). This equation assumes that the soil is wet enough to freeze at a given temperature, which means that ice must be present for the relationship between the temperature and the soil water potential to be valid. Simpler versions of Equation 2-16 have been proposed by various authors (Azmatch et al. 2012a, Liu et al. 2012). These equations generally do not account for the temperature dependency of the latent heat of fusion of water. Konrad (1994) suggested that the suction at an ice lens under atmospheric pressure increases linearly with decreasing temperature at a rate of approximately 1250 kPa/°C. This relation assumes that the effects of solutes are negligible and that the osmotic potential is negligible.

One major downfall of estimating the SWCC from the SFCC is the influence of solutes in the soil. The SWCC is not impacted by the presence of solutes in the soil (Azmatch et al. 2012a). In contrast, solutes will result in a decrease in the freezing point of the pore water, which leads to a decrease in the unfrozen water content at a given temperature (Hivon 1991). Ultimately, this leads to a mismatch in the SWCC and SFCC. This is discussed further in Section 2.5.3. Additionally, the SWCC is known to change with the degree of consolidation and the wetting/drying history of the soil (Williams 1964). This effect has also been observed in the SFCC with successive freeze/thaw cycles and as the degree of consolidation changes (Azmatch et al. 2012b, Williams 1964).

Liu et al. (2011) conducted a study to investigate the validity of using the SFCC as an analogue for the SWCC by testing two colloidal soils that were predominately clay. The SFCC was determined using a thermo-TDR sensor that measured the dielectric constant and temperature of the soil during thawing. The SWCC was determined using the filter paper method (ASTM D5298). This experiment showed good agreement between the SFCC and SWCC and suggested

that the SFCC could be used to determine the SWCC. The authors also stressed the importance of controlling the rate of freezing/thawing to achieve thermal equilibrium and a uniform temperature distribution. This experiment showed that as the rate of thawing increased, the SFCC tended to deviate from the SWCC, which is likely due to non-equilibrium conditions. It is common for researchers to determine the SFCC from a thawing cycle instead of a freezing cycle as supercooling may occur during freezing (Flerchinger et al. 2006). This concept is discussed further in Section 2.5.5.

Azmatch et al. (2012a and 2012b) compared the SFCC of Devon silt to the SWCC using different consolidation pressures and freezing temperatures. The SFCC was determined using a TDR to measure the dielectric constant and RTDs to measure the temperature. The unfrozen water content was then calculated from the dielectric constant using the Topp et al. (1980) calibration equation discussed in Section 2.6.2. The suction was correlated to the temperature using the Clapeyron equation and calculated assuming that the suction increased linearly with decreasing temperature at a rate of 1250 kPa/°C (Konrad 1994). The experiment showed that the SFCC changed with changing consolidation pressure. These changes were also reflected in the SWCC. Additionally, it was observed that the SFCC was influenced by the freezing temperature. As the freezing temperature increased, the ice entry value (IEV) increased. The IEV is similar to the AEV and describes the suction or temperatures where ice first begins to enter the largest soil pores. This may result in errors between the SFCC and SWCC as methods to determine the SWCC will not be impacted by the freezing temperature or rate of freezing. The Devon silt was also subjected to three freeze-thaw cycles to determine the impact on the SFCC. This showed that the SFCC experiences hysteresis with successive freezing and thawing cycles. The SFCC from the first freeze cycle was different than the SFCC from the following freeze cycles and the SFCCs for the thaw cycles were almost identical. The authors suggest that this is due to structural changes that occur when a soil freezes for the first time. The impact of solutes on the SFCC was also investigated by determining the SFCC and SWCC for a sample of Devon silt with a salinity of 5 g/l. These results showed a very poor correlation between the SFCC and SWCC for a saline sample.

Hysteresis between successive freeze cycles was also observed by Patterson and Smith (1981). The study conducted by Patterson and Smith (1981) showed a difference in the unfrozen water content for a given water content between successive freezing and thawing cycles. This difference was reflected in two different methods (TDR and dilatometry) and was thought to be due to structural changes in the soil during the first freeze cycle. As the SWCC is also hysteretic, the first drying cycle can only be compared to the first freezing cycle and the first wetting cycle can only be compared to the first thawing cycle and so on (Spaans 1994). Li et al. (2016) also investigated the hysteretic behavior of freezing and thawing of a clay and noted that the unfrozen water content in the freezing process is always greater than that in the thawing process with a maximum difference of 4.3 percent to 4.6 percent for temperatures in the range of -4°C to -5°C for the soil tested, which shows the importance of considering the impacts of hysteresis.

2.5.3 Osmotic and Matric Contributions to the Total Suction

The relative contributions of the osmotic and matric suction to the total suction have been debated throughout literature. This concept is difficult to quantify due to the inability of typical suction measurement tools to operate at sub-zero temperatures (i.e. tensiometer). As a result, a lot of reliance is placed on estimating the suction in the sample from temperature measurements using methods such as the Clapeyron equation or the freezing point depression method discussed by Drotz et al. (2009).

Ma et al. (2015a) conducted a study where they determined the SWCC of clay and silt using the pressure plate extractor method and the vapour pressure method and determined the SFCC using NMR and temperature measurements. A series of experiments was conducted on the soils that were saturated with different concentrations of NaCl solutions ranging from 0 mol/L to 1.0 mol/L (0 g/L to 58.44 g/L). The pore water potential of the frozen soil is determined based on the Clapeyron equation that accounts for the effects of capillary, sorption, and osmosis. Ma et al. (2015a) noted that the total water potential includes the matric potential, which is a result of the adsorptive and capillary effects in the soil and the osmotic potential, which depends on the solutes and their concentrations in the pore water. Drying and freezing tends to occur in the larger pores first with wetting and thawing occurring in the smaller pores first. The pressure

plate was capable of measuring the matric potential while the vapor equilibrium method measures the total water potential. This has important implications as the solute concentration will have a slight impact on the matric potential but can significantly influence the total potential. This experiment showed that the total water potential of an unsaturated soil is more negative than that of its frozen counterpart at the same water content. This is due to two competitive mechanisms, as follows:

- Matric potential increases as temperature decreases; and,
- Osmotic potential decreases as temperature decreases.

Wen et al. (2012) conducted an experiment to investigate the characteristics of the unfrozen water content, soil matric potential and the temperature. The results of the experiment showed that the actual soil matric potential in a frozen soil was significantly higher (less negative) than the theoretical values inferred from the freezing point depression method. This was attributed to the discrepancy between the adsorptive and osmotic effects. The matric potential was found to control the direction of moisture migration and results in the change of total water content. This experiment also showed that the initial water content has an impact on the freezing point and the unfrozen water content where a higher initial water content will result in an increase in the freezing point.

Drotz et al. (2009) investigated the contributions of the matric and osmotic potentials to the unfrozen water content in a frozen soil. The result of the experiment showed that the unfrozen water content in a mineral soil is governed by the osmotic suction, but the unfrozen water content in samples of humus from the boreal forest was controlled by the osmotic and matric suction with the osmotic potential contributing to 20 percent to 69 percent of the total potential. It should be noted that the tested soils had a low clay content, but a high soil organic matter content. The results from this experiment contradicted the results from Suzuki (2004) who found that the contribution of the osmotic potential to unfrozen water content was negligible for soils with a high clay content.

2.5.4 Impacts of Salinity on Freezing Characteristics

As discussed in Section 2.5.3, solutes increase the level of difficulty in determining the SWCC from the SFCC. Solutes tend to shift the SFCC towards lower temperatures (Anderson and Morgenstern 1973). This shift is believed to correspond to a magnitude comparable with the freezing point depression corresponding to the osmotic potential of solutes added (Anderson and Morgenstern 1973). The freezing point of a soil is the temperature where ice crystals will first start to form (Spaans 1994) and it can be depressed as a result of:

1. Matric pressure that the soil matrix exerts on the pore water
2. Solutes dissolved in the pore water
3. Supercooling of the pore water

The freezing point depression due to dissolved solutes can result in a mismatch between the SWCC and the SFCC as the SWCC is not impacted by the presence of solutes. When a soil begins to freeze, some of the pore water will change phase forming ice. The solutes present in the pore water will be rejected from the ice phase to the liquid phase (Banin and Anderson 1974, Cary and Mayland 1972, Hivon 1991, Williams 1964). As a result, the osmotic pressure in the ice will be negligible. This process results in an increase in the salinity of the liquid phase that corresponds with the binary phase diagram for the solute. The binary phase diagram for NaCl is provided in Figure 2-3. As a result, the freezing of a saline soil occurs progressively where the amount of unfrozen water will decrease and the concentration of the pore water will increase resulting in a continuous decrease in the freezing point (Hivon 1991). This process will continue to occur until the eutectic point is reached. The freezing point depression is affected by the number of solutes present and the associated unfrozen water content may be influenced by the electrolytic dissociation of the solute and the interaction between the ions and the clay surface (Watanabe and Mizoguchi 2002).

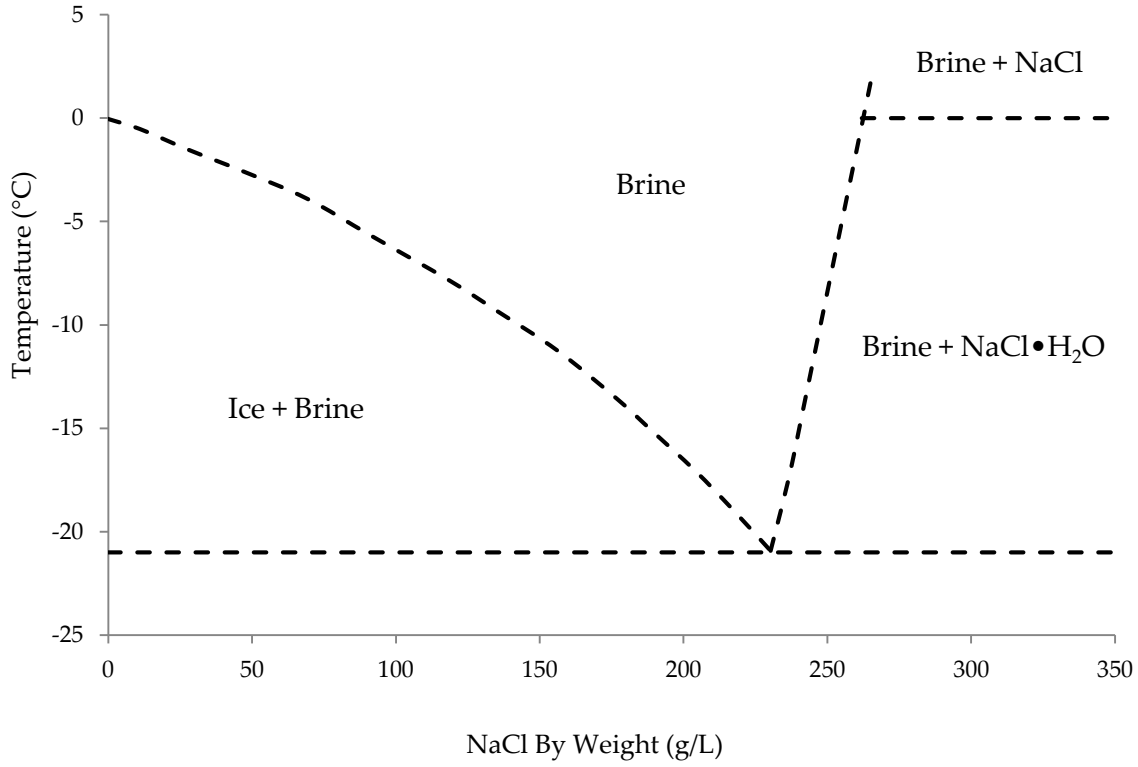

Figure 2-3: NaCl Binary Phase Diagram (after Biggar and Sego 1993)

Williams (1964) suggested that the increase in the freezing point depression due to salinity is approximately proportional to the concentration of the salts present in the pore fluid. The freezing point depression of the soil will increase with increasing molality of the pore fluid (Cheung 1979). This effect is summarized in Equation 2-17 and Equation 2-18.

$$\Delta T = iK_f m \qquad \textbf{2-17}$$

$$K_f = \frac{RT_o^2}{L_f} \qquad \textbf{2-18}$$

Where ΔT is the freezing point depression in °C, i is the van't hoff factor, m is the molality in mol/kg. K_f is the molal freezing point depression constant in °C/molality, R is the universal gas constant in $Jmol^{-1}K^{-1}$, T_o is the freezing temperature of pure water in K, and L_f is the latent heat of fusion J/m^3. The van't hoff factor describes the degree of dissociation or association of the solute in the solvent. The van't hoff factor will be equal to 1 for non-electrolyte solutions (Cheung 1979).

If there is no interionic attraction, the factor will be equal to the number of ions formed per molecule when the electrolyte dissociates (Cheung 1979). For solutions with a high solute concentration, the van't hoff factor may not equal the number of ions per molecule due to interionic attractions (Cheung 1979). Cheung (1979) noted that the unfrozen water content of a soil is due to the combined effect of the salt exclusion mechanism and the osmotic pressure of phenomenon. This depends on the salt concentration. The unfrozen water content increases with increasing salt concentration due to the freezing point depression from the physical presence of the salt. In contrast, the unfrozen water content decreases with increasing salt concentration due to reducing osmotic pressure. These two mechanisms are inversely related. Cheung's (1979) results showed that:

- The unfrozen water content is less than that of a salt-free clay at NaCl concentrations of less than 10^{-3} M, and;
- The unfrozen water content is more than that of a salt-free clay at NaCl concentrations of more than 10^{-2} M.

Banin and Anderson (1974) developed an equation for calculating the freezing point depression due to gradual removal of water upon freezing in porous bodies. Banin and Anderon (1974) proposed that the freezing point depression is primarily due to the direct effect of solutes on the activity and free energy of the water in the solution. This was based on the assumption that the pore fluid behaves as an ideal solution throughout the range of freezing. Cheung (1979) argues that the model based on salt exclusion of pure solution by Banin and Anderson (1974) can not be substantiated for saline soils due to an observed mismatch of measured and predicted values of unfrozen water content in low temperature ranges. The model by Banin and Anderson (1974) assumes that any change in the freezing point can be attributed to the salt treatment as described by the pure solution theory and the interaction with the bound water films can be neglected.

Wu et al. (2015) conducted laboratory experiments to study the effects of water and solutes on soil freezing using TDR and temperature sensor combo methods. The results of the experiment showed that solute content and type had significant effects on the soil freezing process (Wu et al.

2015). It should be noted that the solute type had a more significant effect on the freezing process than the solute content. It was noted that solutes tended to lower the freezing point of the soil and that the solute concentration would increase in the soil as the unfrozen water content decreased, which would decrease the osmotic potential and impede freezing. The osmotic potential was noted to be a major contributor to the soil potential when the soil temperature was close to 0°C. As the temperature in the soil dropped below -1°C, the matric potential rapidly decreased and became the major contributor to the soil potential. The osmotic potential can be calculated based on Equation 2-19.

$$\pi = -cRT_K/g \qquad \textbf{2-19}$$

Where π is the osmotic suction in m, c is the solute concentration in mol/kg, R is the general gas constant (8.3143 J/(mol K), T_k is the temperature in K, and g is the gravitational constant.

Bing and Ma (2011) studied the influence of the initial water content and solute content on the freezing point of soil and concluded that the freezing point of soil will increase with an increase in initial water content and will decline as the solute content increases. It was also noted that the effect of the soil particle size on the freezing point decreased with increasing initial water content. This has important implications for the testing of oil sands materials that have a very high initial water content and a relatively low solute content when compared to saline soils.

2.5.5 Supercooling Phenomenon

Another phenomenon that can complicate the process of estimating the SWCC from the SFCC is supercooling. This process is shown in Figure 2-4. Supercooling is a drop in sample temperature below the freezing point T_f without phase change as represented by the constant volumetric water content curve shown in Figure 2-4 (Kozlowski 2009). The temperature in the sample will continue to drop until it reaches the spontaneous nucleation temperature T_{sn}. At this temperature, latent heat will be released and ice will start to form as nucleation occurs (Kozlowski 2009). This will cause a rise in the sample temperature to the freezing temperature. At this point, phase change will occur, which is represented by the decreasing volumetric water content in Figure 2-4. This

process can have a huge impact on the shape of the SFCC and can make it difficult to estimate the air entry value. It should be noted that supercooling does not occur during the thawing process as thawing is a single step process that occurs at the melting point of the ice (Kozlowski 2009). In contrast, the freezing process involves ice nucleation and crystal growth. As a result, it is generally more desirable to estimate the SWCC from the thawing SFCC. However, it should be noted that the SWCC exhibits hysteretic behavior for the processes of wetting and drying (Williams 1964). This effect has also been observed in the SFCC for the processes of freezing and thawing (Azmatch et al. 2012b, Williams 1964). As a result, it is important that similar processes are matched up when estimating the SWCC from the SFCC. This means that the freezing SFCC should be used to estimate the drying SWCC and the thawing SFCC should be used to estimate the wetting SWCC.

Kozlowski (2009) investigated the impact of various factors on the supercooling phenomenon and the equilibrium freezing point in soil-water systems and noted that the equilibrium freezing point was strongly dependent on the water content of the soil. This has important implications for estimating the SWCC from the SFCC as the equilibrium freezing point is correlated with the AEV on the SWCC. Kozlowski (2009) provided an empirical equation for estimating the freezing temperature based on the plastic limit of the soil and the water content as shown in Equation 2-20.

$$T_f = -0.0729 w_p^{2.462} w^{-2} \qquad \textbf{2-20}$$

Where T_f is the freezing temperature in °C, w_p is the plastic limit of the soil in %, and w is the water content. This equation provided a good fit to the experimental data obtained on melting, but was unable to describe the behavior at water contents that were close to the unfreezable water content (Kozlowski 2009). While Equation 2-20 adequately described the relationship between the water content and the freezing temperature, Kozlowski (2009) noted that a simple relationship between the water content and the spontaneous nucleation temperature did not exist as the spontaneous nucleation temperature is dependent on a number of factors (Kozlowski 2009), including:

- Sample volume;
- Cooling velocity;
- Presence and concentration of solutes;
- Presence of solid impurities; and,
- Effect of external fields.

Kozlowski (2009) did note that the temperature of spontaneous nucleation would decrease with decreasing water content and that the higher the plastic limit, the lower the temperature of spontaneous nucleation for a constant water content and sample mass. It should also be noted that there is a critical water content where supercooling is at a maximum (Kozlowski 2009). At water contents above and below the critical water content, supercooling will be less than the maximum (Kozlowski 2009). It was also noted that the supercooling would gradually decrease with the increasing water content when the water content exceeded the liquid limit. Kozlowski (2009) suggested that some degree of supercooling is needed for freezing to occur in laboratory experiments, but that soils in the natural environment may freeze without supercooling.

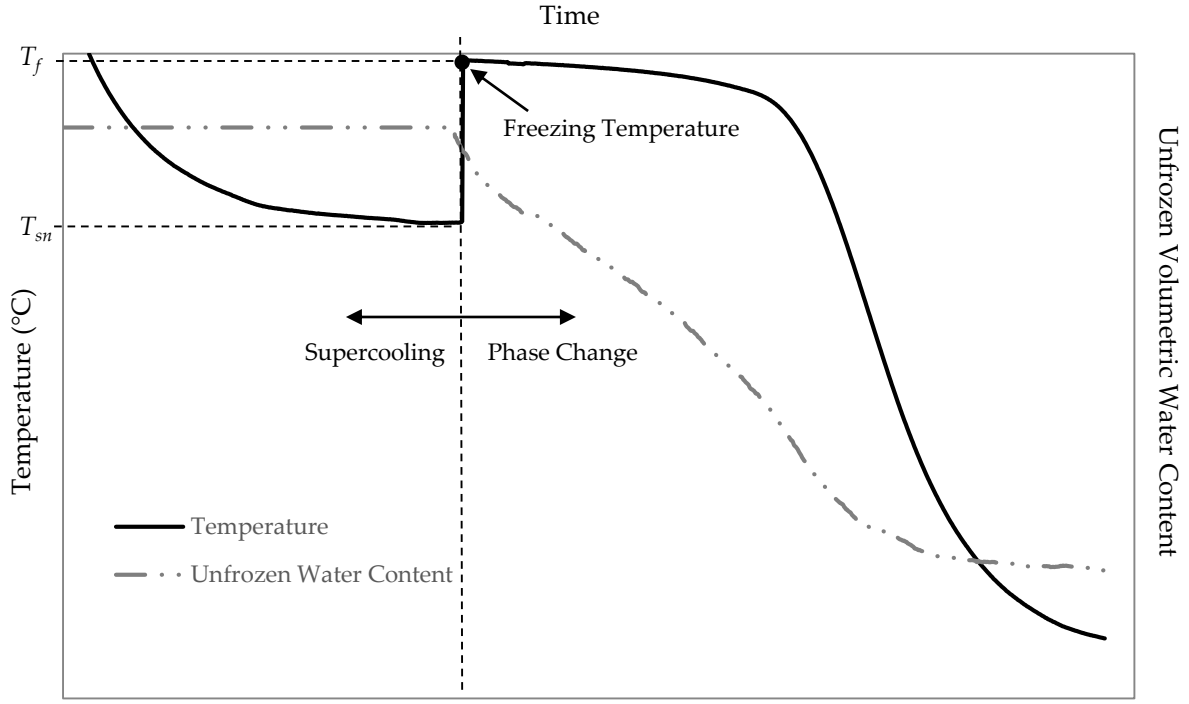

Figure 2-4: Supercooling Phenomenon and the Impact on the Unfrozen Water Content versus Time

2.6 Time Domain Reflectometry

2.6.1 General

Time domain reflectometry (TDR) is a guided radar technology that was initially used by electrical engineers to locate discontinuities in electrical cables (Liu et al. 2012). The technology was later extended to measure the water content in soil for irrigation purposes after the work performed by Topp et al. (1980). TDR is an electromagnetic technique that measures the dielectric constant of soil by measuring the travel time of an electromagnetic wave in the soil (Benson and Bosscher 1999, Sorta et al. 2013). The water content (frozen or unfrozen) of the soil can then be determined using empirical correlation equations or dielectric mixing models that relate the water content to the apparent dielectric constant. TDR has a lot of advantages over previous methods used to determine the water content of a soil. It is cost effective, fast, rugged, non-destructive, accurate, automatic, and can be used in the laboratory or field (Benson and Bosscher 1999, Liu et al. 2012, Patterson and Smith 1981, Sorta et al. 2013). Additionally, the dielectric constant is a function of the liquid water content and can be measured directly (Benson and Bosscher 1999, Patterson and Smith 1981).

2.6.2 Dielectric Constant

The dielectric constant indicates the ability of a substance to store electrical potential energy in an electrical field relative to that of air (Patterson and Smith 1980). The complex dielectric constant (K*) is shown in Equation 2-21 and is composed of a real term and an imaginary term.

$$K^* = K' + j * (K'' + \frac{\sigma_{dc}}{\omega \varepsilon_o}) \quad \textbf{2-21}$$

Where K′ is the real part of the dielectric constant and the second term is the imaginary part that represents the dielectric and conductive losses in the material during wave propagation (Patterson and Smith 1980). Additionally, an electrical loss term tan δ is defined in Equation 2-22.

$$tan\delta = \frac{K'' + \frac{\sigma_{dc}}{\omega \varepsilon_o}}{K'} \quad \textbf{2-22}$$

Where σ_{dc} is the direct current electrical conductivity, ω is the frequency, and ε is the permittivity of the free space. Clay soils tend to have more electrical loss and the loss will increase with water content and salt concentration (Patterson and Smith 1980). TDR measures both the real and imaginary parts of the dielectric constant and is often referred to as the apparent dielectric constant (K_a). There is a large difference between the apparent dielectric constant of water and soil solids. The K_a of water is approximately 81, the K_a of soil solids varies from 3 to 7, the K_a of air is about 1 (Liu et al. 2012, Patterson and Smith 1980). This contrast makes it possible for TDR to be used to measure the volumetric water content as the apparent dielectric constant of the soil changes as the volume fraction of water changes (Benson and Bosscher 1999, Patterson and Smith 1980). The K_a of ice is similar to that of soil solids with a value of about 3.2 (Benson and Bosscher 1999, Patterson and Smith 1980). As a result, the liquid water that remains when the soil is frozen has a much higher K_a (approximately 81) than the other phases (3 to 7 for soil solids, 1 for air and 3.2 for ice) (Benson and Bosscher 1999, Patterson and Smith 1980). Due to this distinct difference, TDR can also be used to measure the unfrozen water content.

2.6.3 TDR System

The TDR system generally consists of a reflectometer, a TDR probe, coaxial cable, a multiplexer, a data processor, and a data logger as shown in Figure 2-5. The reflectometer generates the pulses and the multiplexer is used to monitor multiple probes using a single reflectometer (Sorta et al. 2013). The TDR probe may consist of two or three metal rods. The soil sampled by the TDR is a cylinder with a diameter that is 1.4 times the spacing between the rods (Topp and Davis 1985). There is no obvious variation in sensitivity along the length of the probes and the area just beyond the tip of the probe is not sampled (Baker and Lascano 1989). Additionally, the ratio of the radius of the probe to the spacing between the probes should be greater than 0.1 and the radius of the probe should be as large as possible compared to the average pore size of the material (Knight 1992).

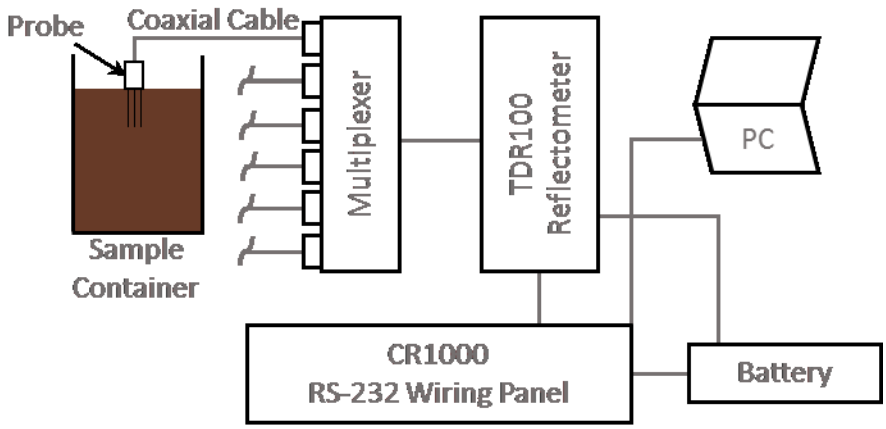

Figure 2-5: Schematic of a TDR system (after Sorta et al. 2013)
Printed in CIM Journal, Vol. 4, 2013. Reproduced with permission from the Canadian Institute of Mining, Metallurgy and Petroleum.

2.6.4 Theory

In TDR, a fast rising step pulse propagates along coaxial cables to the measurement probe in the soil (Benson and Bosscher 1999, Liu et al. 2012). When the electrical signal encounters a change in the dielectric properties, a partial signal is reflected back towards the generator (Benson and Bosscher 1999). As shown in Figure 2-6, there will be two reflections that occur due to large contrasts in the dielectric properties. The first reflection occurs when the pulse reaches the top of the TDR probe and the second reflection occurs when the pulse reaches the bottom of the TDR

probe. The waveform curve defines the apparent length (L_a), which is used to calculate the time between the two reflections as shown in Equation 2-23. This can then be used to calculate the velocity of the electromagnetic wave using Equation 2-24.

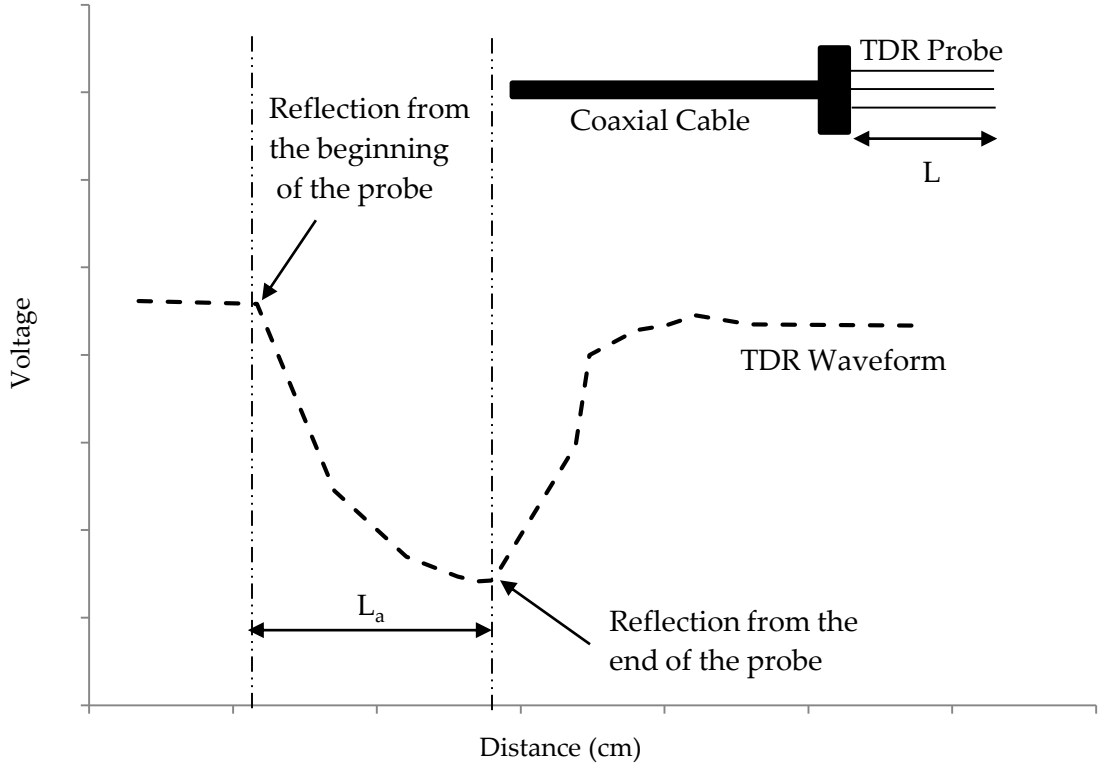

Figure 2-6: Typical TDR Curve for Soil and Measurement of Apparent Length (after Sorta et al. 2013)
Printed in CIM Journal, Vol. 4, 2013. Reproduced with permission from the Canadian Institute of Mining, Metallurgy and Petroleum.

$$t = \frac{2L_a}{c} \qquad \textbf{2-23}$$

$$v = \frac{2L}{t} = \frac{2L}{2L_a/c} = \frac{L}{L_a}c \qquad \textbf{2-24}$$

Where L_a is the apparent length, c is the speed of the electromagnetic wave in a vacuum (3.0×10^8 m/s), t is the time difference between the two reflections, v is the velocity of an electromagnetic wave travelling in the material, L is the physical length of the TDR sensor section. The velocity can then be described by Equation 2-25. If electrical losses are small, then tanδ is much less than 1 and Equation 2-26 is applicable. Finally, Equation 2-24 and 2-27 can then be

combined to define the apparent dielectric constant in terms of the apparent length and the physical length as shown in Equation 2-28.

$$v = \frac{c}{\sqrt{K' \times \frac{1+(1+tan^2\delta)^{1/2}}{2}}} \quad \textbf{2-25}$$

$$K_a \approx K' \quad \textbf{2-26}$$

$$v = \frac{c}{\sqrt{K_a}} \quad \textbf{2-27}$$

$$K_a = \left(\frac{L_a}{L}\right)^2 \quad \textbf{2-28}$$

2.6.5 Volumetric Water Content and Apparent Dielectric Constant Correlation

In order to determine the volumetric water content or the unfrozen water content from the K_a of a soil, a correlation between K_a and the water content is needed. Topp et al. (1980) conducted a series of experiments on four types of soils (sandy loam to heavy clay) and glass beads. The results from these experiments were used to develop a third order polynomial empirical relationship between K_a and volumetric water content (θ) as shown in Equation 2-29. The experiments showed that the relationship was relatively independent of soil type, temperature, density, and salinity. As a result, this equation was considered universal.

$$\theta = -0.053 + 0.0292K_a - 0.00055{K_a}^2 + 4.3 \times 10^{-6}{K_a}^3 \quad \textbf{2-29}$$

(Topp et al. 1980)

After the development of Topp et al.'s (1980) equation, many other empirical equations and mixing models have been developed to relate K_a to θ. The empirical equations fit a mathematical model of measured K_a to measured θ, whereas mixing models use the dielectric constants and volumetric fraction of each phase to derive a relationship describing the K_a (Sorta et al. 2013). Empirical equations are considered the most accurate method to determine the θ from the K_a as

these methods account for the unique physical characteristics of the soil (Nagare et al. 2011). The development of different calibration curves demonstrated the non-universality of Topp et al.'s (1980) equation. A study conducted by Herkelrath et al. (1991) showed that θ values predicted by Topp et al.'s (1980) equation were as much as 30 percent too low. This is thought to be a result of a high content of soil organic matter, which was not considered in Topp et al.'s (1980) equation. This led to the development of a linear fit calibration model that is dependent on the square root of K_a. A study conducted by Jacobsen and Schjonning (1993) aimed to develop a calibration equation that included linear terms for dry bulk density, clay content, and organic matter using 10 soils that varied in texture and organic content. The study showed that Topp et al.'s (1980) equation adequately predicted the θ to an upper boundry of 0.18 m^3/m^3. Above this boundary, the prediction was poor and under predicted the θ. Ponizovsky et al. (1999) conducted a study on seven different types of soil to evaluate the ability of existing models to adequately predict the θ and to explore the use of a piecewise-constant function with three adjustable parameters to fit the data. The results indicated that Topp et al.'s (1980) equation performed well for certain soils, but the error increased with an increase in fine fraction. This can be explained by the increasing amount of confined water with an increase of soil or clay specific surface, which is related to organic content and clay content. This impacts the dependence of the K_a value on the θ. These studies demonstrate the shortcomings of Topp et al.'s (1980) equation and show the importance of deriving soil specific calibrations or using a calibration that best describes the soil being tested (Benson and Bosscher 1999, Drnevich et al. 2005, Herkelrath et al. 1991, Jacobsen and Schjonning 1993, Ponizovsky et al. 1999).

Sorta et al. (2013) conducted a series of tests to investigate the impact of temperature, solute, texture, and thixotopic effects on determining the water content of oil sands tailings using TDR. While many different calibration equations have been developed, most of them are based on lower water contents and thus higher solids contents with θ that are generally less than 50 percent. This is not typical of oil sands tailings. The results of the investigation showed that Topp et al.'s (1980) equation for predicting the θ would result in values that are up to 28 percent lower than the actual θ. Sorta et al. (2013) suggested that the K_a is better correlated with the gravimetric

water content or the solids content of the slurry instead of the θ. The results show that the TDR measurements are influenced by temperature, residual bitumen, and percent clay in the tailings. Thixotropy and the addition of phosphogypsum did not influence the TDR measurements. Sorta et al. (2013) investigated the impact of temperature on the TDR measurements by varying the temperature of the tailings from 15°C to 75°C. The research indicated that the TDR measurements were impacted by the temperature due to the dependence of the K_a of the water on the temperature and the effects of the temperature on the interaction of the water phase and the solid phase. This demonstrates the importance of a soil specific calibration for oil sands tailings.

2.6.6 Unfrozen Water Content and Apparent Dielectric Constant Correlation

As discussed in Section 2.6.5, it is important to develop a soil specific correlation between the K_a and the θ. There has been a lot of discussion over the years regarding if correlations developed to determine the θ can be used to determine the θ_u in a frozen or partially frozen soil. This section provides a brief discussion on the different viewpoints on this subject.

Patterson and Smith (1981) investigated the possibility of determining the θ_u from K_a measurements by TDR and assessing the impact of the ice content on the K_a. This experiment involved testing clay loam and silt loam that were brought to a slurried state using a combined TDR-dilatometer apparatus. The results indicated that the ice content has little impact on the K_a value and suggested that Topp et al.'s (1980) equation could be used to evaluate the θ_u in frozen soils. The results were restricted to temperatures above -3°C or -4°C due to dilatometer errors. As a result, it is expected that this relationship would depart from Topp et al.'s (1980) curve at lower temperatures where the ice contents are higher and the θ_u are lower (Smith and Tice 1988).

Smith and Tice (1988) recognized the need for a θ_u-K_a calibration that was specific to freezing conditions and conducted a calibration experiment using nuclear magnetic resonance (NMR) and TDR. The experiment was conducted on 17 different soil types that had varying specific surface areas (SSAs) from 15 m^2/g to 714 m^2/g. Using this data, a third-degree polynomial calibration equation was developed as shown in Equation 2-30. The impact of soil type on the relationship was investigated due to data scatter. The results suggested that the K_a for a given θ_u decreases

with increasing fines content. As the fines content increases (and the SSA), the amount of adsorbed water will also increase. The adsorbed water has a lower dielectric constant than that of bulk water. The larger proportion of adsorbed water will result in an overall decrease in K_a at a given θ_u. This testing was conducted on fully saturated samples with θ_u less than 0.6. Additional testing was conducted to evaluate if the equation was valid for other soil types. In general, the equation performed well, except for hectorite and volcanic ash where the predicted water contents were noticeably lower than the corresponding NMR values. Both of these soils had high SSAs.

$$\theta_u = -0.1458 + 0.03868K_a - 0.0008502{K_a}^2 + 9.920 \times 10^{-6}{K_a}^3 \qquad \textbf{2-30}$$

The study conducted by Smith and Tice (1988) was conducted on saturated soils. As a result, it is expected that this equation should consistently underestimate θ_u if applied to unsaturated frozen soils as the air and ice mixture will lead to a lower K_a then ice alone (Spaans and Baker 1995). Spaans and Baker (1995) also argue that calibrations derived from drying an unfrozen soil cannot be used for determining the θ_u from K_a for a frozen soil. In a drying soil, the water is replaced by air, but the water is replaced by ice in a freezing soil. This will result in errors as the dielectric constant of air is about 1 and the dielectric constant of ice is about 3.2 (Benson and Bosscher 1999, Patterson and Smith 1980).

Spaans and Baker (1995) conducted a study to demonstrate a new method to calibrate the θ_u-K_a relationship from TDR and to determine the impact of initial water content on the calibration on saturated to unsaturated samples. Their results indicated that no unique calibration exists for determining the θ_u from the K_a from TDR, but rather a family of calibration curves should be used where each curve corresponds to a different total water content. The θ_u of a soil is determined by the temperature in the soil, but the K_a depends on the θ_u and the amount of ice present, which may vary depending on the conditions before and after freezing.

A study conducted by Seyfried and Murdock (1996) showed that there was an increase in the θ_u with an increase in the total water content at a constant temperature. These results conflicted

with previous modelling assumptions that assumed θ_u was independent of the total soil water content at a constant temperature. Due to limitations of their testing methods, they were not able to determine if this phenomenon was real or if it was a result of errors in the TDR calibration equations. This study involved applying six calibration equations to three natural soils under frozen and unfrozen conditions. The samples were air-dried and then mixed with deionized water to saturation. Three of the equations used were empirical calibration equations and three of the equations were dielectric mixing models that assume that K_a depends only on the volumetric composition of the components. The different calibration methods exhibited similar results for the unfrozen condition. When applied to the frozen condition, the models predicted very different behaviour with some providing poor to unusable results. This difference may be due to the ability of each method to account for ice effects. The authors recommended further investigation to determine the validity of the θ_u dependence on the total water content.

Flerchinger et al. (2006) investigated the validity of deducing the SWCC curve from the SFCC curve by installing TDRs and thermocouples in situ at different field sites in natural soils. This involved performing soil freezing tests with a TDR to determine the θ_u. This was done using a manufacturer specific calibration that was similar to Topp et al.'s (1980) equation and then correcting for the ice content. The results indicated that neglecting the effect of ice on TDR-measured θ_u resulted in higher estimated θ_u. This effect tended to increase at lower θ_u and to increase with increasing total water content. This is thought to be a result of the mismatch of the dielectric constant of ice and air. As the dielectric constant of ice is higher than air, calibrations performed on unfrozen soil will result in overestimation of θ_u in frozen soils. In order to accurately correct for the ice content, the total water content or the ice content must be measured. This study suggests that the increase in the θ_u observed by Seyfried and Murdock (1996) with increasing total water content at a given temperature is due to errors in the TDR calibrations.

Kahimba and Sri Ranjan (2007) conducted a study to develop a temperature calibration method for field TDR measurements at different soil temperatures. The measurements were taken in situ on natural soils. This was achieved by using a neutron moisture meter (NMM) to measure the total water content and a TDR to measure the unfrozen water content. The temperature

calibration was conducted at temperatures above zero and then applied to partially frozen conditions. Before soil freezing conditions, the NMM and TDR should theoretically be the same. Prior to the temperature correction, the TDR method overestimated the water content by an average of 0.10 m^3/m^3. The application of this temperature correction under soil freezing conditions was not confirmed with a secondary method. It is not clear if the ice content had an impact on the TDR readings (Kahimba and Sri Ranjan 2007).

Watanabe and Wake (2009) performed a study to investigate the influence of freezing conditions on TDR measurements of K_a by measuring θ_u using NMR and K_a using TDR on unsaturated soils. The NMR results indicated that the θ_u corresponded to the total water content above 0°C and decreased as the temperature decreased below zero. With different total water contents, the θ_u decreased proportionally with total water content between 0°C and -1°C and then had the same θ_u – T relationship below about -1°C. The measured K_a values were used to determine the θ_u using Smith and Tice's equation (Equation 2-30) and Topp et al.'s (1980) equation (Equation 2-29). These results were then compared with the NMR determined θ_u, which demonstrated how poorly these equations compute the θ_u for varying total water contents, especially for soils with a high amount of adsorbed water. The authors emphasize the principle that calibration of the $K_a - \theta_u$ relationship without consideration of the K_a dependency on the total water content will lead to inaccurate estimations of θ_u. Using a four-phase mixing model to predict the θ_u from the K_a value yielded good results for the soils with a low unfrozen water content (sand); however, these models failed to provide good results for soil that had a large amount of unfrozen or adsorbed water. For these materials, the mixing model estimated higher θ_u than measured from NMR as the total water content increased. This is thought to be a result of adsorbed water that tends to behave more like a solid than bulk water due to the influence of surface forces. As a result, the adsorbed water generally has a lower dielectric constant than the bulk water. To solve for this, the four-phase mixing model was modified to account for the surface forces associated with adsorbed water and to account for the change in the K_a with a different total water content.

Zhou et al. (2014) conducted a study to develop a method to measure the total water content, unfrozen water content, and ice content in an unsaturated silt loam during column freezing

experiments and to quantify the overestimation of unfrozen water measured by TDR alone. This was done using gamma ray attenuation to determine the total water content and TDR to measure the K_a. The K_a value measured by TDR is affected by the unfrozen water, ice, air, and soil while the θ_u is only affected by the temperature. As a result, it is necessary that TDR be calibrated using a secondary method to determine unfrozen water content for empirical methods or to determine the total water content or ice content for dielectric mixing models. In this study, the θ_u was calculated from the measured K_a using a four-phase mixing model. The study showed that the θ_u measured by TDR alone tends to overestimate the unfrozen water content compared to the combined method. The overestimation increases as the ice content increases and as the initial total water content increases. The combined method was successful in determining the unfrozen water content and ice content in the frozen silt loam. This study showed that the θ_u is independent of total water content and affected only by temperature when the freezing point is reached.

Based on the literature review, it appears that θ_u – K_a calibrations developed for unfrozen soils should not be applied to frozen or partially frozen soils for unsaturated soils. In general, it is recommended to conduct a soil specific empirical correlation using TDR and a secondary method such as NMR or to use a dielectric mixing model, which requires a method to measure the ice content or the total water content. If these steps are not taken, the θ_u will generally be overestimated with increasing total water content or increasing SSA due to the following:

- The dielectric constant of ice (3.2) is higher than air (Flerchinger et al. 2006, Spaans and Baker 1995, Watanabe and Wake 2009).
- The K_a of the soil is influenced by the unfrozen water content, ice content, air, and soil; however, the θ_u is only affected by the temperature (Flerchinger et al. 2006, Seyfried and Murdock 1996, Spaans and Baker 1995, Watanabe and Wake 2009, Zhou et al. 2014).
- As the SSA of a soil increases, the amount of adsorbed water will increase. The adsorbed water has a lower dielectric constant than the bulk water (Smith and Tice 1988, Watanabe and Wake 2009).

2.6.7 Errors in TDR Measurements

Using TDR to determine the K_a can have a number of potential sources of error. One source of error is the potential for air gaps to occur between the probe and the soil when the probe is installed, which can result in significant underestimation of the K_a of the soil (Sorta et al. 2013, Topp and Davis 1985). Air gaps may also develop after installation due to shrinkage and swelling (Topp and Davis 1985).

Herkelrath et al. (1991) investigated the influence of cable length on the TDR signal. This study showed that long cables (greater than 27 m) result in signal attenuation making the measurement impractical. Long cables tend to smooth, spread, and attenuate the waveform, which may make it difficult to identify different reflections. It should be noted that the upper limit of the cable length depends on the soil type as the soil disperses and attenuates the waveform.

Flerchinger et al. (2006) conducted a study to investigate the applicability of deducing the SWCC from the SFCC. The results showed two major issues, as follows:

- The influence of solutes is more critical at higher water contents. This is due to the impact on the osmotic potential, which becomes a larger component of the total water potential when the soil is relatively wet. The osmotic potential should be determined in order to accurately predict the SWCC, especially for soils that are high in solutes.
- The accuracy of temperature measurements is more critical at higher water contents (or near saturation) as a lot of the water freezes over a small temperature range. As an example, each 0.1°C is equal to about 120 J/kg.

These results are significant with respect to oil sands tailings that are generally tested at high water contents. In this study, the samples had an upper limit of 50 percent for the water content. Additionally, Flerchinger et al. (2006) showed that the ice in the soil can influence the θ_u to a small degree as the dielectric constant of ice is greater than air. This will result in an overestimation of the θ_u if the ice content is neglected. This error was greater at lower liquid water contents and increased as the ice content increased.

The accuracy of TDR with saline soils is impacted by the combined effect of pore water salinity, water content, temperature, and the cable length (Patterson and Smith 1985, Patterson and Smith 1983). The impact of the transmission length has previously been discussed. The salinity and temperature can also impact the TDR measurement as they can result in signal attenuation making it difficult to distinguish the reflection points (Patterson and Smith 1985). Signal attenuation increases as the temperature increases and as the salinity due to the conductive pore water (Patterson and Smith 1985, Patterson and Smith 1983). As discussed in Section 2.6.2, the dielectric constant consists of a real component and an imaginary component. Generally, the imaginary component is assumed to be negligible; however, salinity can impact the bulk electrical conductivity (EC_a), which affects the imaginary part of the dielectric constant and the resulting K_a (Bouksila et al. 2008). The study conducted by Bouksila et al. (2008) showed that TDR became unrealistic at EC_a values above 11 dS m^{-1}. Patterson and Smith (1985) conducted an investigation to determine if salinity impacted the estimate of θ_u using TDR by comparing the results with prediction by dilatometer. The pore water salinities ranged from 5 g NaCl/L to 35 g NaCl/L. Overall, the study showed that high pore water salinity does not seem to significantly affect the θ_u estimates obtained by TDR. In general, the two methods were normally distributed, but the TDR values tended to be slightly higher than the dilatometer values. Additionally, there was more scatter of the data at water contents that were greater than 30 percent. It should be noted that this investigation utilized Topp et al.'s (1980) equation to determine the θ_u from the K_a.

2.7 Implications for the Current Research

As discussed in Sections 2.6.6 and 2.6.7, there are issues associated with using TDR to measure the SFCC that are primarily related to estimating the unfrozen water content from the apparent dielectric constant. There are different methods for estimating the unfrozen water content from the apparent dielectric constant, including:

- Conduct a soil specific empirical correlation using TDR and a secondary method under freezing conditions;
- Conduct a soil specific empirical correlation on an unfrozen soil and apply the calibration to a frozen soil;

- Use a dielectric mixing model; and,
- Use an existing calibration.

For the purposes of this research, a soil specific empirical correlation on an unfrozen soil will be performed and applied to the frozen soil. This will be combined with existing calibrations, including Topp et al. (1980) and Smith and Tice (1988). A substantial amount of research suggests that that $\theta_u - K_a$ calibrations developed for unfrozen soils should not be applied to frozen or partially frozen soils (Flerchinger et al. 2006, Seyfried and Murdock 1996, Spaans and Baker 1995, Watanabe and Wake 2009, Zhou et al. 2014). However, the majority of this body of research was conducted on unsaturated natural soils, many of which were tested in situ where the total water content is unknown. The mine waste tailings that will be tested for this research will be fully saturated. Additionally, a number of authors have shown that calibrations developed for unfrozen saturated soils have been used on frozen soils with success including Patterson and Smith (1981) and Azmatch et al. (2012a, 2012b).

Furthermore, the purpose of this research is to provide a simple alternative to conducting a time-consuming, challenging SWCC test. As a result, it would be ideal to avoid the use of a secondary method for calibration as this adds a substantial amount of time and requires a secondary instrument. A dielectric mixing model would require the volumetric component of each phase to be known, including the ice content and the amount of adsorbed unfrozen water versus free unfrozen water. As a result, a soil specific empirical correlation on an unfrozen soil will be performed and applied to the frozen soil.

The literature review suggests that there may be issues with estimating the SWCC from the SFCC in saline soils due to the depression of the freezing point. As will be presented in subsequent sections, the solute concentrations in the mine waste samples to be tested are lower than the results presented by Azmatch et al. (2012a) and Ma et al. (2015a). As a result, salinity is expected to have a minimal impact on estimating the SWCC from the SFCC for the mine waste tailings. It is expected that some issues may arise due to the increased SSA of high clay content materials based on the research presented by Smith and Tice (1988) and Watanabe and Wake (2009).

The laboratory program took place in two stages. In both stages, SFCC testing was performed and used to estimate the SWCC. The estimated SWCCs were then compared to SWCCs measured using traditional laboratory methods. The first stage involved determining the SFCC of Devon silt and comparing the results to those presented by Azmatch et al. (2012a, 2012b). The purpose of this phase was to develop and validate the experimental methodology and apparatus. The experimental results from the first stage off testing and the development of the experimental methodology are provided in Section 3. The experimental results from the second stage of testing are provided in Section 4. A comparison between the estimated and measured SWCCs is provided in Section 5. The experimental results are discussed in Section 6, and conclusions and recommendations for future research are provided in Section 7.

3 Laboratory Methods

3.1 General

This chapter describes the laboratory methods used for the research program and the development of the methodology for the SFCC testing. The research program involved testing Devon silt, copper tailings, gold tailings, and oil sands centrifuge cake.

3.2 Index Testing

The following index tests were performed on the tested soils where relevant to help classify the material behavior:

- Water content determination;
- Atterberg limits testing;
- Specific gravity testing; and,
- Grain size distribution (GSD).

The water content of each soil was determined according to ASTM D2216-10 where the sample was weighed and oven dried at 110°C for 24 hours. The Atterberg limits (liquid limit and plastic limit) were determined according to ASTM D4318-10. Specific gravity was determined according to ASTM D854-14 using vacuum deairing. An example of a specific gravity test is shown in Figure 3-1. The specific gravity of a soil is needed to determine the density of the solids and is needed for shrinkage testing and SWCC testing.

The grain size distribution was determined according to ASTM D422-63 and involved a combination of sieving and a sedimentation process using a hydrometer. An example of the hydrometer portion of the grain size distribution test on Devon silt is shown in Figure 3-2. The grain size distribution test is used to characterize the gradation of the sample for correlation to other soil parameters.

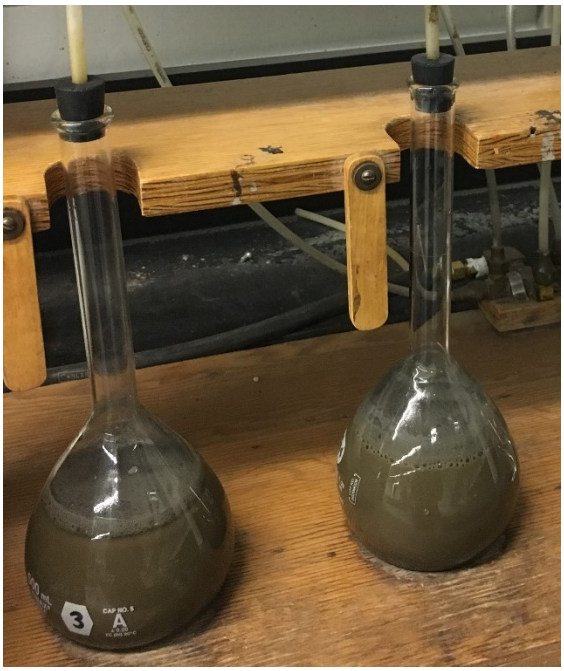

Figure 3-1: Specific Gravity Test on Gold Tailings

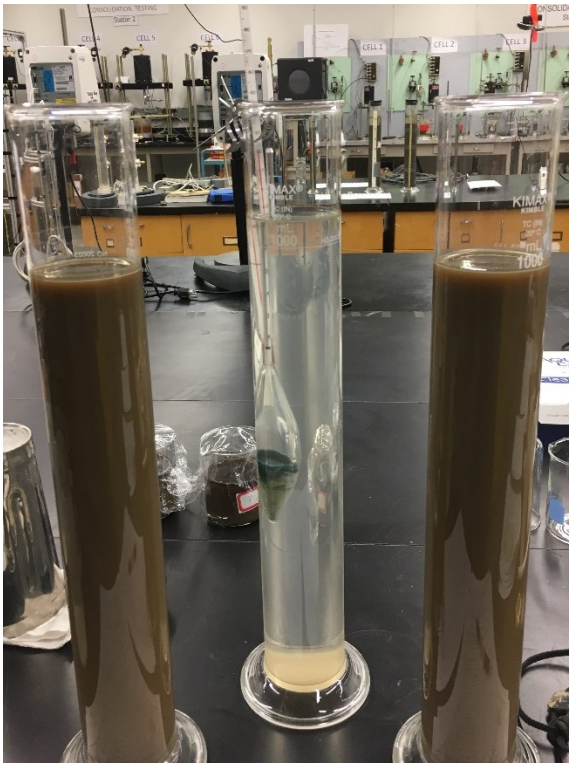

Figure 3-2: Hydrometer Test on Devon Silt

3.3 Unsaturated Soil Properties

Traditional SWCC tests were conducted on the soils for comparison to the SWCCs estimated from the SFCC. The SWCCs were conducted in accordance with ASTM D6836 using Method A, Method C, and Method D. Small pressure cells were used to measure the SWCC points from saturated conditions to a suction of 400 kPa. Method A (hanging water column) was used for suctions less than 5 kPa in small pressure cells. Method C was used for suctions from 5 kPa to 400 kPa. An example of a single-specimen pressure plate is shown in Figure 3-3. Method D was used for suctions greater than 2000 kPa using a chilled mirror hygrometer. It should be noted that Method A and Method C yield matric suction while Method D yields total suction.

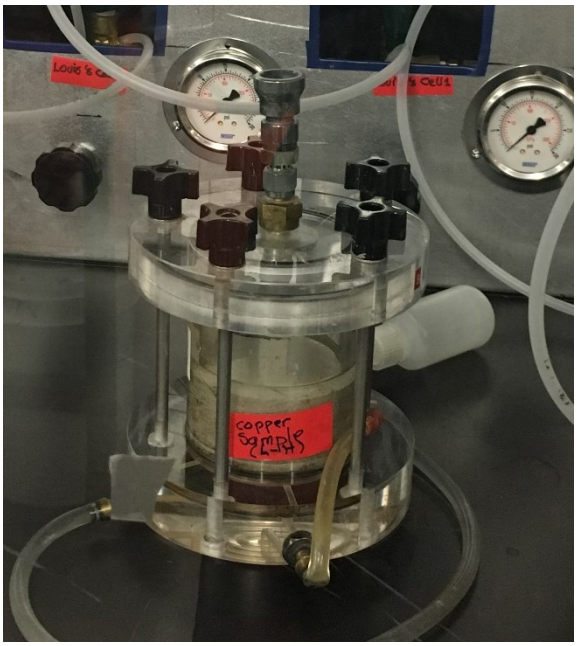

Figure 3-3: SWCC Measurement in Low Suction Range Using Single-Specimen Pressure Plate for Copper Tailings

Shrinkage testing was also conducted to measure the relationship between the void ratio and gravimetric water content of a soil during drying. The shrinkage testing methodology is described by Zhang (2016) and Fredlund et al. (2011). The results from the shrinkage testing was used to interpret the results from the SWCC testing for high volume change materials. It should be noted that all of the shrinkage testing and the majority of the SWCC testing was conducted by third parties. This has been noted where relevant.

3.4 Solids Mineralogy and Pore Water Chemistry

The laboratory testing for the solids mineralogy and the pore water chemistry was completed by AGAT Laboratories Ltd. They followed standard ASTM and accepted lab practices to conduct XRD, chemical speciation analyses, and methylene blue index testing.

3.5 TDR Calibration

A soil specific TDR calibration was conducted for the copper tailings, gold tailings, and the centrifuge cake on unfrozen material. The calibration procedure consisted of preparing samples to different gravimetric water contents and measuring the K_a of the mixture by fully inserting the TDR probe into the center of the sample. The samples were brought to a temperature of 1°C to minimize the temperature dependency of the TDR calibration noted by Sorta et al. (2013).

Approximately seven to eight samples of gold and copper tailings were mixed to different gravimetric water contents that ranged from approximately 15 percent to 95 percent using distilled water. Samples were not mixed to gravimetric water contents less than 15 percent as it was difficult to create a homogeneous mix and place the samples into a container without significant air voids due to the low water content.

The as received solids content of the centrifuge cake was approximately 52 percent (gravimetric water content of 92 percent). Eight samples of centrifuge cake were mixed to a gravimetric water content from approximately 100 percent to 450 percent (solids content of about 50 percent to 18 percent). Four samples of the centrifuge cake were air-dried to gravimetric water contents of approximately 35 percent to 70 percent (solids content of about 74 percent to 59 percent) and then mixed prior to testing. It was very difficult to ensure these samples were dried homogeneously. As a result, the reliability of these points is unknown.

For each sample, 10 TDR measurements were taken to ensure that the TDR reading was repeatable and reliable. The average standard deviation of all of the measurements was approximately 0.04. It should be noted that the TDR yields a L_a/L measurement. The K_a is then calculated using Equation 2-28. The TDR readings were averaged to determine the correlation

between the K_a and the volumetric water content. The TDR probes used in this experiment had three rods with a free length of 75 mm. The rods have a diameter of 1.6 mm with a spacing of 8 mm. This fulfills the Knight (1992) recommendation discussed in Section 2.6.3, which includes:

- The ratio of the radius of the rods to the spacing should be greater than 0.1; and,
- The radius of the rod should be as large as possible compared to the average pore size of the material.

The container used for the calibration was a PVC cylinder with a height of approximately 151 mm and a diameter of about 77 mm. According to Topp and Davis (1985), a cylinder of soil with a diameter that is 1.4 times the spacing between the rods is sampled by the TDR probe. According to Baker and Lascano (1989), the area just beyond the tip of the rods does not affect the TDR readings. The container used in this calibration was much greater than the zone of influence with a diameter that was about 9.5 times the spacing of the rods and a height that was approximately double the length of the rods. The probes were inserted into the middle of the sample to limit the impact of boundary effects. The probes were also inserted to minimize the introduction of air gaps between the soil and the probe. An example of a TDR calibration test is shown in Figure 3-4.

Figure 3-4: Example of a TDR calibration test

3.6 Soil Freezing Characteristic Curve Testing

The experimental methodology and apparatus was developed and validated by determining the SFCC for Devon silt and comparing the results to those presented by Azmatch et al. (2012a, 2012b). The testing performed by Azmatch et al. (2012a, 2012b) is detailed in Appendix 1: Development of SFCC Methodology. SFCC testing was then performed on Devon silt and compared to the results from Azmatch et al. (2012a, 2012b) to validate the experimental apparatus and methodology. The validation of the experimental method is discussed in Appendix 1: Development of SFCC Methodology. The finalized experimental method is presented in Section 3.6.1. The results from the testing on the Devon silt are presented in Section 3.6.2

3.6.1 Experimental Method

Testing on Devon silt aided in the development of the experimental apparatus and methodology. Following the completion of the testing of the Devon silt, the experimental method was finalized and extended to apply to slurries by the introduction of a container. The experimental apparatus consists of a temperature control bath that circulates glycol into an insulated box. The glycol is then circulated around the sample using brass coils. The sample sits on an elevated platform to promote isotropic freezing. One RTD probe and one TDR probe are inserted into the sample at marked locations to measure the temperature and the dielectric constant of the soil, respectively. The probes are stabilized using a clamping system. Two additional RTD probes are placed in the insulated box to monitor the ambient air temperature. A fan is placed in the corner of the box to circulate air. The entire apparatus is placed in a temperature controlled room to limit the impacts of room temperature fluctuations on the testing. A schematic of the apparatus is shown in Figure 3-5. The freezing cell is shown in Figure 3-6 and an example of a test set-up inside the cell is shown in Figure 3-7.

The experimental method is as follows:

1. Prepare sample. This may include mixing the sample with process water or distilled water from a dry state to a non-segregating slurry and allowing to sit for 24 hours.

2. The diameter, length, and mass of the container are recorded and gravimetric water content measurements are made.
3. The sample is transferred into a container with a diameter of approximately 99 mm and a height of approximately 111 mm. Care should be taken to limit the introduction of air voids. The combined mass of the sample and the container are determined.
4. The top of the sample is marked to determine the locations that the RTD and TDR should be inserted to ensure that they are equidistant from the edges. The TDR and RTD are inserted at a distance of 30 mm from the outer edge of the container. The purpose of this is to prevent interference between the probes and encourage simultaneous freezing of the soil adjacent to the two probes for accurate test results. The RTD is considered accurate to the nearest 0.01°C. The error associated with TDR measurements is dependent on a variety of factors, including the material, salinity, and water content. In general, TDR errors resulted in a maximum of a 2.5 percent volumetric water content spread at a given temperature. The highest errors were observed with the Devon silt which is attributed to the consolidation of the material and the potential for air voids adjacent to probes.
5. The sample is placed in the freezing cell on the platform and the RTD and TDR are inserted to the same depth, which is equivalent to the length of the TDR probe (75 mm). The inside dimensions of the insulated box are approximately 520 mm x 405 mm x 285 mm. The outside dimensions of the insulated box are approximately 725 mm x 535 mm x 470 mm.
6. The temperature of the cell is set at approximately 0°C.
7. The freezing test is initiated when the temperature in the sample reaches 0.5°C.
8. The temperature in the freezing cell is then decreased to about -2°C to initiate freezing.
9. The sample is then monitored until the temperature and the output from the TDR (K_a) in the sample stabilizes. At this point, the temperature in the freezing cell is decreased again by decreasing the temperature bath. The temperature bath is decreased in 4°C increments. It should be noted that this does not result in 4°C drops in the freezing cell. As the temperatures get lower, the efficiency of the temperature bath decreases and the temperature drops in the freezing cell and sample will decrease.

10. This process is continued until minor changes in the K_a value are observed.
11. The temperature in the cell is then increased to 0°C to initiate thawing.
12. Once thawing is complete, photographs are taken of the sample and gravimetric water content measurements are made.

To estimate the SWCC from the SFCC, the following is performed:

1. The material is assumed to be colloidal or non-colloidal and an appropriate soil dependent constant is used based on Koopmans and Miller (1966).
2. The w_u and the θ_u were assumed to be equal to the gravimetric water content and the volumetric water content during drying, respectively. This yields an estimated θ-SWCC and a w-SWCC.
3. High volume change property functions are applied (if appropriate) to attain the θ_i-SWCC and the S-SWCC based on Section 2.4.3.

With high volume change materials, it is important to develop the S-SWCC using the shrinkage curve to attain the true AEV. Due to the volume change, the suction at the first breaking point between the different SWCCs will vary and may not be representative of the AEV. For a high volume change material, the AEV must be estimated from the S-SWCC. The AEV can be estimated using the graphical method presented by Vanapalli et al. (1998).

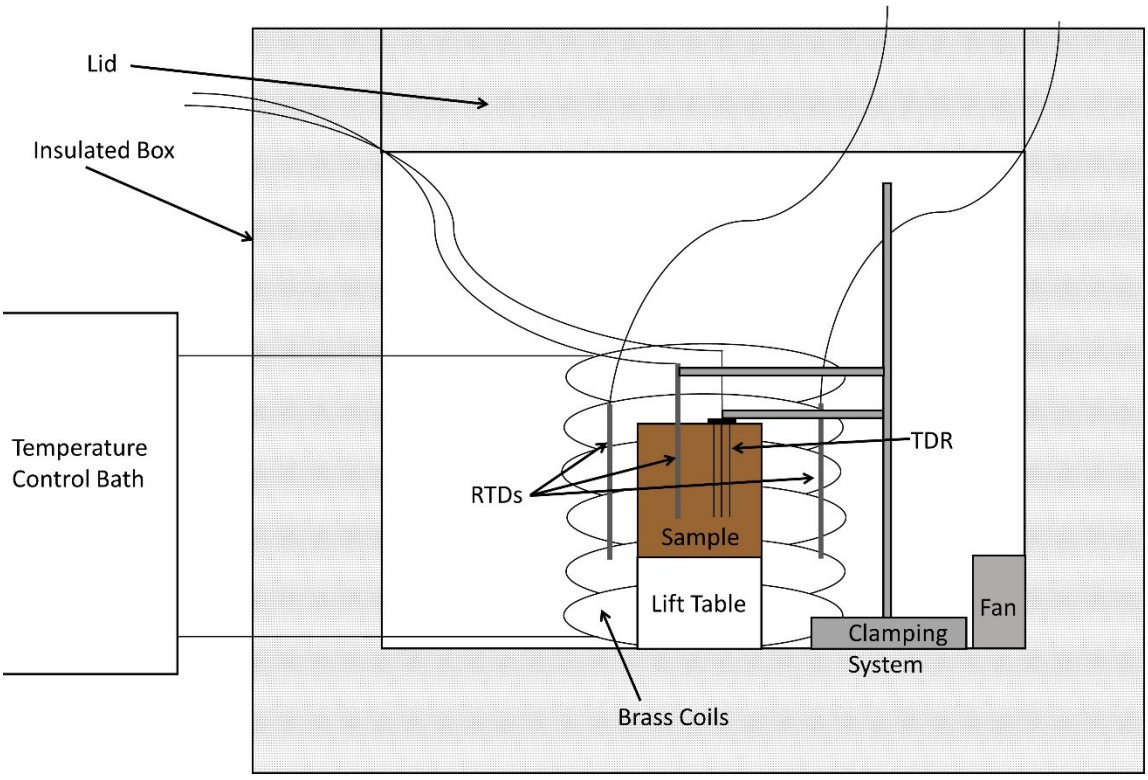

Figure 3-5: Schematic of Freezing Cell

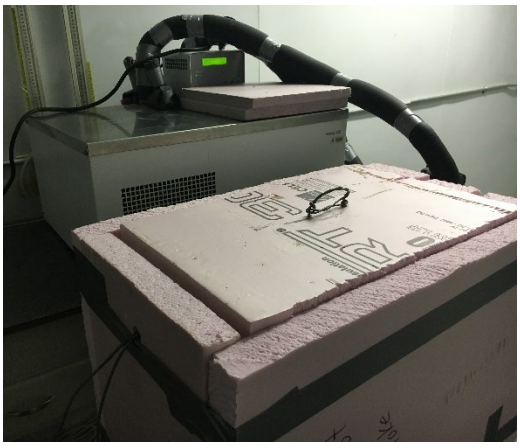

Figure 3-6: Final Freezing Cell

Figure 3-7: Example of a Test Set-up

3.6.2 Devon Silt Results

3.6.2.1 Devon Silt Index Testing

The following index tests were performed on the Devon silt to help classify the material behavior:

- Atterberg limits;
- Grain size distribution (GSD); and,
- Specific gravity testing.

The Devon silt had a liquid limit of 35 percent, a plastic limit of 20 percent, and a plasticity index of 15 percent (Zhang 2016). The GSD of the Devon silt is provided in Figure 3-8. The specific gravity of the Devon silt was 2.66.

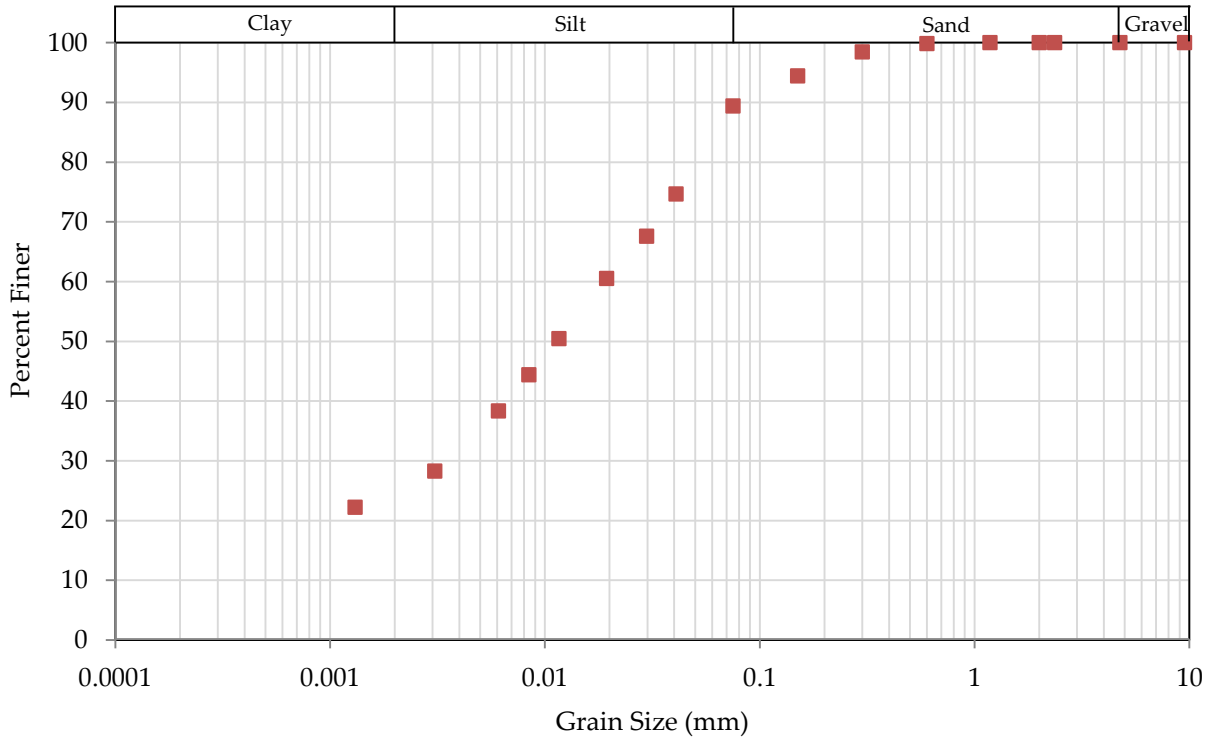

Figure 3-8: Devon Silt Grain Size Distribution

3.6.2.2 Devon Silt SWCC and Shrinkage Testing Results

Zhang (2016) conducted SWCC and shrinkage testing on Devon silt as part of her Phd thesis. Zhang (2016) noted that the Devon silt is a high volume change material. Zhang (2016) measured the SWCC for the Devon silt using single-specimen pressure plate devices up to an applied suction of 500 kPa and then a WP4-T (Water PotentiaMeter with internal temperature control) for the higher suction range. This yielded the w-SWCC as shown in Figure 3-9, which was fit with Zhang and Chen's (2005) simplified bimodal equation (Equation 2-5). The best-fitting parameters of Equation 2-5 are provided on Figure 3-9. The Devon silt shrinkage curve and the best-fitting parameters of Equation 2-6 are provided on Figure 3-10. The shrinkage curve was then used to determine the S-SWCC and the θi-SWCC from the w-SWCC as shown in Figure 3-11. The w-SWCC is also presented on Figure 3-11 for comparison purposes.

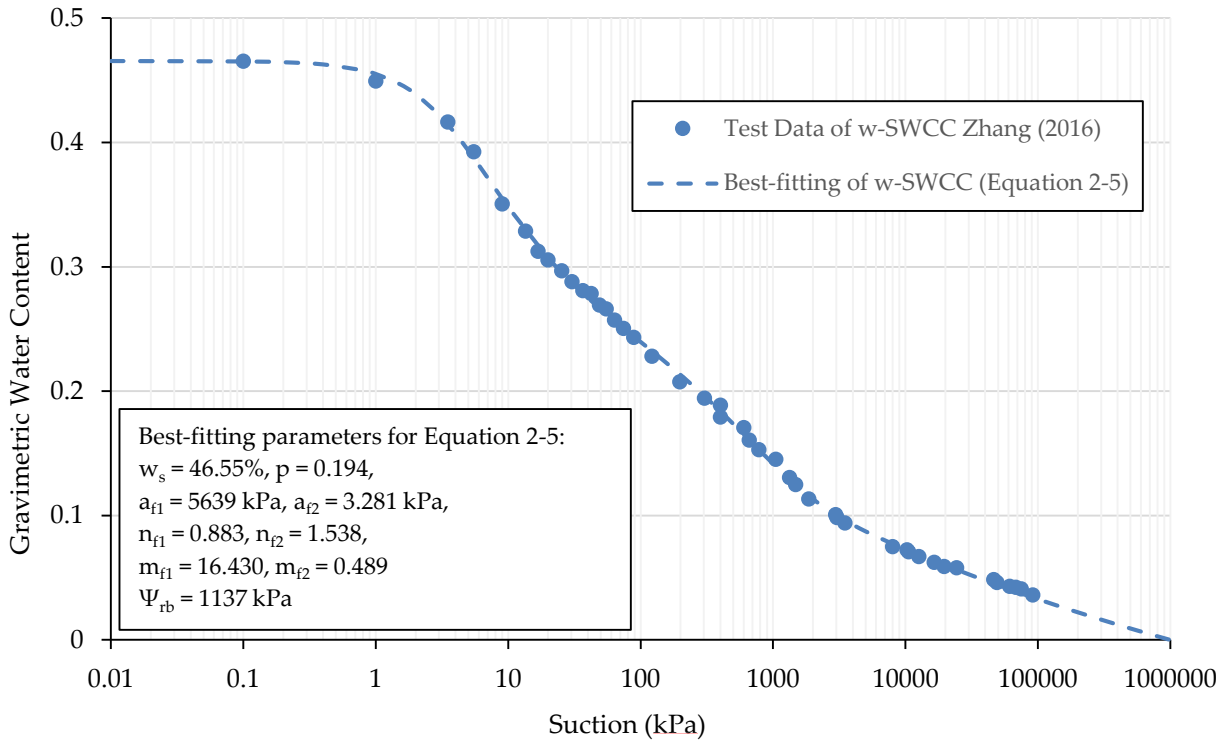

Figure 3-9: Measured w-SWCC using Traditional Methods for Devon Silt (Equation 2-5 Simplified Bimodal Zhang and Chan (2005)) (after Zhang 2016)

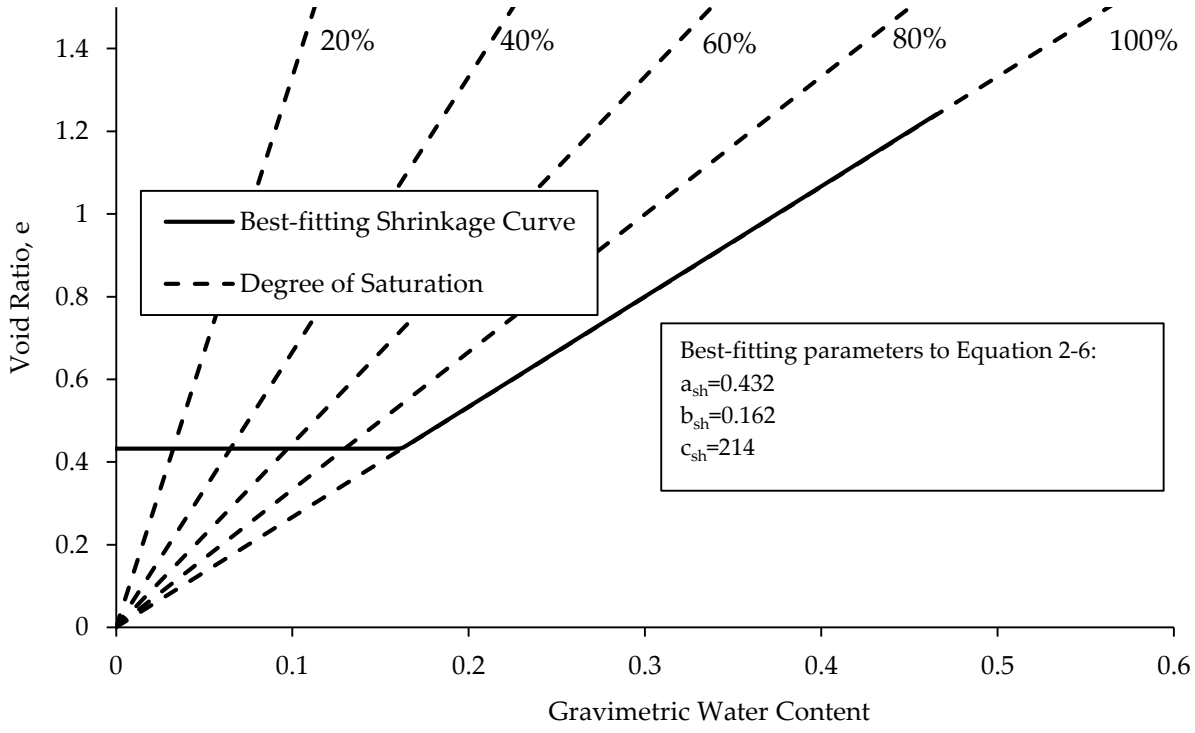

Figure 3-10: Shrinkage Curve for Devon Silt (after Zhang 2016)

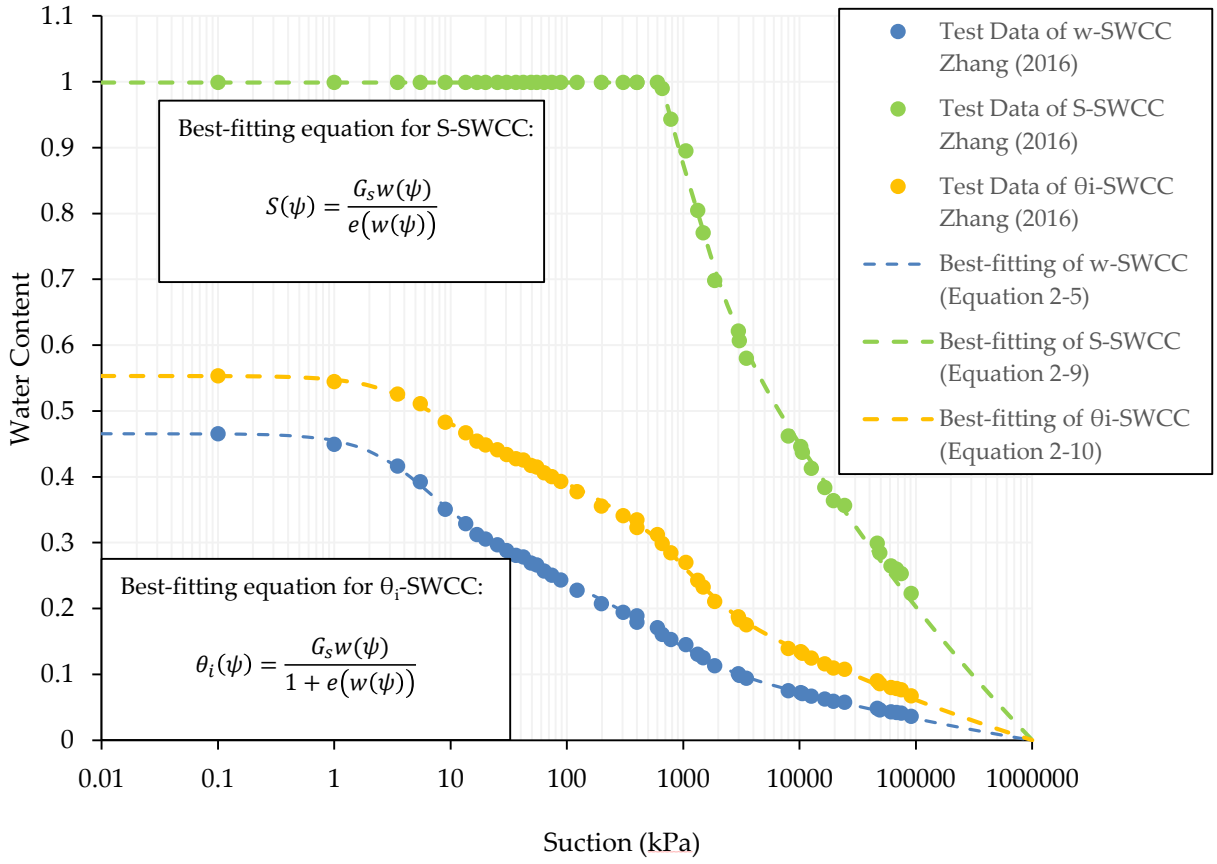

Figure 3-11: Measured SWCCs using Traditional Methods for Devon Silt (after Zhang 2016)

The suction at the first breaking point between the different SWCCs is provided in Table 3-1. As this is a high volume change material, the AEV must be estimated from the S-SWCC. Based on this, the AEV of Devon Silt is about 593 kPa.

Table 3-1: Suction at the First Breaking Point for Different SWCCs for Devon Silt

Type of SWCC	Suction at First Breaking Point (kPa)
w-SWCC	1.89
S-SWCC	593
θi-SWCC	2.35

3.6.2.3 Devon Silt SFCC Results

Six samples (DS4, DS5, DS6, DS8, DS9, and DS10) were mixed to a water content of 60 percent. The water was de-aired prior to mixing using the Nold DeAerator. The samples were hand mixed slowly to avoid the introduction of air bubbles. The samples were consolidated using a combination of self-weight consolidation, dead weights, and air pressure to a consolidation

pressure of 100 kPa, which took about a month per sample. The consolidation cells had a diameter of approximately 100 mm with a height of approximately 230 mm. The samples were extruded from the consolidation cell using a hydraulic extruder. The samples were trimmed to a height of approximately 110 mm to 120 mm with a diameter of approximately 100 mm. Water content determinations were performed on the trimmed material. The SFCC testing was performed in accordance with the method described in Section 3.6.1. The volumetric unfrozen water content (θ_u) was determined from the dielectric constant using Topp et al.'s (1980) equation in accordance with the procedure followed by Azmatch et al. (2012a, 2012b). The suction was calculated using Konrad's (1994) relationship in the same manner as Azmatch et al. (2012a, 2012b). The Clapeyron Equation (Equation 2-16) was also used to determine the suction and yielded very similar results to the method used by Azmatch et al. (2012a, 2012b). The presented results for Devon silt use Konrad's (1994) relationship for comparison. The gravimetric unfrozen water content (w_u) was computed using Equation 2-3. To estimate the SWCC from the SFCC, the Devon silt was assumed to be colloidal and a soil dependent constant of about 1.0 was used to estimate the SWCC from the SFCC based on Koopmans and Miller (1966).

The remainder of this section provides estimated θ-SWCCs assuming no volume change. The estimated θ-SWCCs and the associated Fredlund and Xing (1994) (Equation 2-4) fits for the six samples are provided in Figure 3-12 to Figure 3-17. The best-fitting parameters of Equation 2-4 for the six samples are provided in Table 3-2. Samples DS5, DS6, and DS8 also exhibited a supercooling behaviour, which is undesirable and difficult to avoid during freezing. The supercooling behaviour of Sample DS6 is shown in Figure 3-18. The zones of supercooling have been indicated on Figure 3-13, Figure 3-14, and Figure 3-15. These zones represent areas of a drop in temperature below the freezing point without an associated phase change as shown in Figure 3-18. As a result, the suctions calculated for these temperatures are not representative of the actual suction in the sample and have been termed "pseudo-suctions".

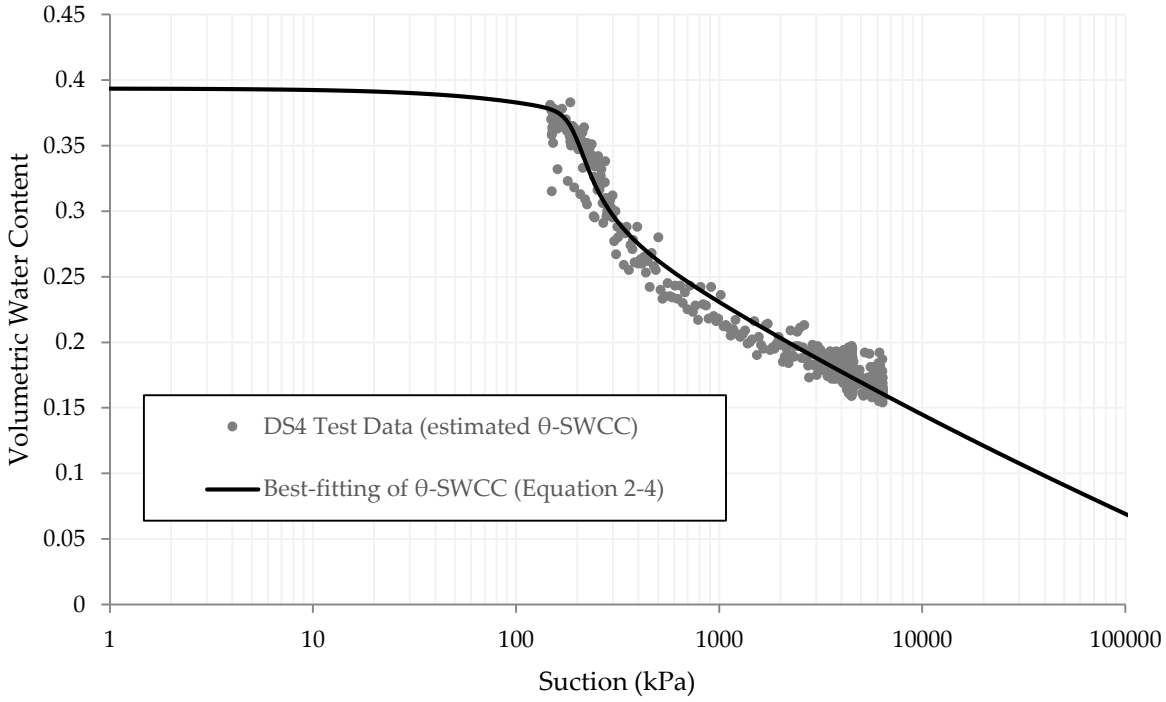

Figure 3-12: Sample DS4 Estimated θ-SWCC from the SFCC and Fredlund and Xing (1994) Fit (Equation 2-4)

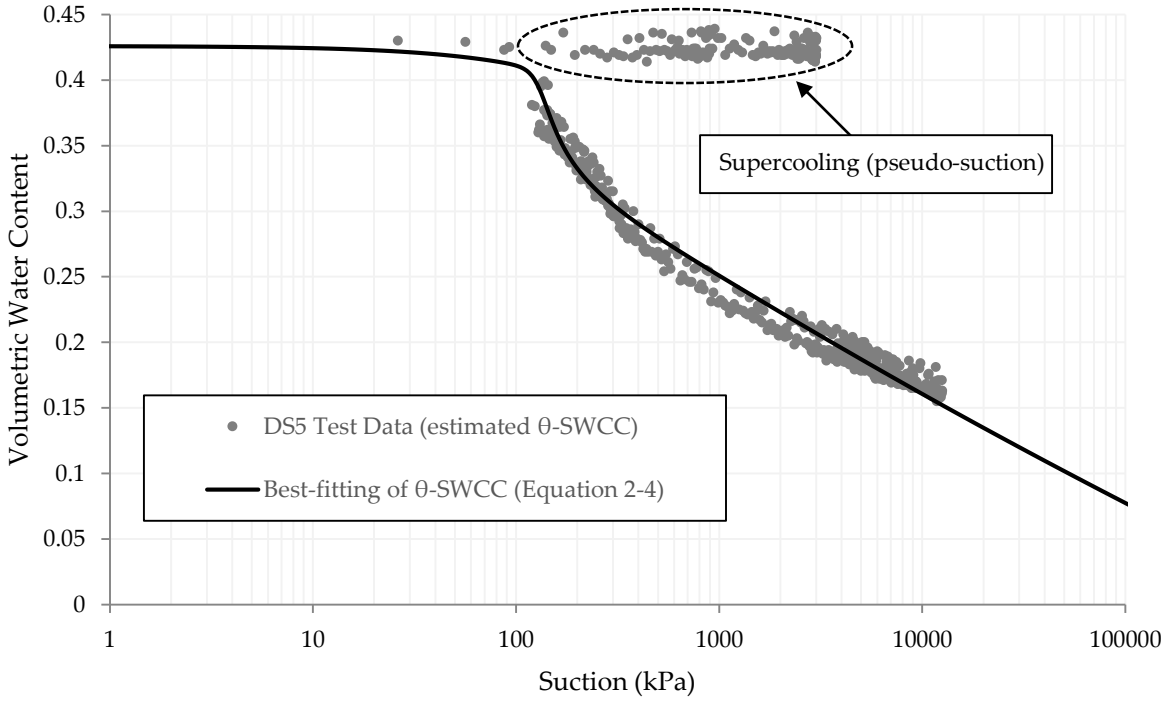

Figure 3-13: Sample DS5 Estimated θ-SWCC from the SFCC and Fredlund and Xing (1994) Fit (Equation 2-4)

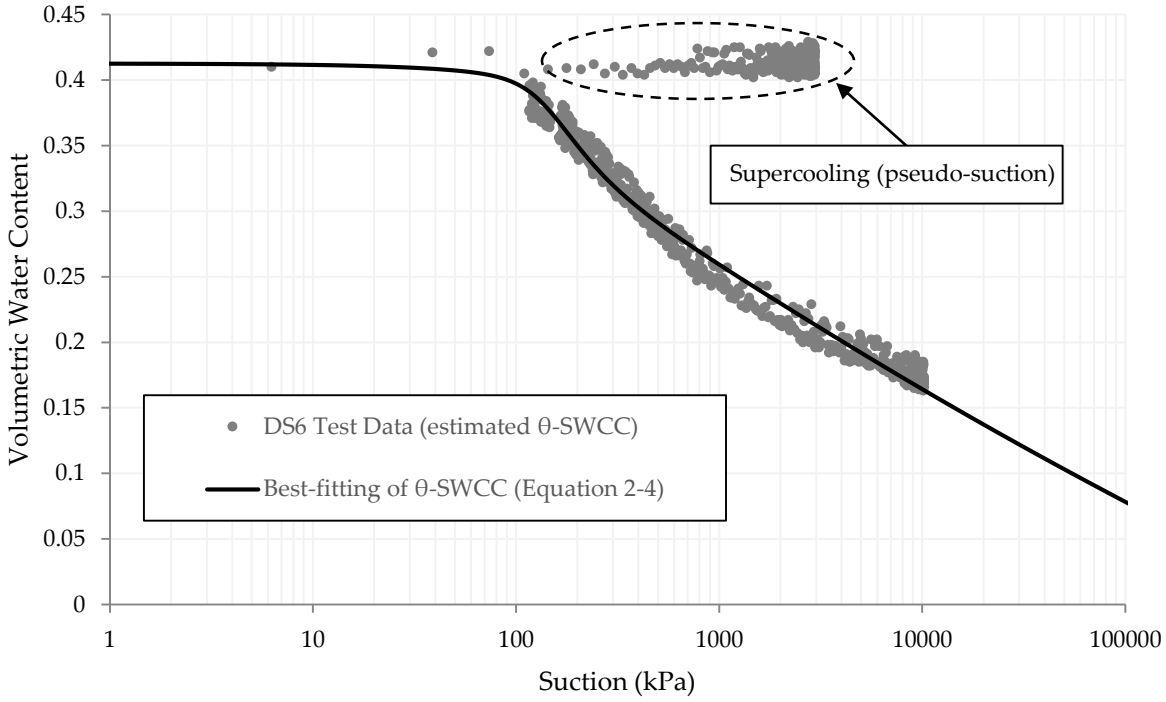

Figure 3-14: Sample DS6 Estimated θ-SWCC from the SFCC and Fredlund and Xing (1994) Fit (Equation 2-4)

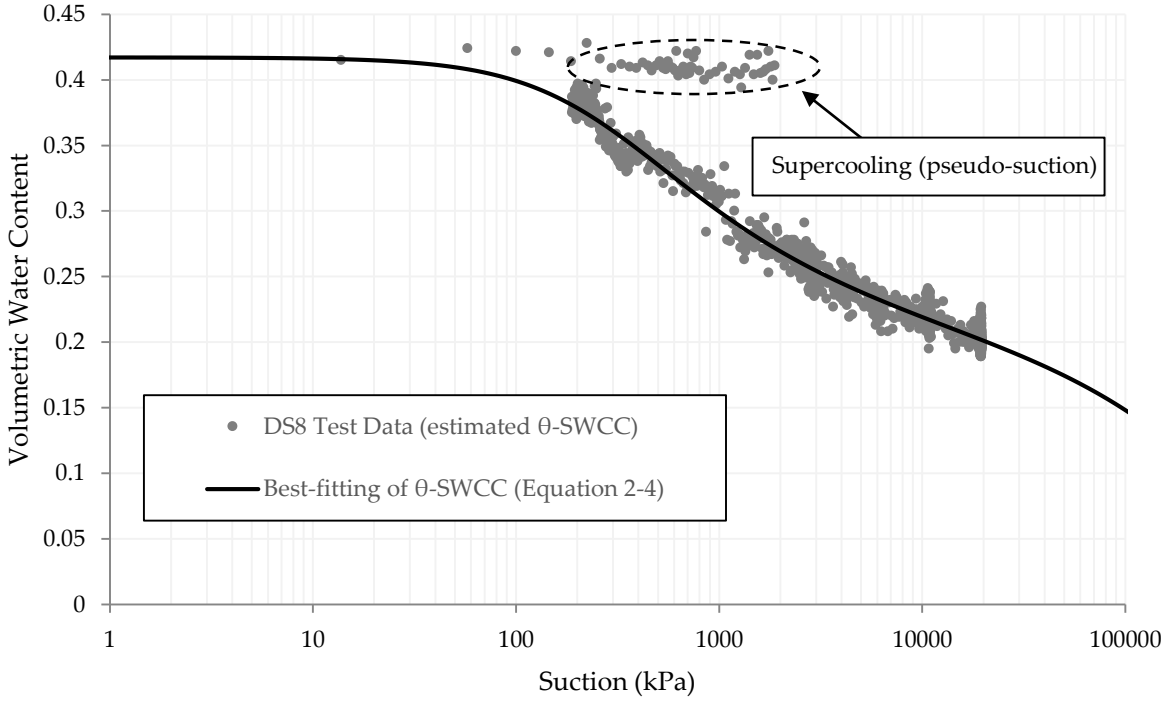

Figure 3-15: Sample DS8 Estimated θ-SWCC from the SFCC and Fredlund and Xing (1994) Fit (Equation 2-4)

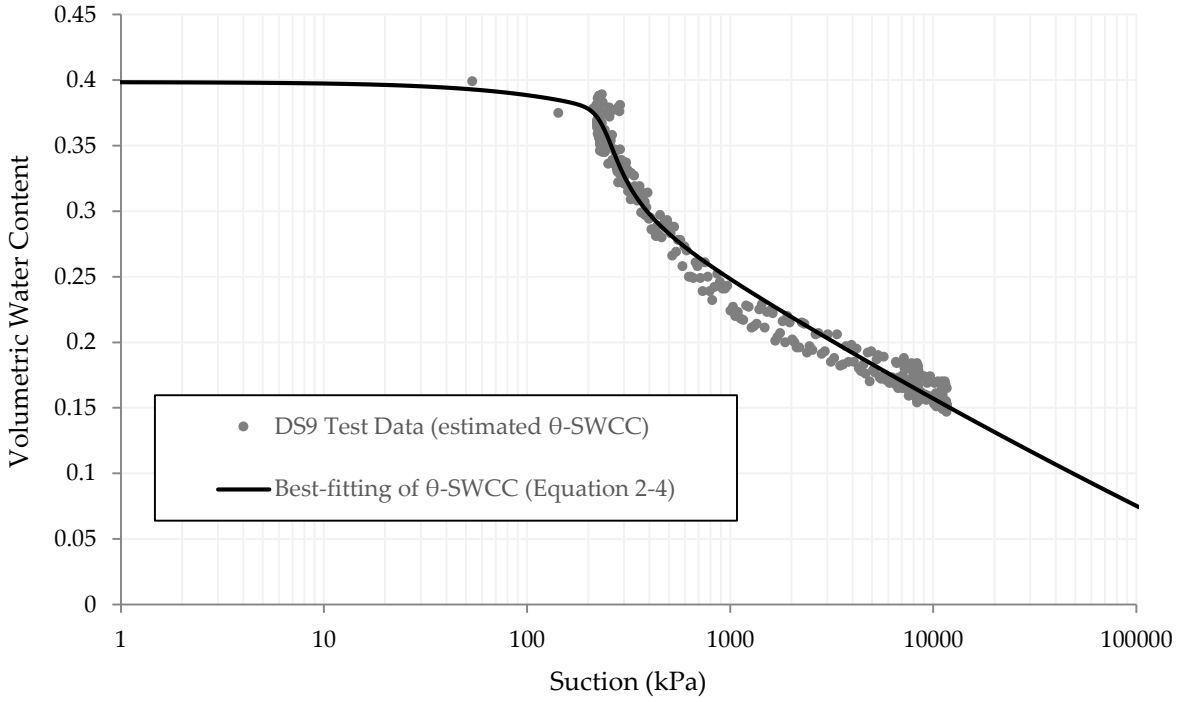

Figure 3-16: Sample DS9 Estimated θ-SWCC from the SFCC and Fredlund and Xing (1994) Fit (Equation 2-4)

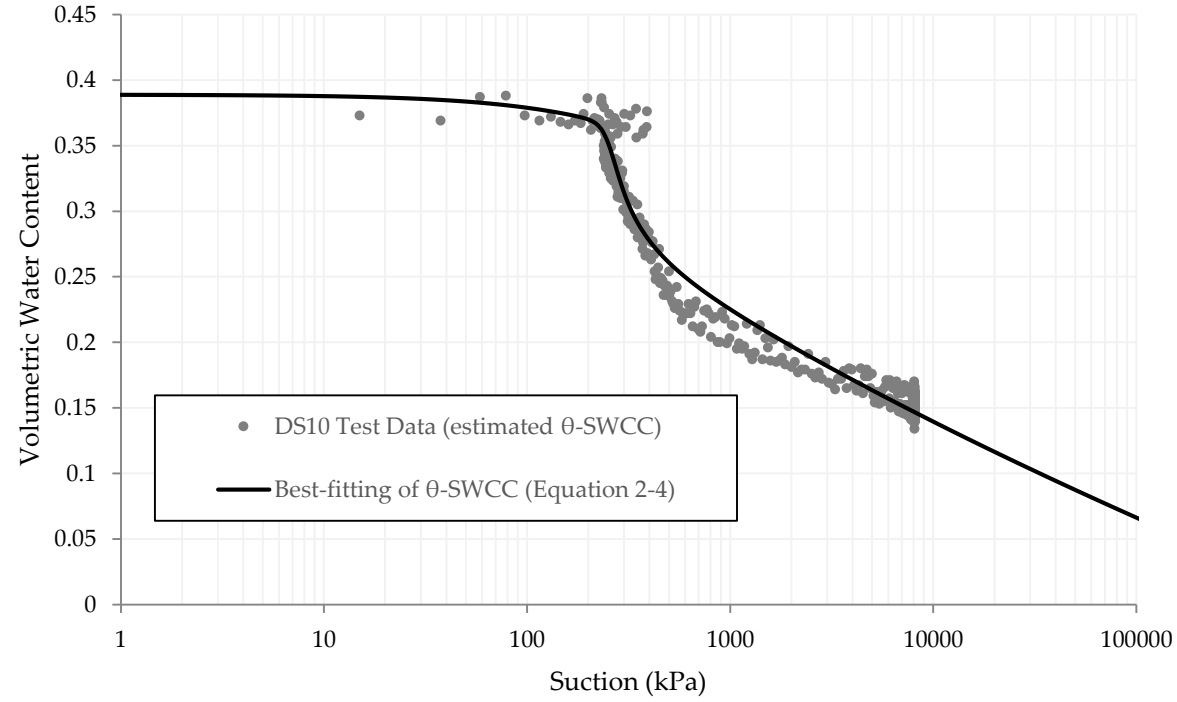

Figure 3-17: Sample DS10 Estimated θ-SWCC from the SFCC and Fredlund and Xing (1994) Fit (Equation 2-4)

Table 3-2: Best-fitting Parameters for Equation 2-4 for Devon Silt

Sample	a_f (kPa)	n_f	m_f	ψ_r (kPa)	w_z
DS4	187.677	12.328	0.1207	427.93	0.245
DS5	126.314	13.819	0.1004	322.09	0.28
DS6	127.707	4.725	0.1368	515.57	0.265
DS8	207.141	1.383	0.367	217390	0.27
DS9	224.395	12.904	0.1063	474.39	0.25
DS10	246.244	15.858	0.124	458.33	0.24

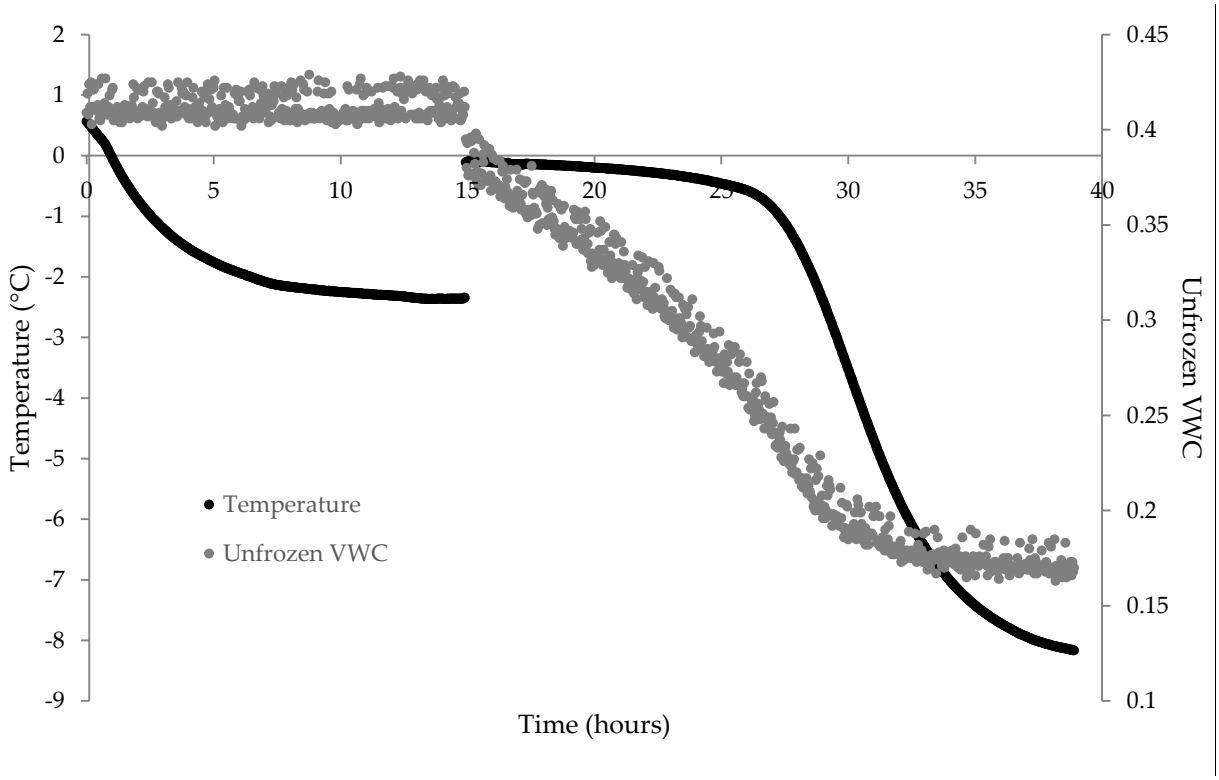

Figure 3-18: Supercooling in Sample DS6

After the completion of the freezing test in samples DS4 and DS5, the TDR probe was removed and replaced with a second RTD probe. The samples were then frozen again and the temperature was monitored at the two different locations to ensure that freezing was occurring at the same rate at the two different locations. The result of the test performed on DS4 is provided in Figure 3-19. The results from these tests indicated that the two locations are freezing simultaneously.

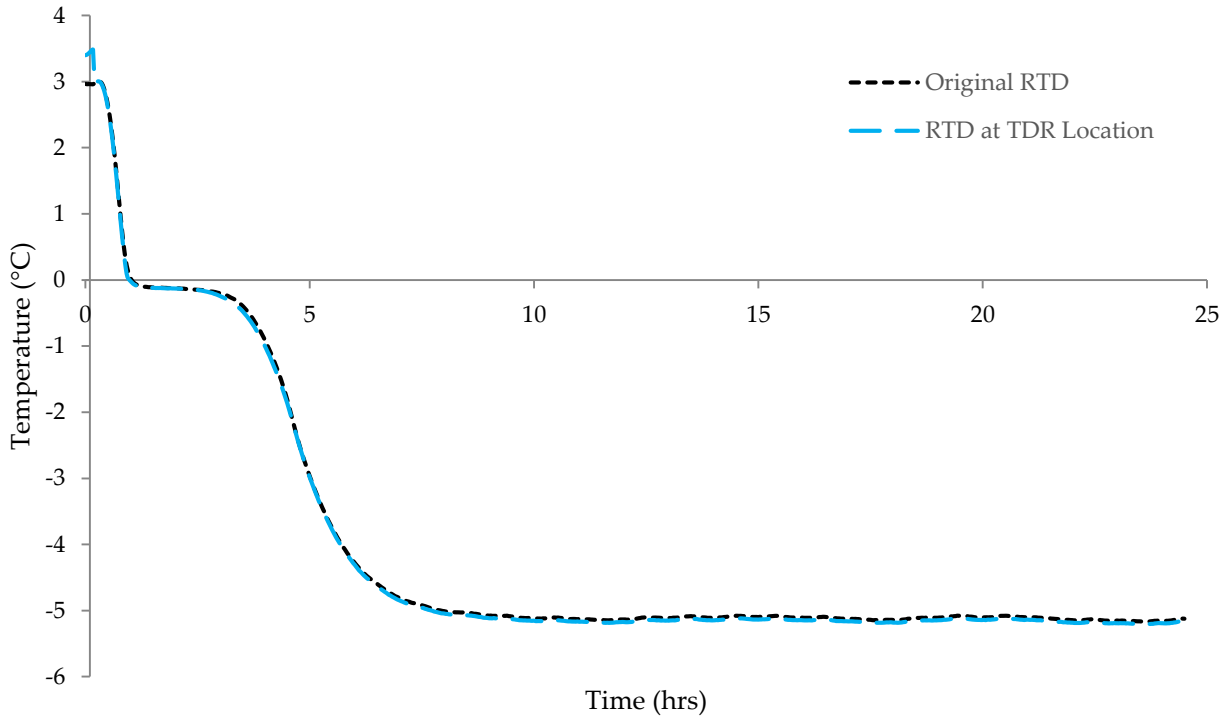

Figure 3-19: RTD Probe Test in Sample DS4

3.6.2.4 Comparison Between the Estimated and Measured SWCC

Of the six tests performed, five showed good agreement with the Fredlund and Xing (1994) fit from Azmatch et al. (2012a) as shown in Figure 3-20. For clarity, the raw test data has not been presented on this figure. Sample DS8 did not show good agreement, which is thought to be a result of segregation prior to the start of consolidation resulting in a different grain size distribution throughout the sample height.

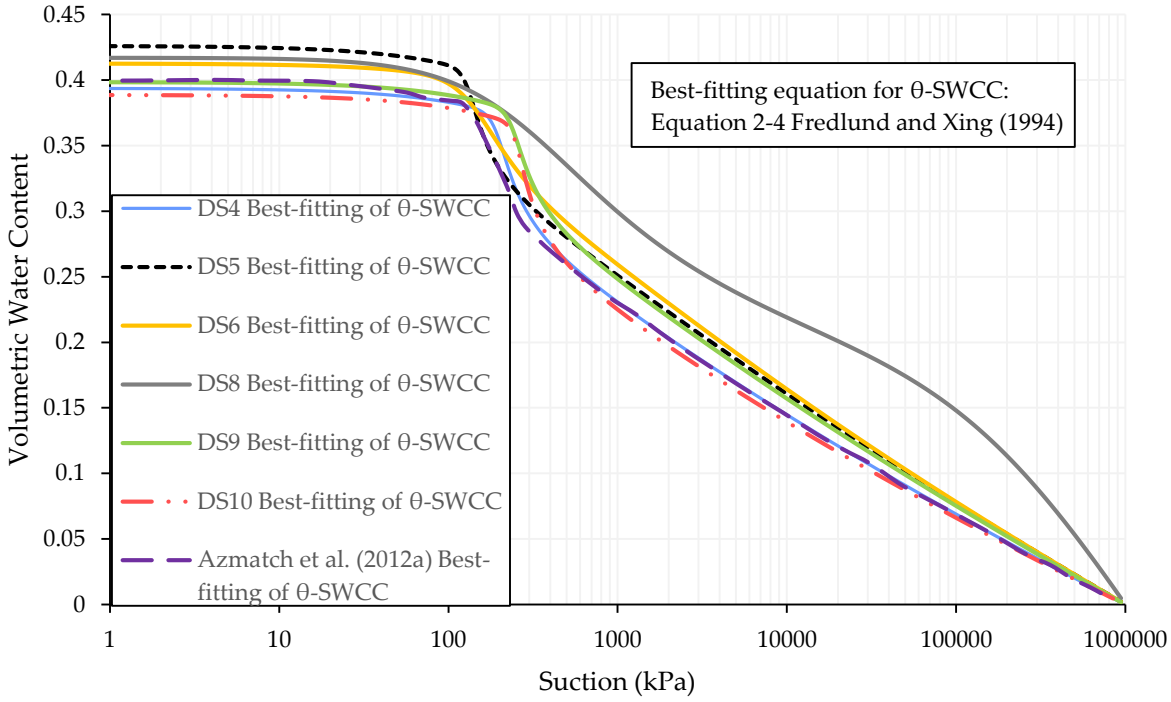

Figure 3-20: Comparison of Estimated θ-SWCC from the SFCC Fredlund and Xing (1994) Fits to Azmatch et al. (2012a)

A comparison between the SWCCs estimated from the SFCC and the SWCCs determined by Zhang (2016) are provided in Figure 3-21 to Figure 3-23. High volume change property functions were used to attain the θi-SWCC and the S-SWCC. For simplicity, only the best-fitting curves are provided. The gravimetric best-fitting curve fits were attained using Equation 2-5 to compare to Zhang (2016). The θ_i-SWCC best-fitting curves were attained using Equation 2-10. The S-SWCC best fitting curves were attained using Equation 2-9. The best-fitting parameters for Equation 2-5 are provided in Table 3-3. The AEV for the different samples estimated from the S-SWCC are provided in Table 3-4. The AEV was estimated using the graphical method presented by Vanapalli et al. (1998).

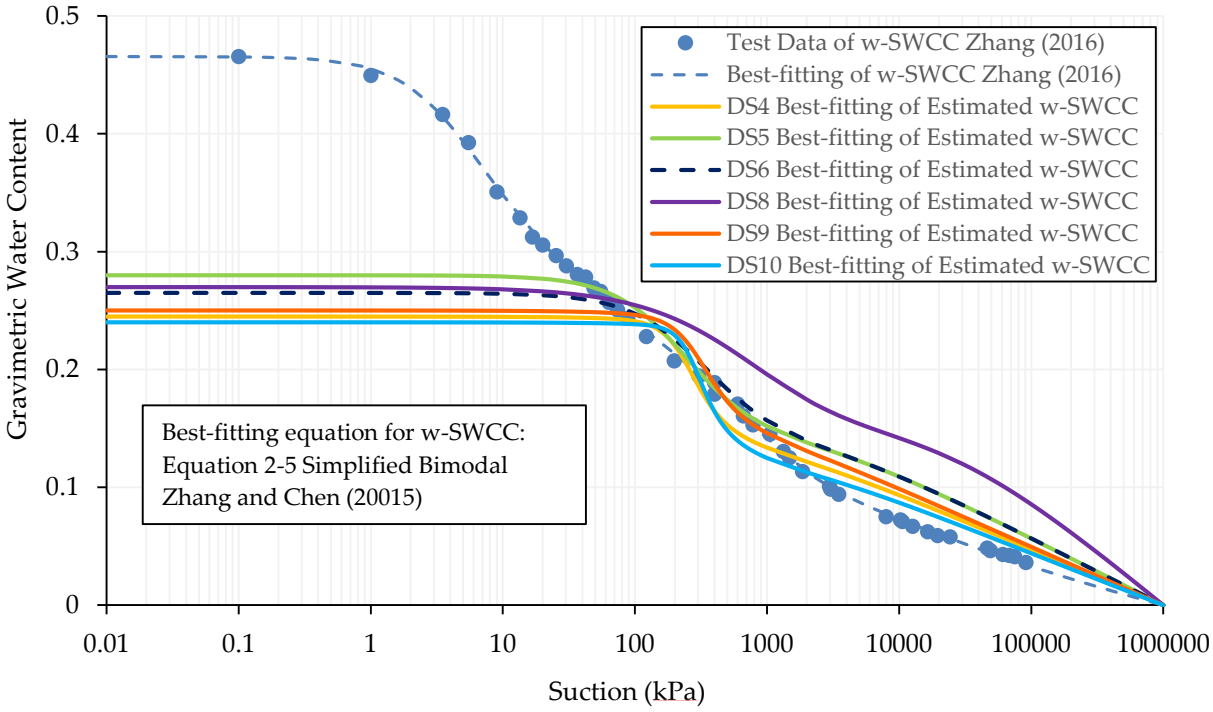

Figure 3-21: Comparison Between w-SWCC Estimated from SFCC and w-SWCC Determined using Traditional Methods (Equation 2-5 Simplified Bimodal Zhang and Chen (2005))

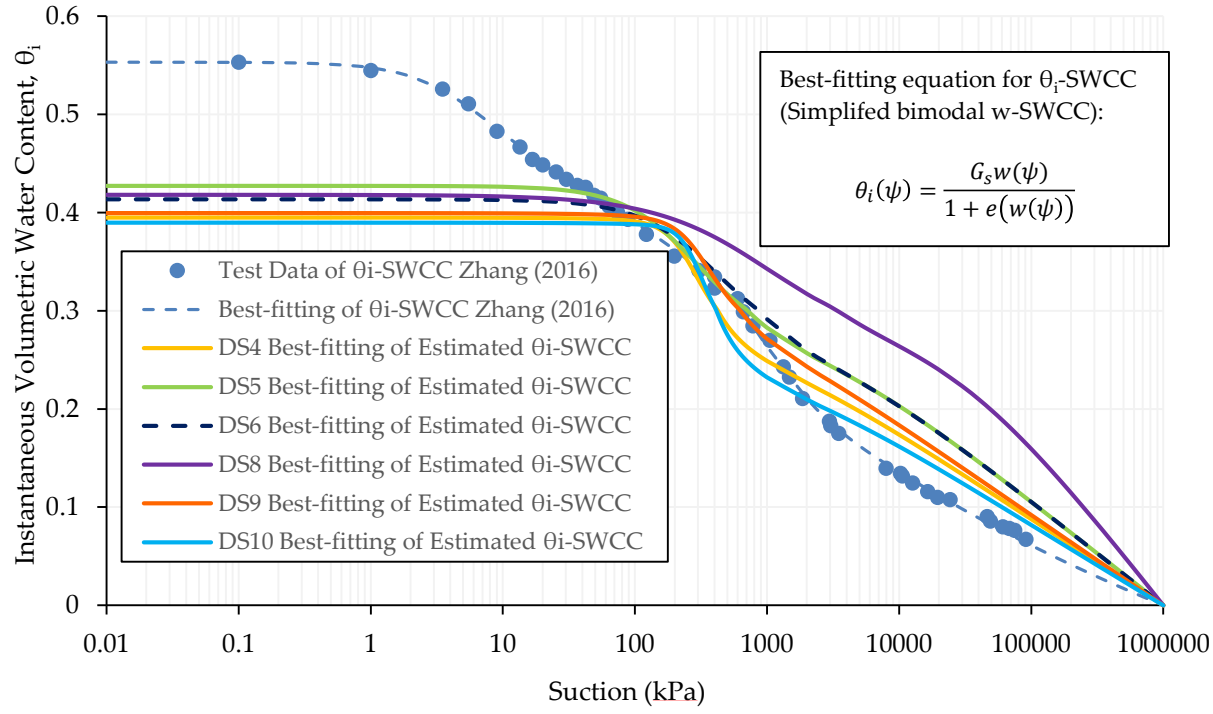

Figure 3-22: Comparison Between θi-SWCC Estimated from SFCC and θi-SWCC Determined using Traditional Methods

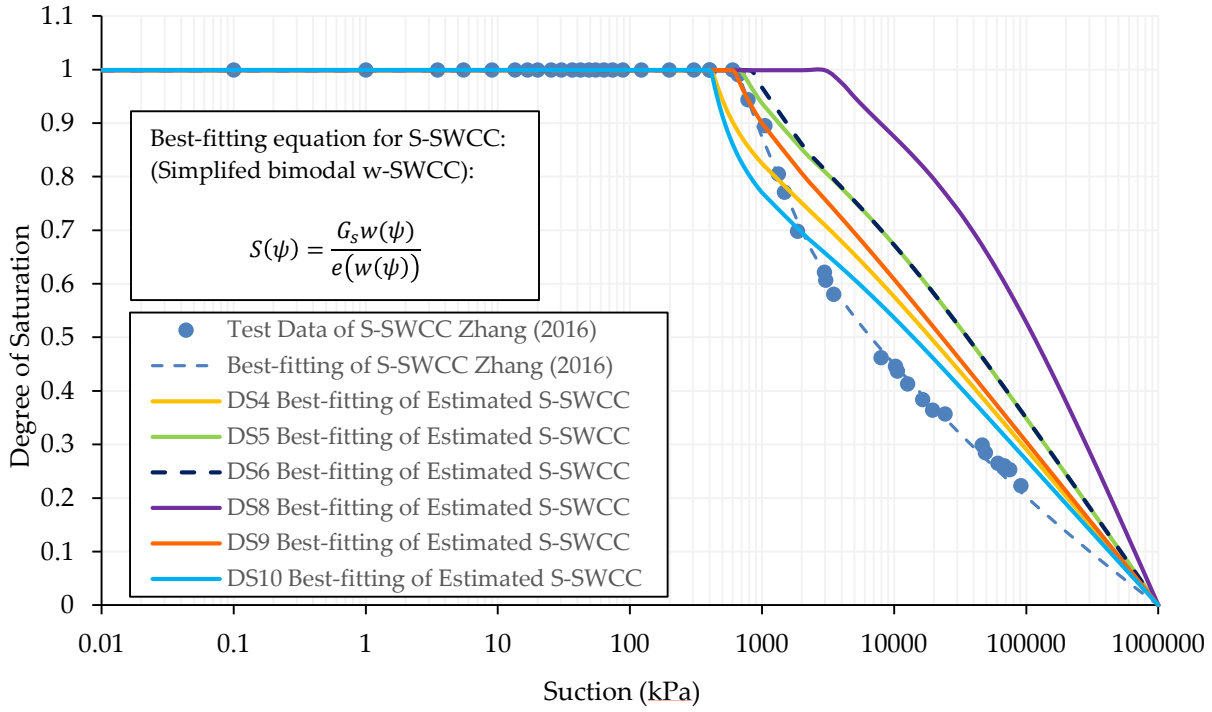

Figure 3-23: Comparison Between S-SWCC Estimated from SFCC and S-SWCC Determined using Traditional Methods

Table 3-3: Best-fitting Parameters for Equation 2-5 for Devon Silt

Sample	a_{f1} (kPa)	a_{f2} (kPa)	n_{f1}	n_{f2}	m_{f1}	m_{f2}	ψ_{rb} (kPa)	p	w_z
DS4	232.571	4.023	3.967	0.608	1.169	0.0002	1627.75	0.470	0.245
DS5	221.063	4.022	1.551	0.609	2.161	0.0002	3291.51	0.495	0.28
DS6	306.172	4.022	1.471	0.608	2.108	0.0002	3838.35	0.480	0.265
DS8	1059.464	4.018	0.945	0.608	3.539	0.0002	24814.83	0.442	0.27
DS9	281.480	4.024	3.604	0.607	1.121	0.0002	1341.825	0.443	0.25
DS10	262.843	4.023	5.406	0.608	0.833	0.0002	2871.83	0.560	0.24

Table 3-4: AEV Estimated from S-SWCC from Simplified Bimodal w-SWCC

Sample	AEV (kPa)
DS4	415
DS5	675
DS6	815
DS8	3182
DS9	629
DS10	410
Zhang (2016)	593

The TDR calibration used to determine the unfrozen water content from the dielectric constant has a large impact on the shape of the resulting estimated SWCC. To demonstrate this principle, the estimated S-SWCC for Sample DS4 is shown in Figure 3-24 using the Topp et al. (1980) calibration and the Smith and Tice (1988) calibration. For comparison purposes, Zhang's data is also shown in Figure 5-8. This shows the high reliance of the estimated SWCC on the TDR calibration.

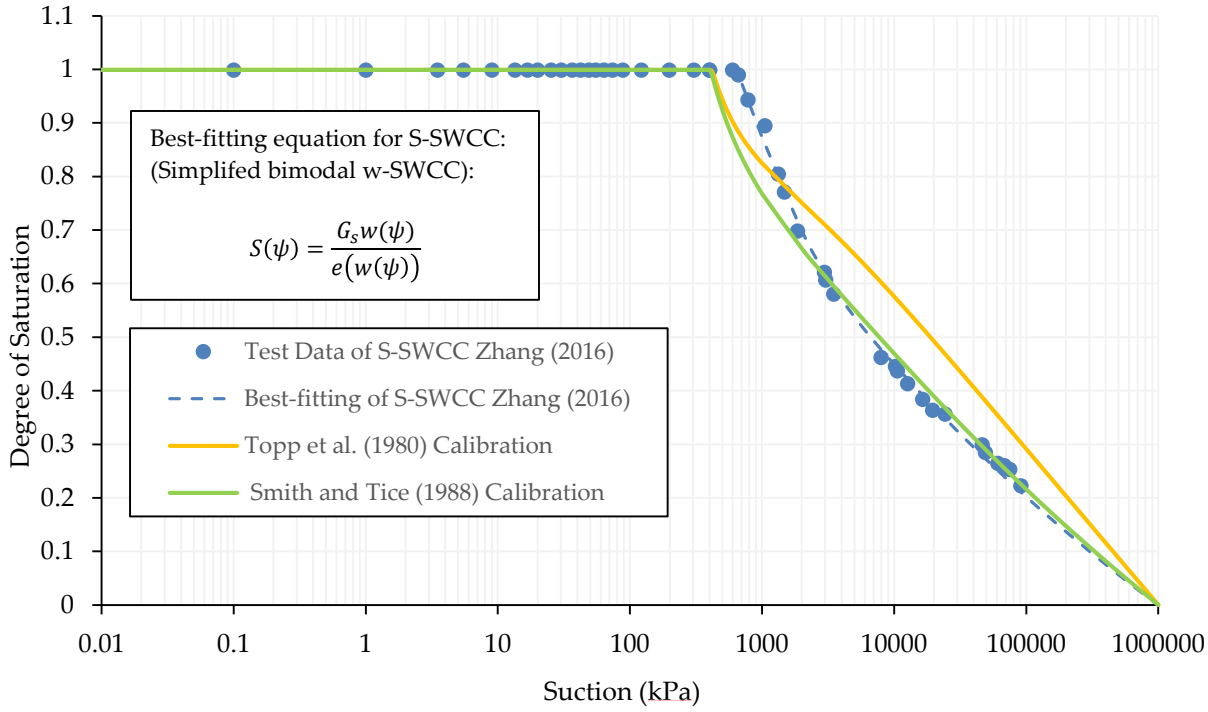

Figure 3-24: Impact of TDR Calibration on the Estimated S-SWCC from the SFCC for Sample DS4

4 EXPERIMENTAL RESULTS

Following the development of the experimental methodology as discussed in Section 3.6, testing commenced on a variety of tailings materials, including:

- Copper tailings;
- Gold tailings; and,
- Oil sands centrifuge cake.

All of these materials were tested in the form of a saturated slurry. Index testing performed on the different materials is provided in Section 4.1. The experimental results for the copper tailings, gold tailings, and centrifuge cake are discussed in Section 4.2, 4.3, and 4.4 respectively. The purpose of testing these three materials was to determine the range of tailings materials that the experimental method was valid.

4.1 Index Testing

The following index tests were performed on the materials where relevant to help classify the material behavior:

- Grain size distribution (GSD);
- Specific gravity testing; and,
- Atterberg limits testing.

The GSDs of the copper tailings, gold tailings, and centrifuge cake are provided in Figure 4-1. Sand tailings from an oil sands site in northern Alberta were also tested to determine the limits of the SFCC test. The GSD of the sand tailings is also provided in Figure 4-1. The results from the Atterberg limits testing and the specific gravity testing are provided in Table 4-1.

Table 4-1: Index Testing Results

Material	Specific Gravity	Liquid Limit (%)	Plastic Limit (%)	Plasticity Index (%)
Copper Tailings	2.65	20	14	6
Gold Tailings	2.82	-	-	-
Centrifuge Cake	2.24	57	26	31

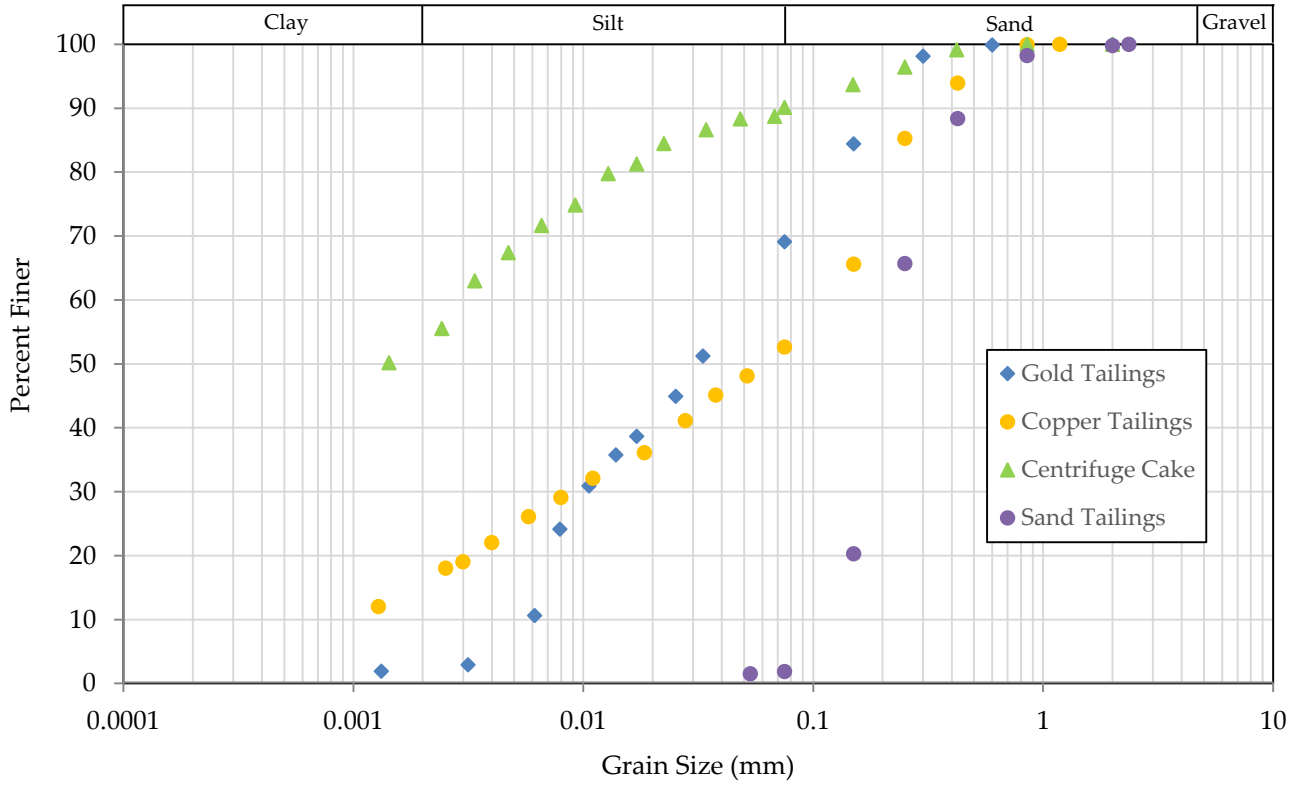

Figure 4-1: Grain Size Distributions

4.2 Copper Tailings Results

SFCC testing was performed on the copper tailings to aid in defining the range of materials that the experimental method is valid. The copper tailings were attained from a copper mine. The location of collection of the tailings from the beach is unknown. The copper tailings contain over 50 percent of sand sized particles with some clay sized particles as shown in Figure 4-1.

4.2.1 Copper Tailings SWCC and Shrinkage Testing Results

SWCC testing was completed on the copper tailings at the University of Alberta and shrinkage testing was conducted by Golder Associates Ltd. Single-specimen pressure plate cells were used up to an applied suction of 500 kPa and then a WP4-T was used (Water PotentiaMeter with

internal temperature control) for the higher suction range. This yielded the w-SWCC as shown in Figure 4-2, which was fit with Zhang and Chen's (2005) simplified bimodal equation (Equation 2-5). The best-fitting parameters of Equation 2-5 are provided on Figure 4-2. The shrinkage curve for the copper tailings and the best-fitting parameters of Equation 2-6 are provided on Figure 4-3. The shrinkage curve was then used to determine the S-SWCC and the θ_i-SWCC from the gravimetric-SWCC as shown in Figure 4-4. The w-SWCC is also presented on Figure 4-4 for comparison purposes.

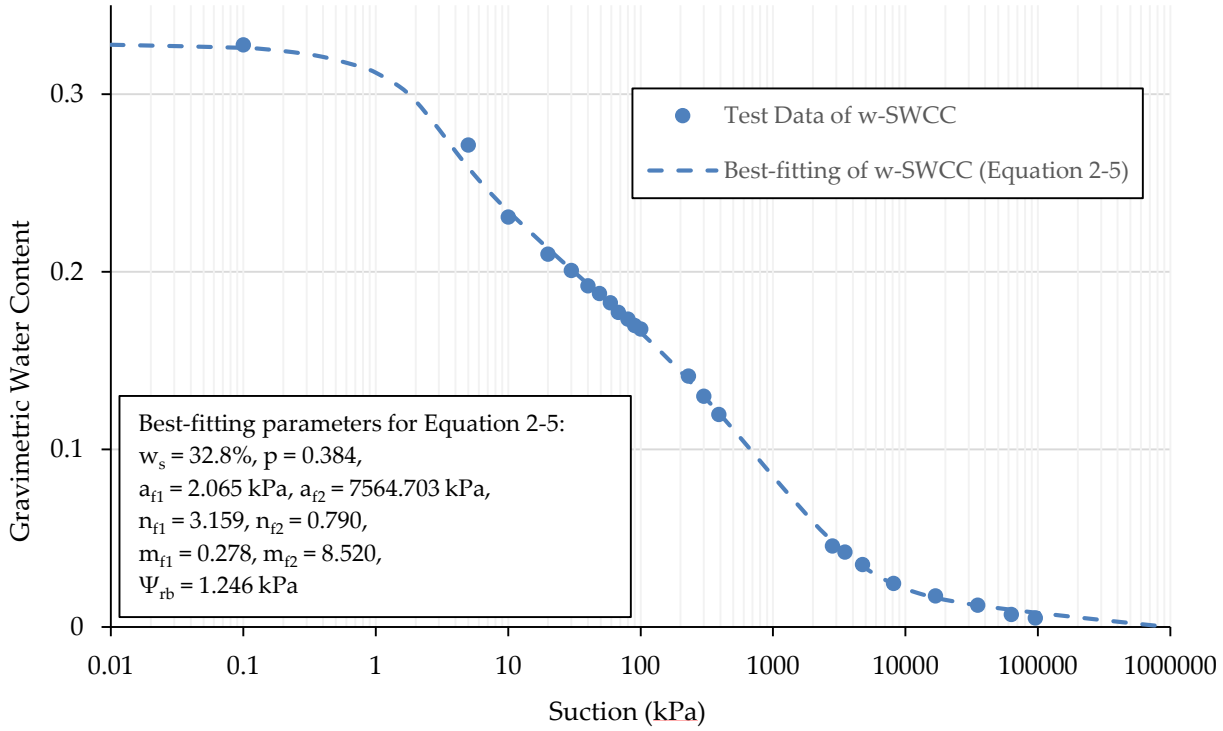

Figure 4-2: Measured w-SWCC using Traditional Methods for Copper Tailings (Equation 2-5 Simplified Bimodal Zhang and Chen (2005))

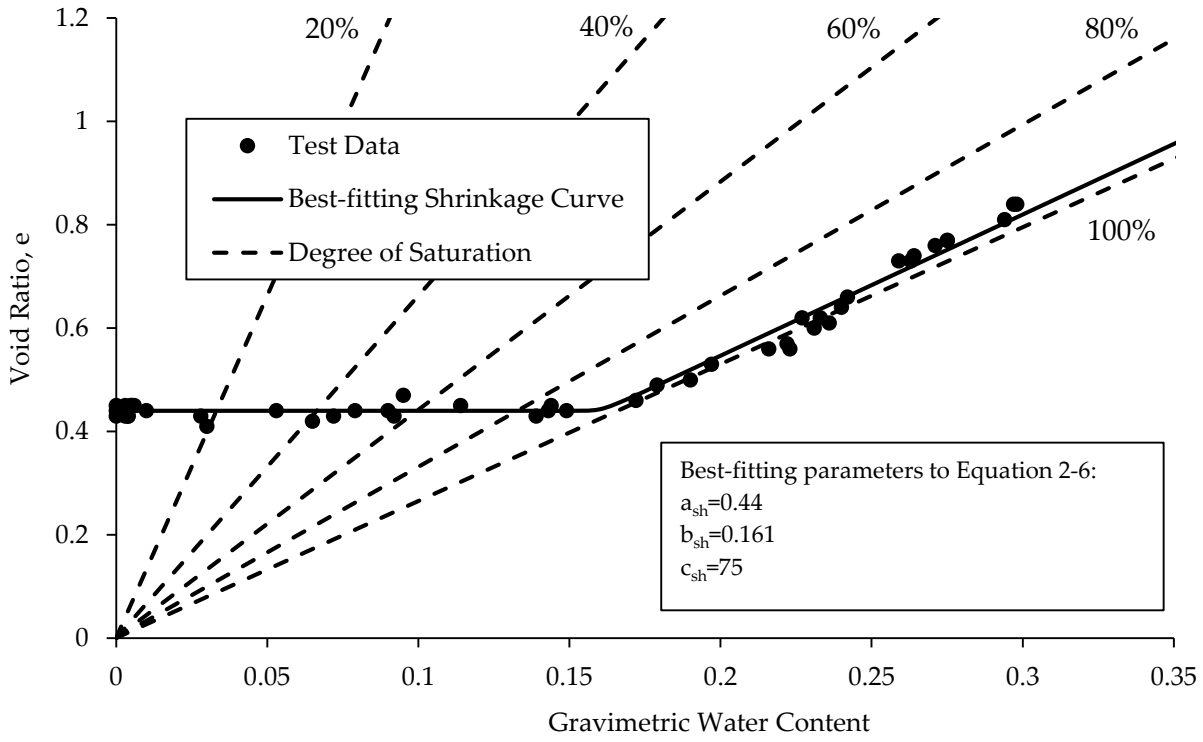

Figure 4-3: Shrinkage Curve for Copper Tailings

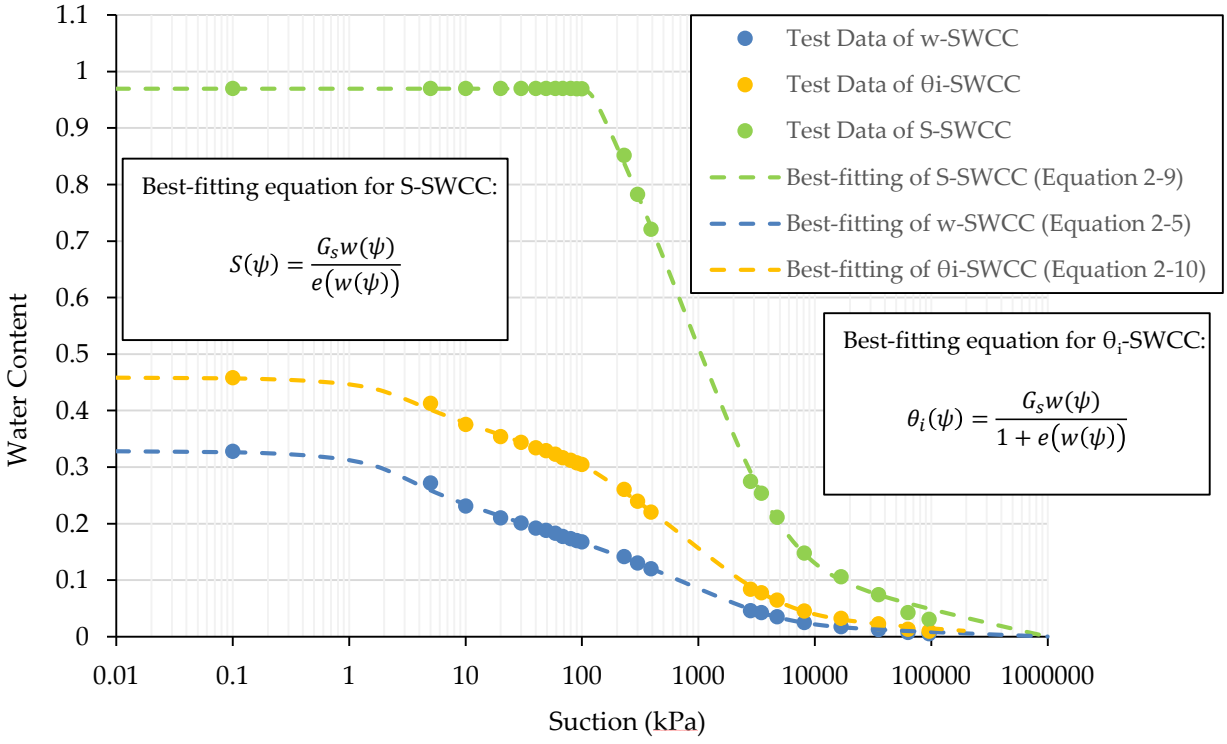

Figure 4-4: Measured SWCCs using Traditional Methods for Copper Tailings

The suction at the first breaking point between the different SWCCs is provided in Table 4-2. As this is a high volume change material, the AEV must be estimated from the S-SWCC. Based on this, the AEV of the copper tailings is about 122 kPa.

Table 4-2: Suction at the First Breaking Point for Different SWCCs for Copper Tailings

Type of SWCC	Suction at First Breaking Point (kPa)
w-SWCC	0.95
S-SWCC	122
θ_i-SWCC	1.03

4.2.2 Copper Tailings TDR Calibration

As discussed in Section 3.5, a soil specific TDR calibration was conducted on the copper tailings by mixing eight samples to varying gravimetric water contents. As noted in Section 3.5, it was very difficult to mix homogeneous samples to a water content less than 15 percent. This is a major limitation to determining the TDR calibration using this method as a large portion of the curve is not computed. The dielectric constant at a volumetric water content of zero was determined based on the Smith and Tice (1988) calibration, which was conducted on frozen material. The copper tailings TDR calibration is shown in Figure 4-5. As discussed, the dielectric constant at a volumetric water content of zero was not determined using the calibration procedure. This point has been indicated on Figure 4-5 by an open circle. The calibration equations provided by Topp et al. (1980) and Smith and Tice (1988) are shown in Figure 4-5 for comparison purposes.

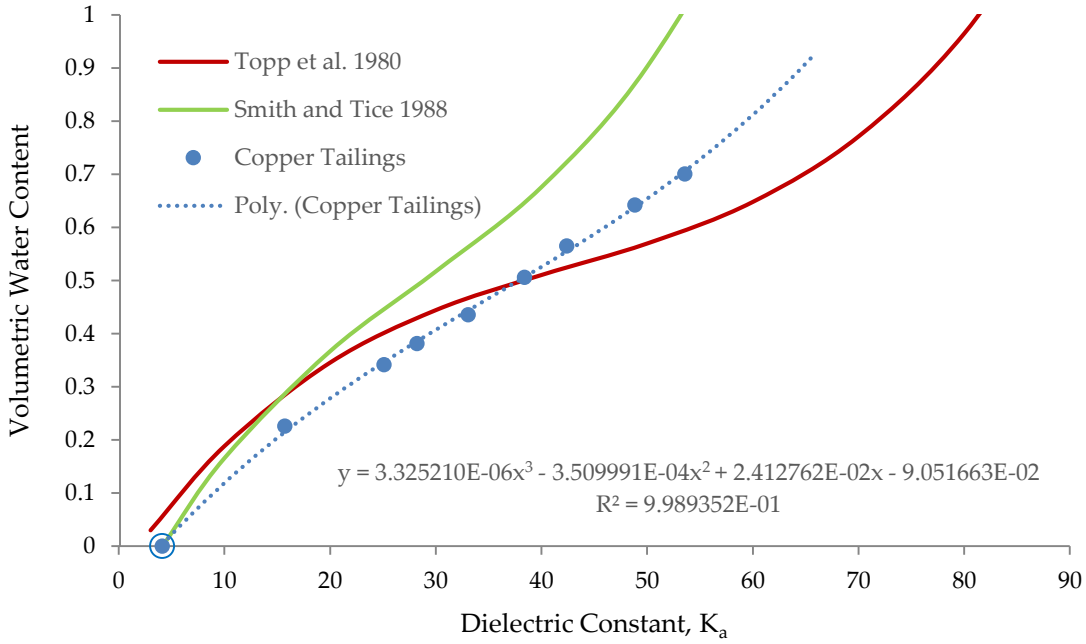

Figure 4-5: Copper Tailings TDR Calibration

4.2.3 Copper Tailings SFCC Results

Three samples (CT1, CT2, and CT3) of copper tailings were mixed to a gravimetric water content of about 45 percent using distilled water. The samples were left to saturate for a period of 24 hours prior to SFCC testing. The samples were approximately 99 mm in diameter with a length of 111 mm. The top of the sample was marked with the location that the TDR and the RTD probe should be inserted to ensure that they were equidistant from the edges.

The SFCC curves are shown in Figure 4-6. The volumetric unfrozen water content was determined from the apparent dielectric constant using the soil specific calibration discussed in Section 3.5 and was taken to be equivalent to the volumetric water content. The suction was determined from the temperature measurements using the Clapeyron equation (Equation 2-16). To estimate the SWCC from the SFCC, the copper tailings were assumed to be colloidal and a soil dependent constant of 1.0 was used to estimate the SWCC from the SFCC based on Koopmans and Miller (1966).

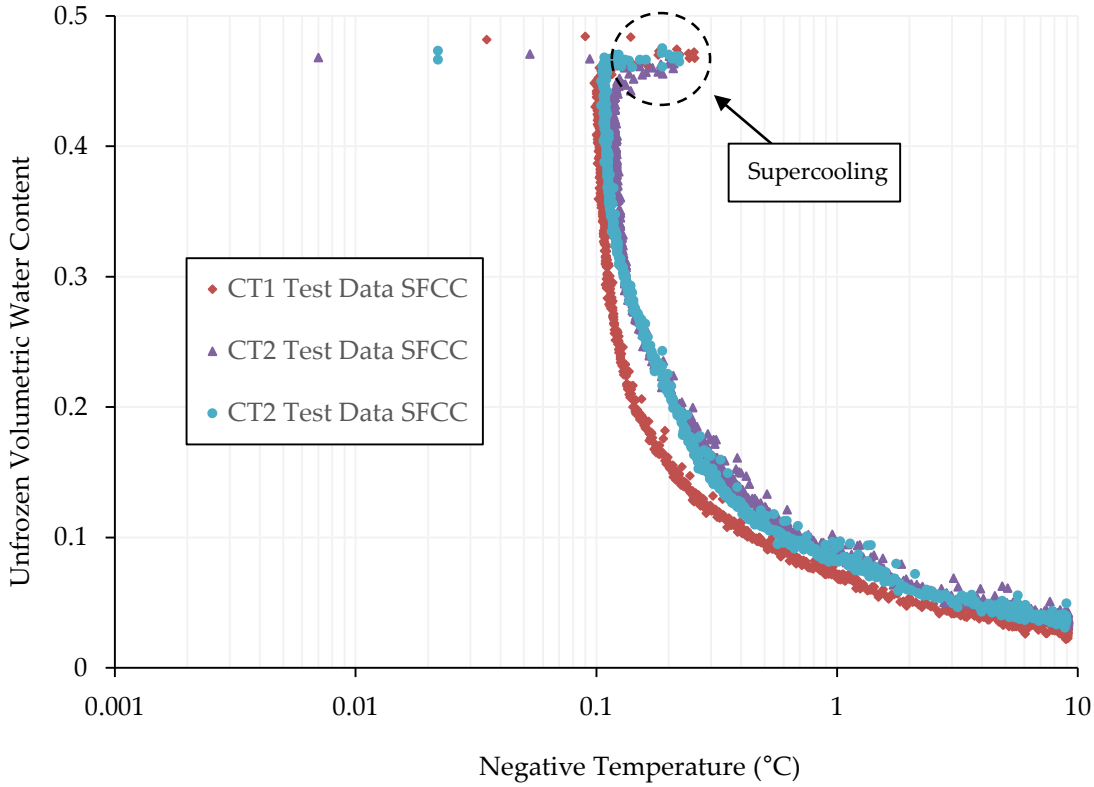

Figure 4-6: Copper Tailings SFCC

The estimated θ-SWCC, w-SWCC, S-SWCC, and θ_i-SWCC for the copper tailings are shown in Figure 4-7 to Figure 4-10. The test data was fit with the Fredlund and Xing (1994) fit (Equation 2-4) and the Zhang and Chen (2005) (Equation 2-5). Minimal differences were observed between the two fits, except in the case of Sample CT1 where the Zhang and Chen (2005) (Equation 2-5) provided a better fit. As a result, the Zhang and Chen (2005) fit (Equation 2-5) was used. The difference between the two fits (Equation 2-4 and Equation 2-5) on the S-SWCC is shown in Figure 4-11. The best-fitting parameters for the three samples for the Fredlund and Xing (1994) fit (Equation 2-4) are provided in Table 4-3. The best-fitting parameters for the Zhang and Chen (2005) fit (Equation 2-5) are provided in Table 4-4. The S-SWCC and θ_i-SWCC were determined using the shrinkage curve measured by Golder Associates Ltd. The test results further supported that this method is repeatable and reliable. Supercooling was observed during testing, which is shown by the scatter in Figure 4-7 to Figure 4-10 at high water contents. These zones represent areas of a drop in temperature below the freezing point without an associated phase change. As

a result, the suctions calculated for these temperatures are not representative of the actual suction in the sample and have been termed "pseudo-suctions". The AEV for the different samples estimated from the S-SWCC are provided in Table 4-5. The AEV was estimated using the graphical method presented by Vanapalli et al. (1998).

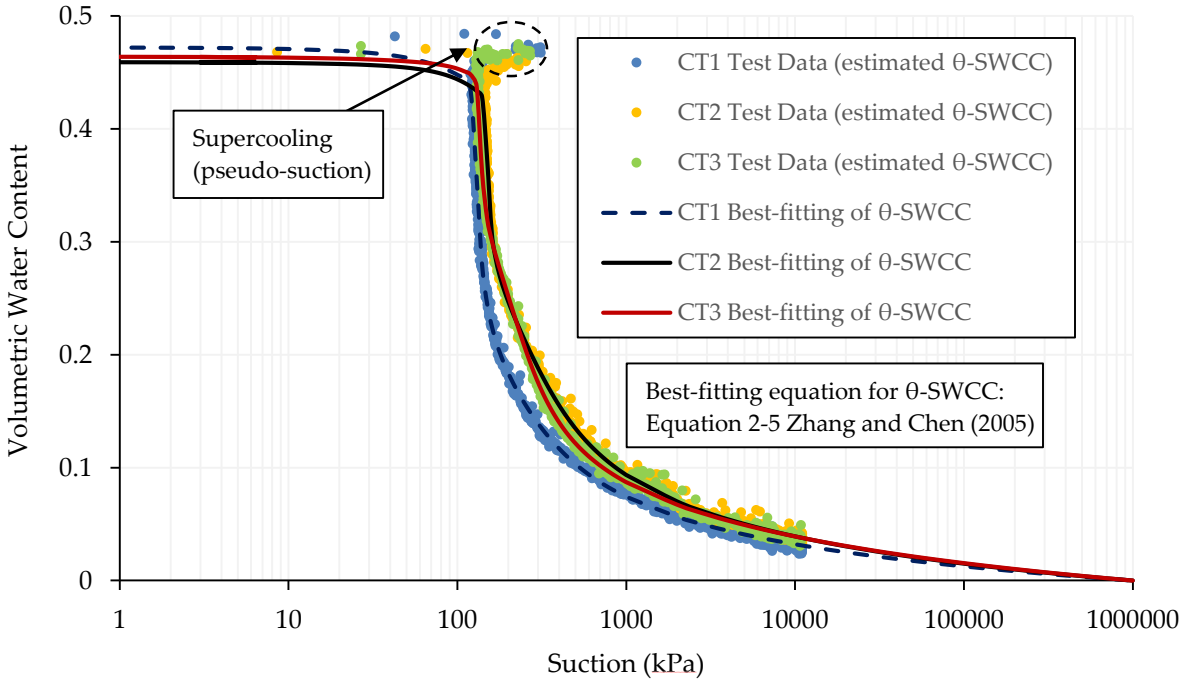

Figure 4-7: Copper Tailings Estimated θ-SWCC from the SFCC and Simplified Bimodal Zhang and Chen (2005) Fit (Equation 2-5)

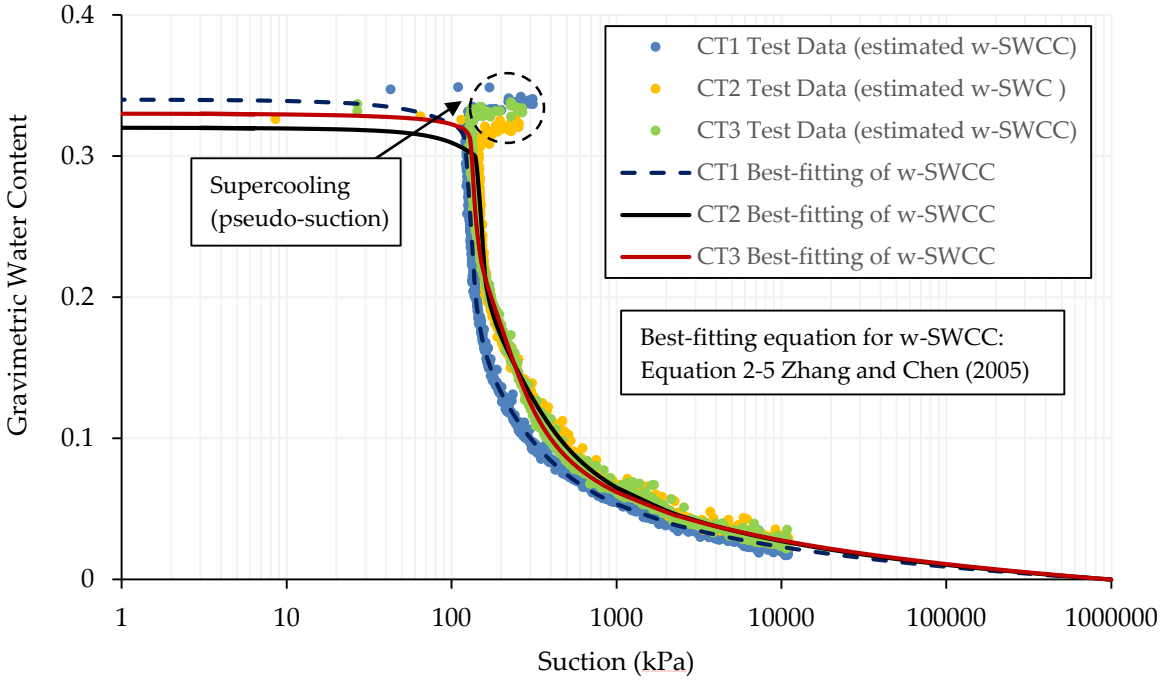

Figure 4-8: Copper Tailings Estimated w-SWCC from the SFCC and Simplified Bimodal Zhang and Chen (2005) Fit (Equation 2-5)

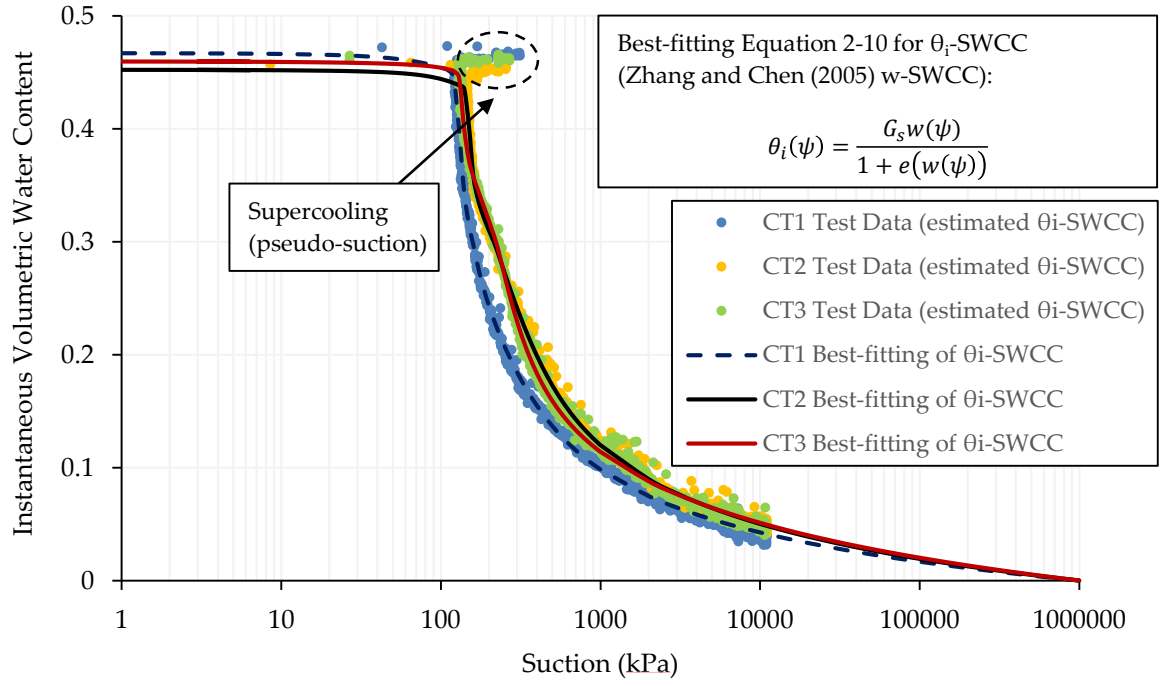

Figure 4-9: Copper Tailings Estimated θi-SWCCs from the SFCC with Equation 2-10 Fit for Zhang and Chen (2005) w-SFCC Fit

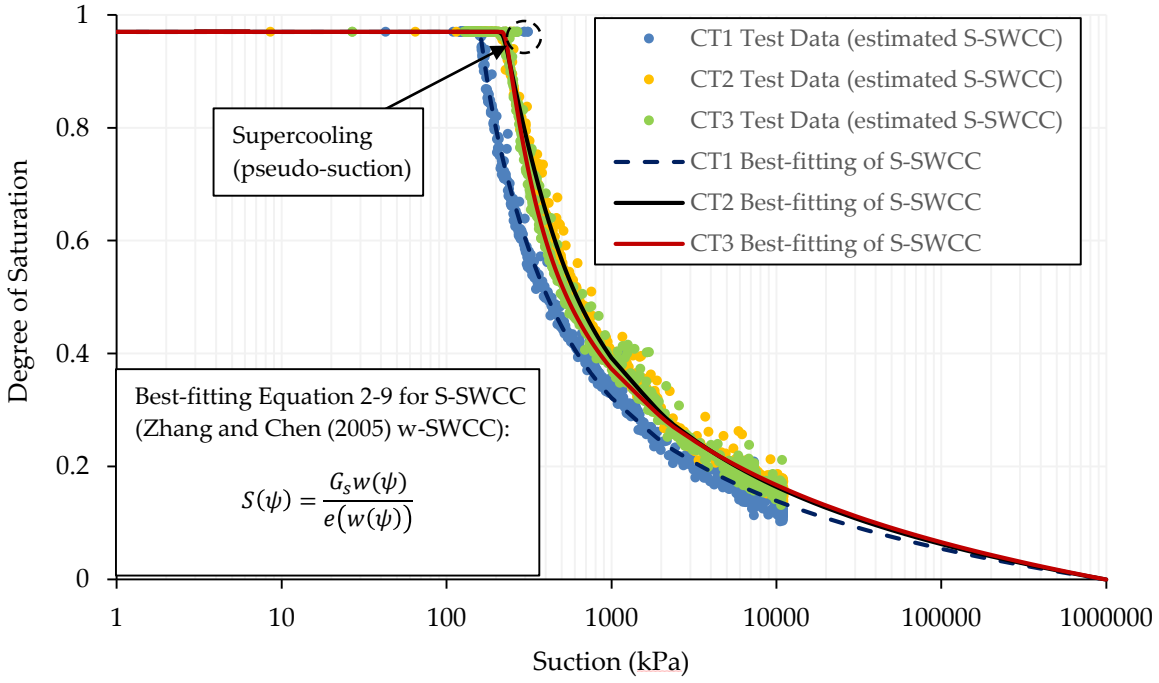

Figure 4-10: Copper Tailings Estimated S-SWCCs from the SFCC with Equation 2-9 Fit for Zhang and Chen (2005) w-SWCC Fit

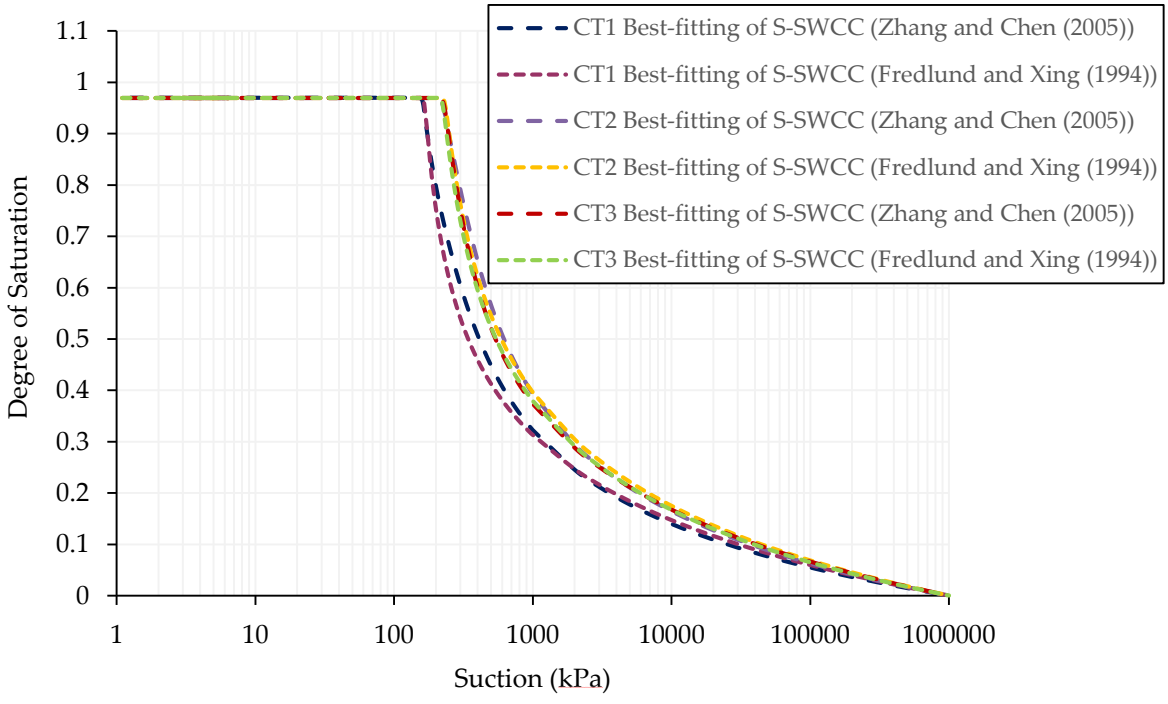

Figure 4-11: Comparison Between Copper Tailings Estimated S-SWCCs from the SFCC with Fredlund and Xing (1994) w-SWCC Fit and Zhang and Chen (2005) w-SWCC Fit

Table 4-3: Best-fitting Parameters for Fredlund and Xing (1994) (Equation 2-4) for Copper Tailings

Sample	a_f (kPa)	n_f	m_f	ψ_r (kPa)	w_s
CT1	122.058	12.431	0.5126	273.932	0.34
CT2	142.958	5.794	0.5839	427.755	0.32
CT3	137.724	5.969	0.6129	591.141	0.33

Table 4-4: Best-fitting Parameters for Zhang and Chen (2005) (Equation 2-5) for Copper Tailings

Sample	a_{f1} (kPa)	a_{f2} (kPa)	n_{f1}	n_{f2}	m_{f1}	m_{f2}	ψ_{rb} (kPa)	p	w_s
CT1	125.546	161.09	41.154	2.414	0.438	0.848	443.890	0.697	0.34
CT2	147.036	194.093	68.782	2.994	0.443	0.696	832.571	0.469	0.32
CT3	133.245	183.217	61.131	4.913	0.452	0.592	787.691	0.425	0.33

Table 4-5: AEV Estimated from S-SWCC for Zhang and Chen (2005) w-SWCC for Copper Tailings

Sample	AEV (kPa)
CT1	161
CT2	219
CT3	224
Traditional Methods	122

The SFCC testing results on the copper tailings showed that the testing method could be easily applied to a coarse tailings material. While this material is coarse, it still contains a substantial amount of fines. This depresses the freezing point and allows the SFCC to be determined by measuring the temperature using a RTD. The RTD is considered accurate to the nearest 0.01°C (approximately 12 kPa to 12.5 kPa). As a result, there are concerns of the reliability of this method for materials that have a freezing point above -0.01°C. To test this, SFCC testing was performed on three samples of sand tailings from the oil sands in northern Alberta (GSD on Figure 4-1). The θ-SWCC for the sand tailings is provided in Figure 4-12. A soil specific TDR calibration was not conducted for the sand tailings. Topp et al.'s (1980) calibration was used to estimate the volumetric water content from the dielectric constant. A soil dependent constant of 2.2 was used to estimate the SWCC from the SFCC as the material is non-colloidal. Sample ST2 and ST3 yielded similar curves, while the estimated SWCC for Sample ST1 was much different. Sample ST1 was mixed to a lower gravimetric water content then Sample ST2 and Sample ST3. As a result, the sample may not have been fully saturated, which could have resulted in the presence of air

pockets along the TDR probe. It is suspected that this contributed to the scatter observed in Figure 4-12 for Sample ST1. Regardless, Sample ST2 and ST3 suggest that the AEV for the sand tailings is greater than 6 kPa (assuming no volume change), which is unlikely for a material that consists of 100 percent sand sized particles. This is largely attributed to the ability of the RTDs to accurately measure the temperature at the freezing temperature of the sand, which is estimated to be between -0.001°C and -0.01°C based on the results of the SFCC testing. As a result, it is not recommended to estimate the SWCC from the SFCC for materials with an AEV less than 10 kPa using RTDs. If a more accurate instrument is used to estimate the temperature, it may be possible the estimate the SWCC from the SFCC for this type of material.

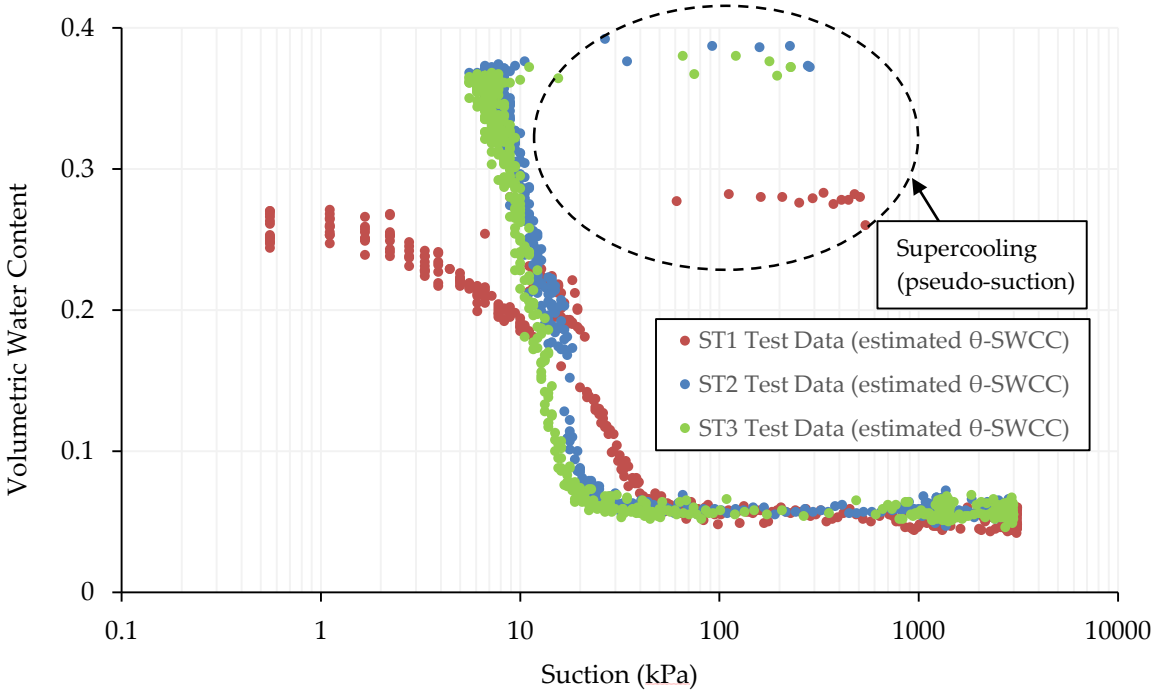

Figure 4-12: Sand Tailings Estimated θ-SWCC from the SFCC

4.3 Gold Tailings Results

SFCC testing was performed on the gold tailings to further show that this method could be used on a non-colloidal material with a substantial amount of sand. The gold tailings only contained about 2 percent clay sized particles. The gold tailings were fully characterized by Zhang (2016)

as part of her Phd thesis, which included SWCC and shrinkage testing. This allowed for comparison with the SWCC estimated from the SFCC.

4.3.1 Gold Tailings SWCC and Shrinkage Testing Results

The gold tailings characterized by Zhang (2016) were considered a high volume change material. Zhang (2016) measured the SWCC for the gold tailings using single-specimen pressure plate devices up to an applied suction of 500 kPa and then used a WP4-T (Water PotentiaMeter with internal temperature control) for the higher suction range. This yielded the w-SWCC as shown in Figure 4-13, which was fit with Zhang and Chen's (2005) simplified bimodal equation (Equation 2-5). The best-fitting parameters of Equation 2-5 are provided on Figure 4-13. The gold tailings shrinkage curve and the best-fitting parameters of Equation 2-6 are provided on Figure 4-14. The shrinkage curve was then used to determine the S-SWCC and the θ_i-SWCC from the w-SWCC as shown in Figure 4-15. The w-SWCC is also presented on Figure 4-15 for comparison purposes.

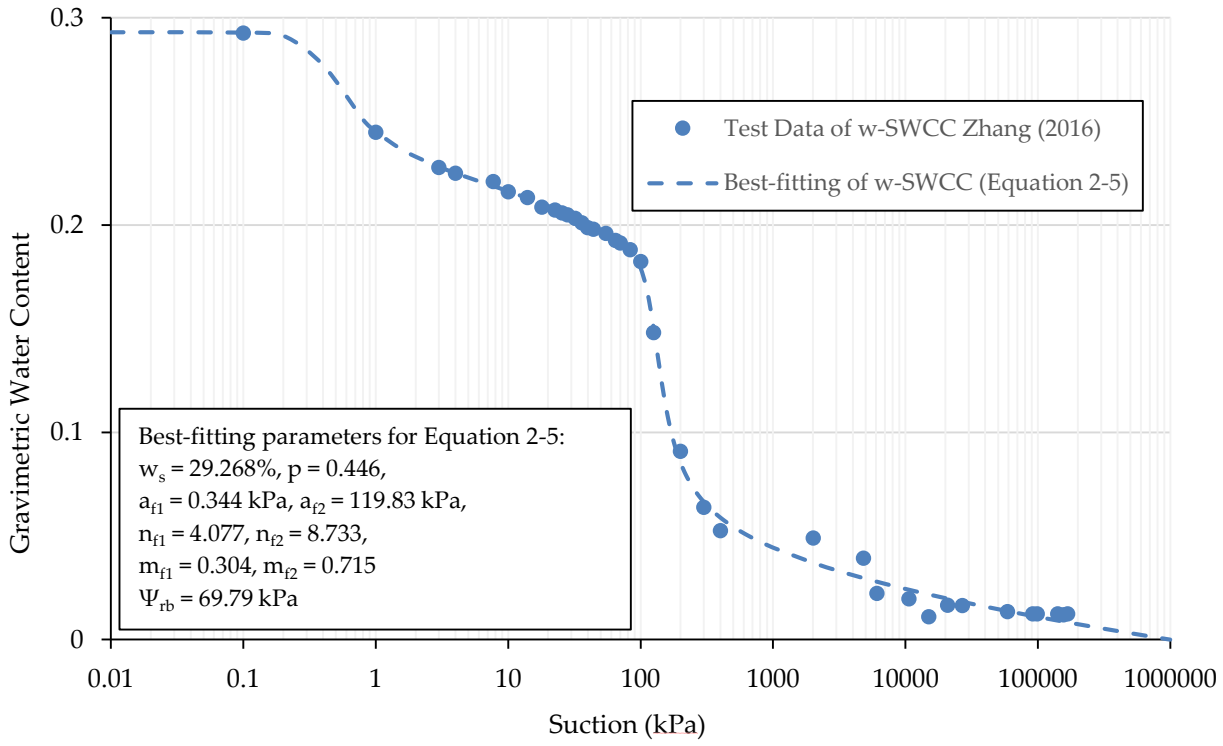

Figure 4-13: Measured w-SWCC using Traditional Methods for Gold Tailings (Equation 2-5 Simplified Bimodal Zhang and Chen (2005)) (after Zhang 2016)

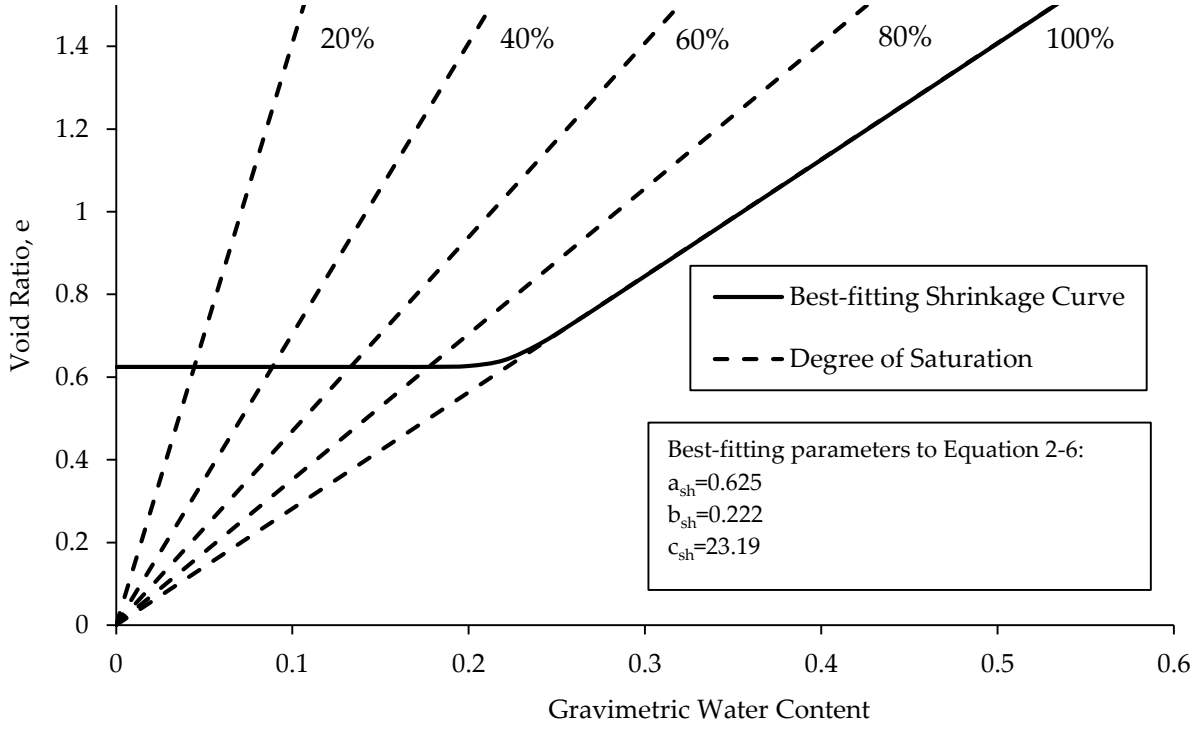

Figure 4-14: Shrinkage Curve for Gold Tailings (after Zhang 2016)

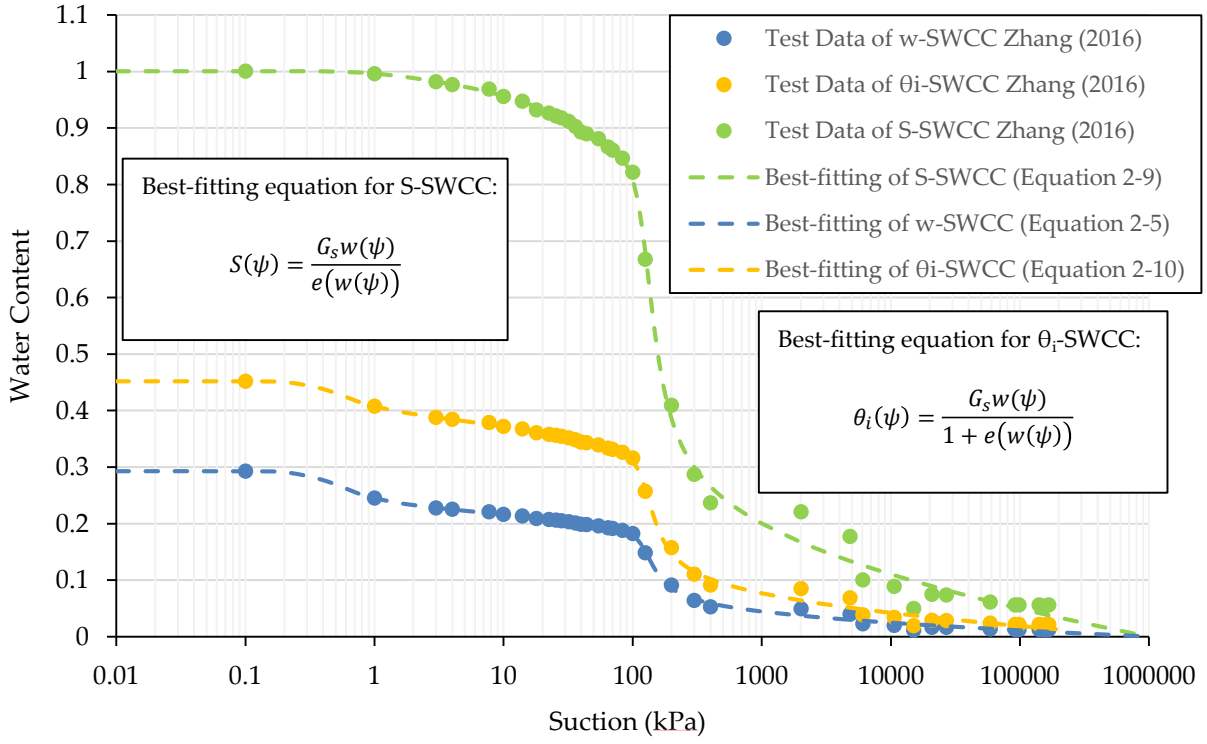

Figure 4-15: Measured SWCCs using Traditional Methods for Gold Tailings (after Zhang 2016)

The suction at the first breaking point between the different SWCCs is provided in Table 4-6. As this is a high volume change material, the AEV must be estimated from the S-SWCC. Based on this, the AEV of the gold tailings is about 86 kPa.

Table 4-6: Suction at the First Breaking Point for Different SWCCs for Gold Tailings

Type of SWCC	Suction at First Breaking Point (kPa)
w-SWCC	0.276
S-SWCC	86
θ_i-SWCC	0.28

4.3.2 Gold Tailings TDR Calibration

As discussed in Section 3.5, a soil specific TDR calibration was conducted on the gold tailings by mixing seven samples to varying gravimetric water contents. As noted in Section 3.5, it was very difficult to mix homogeneous samples to a water content less than 15 percent. This is a major limitation to determining the TDR calibration using this method as a large portion of the curve is not computed. The dielectric constant at a volumetric water content of zero for the gold tailings was determined based on two considerations, as follows:

- The Smith and Tice (1988) calibration, which was conducted on frozen material. At an unfrozen water content of zero, the K_a is approximately 4.1 for this calibration.
- Below a temperature of -15°C, the gold tailings were considered to be completely frozen with an unfrozen water content of zero. The minimum K_a value measured by the TDR for all samples under these conditions was approximately 5.2.

Based on these considerations, a K_a value of 5.2 was used for an unfrozen volumetric water content of zero. The gold tailings TDR calibration is shown in Figure 4-16. As discussed, the dielectric constant at a volumetric water content of zero was not determined using the calibration procedure. This point has been indicated on Figure 4-16 by an open circle. The calibration equations provided by Topp et al. (1980) and Smith and Tice (1988) are shown in Figure 4-16 for comparison purposes.

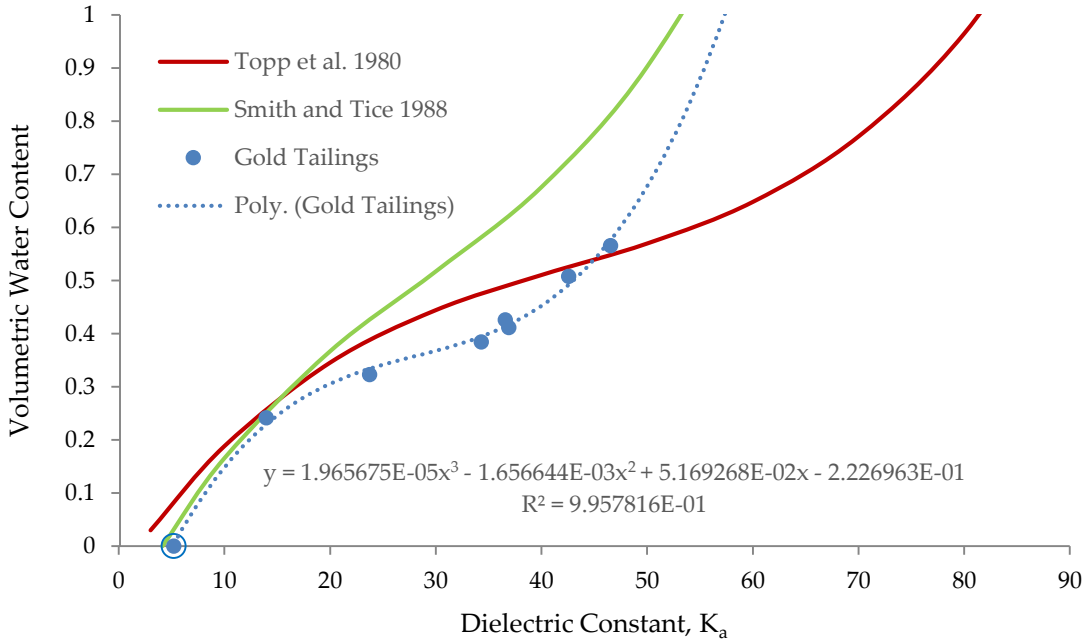

Figure 4-16: Gold tailings TDR Calibration

4.3.3 Gold Tailings SFCC Results

Three samples (BG1, BG2, and BG3) of gold tailings were mixed to a gravimetric water content of about 30 percent using distilled water. The samples were left to saturate for a period of 24 hours prior to SFCC testing. The samples were approximately 99 mm in diameter with a length of 111 mm. The top of the sample was marked with the location that the TDR and the RTD probe should be inserted to ensure that they were equidistant from the edges.

The SFCC curves are shown in Figure 4-17. The volumetric unfrozen water content was determined from the apparent dielectric constant using the soil specific calibration discussed in Section 3.5 and was taken to be equivalent to the volumetric water content. The suction was determined from the temperature measurements using the Clapeyron Equation (Equation 2-16). To estimate the SWCC from the SFCC, the gold tailings were assumed to be non-colloidal and a soil dependent constant of 2.2 was used to estimate the SWCC from the SFCC based on Koopmans and Miller (1966).

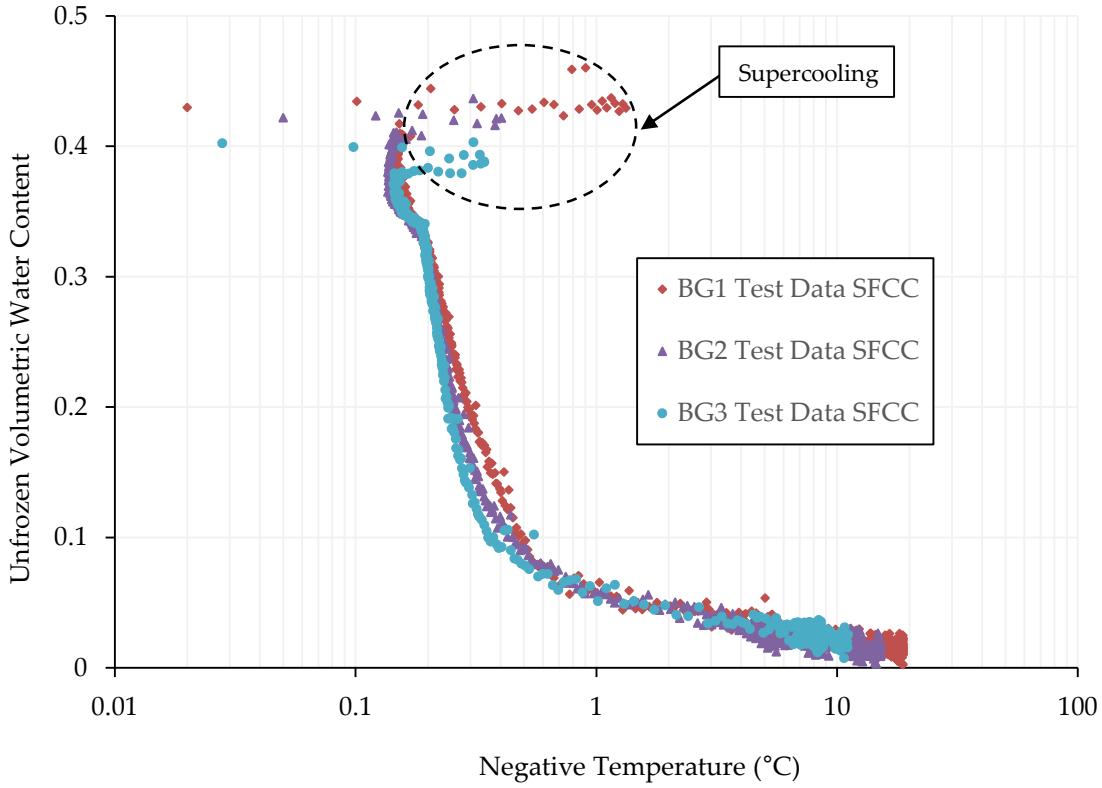

Figure 4-17: Gold Tailings SFCC

The estimated θ-SWCC, w-SWCC, S-SWCC, and θ_i-SWCC for the gold tailings are shown in Figure 4-18 to Figure 4-21. The test data was fit with the Fredlund and Xing (1994) fit (Equation 2-4) and the Zhang and Chen (2005) (Equation 2-5). Minimal differences were observed between the two fits, so the Fredlund and Xing (1994) fit (Equation 2-4) was used. The difference between the two fits (Equation 2-4 and Equation 2-5) on the S-SWCC is shown in Figure 4-22. The best-fitting parameters for the three samples for the Fredlund and Xing (1994) fit (Equation 2-4) are provided in Table 4-7. The best-fitting parameters for the Zhang and Chen (2005) fit (Equation 2-5) are provided in Table 4-8. The S-SWCC and θ_i-SWCC were determined using the shrinkage curve measured by Zhang (2016). The test results further supported that this method is repeatable and reliable. Supercooling was observed during testing, which is shown by the scatter in Figure 4-18 to Figure 4-21 at high water contents. These zones represent areas of a drop in temperature below the freezing point without an associated phase change. As a result, the suctions calculated for these temperatures are not representative of the actual suction in the

sample and have been termed "pseudo-suctions". The AEV for the different samples estimated from the S-SWCC are provided in Table 4-9. The AEV was estimated using the graphical method presented by Vanapalli et al. (1998).

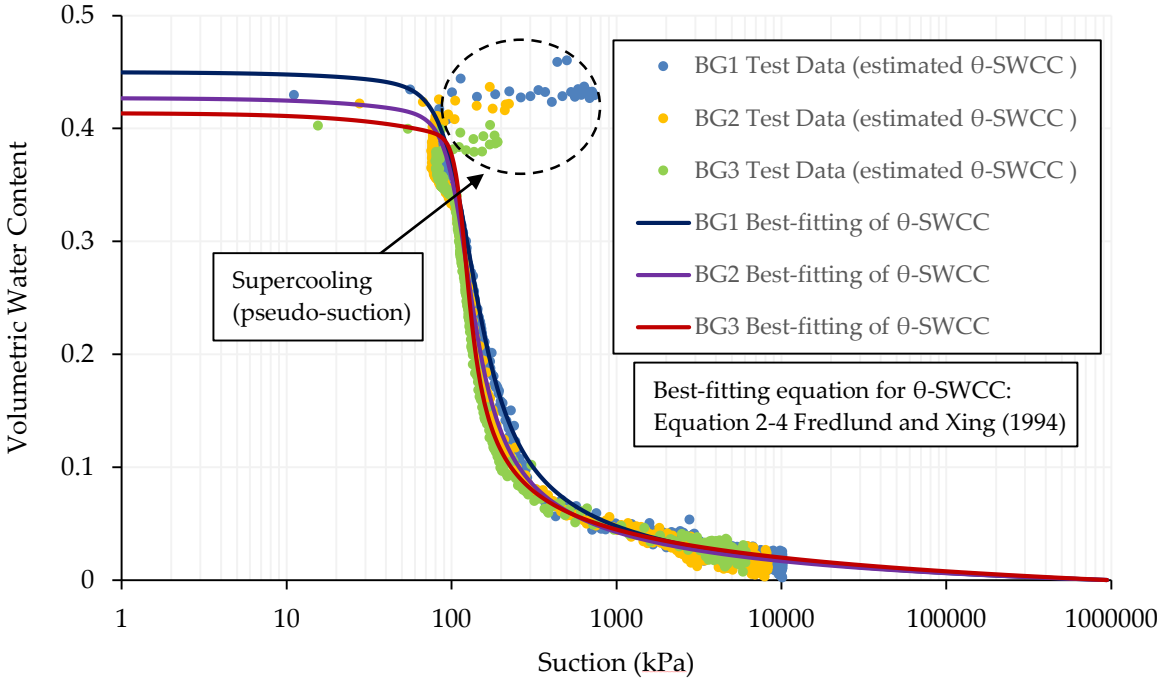

Figure 4-18: Gold Tailings Estimated θ-SWCC from the SFCC and Fredlund and Xing (1994) Fit (Equation 2-4)

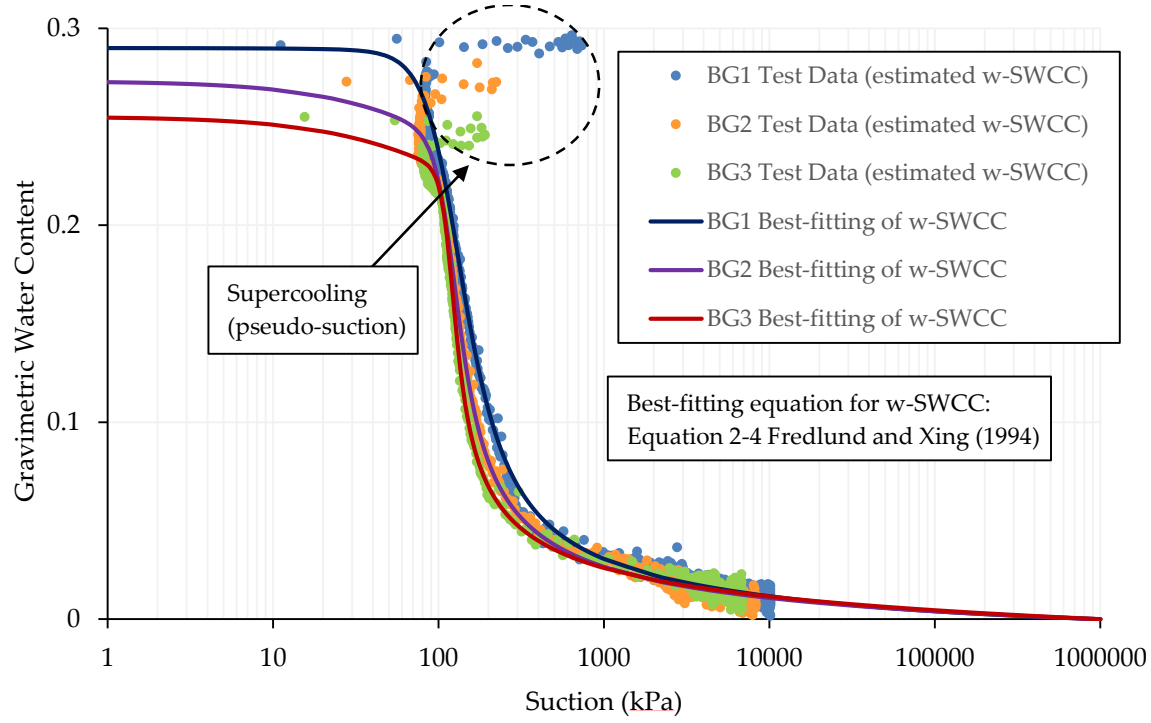

Figure 4-19: Gold Tailings Estimated w-SWCC from the SFCC and Fredlund and Xing (1994) Fit (Equation 2-4)

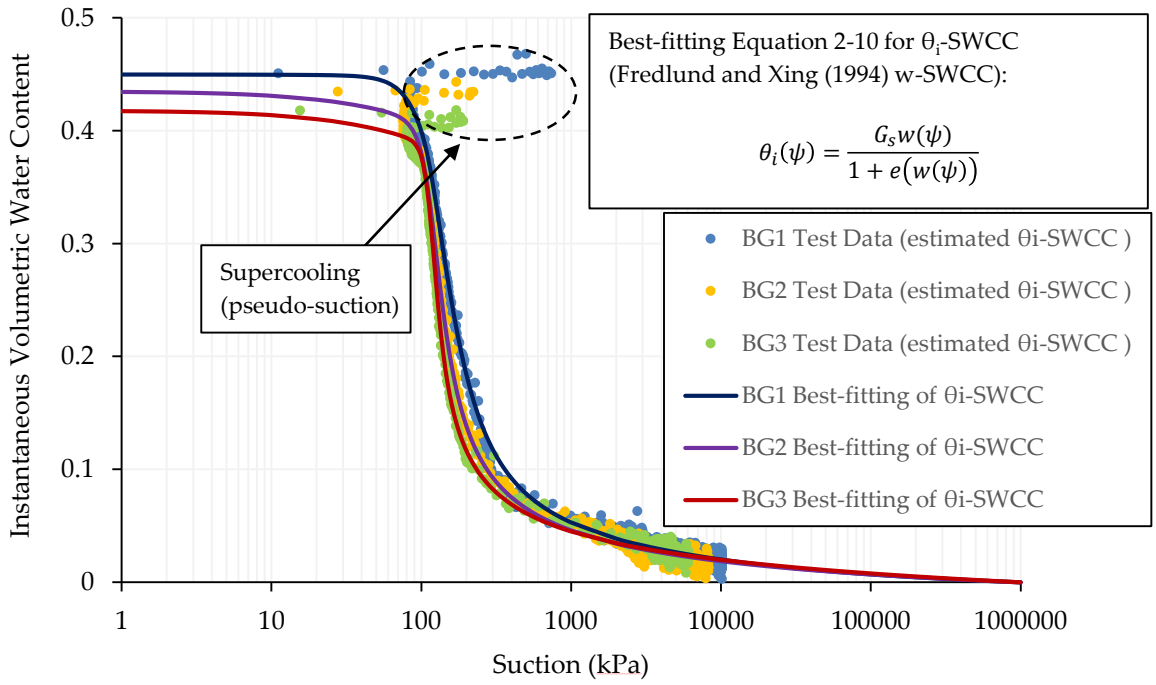

Figure 4-20: Gold Tailings Estimated θi-SWCCs from the SFCC with Equation 2-10 Fit for Fredlund and Xing (1994) w-SFCC fit

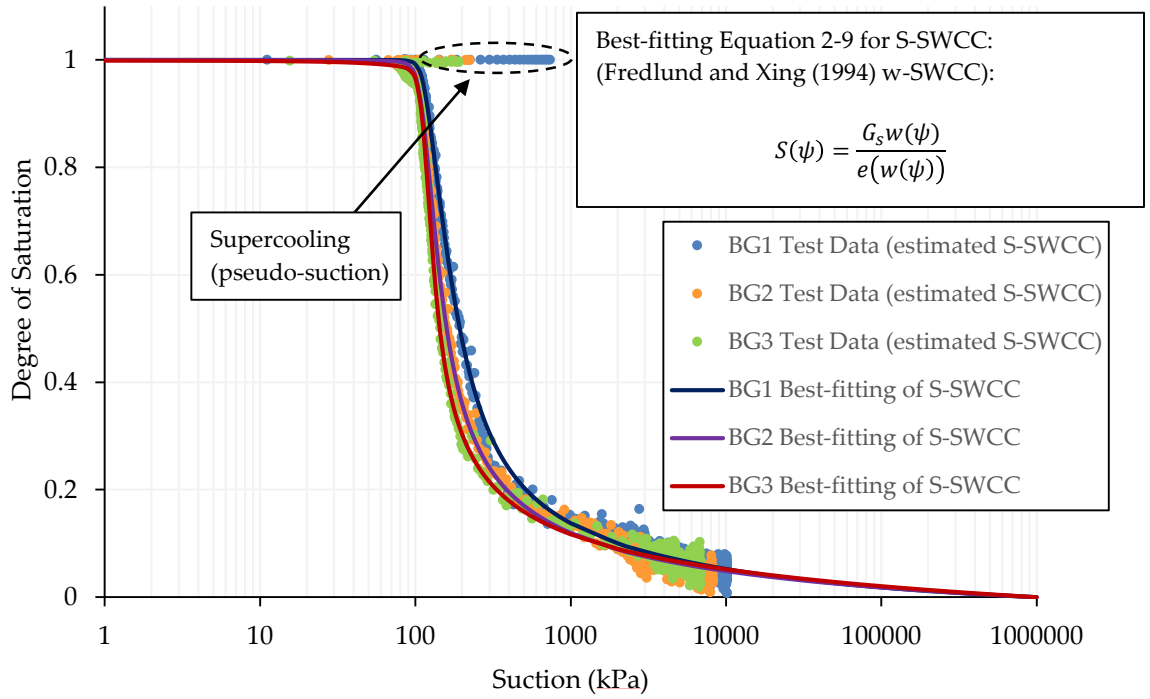

Figure 4-21: Gold Tailings Estimated S-SWCCs from the SFCC with Equation 2-9 Fit for Fredlund and Xing (1994) w-SWCC Fit

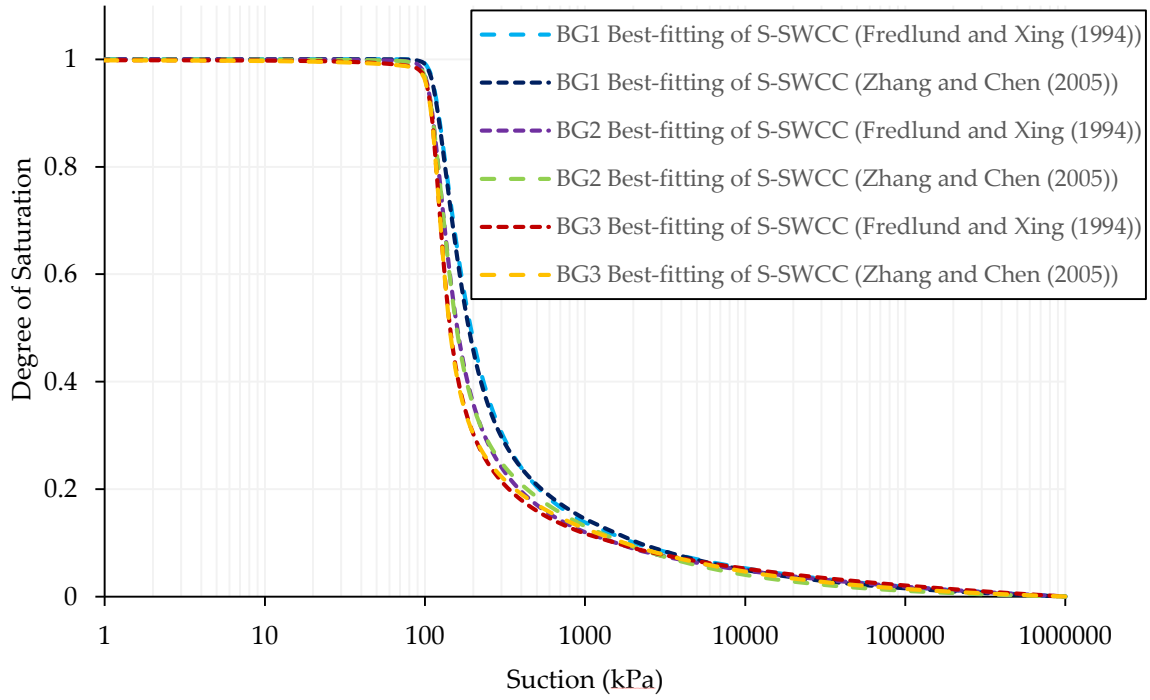

Figure 4-22: Comparison Between Gold Tailings Estimated S-SWCCs from the SFCC with Fredlund and Xing (1994) w-SWCC Fit and Zhang and Chen (2005) w-SWCC Fit

Table 4-7: Best-fitting Parameters for Fredlund and Xing (1994) (Equation 2-4) for Gold Tailings

Sample	a_f (kPa)	n_f	m_f	ψ_r (kPa)	w_s
BG1	109.697	4.333	0.9652	1956.118	0.29
BG2	110.466	7.676	0.7013	62.100	0.273
BG3	112.036	13.147	0.5756	60.472	0.255

Table 4-8: Best-fitting Parameters for Zhang and Chen (2005) (Equation 2-5) for Gold Tailings

Sample	a_{f1} (kPa)	a_{f2} (kPa)	n_{f1}	n_{f2}	m_{f1}	m_{f2}	ψ_{rb} (kPa)	p	w_s
BG1	118.568	230.394	4.328	0.969	1.389	1.047	1626.604	0.839	0.29
BG2	115.334	266.041	7.169	0.615	1.114	1.806	218.874	0.772	0.273
BG3	113.763	262.982	12.221	0.480	0.800	1.938	195.648	0.818	0.255

Table 4-9: AEV Estimated from S-SWCC for Fredlund and Xing (1994) w-SWCC

Sample	AEV (kPa)
BG1	108
BG2	102
BG3	104
Zhang (2016)	86

4.4 Centrifuge Cake Results

SFCC testing was performed on an oil sands tailings sample from a mine site in northern Alberta. The material has a solids content of about 52 percent. To prepare this material, tailings were dredged from a settling basin (Spence et al. 2015). The tailings were then mixed with gypsum and a flocculant and processed using a centrifuge (Spence et al. 2015). This results in the formation of a centrifuge cake and a centrate that can be disposed of separately (Spence et al. 2015). After formation on site, a sample of the centrifuge cake was placed into totes and shipped to the University of Alberta for characterization and SFCC testing.

4.4.1 Centrifuge Cake Solids Mineralogy and Pore Water Chemistry

Table 4-10 provides a summary of the solids mineralogy of the centrifuge cake. The centrifuge cake is composed of approximately 48 percent non-clay minerals and 52 percent clay minerals. The tailings contain mainly quartz, kaolinite, and illite with minor amounts of siderite, pyrite, and dolomite. The pore water chemistry of the centrifuge cake is summarized in

Table 4-11. The laboratory testing for the solids mineralogy and the pore water chemistry was completed by AGAT Laboratories.

Table 4-10: Centrifuge Cake Solids Mineralogy

Property	Value
Minerals (%)	Non-clay: Quartz (40); Potassium Feldspar (2); Siderite (3); Pyrite (2); Dolomite (1)
	Clay: Kaolinite (36); Illite (15)
Methylene Blue Index (meq/100g)	4.91

Table 4-11: Centrifuge Cake Pore Water Chemistry

Property	Value
pH	8.17
Electrical Conductivity (μs/cm)	3890
Dissolved Ions (mg/L)	Cations: Na^+ (780); Ca^{2+} (36.5); Mg^{2+}(15.9); K^+(14.6)
	Anions: Cl^- (446); NO_3^- (0.26); SO_4^{2-} (17.7); F^- (2.47); Br^- (0.53)

4.4.2 Centrifuge Cake SWCC and Shrinkage Testing Results

SWCC and shrinkage testing was completed on the centrifuge cake by Golder Associates Ltd. Single-specimen pressure plate cells were used up to an applied suction of 500 kPa and a chilled mirror hygrometer was used for suctions greater than 2000 kPa. This yielded the w-SWCC as shown in Figure 4-23, which was fit with Zhang and Chen's (2005) simplified bimodal equation (Equation 2-5). The best-fitting parameters of Equation 2-5 are provided on Figure 4-23. The centrifuge cake shrinkage curve and the best-fitting parameters of Equation 2-6 are provided on Figure 4-24. The shrinkage curve was then used to determine the S-SWCC and the θ_i-SWCC from the gravimetric-SWCC as shown in Figure 4-25. The w-SWCC is also presented on Figure 4-25 for comparison purposes.

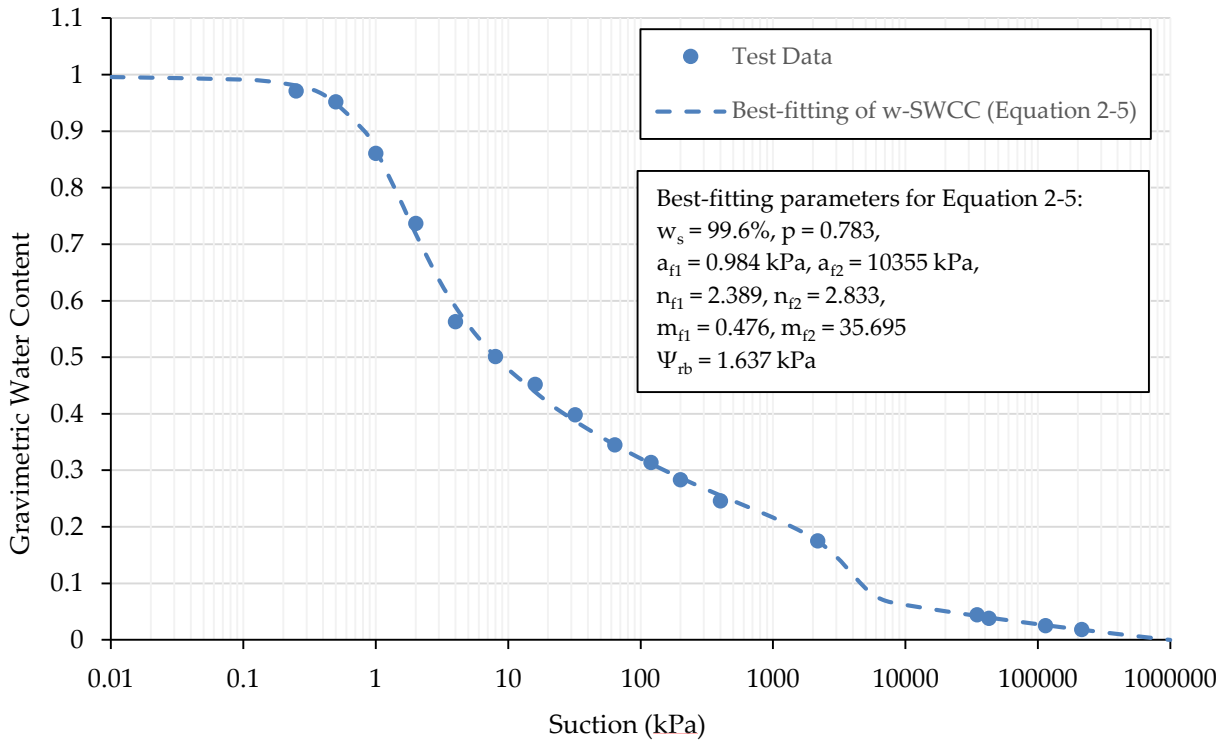

Figure 4-23: Measured w-SWCC using Traditional Methods for Centrifuge Cake (Equation 2-5)

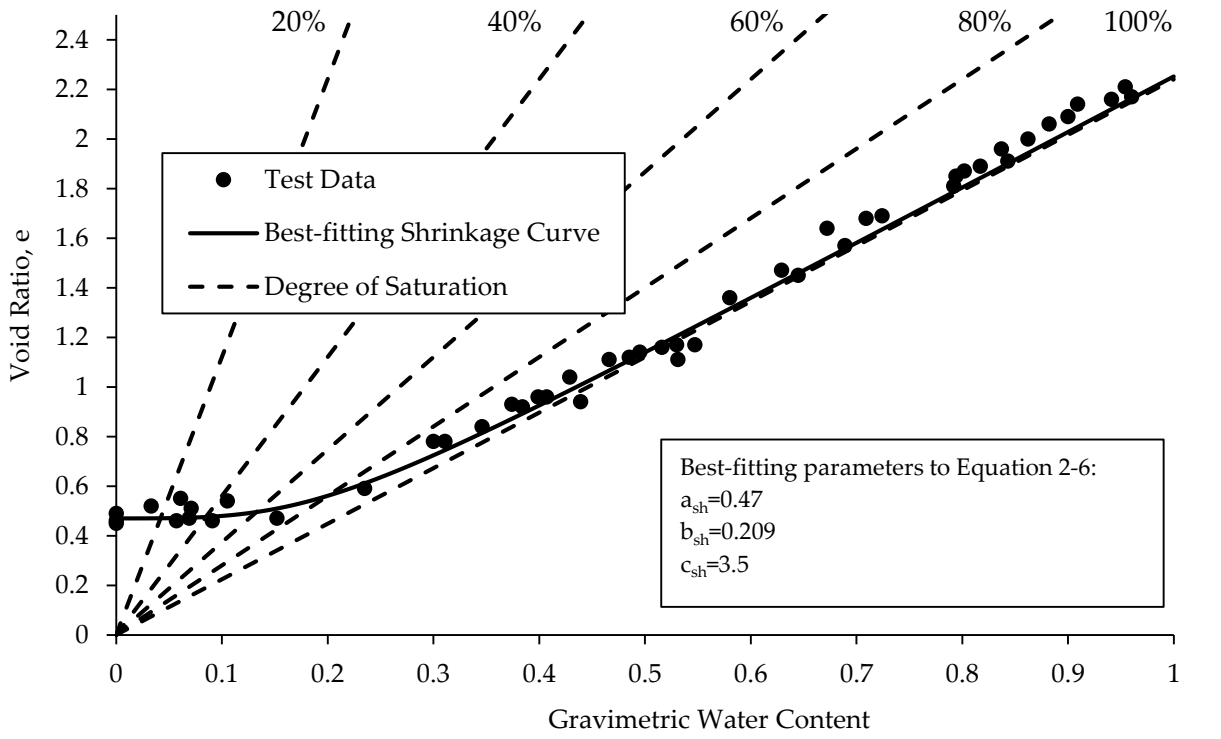

Figure 4-24: Shrinkage Curve for Centrifuge Cake

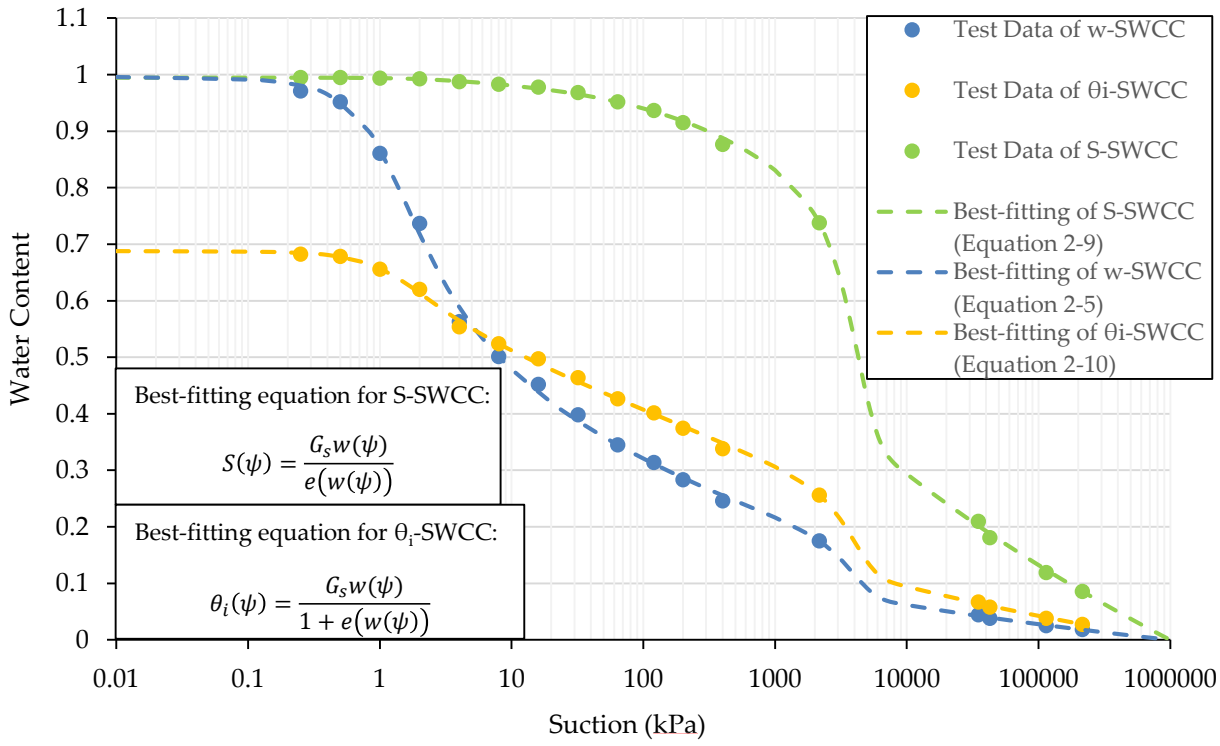

Figure 4-25: Measured SWCCs using Traditional Methods for Centrifuge Cake

The suction at the first breaking point between the different SWCCs is provided in Table 4-12. As this is a high volume change material, the AEV must be estimated from the S-SWCC. Based on this, the AEV of the centrifuge cake is about 1449 kPa.

Table 4-12: Suction at the First Breaking Point for Different SWCCs for Centrifuge Cake

Type of SWCC	Suction at First Breaking Point (kPa)
w-SWCC	0.55
S-SWCC	1449
θi-SWCC	0.65

4.4.3 Centrifuge Cake TDR Calibration

The in situ solids content of the centrifuge cake was approximately 52 percent (gravimetric water content of 93 percent). A soil specific TDR calibration was conducted on the centrifuge cake by mixing eight samples to varying gravimetric water contents from 100 percent to 450 percent and air-drying four samples to gravimetric water contents of approximately 35 percent to 70 percent. As noted in Section 3.5, it was very difficult to air-dry samples of the centrifuge cake and the reliability of these points is not known. This is a major limitation to determining the TDR

calibration using this method as a large portion of the curve is not computed. The dielectric constant at a volumetric water content of zero was determined based on the Smith and Tice (1988) calibration, which was conducted on frozen material. The centrifuge cake TDR calibration is shown on Figure 4-26. As discussed, the dielectric constant at a volumetric water content of zero was not determined using the calibration procedure. This point has been indicated on Figure 4-26 by an open circle. The calibration equations provided by Topp et al. (1980), Smith and Tice (1988), and Sorta et al. (2013) are shown in Figure 4-26 for comparison purposes.

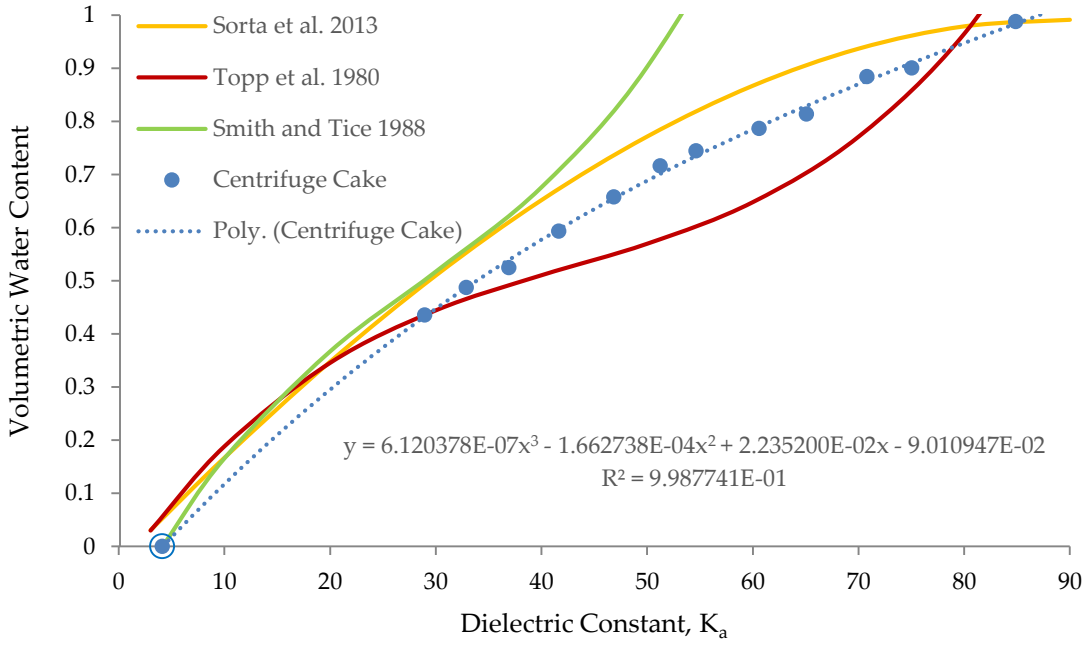

Figure 4-26: Centrifuge Cake TDR Calibration

4.4.4 Centrifuge Cake SFCC Results

Four samples (CC1, CC2, CC3, and CC4) of centrifuge cake were tested at the in situ solids content of 52 percent. The samples were approximately 99 mm in diameter with a length of 111 mm. The top of the sample was marked with the location that the TDR and the RTD probe should be inserted to ensure that they were equidistant from the edges.

The SFCC curves are shown in Figure 4-27. The volumetric unfrozen water content was determined from the apparent dielectric constant using the soil specific calibration discussed in Section 3.5 and was taken to be equivalent to the volumetric water content. The suction was

determined from the temperature measurements using the Clapeyron Equation (Equation 2-16). To estimate the SWCC from the SFCC, the centrifuge cake was assumed to be colloidal and a soil dependent constant of 1.0 was used to estimate the SWCC from the SFCC based on Koopmans and Miller (1966).

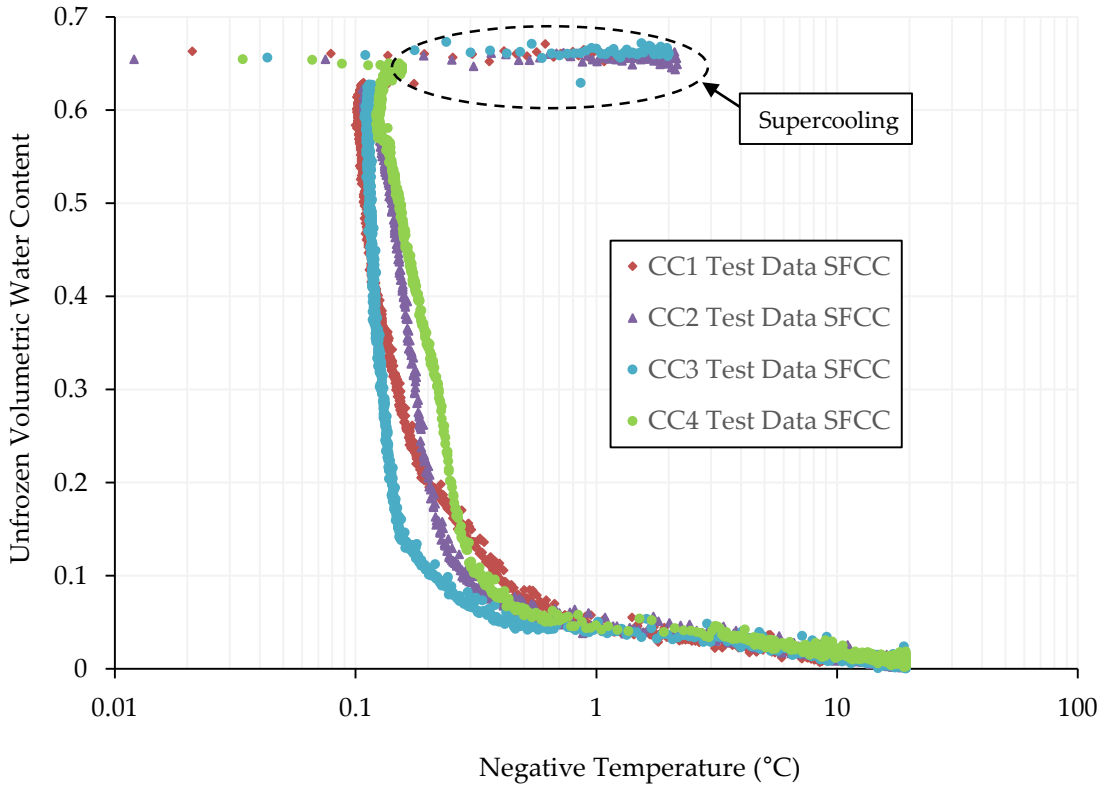

Figure 4-27: Centrifuge Cake SFCC

The estimated θ-SWCC, w-SWCC, S-SWCC, and θ_i-SWCC for the centrifuge cake are shown in Figure 4-28 to Figure 4-31. Zhang and Chen's (2005) simplified bimodal equation (Equation 2-5) was used to fit the data. For comparison purposes, the test data was also fit with the Fredlund and Xing (1994) fit (Equation 2-4). The difference between the two fits (Equation 2-4 and Equation 2-5) on the S-SWCC is shown in Figure 4-32. The best-fitting parameters for the four samples for the Fredlund and Xing (1994) fit (Equation 2-4) are provided in Table 4-13. The best-fitting parameters for the Zhang and Chen (2005) fit (Equation 2-5) are provided in Table 4-14. The S-SWCC and θ_i-SWCC were determined using the shrinkage curve measured by Golder Associates Ltd. Supercooling was observed during testing, which is shown by the scatter in

Figure 4-28 to Figure 4-31 at high water contents. These zones represent areas of a drop in temperature below the freezing point without an associated phase change. As a result, the suctions calculated for these temperatures are not representative of the actual suction in the sample and have been termed "pseudo-suctions". The AEV for the different samples estimated from the S-SWCC are provided in Table 4-15. The AEV was estimated using the graphical method presented by Vanapalli et al. (1998).

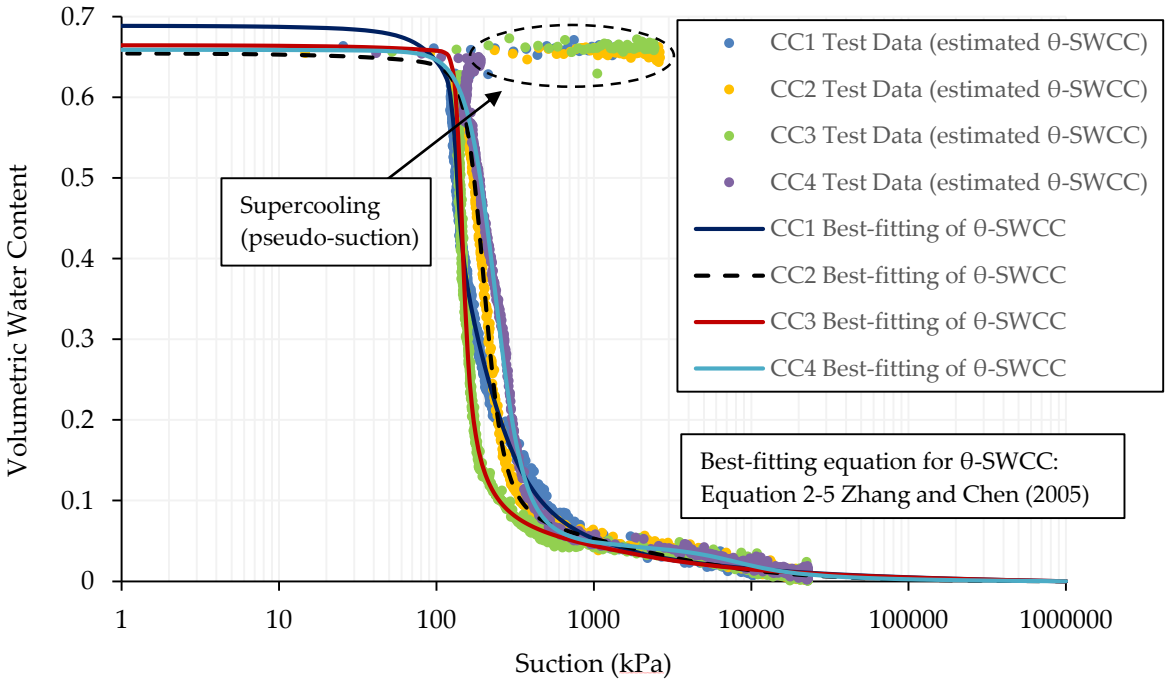

Figure 4-28: Centrifuge Cake Estimated θ-SWCC from the SFCC and Simplified Bimodal Zhang and Chen (2005) Fit (Equation 2-5)

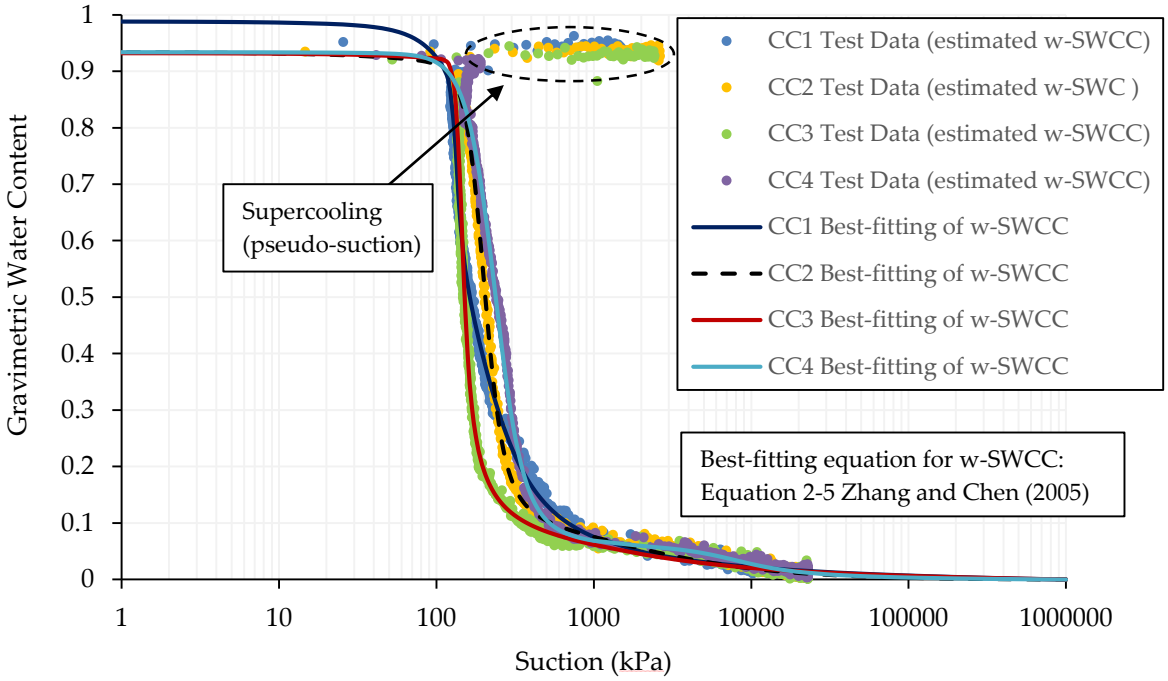

Figure 4-29: Centrifuge Cake Estimated w-SWCC from the SFCC and Simplified Bimodal Zhang and Chen (2005) Fit (Equation 2-5)

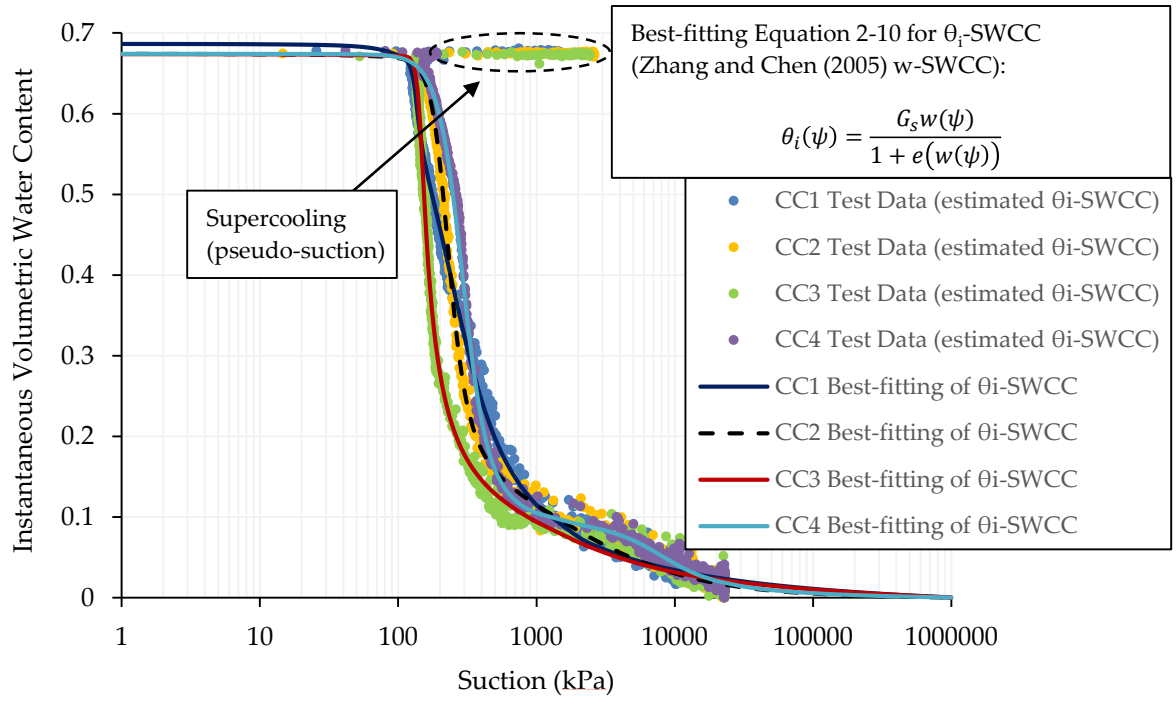

Figure 4-30: Centrifuge Cake Estimated θ_i-SWCCs from the SFCC with Equation 2-10 Fit for Zhang and Chen (2005) w-SFCC fit

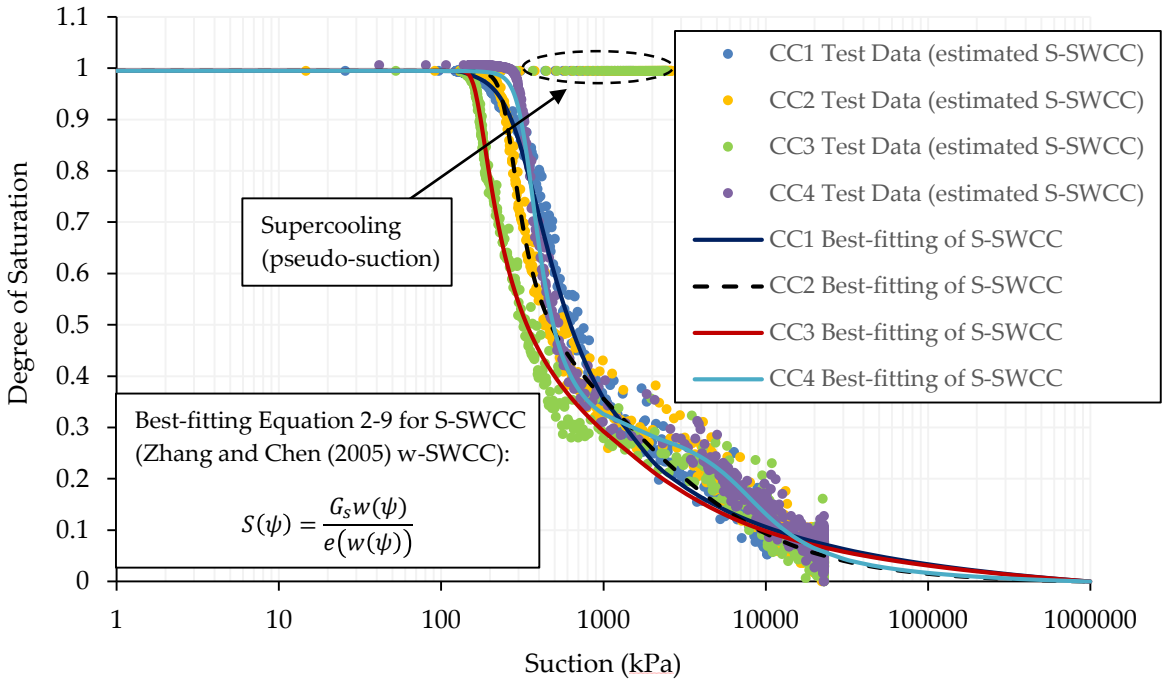

Figure 4-31: Centrifuge Cake Estimated S-SWCCs from the SFCC with Equation 2-9 Fit for Zhang and Chen (2005) w-SWCC Fit

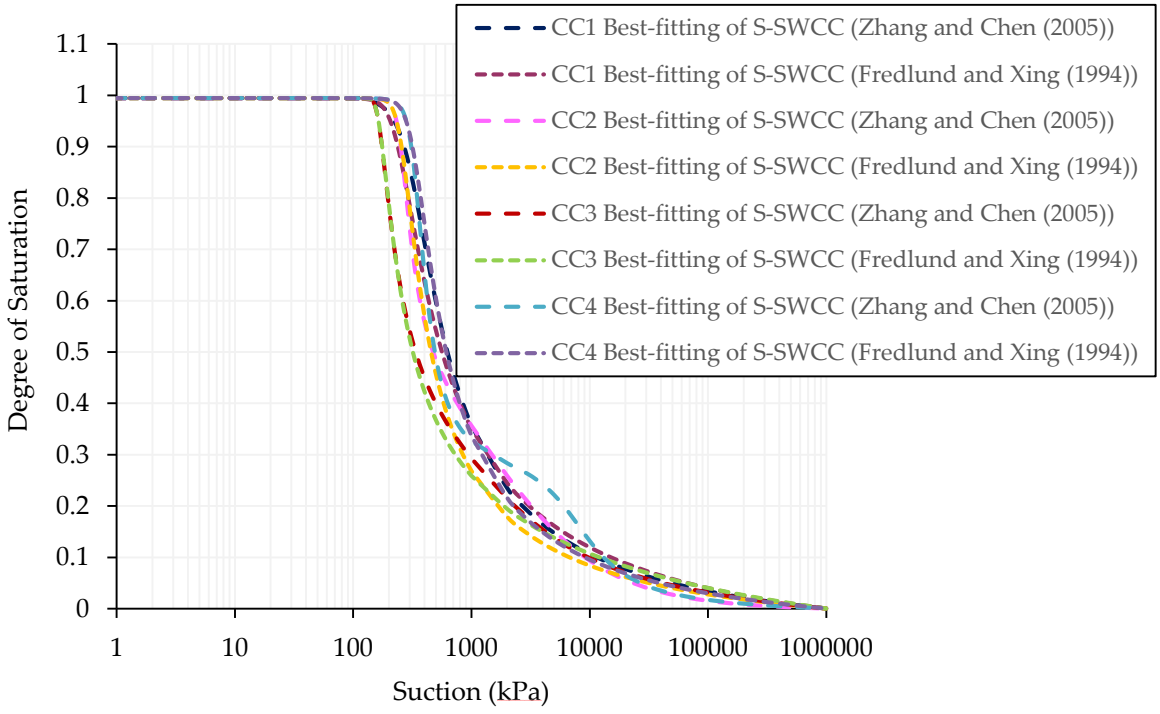

Figure 4-32: Comparison Between Centrifuge Cake Estimated S-SWCCs from the SFCC with Fredlund and Xing (1994) w-SWCC Fit and Zhang and Chen (2005) w-SWCC Fit

Table 4-13: Best-fitting Parameters for Fredlund and Xing (1994) (Equation 2-4) for Centrifuge Cake

Sample	a_f (kPa)	n_f	m_f	ψ_r (kPa)	w_s
CC1	132.865	6.152	0.972	618.081	0.988
CC2	177.879	9.395	0.935	291.655	0.934
CC3	138.858	24.409	0.697	618.149	0.932
CC4	196.183	6.283	1.049	643.162	0.934

Table 4-14: Best-fitting Parameter for Zhang and Chen (2005) (Equation 2-5) for Centrifuge Cake

Sample	a_{f1} (kPa)	a_{f2} (kPa)	n_{f1}	n_{f2}	m_{f1}	m_{f2}	ψ_{rb} (kPa)	p	w_s
CC1	129.742	161.518	28.915	3.329	0.770	1.189	705.450	0.407	0.988
CC2	192.470	1523.662	7.266	0.812	7.863	2.105	1657.540	0.878	0.934
CC3	139.082	1523.434	22.738	1.188	0.799	1.769	1657.389	0.965	0.932
CC4	231.272	6592.687	4.639	2.760	2.250	1.003	4700.570	0.936	0.934

Table 4-15: AEV Estimated From S-SWCC for Zhang and Chen (2005) w-SWCC

Sample	AEV (kPa)
CC1	236
CC2	232
CC3	155
CC4	285
Traditional Methods	1449

5 COMPARISON BETWEEN THE ESTIMATED AND MEASURED SWCC

5.1 Copper Tailings

A comparison between the SWCCs estimated from the SFCC and the SWCCs determined using traditional methods are provided in Figure 5-1 to Figure 5-3. High volume change property functions were used to attain the θ_i-SWCC and the S-SWCC. Temperatures are shown on the S-SWCC to aid in visualizing the comparison to the SFCC. For simplicity, only the best-fitting curves are provided. The gravimetric best-fitting curve fits were attained using Equation 2-5. The θ_i-SWCC best-fitting curves were attained using Equation 2-10. The S-SWCC best-fitting curves were attained using Equation 2-9.

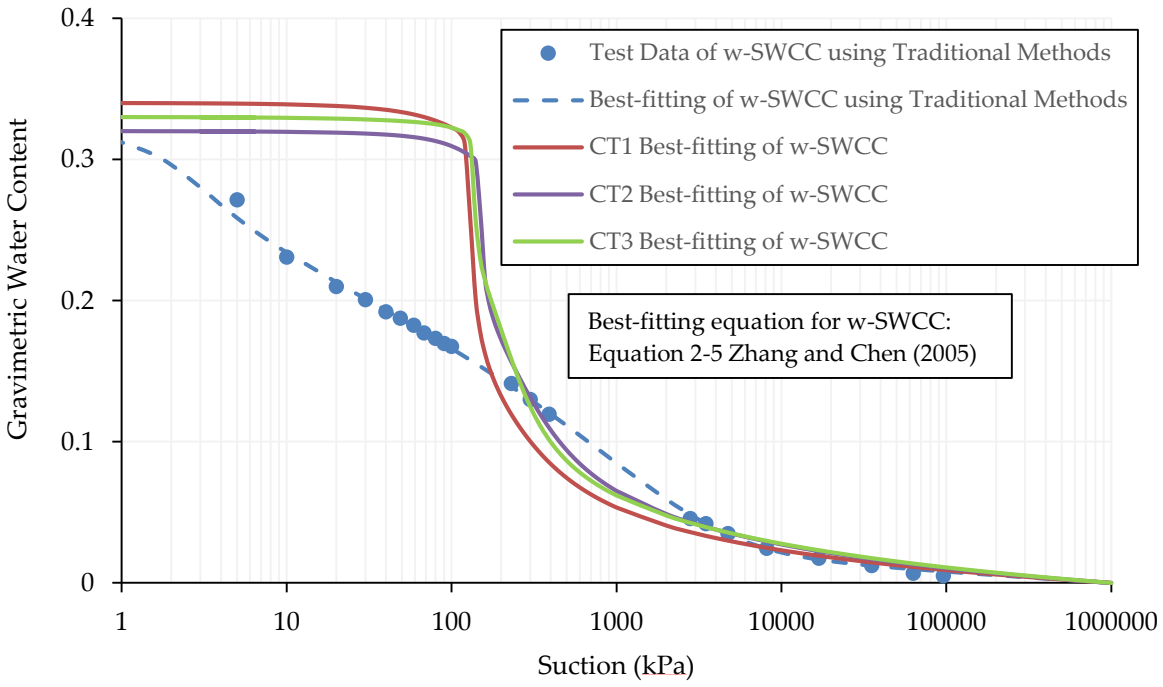

Figure 5-1: Comparison Between w-SWCC Estimated from SFCC and w-SWCC Determined using Traditional Methods for Copper Tailings (Equation 2-5 Zhang and Chen (2005))

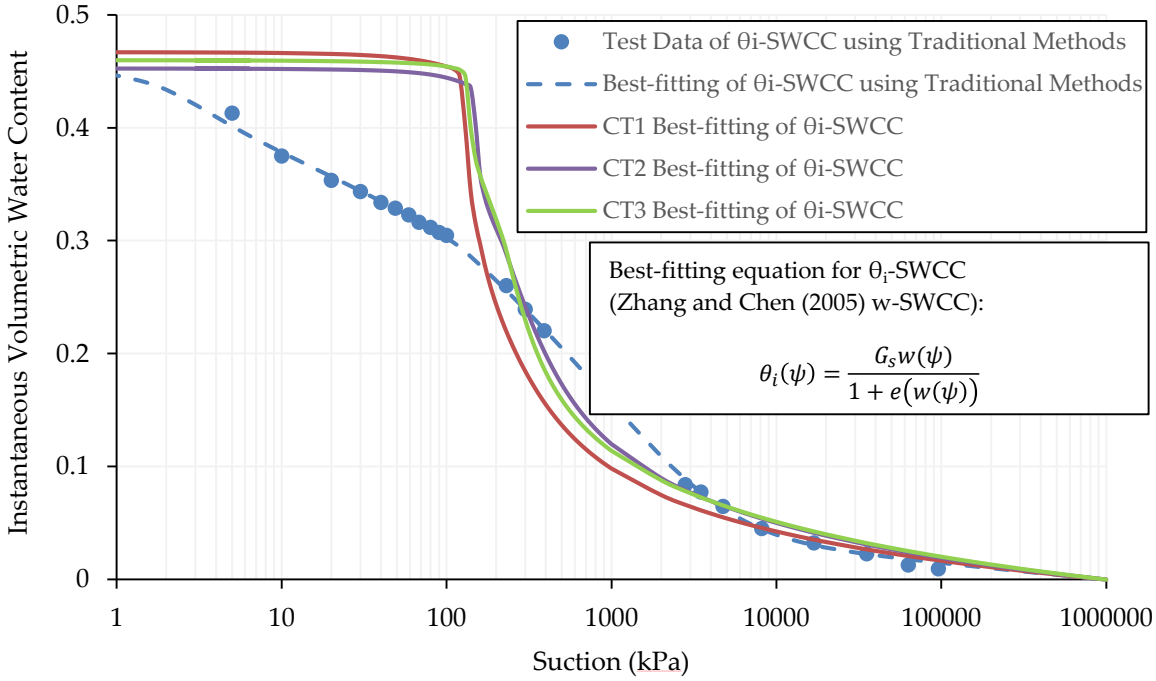

Figure 5-2: Comparison Between θi-SWCC Estimated from SFCC and θi-SWCC Determined using Traditional Methods for Copper Tailings

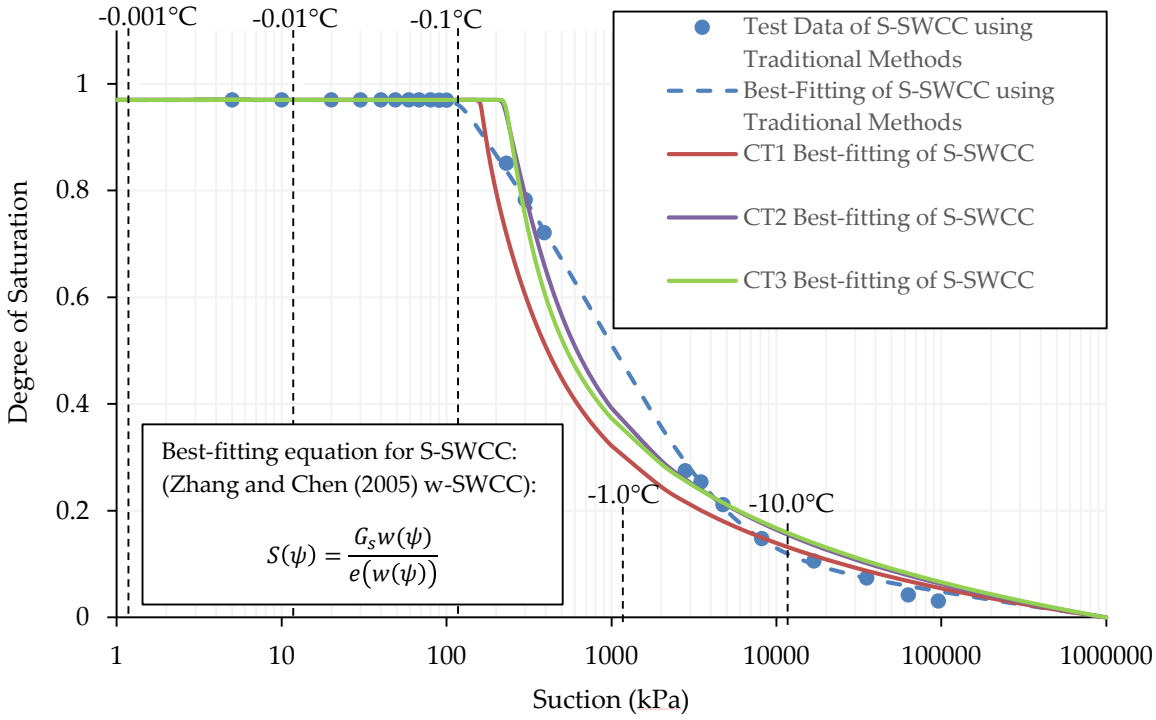

Figure 5-3: Comparison Between S-SWCC Estimated from SFCC and S-SWCC Determined using Traditional Methods for Copper Tailings

The TDR calibration used to determine the unfrozen water content from the dielectric constant has a large impact on the shape of the resulting estimated SWCC. To demonstrate this principle, the estimated S-SWCC for Sample CT2 is shown in Figure 5-4 using the Topp et al. (1980) calibration, the Smith and Tice (1988) calibration, and the soil specific calibration. For comparison purposes, the S-SWCC determined using traditional methods is also shown in Figure 5-4. This shows the high reliance of the estimated SWCC on the TDR calibration.

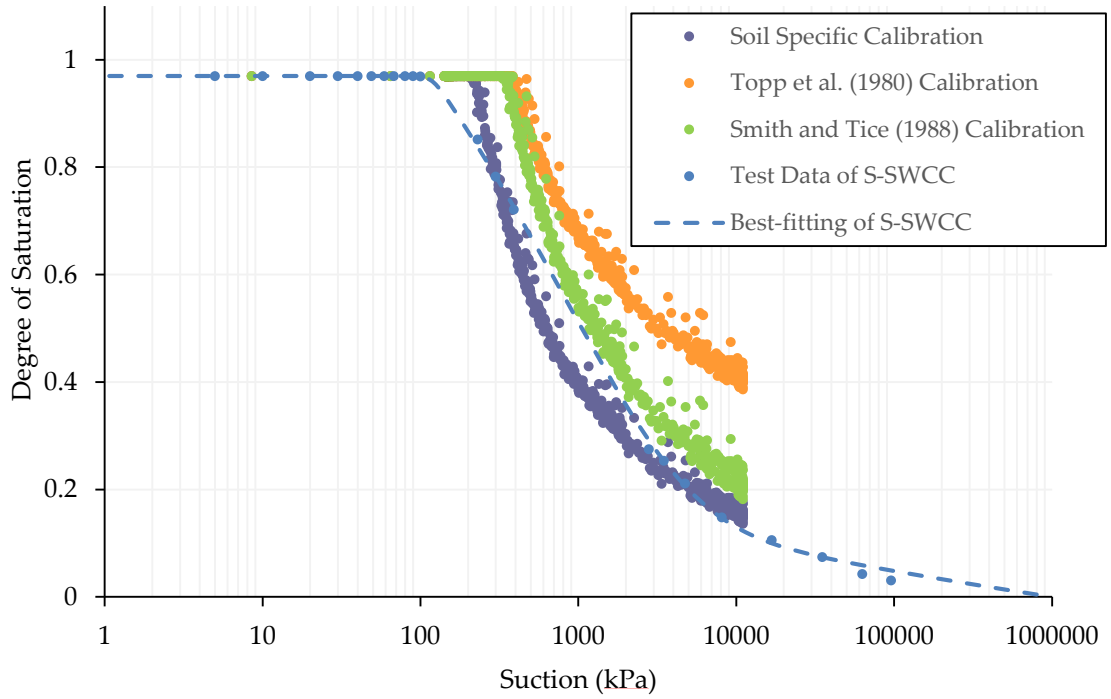

Figure 5-4: Impact of TDR Calibration on the Estimated S-SWCC from the SFCC for Sample CT2

5.2 Gold Tailings

A comparison between the SWCCs estimated from the SFCC and the SWCCs determined by Zhang (2016) are provided in Figure 5-5 to Figure 5-7. High volume change property functions were used to attain the θ_i-SWCC and the S-SWCC. Temperatures are shown on the S-SWCC to aid in visualizing the comparison to the SFCC. For simplicity, only the best-fitting curves are provided. The gravimetric best-fitting curve fits were attained using Equation 2-4. The θ_i-SWCC best-fitting curves were attained using Equation 2-10. The S-SWCC best-fitting curves were attained using Equation 2-9.

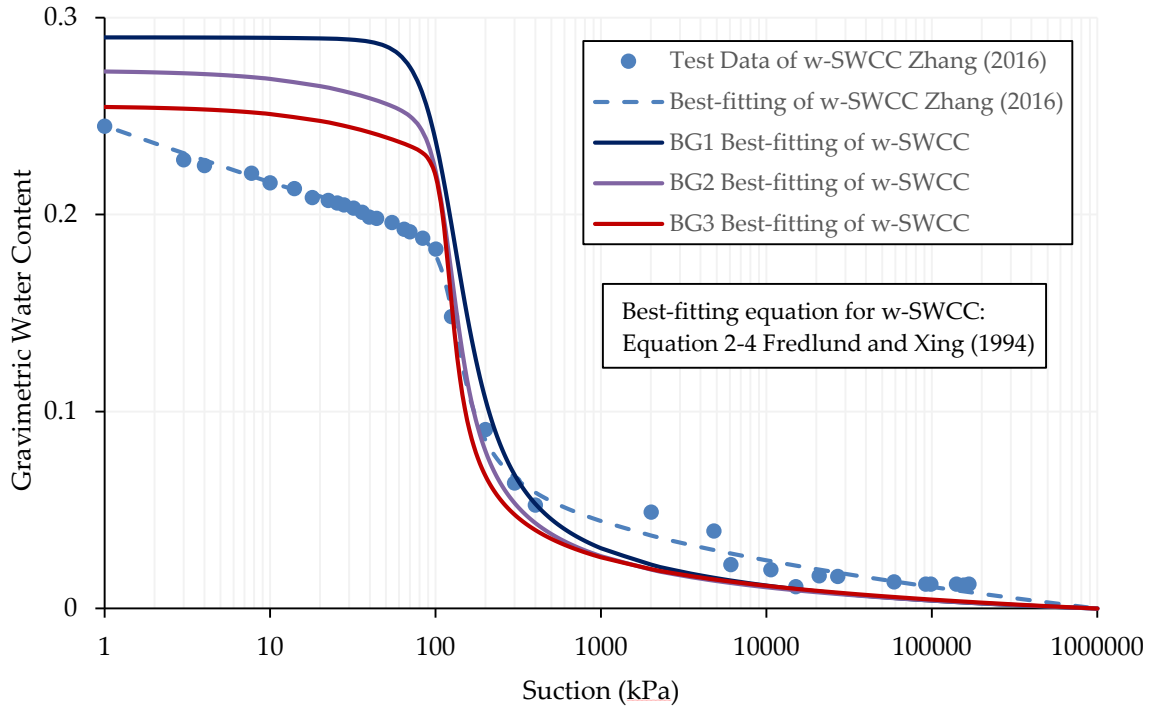

Figure 5-5: Comparison Between w-SWCC Estimated from SFCC and w-SWCC Determined using Traditional Methods for Gold Tailings (Equation 2-5 Fredlund and Xing (1994))

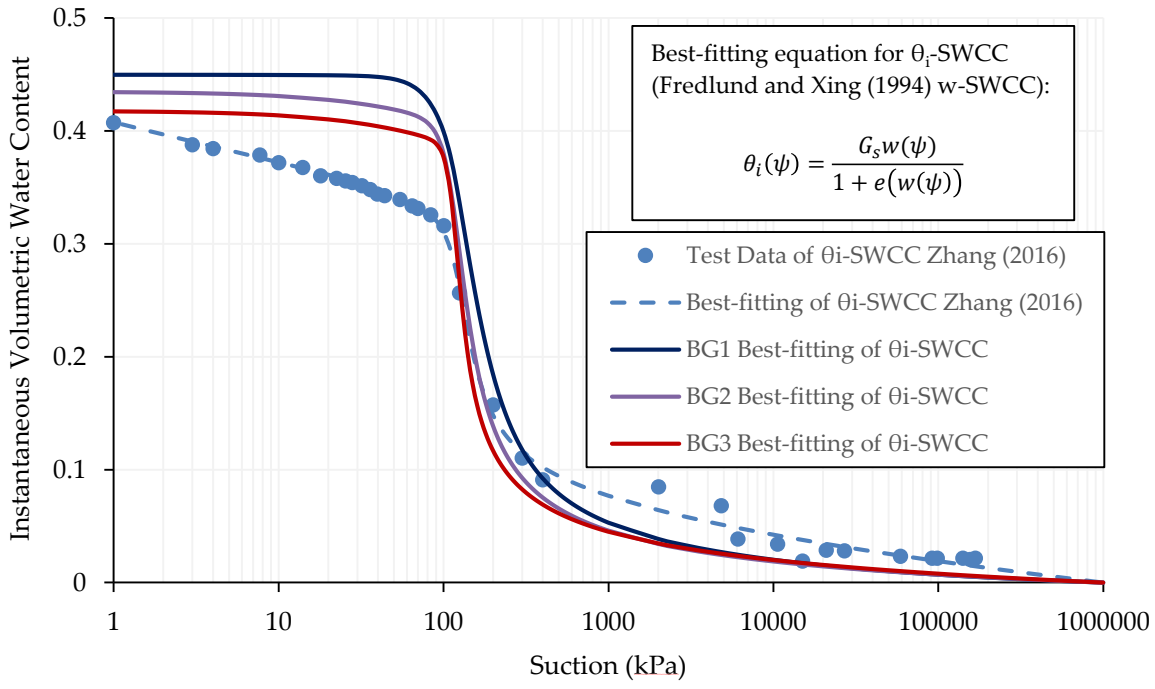

Figure 5-6: Comparison Between θi-SWCC Estimated from SFCC and θi-SWCC Determined using Traditional Methods for Gold Tailings

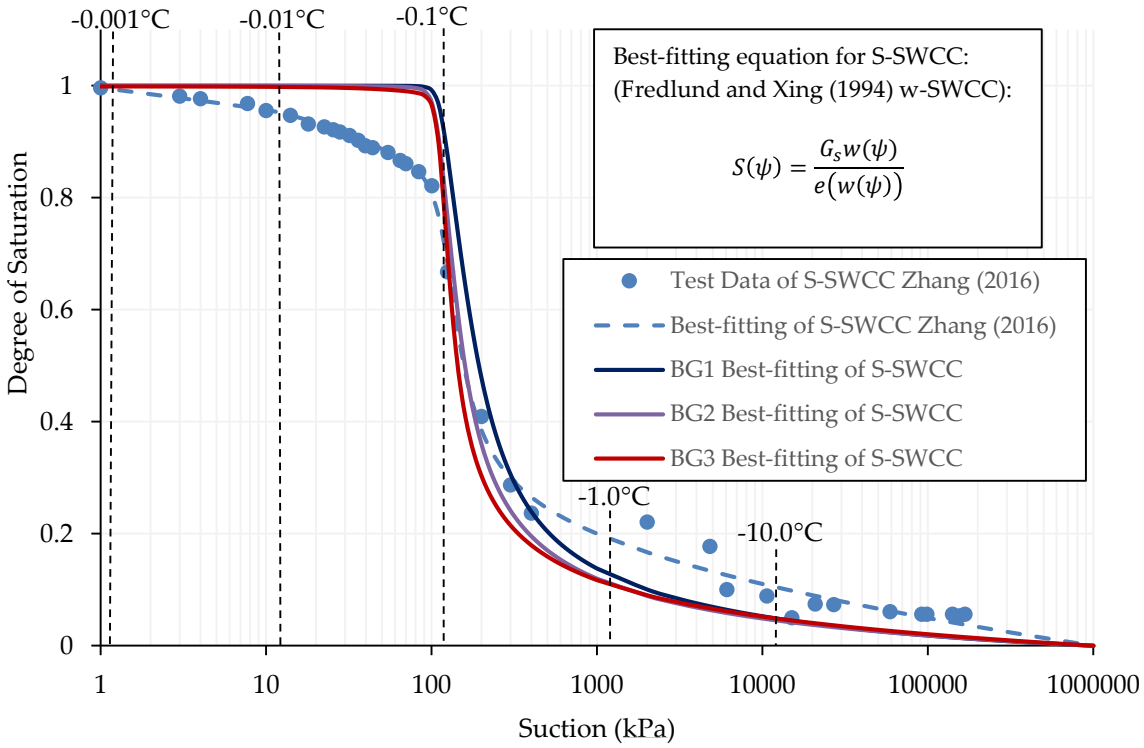

Figure 5-7: Comparison Between S-SWCC Estimated from SFCC and S-SWCC Determined using Traditional Methods for Gold Tailings

The TDR calibration used to determine the unfrozen water content from the dielectric constant has a large impact on the shape of the resulting estimated SWCC. To demonstrate this principle, the estimated S-SWCC for Sample BG1 is shown in Figure 5-8 using the Topp et al.(1980) calibration, the Smith and Tice (1988) calibration, and the soil specific calibration. For comparison purposes, Zhang's data is also shown in Figure 5-8. As the Smith and Tice (1988) calibration provided a better fit to the data presented by Zhang (2016), the soil specific calibration was altered to mimic the conditions of the Smith and Tice (1988) calibration at a volumetric water content of zero. This altered calibration is shown on Figure 5-8. This shows the high reliance of the estimated SWCC on the TDR calibration, especially at low water contents or saturation where it is very difficult to properly mix samples for calibration purposes.

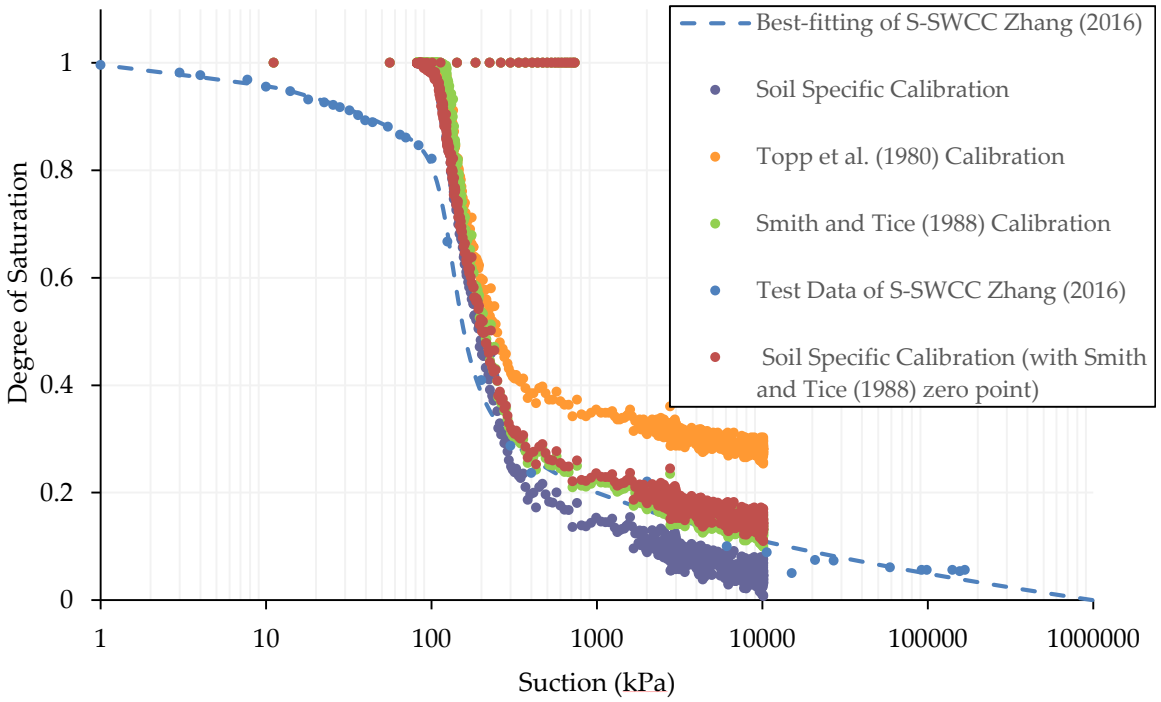

Figure 5-8: Impact of TDR Calibration on the Estimated S-SWCC from the SFCC for Sample BG1

5.3 Centrifuge Cake

A comparison between the SWCCs estimated from the SFCC and the SWCCs determined using traditional methods are provided in Figure 5-9 to Figure 5-11. High volume change property functions were used to attain the θ_i-SWCC and the S-SWCC. Temperatures are shown on the S-SWCC to aid in visualizing the comparison to the SFCC. For simplicity, only the best-fitting curves are provided. The gravimetric best-fitting curve fits were attained using Equation 2-5. The θ_i-SWCC best-fitting curves were attained using Equation 2-10. The S-SWCC best-fitting curves were attained using Equation 2-9.

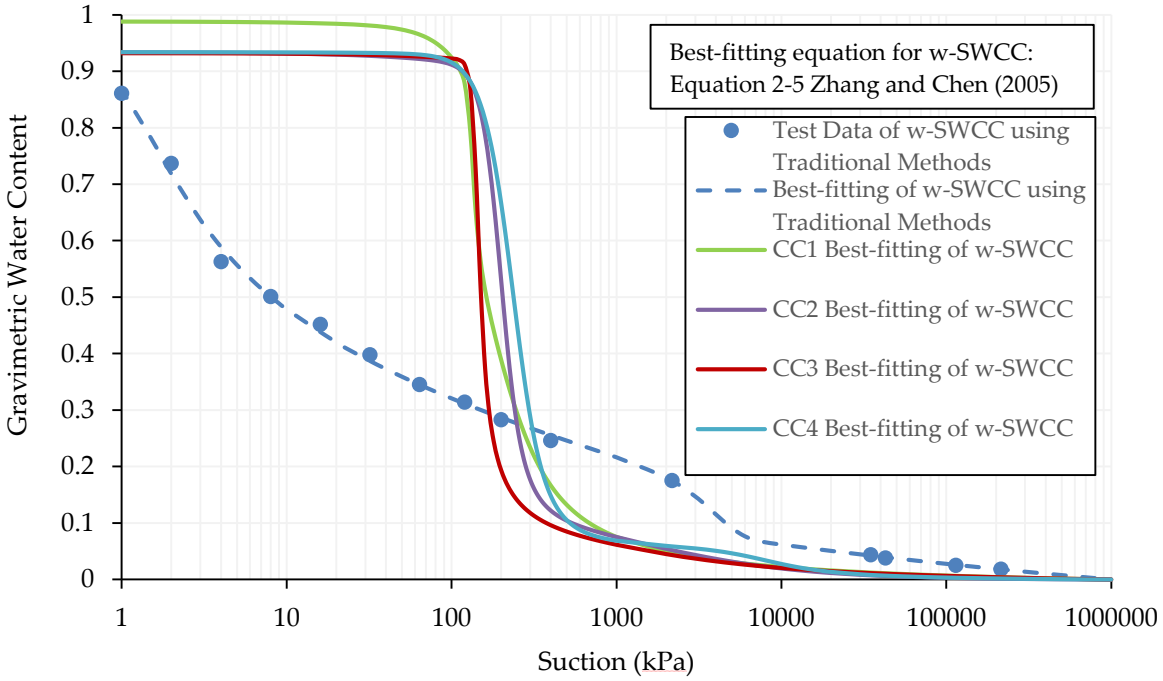

Figure 5-9: Comparison Between w-SWCC Estimated from SFCC and w-SWCC Determined using Traditional Methods for Centrifuge Cake (Equation 2-5 Zhang and Chen (2005))

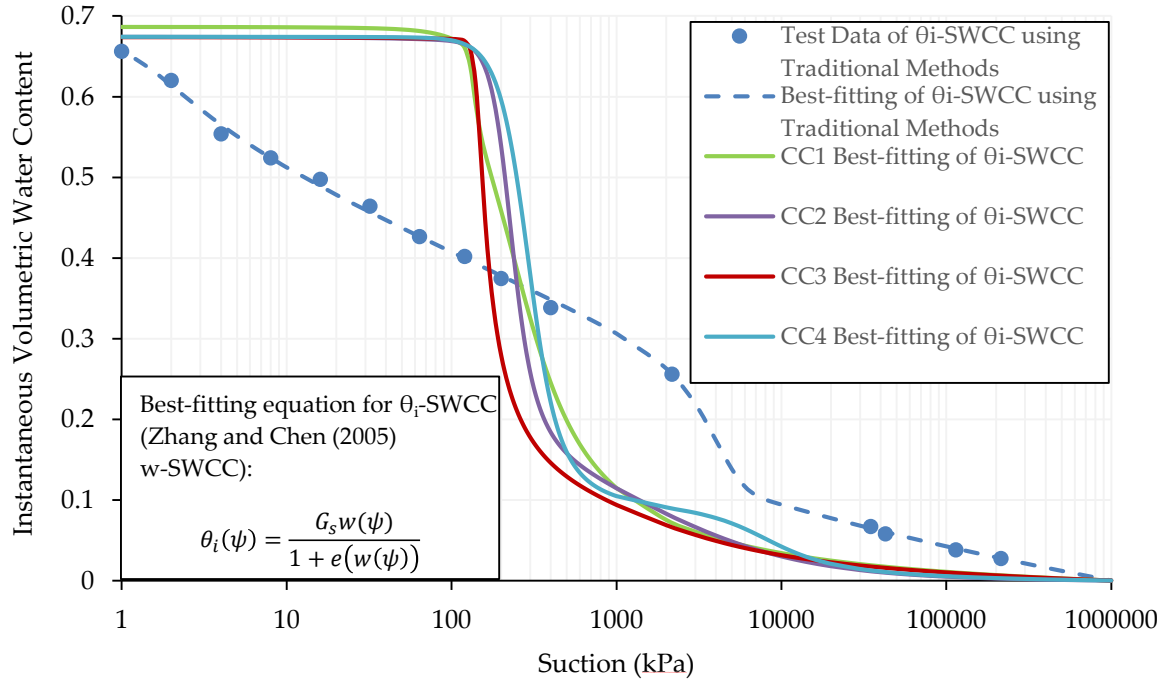

Figure 5-10: Comparison Between θi-SWCC Estimated from SFCC and θi-SWCC Determined using Traditional Methods for Centrifuge Cake

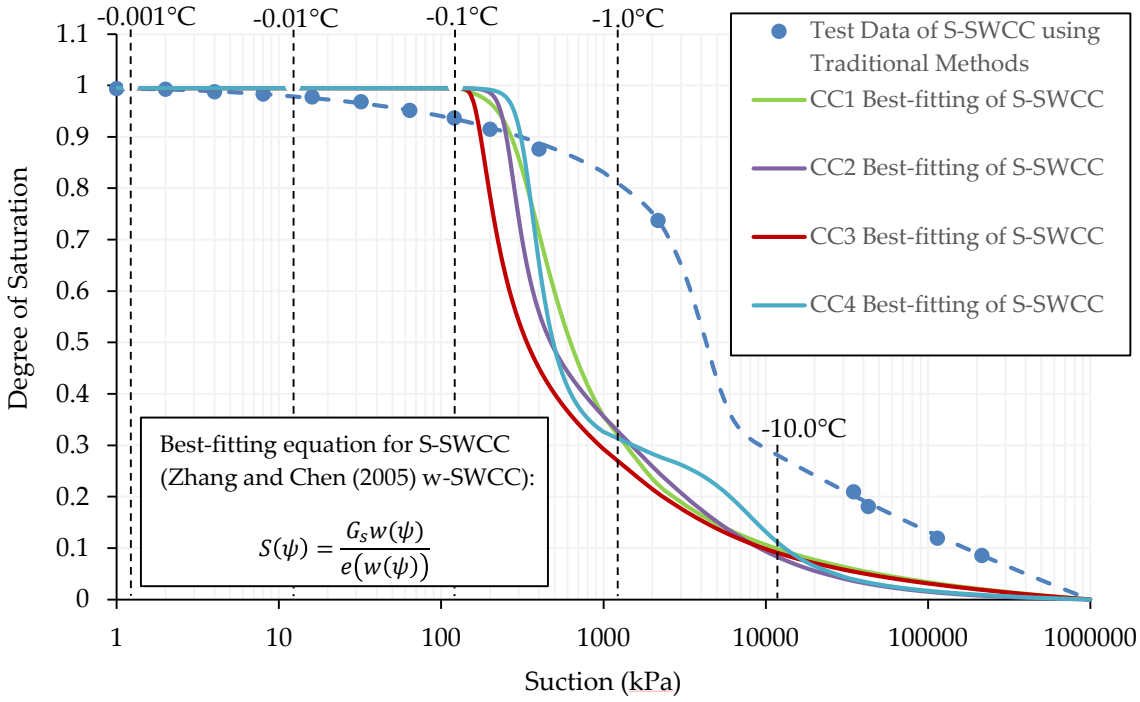

Figure 5-11: Comparison Between S-SWCC Estimated from SFCC and S-SWCC Determined using Traditional Methods for Centrifuge Cake

The TDR calibration used to determine the unfrozen water content from the dielectric constant has a large impact on the shape of the resulting estimated SWCC. To demonstrate this principle, the estimated S-SWCC for Sample CC1 is shown in Figure 5-12 using the Topp et al. (1980) calibration, the Smith and Tice (1988) calibration, Sorta et al. (2013) calibration and the soil specific calibration. For comparison purposes, the S-SWCC determined used traditional methods is also shown in Figure 5-12. This shows the high reliance of the estimated SWCC on the TDR calibration.

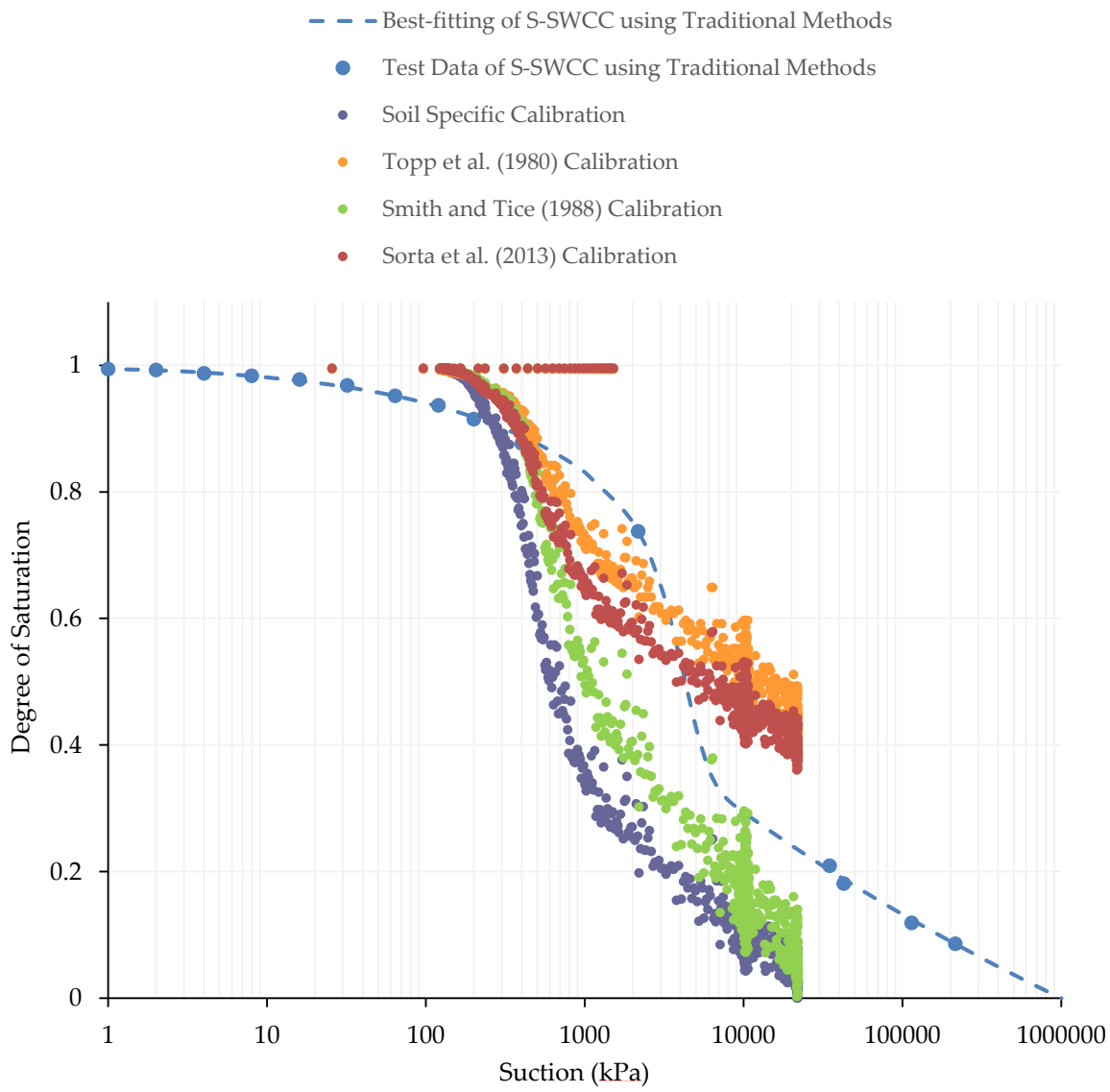

Figure 5-12: Impact of TDR Calibration on the Estimated S-SWCC from the SFCC for Sample CC1

6 DISCUSSION

6.1 Devon Silt

SFCC testing was performed on Devon silt to validate the experimental apparatus and method. The SWCC for the Devon silt was estimated from the SFCC results and compared to the results presented by Azmatch et al. (2012a, 2012b) and Zhang (2016). A good fit was attained with the θ-SWCC presented by Azmatch et. al (2012a, 2012b) for five of the six samples as shown in Figure 3-20. High volume change property functions were applied to the experimental data to attain the θ_i-SWCC and the S-SWCC to allow for comparison to the data presented by Zhang (2016) as shown in Figure 3-21 to Figure 3-23 . The AEV value varied greatly between the six samples ranging from 410 kPa to 3182 kPa. If Sample DS8 is eliminated, the AEV ranged from 410 kPa to 815 kPa. The AEV determined by Zhang (2016) was 593 kPa.

Errors in TDR measurements may occur when there are air gaps between the probe and the soil when the probe is inserted into the soil, which can result in significant underestimation of the K_a of the soil (Sorta et al. 2013, Topp and Davis 1985). Air gaps may also develop after installation due to shrinkage and swelling (Topp and Davis 1985). The Devon silt was consolidated to a pressure of 100 kPa prior to testing resulting in a solid free standing sample with water contents that ranged from approximately 20 percent to 25 percent, which is close to the Devon silt's plastic limit of 20 percent. As a result, it is suspected that air gaps are responsible for the variation in the AEV. It should also be noted that the research conducted by Azmatch et al. (2012b) showed that the ice entry value (IEV) increased with a decrease in the initial void ratio. The IEV is considered to be an analogue for the AEV and is the suction or temperature that ice first begins to enter the largest pores in the soil (Azmatch et al. 2012b). This may have also contributed to the variation in the AEV.

Variation was also observed between the experimental data and the data presented by Zhang (2016) at higher suctions. In the higher suction range, Zhang's best fitting curve yields a lower water content/degree of saturation for a given suction. This is attributed to the use of Topp et al.'s (1980) TDR calibration to attain the θ_u from the K_a, which generally results in an

overestimation of the unfrozen volumetric water content. This is a result of the calibration being conducted on an unfrozen soil and then applied to a frozen or partially frozen soil (Flerchinger et al. 2006, Seyfried and Murdock 1996, Spaans and Baker 1995, Watanabe and Wake 2009, Zhou et al. 2014). The calibration conducted by Smith and Tice (1988) was used to determine the S-SWCC for Sample DS4 for comparison to the Topp et al. (1980) calibration and Zhang's (2016) S-SWCC as shown in Figure 3-24. A better fit to the Zhang (2016) S-SWCC was attained using the Smith and Tice (1988) calibration. The Smith and Tice (1988) calibration was conducted under freezing conditions using NMR and TDR, which is likely the reason that a better fit was attained. The impact of the TDR calibration on the resulting estimated SWCC is discussed further in Section 6.5.

6.2 Copper Tailings

SFCC testing was performed on three samples of copper tailings. The results were used to estimate the θ-SWCC, w-SWCC, θ_i-SWCC, and the S-SWCC. The results of the testing on the three samples further showed that this method was repeatable and reliable for a material with a mixture of coarse and fine material as the estimated SWCCs all yielded similar curves. The AEV for the three samples estimated from the S-SWCCs ranged from 161 kPa to 224 kPa. The estimated SWCCs were compared to the results presented by Zhang (2016) as shown in Figure 5-1 to Figure 5-3. Overall, a good fit was attained between the estimated S-SWCCs and the S-SWCC determined using traditional methods, particularly in the high suction range. The AEV determined using traditional methods from the S-SWCC was 122 kPa, which is approximately 39 kPa to 102 kPa less than the AEVs determined for Sample CT1, CT2, and CT3. Additionally, the slope of the estimated S-SWCCs and the S-SWCC determined using traditional methods differed. The difference in the AEVs and the slopes is thought to be due to one of the following (or a combination):

- The copper tailings were assumed to be colloidal due to the clay content of the material. As a result, a soil dependent constant of 1.0 was used for this material. Due to the mixture of coarse and fine sized particles present in this material, it is possible that it cannot be simply classified as a colloidal or colloid-free soil. As discussed by Koopmans and Miller

(1966), the soil dependent constant for a material that is a mixture of these two extreme types will be somewhere in between 1.0 and 2.2. Ultimately, the soil dependent constant that is utilized for the material will impact the AEV determined from the S-SWCC. To demonstrate this, the S-SWCC has been determined for Sample CT2 with soil dependent constants (SDC) of 1.0, 1.5, and 2.2 as shown in Figure 6-1. The soil dependent constant of 1.5 appears to provide the best fit to the SWCC determined using traditional methods in terms of the AEV. Based on this, it may be likely that the soil dependent constant for the copper tailings is in between 1.0 and 2.2.

- As shown by Figure 5-4, the Topp et al. (1980) calibration, the Smith and Tice (1988) calibration, and the soil specific calibration yielded very different S-SWCCs. This calibration was developed by testing unfrozen samples and then applying the calibration to frozen or partially frozen conditions. Samples were tested for gravimetric water contents greater than 15 percent. The lower bound of the calibration curve was determined based on the Smith and Tice (1988) calibration. The calibration conducted by Topp et al. (1980) and Smith and Tice (1988) was used to determine the S-SWCC for Sample CT1 as shown in Figure 5-4. Overall, the Smith and Tice (1988) calibration and the soil specific calibration provided the best fit to the S-SWCC determined using traditional methods. However, the Topp et al. (1980) calibration had the closest slope to the S-SWCC determined using traditional methods. This suggests that the calibration for freezing conditions for this material is somewhere in between these three calibrations. The impact of the TDR calibration will be discussed further in Section 6.5.

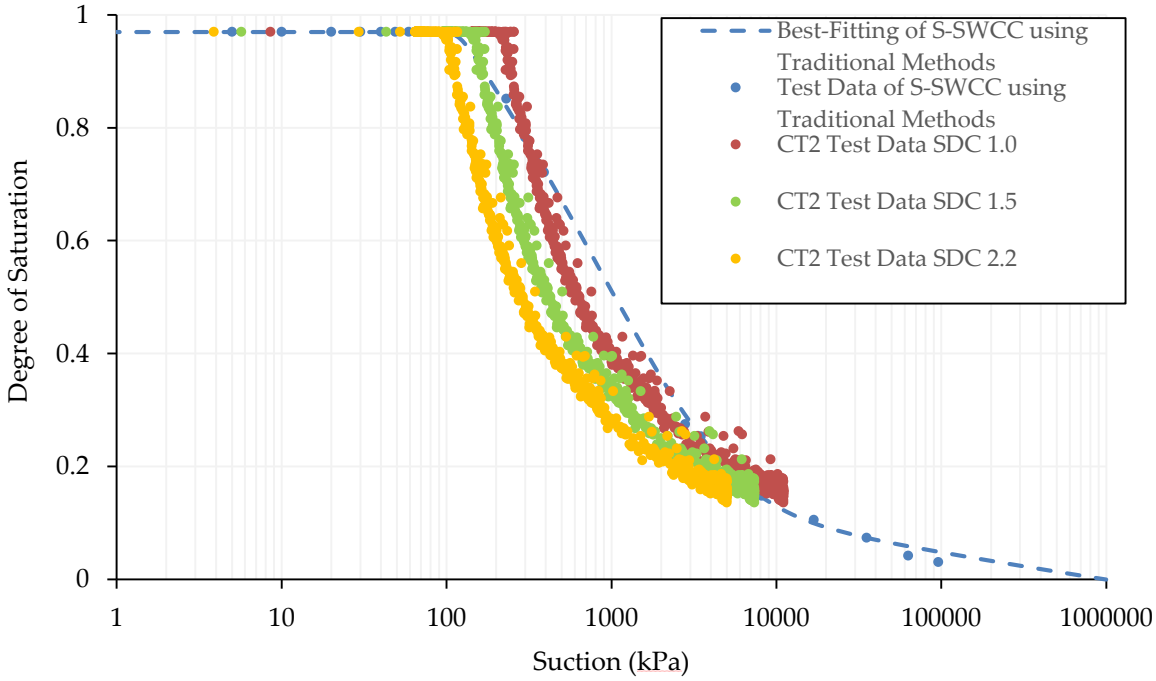

Figure 6-1: S-SWCC for Sample CT2 with Different Soil Dependent Constants

After the completion of the freezing and thawing test on the copper tailings samples, there was free water present as shown in Figure 6-2. This suggests that there may have been significant ice lensing during the freezing process, which may have resulted in the movement of probes and contributed to variation in the results between samples.

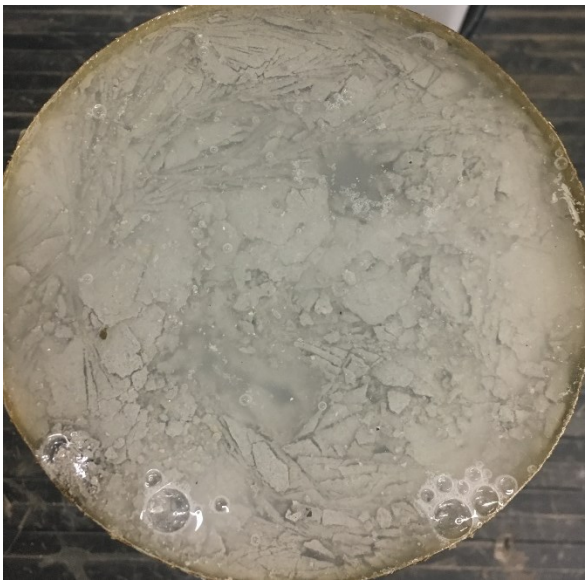

Figure 6-2: Sample CT2 Following Completion of Freezing

6.3 Gold Tailings

SFCC testing was performed on three samples of gold tailings. The results were used to estimate the θ-SWCC, w-SWCC, θ_i-SWCC, and the S-SWCC. The results of the testing on the three samples further showed that this method was repeatable and reliable for a slurry as the estimated SWCCs all yielded similar curves. All three samples exhibited an abrupt change in slope in the range of 70 kPa to 100 kPa. This is thought to be a result of volume change occurring during the freezing process as the new slope corresponds with the AEV determined from the S-SWCC. Interestingly, this observation was not made with any of the other materials tested and is likely a result of the minimal amount of clay present in the sample, which allowed for the volume change to occur more rapidly than in the other samples. In general, it is assumed that zero volume change occurs during the freezing process and the θ_u-SWCC and the w_u-SWCC are equivalent to the θ-SWCC and the w-SWCC, respectively. Regardless of if the transition in slope is due to volume change or not, the results from the SFCC testing would be the same.

The AEV for the three samples estimated from the S-SWCCs ranged from 102 kPa to 108 kPa. The estimated SWCCs were compared to the results presented by Zhang (2016) as shown in Figure 5-5 to Figure 5-7. Overall, a good fit was attained between the estimated SWCCs and the results presented by Zhang (2016). The best-fitting curves all had similar slopes. The AEV determined

by Zhang (2016) was 86 kPa, which is approximately 16 kPa to 22 kPa less than the AEVs determined for Sample BG1, BG2, and BG3.

Variation was observed between the experimental data and the data presented by Zhang (2016) at higher suctions. In the higher suction range, Zhang's best fitting curve yields a higher water content/degree of saturation for a given suction. This is attributed to the soil specific TDR calibration used for the gold tailings. This calibration was developed by testing unfrozen samples and then applying the calibration to frozen or partially frozen conditions. Samples were tested for gravimetric water contents greater than 15 percent. The lower bound of the calibration curve was determined based on the K_a value of the gold tailings at temperatures less than -15°C where the gold tailings were considered completely frozen with an unfrozen water content of zero. This assumption was not made for the copper tailings or the centrifuge cake as these materials have a significant clay content. As a result, it was assumed that these tailings would have adsorbed water present at -15°C where as the gold tailings wouldn't due to the very low clay content. The calibration conducted by Topp et al. (1980) and Smith and Tice (1988) was used to determine the S-SWCC for Sample BG1 as shown in Figure 5-8. The Smith and Tice (1988) calibration provided the best fit to the Zhang (2016) S-SWCC. As a result, the soil specific calibration was altered to mimic the conditions of the Smith and Tice (1988) calibration at a volumetric water content of zero for Sample CT2 in Figure 5-8 where the dielectric constant at a volumetric water content of zero was changed from 5.2 to 4.1. As can be seen in Figure 5-8, this very minor change has a huge impact on the resulting S-SWCC and changes the degree of saturation by as much as 10 percent in the higher suction range. Ultimately, the better fit with the Smith and Tice (1988) calibration suggests that the assumption made for the lower bound of the soil specific TDR calibration was incorrect. This could be due to two potential reasons:

- The gold tailings do not completely freeze and there is always some degree of unfrozen water present in the sample. As a result, the assumption of a water content of zero percent at a temperature of -15°C is incorrect.
- The TDR has a lower bound K_a value below which it cannot measure.

The impact of the TDR calibration on the resulting estimated SWCC is discussed further in Section 6.5.

As shown in Figure 6-3, free water was not released during the freezing and thawing of the gold tailings. This suggests that there was not significant ice lensing during the freezing and thawing process of the gold tailings. As a result, there is less variation in the results of the testing on the gold tailings compared to the copper tailings.

Figure 6-3: Sample BG3 Following Completion of Freezing

6.4 Centrifuge Cake

SFCC testing was performed on four samples of centrifuge cake. The results were used to estimate the θ-SWCC, w-SWCC, θ_i-SWCC, and the S-SWCC. The results of the testing on the four samples further showed that this method was repeatable and reliable for a slurry as the estimated SWCCs all yielded similar curves; however, more variation was observed between the four samples compared to the copper tailings and the gold tailings samples. This is likely a result of the high gravimetric water content (approximately 93 percent) of the centrifuge cake. This has two direct impacts:

- Increased probability of movement of probes after insertion; and,
- Increased water migration and potential for ice pockets to develop adjacent to probes.

The AEV for the four samples ranged from 155 kPa to 285 kPa. The estimated SWCCs were compared to the SWCCs determined used traditional methods as shown in Figure 5-9 to Figure 5-11. A poor fit was attained between the estimated SWCCs and the SWCCs determined using traditional methods. The AEV determined from the S-SWCC measured using traditional methods was 1449 kPa. This is significantly higher than the AEVs determined from the S-SWCC estimated from the SFCC for Samples CC1 to CC4.

The mismatch between the SWCCs estimated from the SFCC and the SWCCs determined using traditional methods was suspected to be due to the high initial water content of the tailings. This was based on the results of the investigation conducted by Flerchinger et al. (2006), which suggested that high initial water contents may create difficulties when estimating the SWCC from the SFCC due to the following:

- The influence of solutes is more critical at higher water contents. This is due to the impact on the osmotic potential, which becomes a larger component of the total water potential when the soil is relatively wet.
- The accuracy of temperature measurements is more critical at higher water contents (or near saturation) as a lot of the water freezes over a small temperature range.

To investigate if the high initial water content influenced the resulting estimated SWCCs for the centrifuge cake, SFCC testing was performed on a sample of kaolinite mixed to a water content of approximately 114 percent (Sample K1) and approximately 67 percent (Sample K2). A shrinkage curve was estimated based on the Atterberg limits of the material to attain the S-SWCC for this material. Kaolinite was chosen for this testing as this is the primary clay mineral in the centrifuge cake. The estimated S-SWCC for the two samples is provided in Figure 6-4. A soil specific TDR calibration was not conducted for the kaolinite. Topp et al.'s (1980) calibration was used to estimate the volumetric water content from the dielectric constant. Based on the results

of the testing completed on the kaolinite, it does not appear that the high water content of the centrifuge cake is responsible for the mismatch between the SWCCs estimated from SFCC and the SWCCS measured using traditional methods. If the high water content was responsible for the mismatch, it is expected that this would be reflected in the S-SWCC in Figure 6-4 with Sample K1 shifted to the left of Sample K2. The shape of the S-SWCC for Sample K1 presented in Figure 6-4 is attributed to volume change of the material during freezing and the formation of soil peds due to water migration during freezing. However, the high water content may increase the probability of movement of the RTD and TDR to different locations. Ultimately, this means that the temperature probe reading may not be representative of the actual temperature along the TDR probe resulting in variation between the four centrifuge cake tests. Additionally, the high water content may result in an increased migration of water during freezing and the formation of ice pockets around probes. This process may contribute to variation between tests.

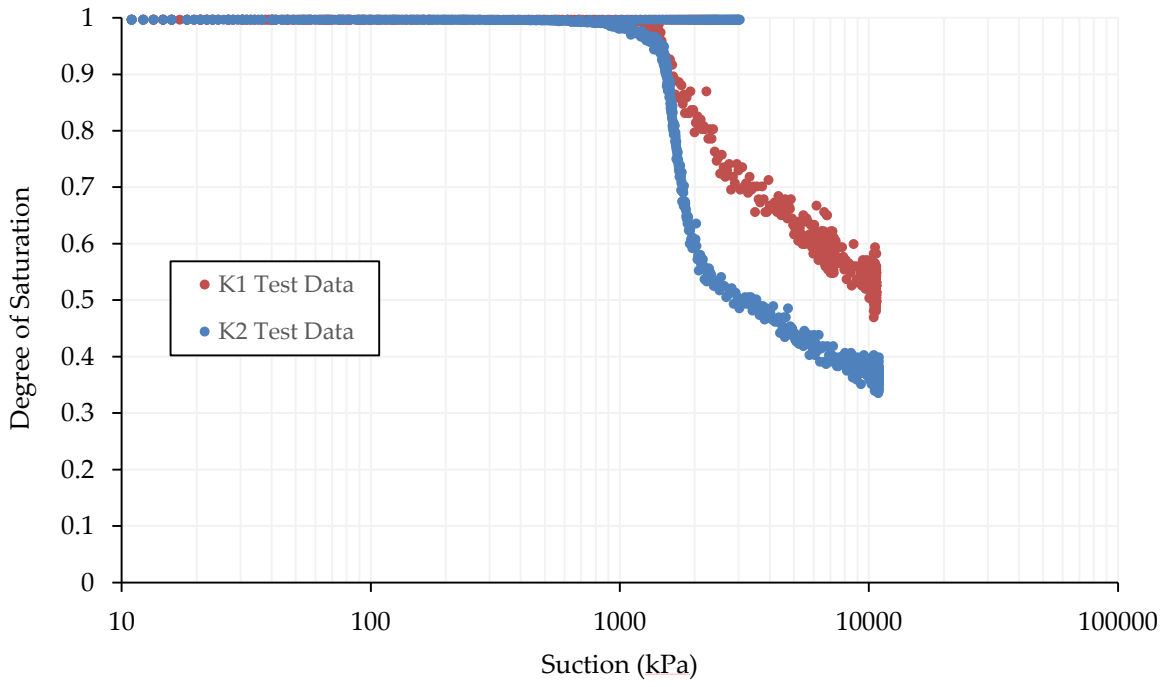

Figure 6-4: Kaolinite Estimated S-SWCC from the SFCC

The calibration conducted by Topp et al. (1980), Smith and Tice (1988), and Sorta et al. (2013) were used to determine the S-SWCC for Sample CC1 as shown in Figure 5-12. The soil specific TDR

calibration and the Smith and Tice (1988) calibration provide very similar curves as expected. The Sorta et al. (2013) and Topp et al. (1980) calibration provide similar results. The soil specific TDR calibration and the Smith and Tice (1988) calibration provide the worst fit of the four calibrations. Smith and Tice (1988) suggested that the K_a for a given θ_u decreases with increasing fines content. As the fines content increases (and the SSA), the amount of adsorbed water will also increase. The adsorbed water has a lower dielectric constant than that of bulk water. The larger proportion of adsorbed water will result in an overall decrease in the K_a at a given θ_u. Smith and Tice's (1988) calibration worked well on a variety of soils with the exception of high SSA soils where the water contents predicted by the calibration were noticeably lower than the corresponding NMR values. As a result, it is likely that the actual calibration is somewhere between the Topp et al. (1980) and Smith and Tice (1988) calibration. Regardless of the TDR calibration, the estimated SWCC from the SFCC will not provide a good fit to the SWCC determined using traditional methods. The impact of the TDR calibration on the resulting estimated SWCC is discussed further in Section 6.5.

After the completion of the freezing and thawing test on the centrifuge cake samples, there was minimal free water present as shown in Figure 6-5. This suggests that there may have been ice lensing during the freezing process, which may have resulted in the movement of probes and contributed to variation in the results between samples.

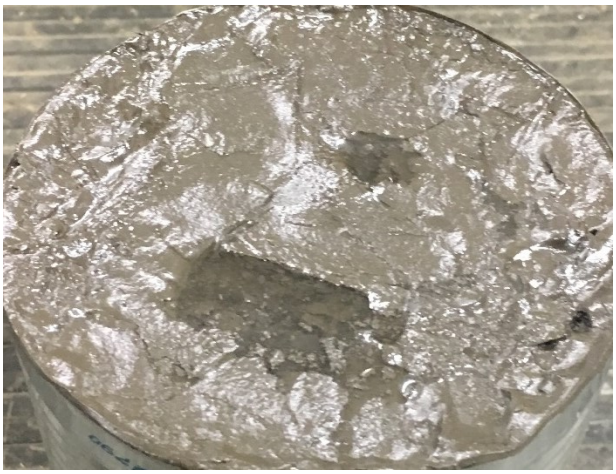

Figure 6-5: Sample CC4 Following Completion of Freezing

6.4.1 Impacts of Salinity on the Centrifuge Cake

A poor fit was observed between the SWCC estimated from the SFCC and the SWCC measured using traditional methods. The poor fit is not thought to be a result of the salinity of the centrifuge cake. In general, solutes tend to shift the SFCC towards lower temperatures (i.e. higher suctions) (Anderson and Morgenstern 1973, Azmatch et al. 2012a). Based on this, it is expected that the SWCC estimated from the SFCC would be shifted to the right of the SWCC measured using traditional methods if the salinity of the centrifuge cake was responsible for the mismatch, which is the opposite of the actual results.

The electrical conductivity of the centrifuge cake was measured to be 3890 μs/cm. Based on the research conducted by Beier (2006), there is an approximate relationship between electrical conductivity (EC) and NaCl concentration as shown in Equation 6-1. Based on this, the NaCl concentration is approximately 2425 mg/L (0.04 mol/L), which is less than the salinity of samples used to study the impacts of salinity on the SFCC. For example, Azmatch et al. (2012a) used Devon silt with a salinity of 5 g/L and Ma et al. (2015a) tested samples with salinities from 0 g/L to 58.44 g/L.

$$C_{NaCl}\left(\frac{\text{mg}}{\text{L}}\right) = 2.55(EC)^2 + 735(EC) - 473 \quad \textbf{6-1}$$

(EC<80 mS/cm)

(Beier 2006)

Cheung (1979) noted that the unfrozen water content of a soil is due to the combined effect of the salt exclusion mechanism and the osmotic pressure of phenomenon. This depends on the salt concentration. The unfrozen water content increases with increasing salt concentration due to the freezing point depression from the physical presence of the salt. In contrast, the unfrozen water content decreases with increasing salt concentration due to reducing osmotic pressure. These two mechanisms are inversely related. Cheung's (1979) results showed that:

- The unfrozen water content is less than that of a salt-free clay at NaCl concentrations of less than 10^{-3} M, and;
- The unfrozen water content is more than that of a salt-free clay at NaCl concentrations of more than 10^{-2} M.

As the NaCl molar concentration of the centrifuge cake is approximately 0.04 mol/L, the centrifuge cake would fall approximately into the second category. Based on this, it would be expected that the unfrozen water content at a given suction for the SWCC estimated from the SFCC would be more than the unfrozen water content at the same suction for the SWCC measured using traditional methods. This behavior was not reflected in the estimated SWCCs and is not responsible for the mismatch in the data. As a result, it is thought that the high water content, clay content, and adsorbed water are responsible for the mismatch between the SWCCs estimated from the SFCC and the SWCC measured using traditional methods.

6.5 Impact of TDR Calibration

The fit of the SWCC estimated from the SFCC with the SWCC measured using traditional methods is highly dependent on the TDR calibration. Without a secondary method, such as NMR, it is not possible to develop a TDR calibration under frozen or partially frozen conditions.

As a result, the TDR calibrations were performed at unfrozen conditions and applied to frozen conditions. This results in a number of complications. The θ_u will generally be overestimated with increasing total water content or increasing SSA due to the following:

- The dielectric constant of ice (3.2) is higher than air (Flerchinger et al. 2006, Spaans and Baker 1995, Watanabe and Wake 2009). When a TDR calibration is conducted under unfrozen conditions, the air phase may be present. When the calibration is then applied to frozen conditions, the air phase (whether or not present) is replaced by the ice phase with a different dielectric constant. These issues will be amplified when the sample is unsaturated prior to the freezing process and there is ice and air present during the freezing process. As the tailings tested were fully saturated, this expected to be a minor contributor to the overestimation of the θ_u.
- The K_a of the soil is influenced by the unfrozen water content, ice content, air, and soil; however, the θ_u is only affected by the temperature (Flerchinger et al. 2006, Seyfried and Murdock 1996, Spaans and Baker 1995, Watanabe and Wake 2009, Zhou et al. 2014). When the sample is fully saturated, as in the case of the tailings, the K_a will be influenced by the unfrozen water content, ice content, and soil during freezing.
- As the SSA of a soil increases, the amount of adsorbed water will increase. The adsorbed water has a lower dielectric constant than the bulk water (Smith and Tice 1988, Watanabe and Wake 2009).

This was clearly observed in the case of the Devon silt where the experimental data showed a higher water content than the measured SWCC data for a given suction using Topp et al.'s (1980) calibration.

The other issue with soil specific TDR calibrations conducted on unfrozen soil is due to the issues associated with testing materials at low water contents. This requires assumptions to be made regarding the dielectric constant of the soil at a water content of zero. The importance of this assumption is clearly shown in the case of the gold tailings where it seems that an incorrect assumption was made regarding this lower bound. While the estimated S-SWCC still provided

a reasonably good fit to the measured S-SWCC, the fit would've been much better if the TDR calibration had been completed under frozen or partially frozen conditions using a secondary method.

Of the four materials tested, it appears that the Smith and Tice (1988) calibration provided a better fit for the Devon silt and gold tailings than the soil specific calibration in the low water content range. For the copper tailings, the Smith and Tice (1988) calibration and the soil specific calibration both provided reasonable fits; however, the fit from the soil specific calibration is considered better based on the AEV. It should be noted that the Smith and Tice (1988) calibration does not provide a good fit in the higher water content range as shown by Figure 4-5 and Figure 4-16. It is unknown if the Smith and Tice (1988) calibration is the best fit for the centrifuge cake due to the poor fit between the estimated SWCC and the measured SWCC. However, it is unlikely that the Smith and Tice (1988) calibration is the best fit for the centrifuge cake due to the high fines content of the centrifuge cake. It is likely that the calibration lies somewhere in between the Smith and Tice (1988) calibration and the Topp et al. (1980) calibration in the low water content range.

After the completion of testing, it was noted that there seemed to be a lower bound K_a value below which the TDR would not read. To investigate this, the K_a value for one sample of each material versus temperature was plotted to determine if they all collapsed to the same value as shown in Figure 6-6. The Devon silt is not included in this figure as the temperature was not lowered far enough to reach the minimum K_a. The minimum K_a value of Sample CT1 (copper tailings) is approximately 5.4 on average with a standard deviation of 0.14 at a temperature of 8.8°C to 9.0°C. The minimum K_a value of Sample BG1 (gold tailings) is approximately 5.5 on average with a standard deviation of 0.13 at a temperature of 18.6°C to 18.8°C. The minimum K_a value of Sample CC1 (centrifuge cake) is approximately 4.4 on average with a standard deviation of 0.14 at a temperature of 18.4°C to 18.6°C. It appears that the K_a does not collapse to a particular value for all materials. This indicates that the K_a value in the low water content range is representative of the actual conditions in all of the different soils. As shown by Figure 5-8, making a very minor change in the dielectric constant has a large impact on the estimated water content.

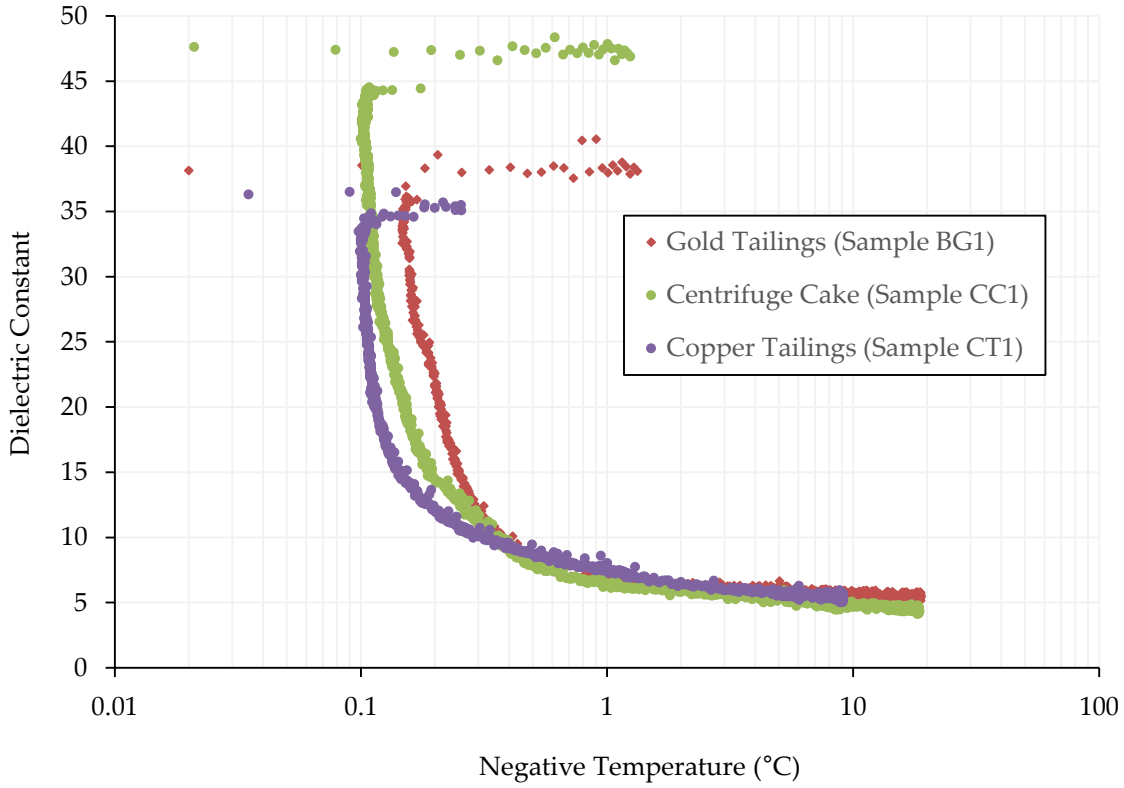

Figure 6-6: Dielectric Constant versus Temperature for Copper Tailings, Gold Tailings, and Centrifuge Cake

A co-blend of MFT and Clearwater shale was prepared for testing; however, testing was unable to proceed as the TDR was unable to take readings of the dielectric constant. This is suspected to be due to the combined effects of the high electrical conductivity of the material and the high degree of adsorption that occurs in this blend. The electrical conductivity of the material was 2490 μs/cm. This material had a significant degree of signal attenuation, which prevents there from being two distinct reflection points for the determination of the apparent length (L_a) and thus the determination of the dielectric constant as discussed in Section 2.6.4. The waveform for the co-blend is shown in Figure 6-7. For comparison purposes, a typical waveform in water is shown in Figure 6-8. This has significant implications to the application of this technology to the oil sands industry.

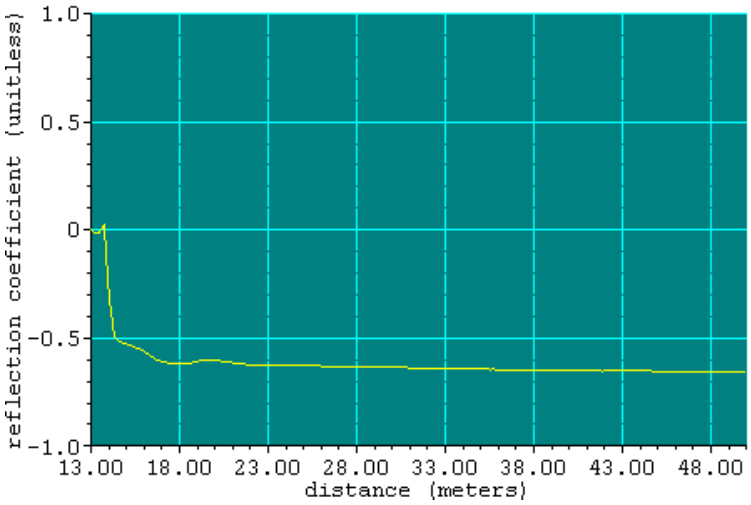

Figure 6-7: Co-blend Waveform

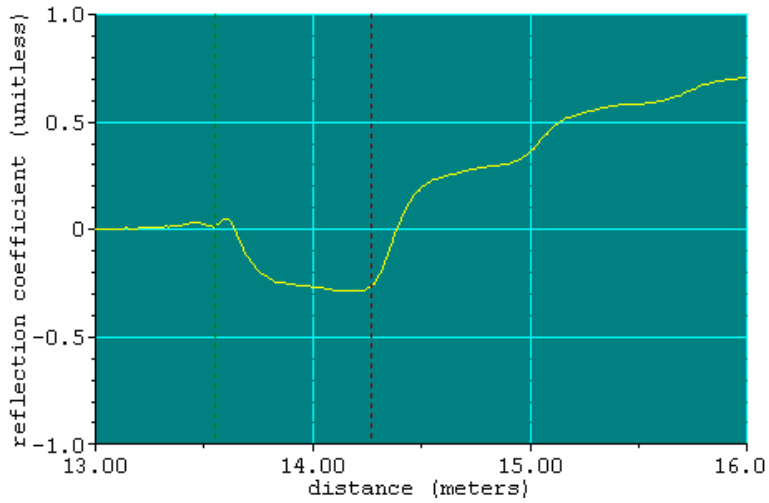

Figure 6-8: Water Waveform

SFCC testing has also been performed on an oil sands sample with a sand to fine ratio (SFR) of 1.0. The material was unable to be tested in the "as received" state due to the very low solids content, which resulted in a highly segregating material. The material was allowed to segregate and then the clarified water was decanted. The material was remixed, and the TDR and RTD were inserted into the top of the sample for testing. Despite this, issues were still encountered with segregation resulting in variation between tests. As a result, segregation will negatively impact the test results as the material tested by the probes may not be representative of the overall soil behavior. Ultimately, this limits the applicability of the method as the material must be non-segregating for SFCC testing to occur.

6.6 Supercooling and Wetting SWCC

As discussed in Section 2.5.5, supercooling is a drop in sample temperature below the freezing plot without a phase change (Kozlowski 2009). The temperature in the sample will continue to drop until the spontaneous nucleation temperature T_{sn} is reached at which point latent heat will be released and nucleation will occur (Kozlowski 2009). The temperature in the sample will then rise to the freezing temperature and phase change will occur. This process can make it difficult to estimate the SWCC from the SFCC as it may result in substantial scatter around the freezing point. It should be noted that all suctions calculated in zones of supercooling represent pseudo-suctions and are not considered representative of the actual suction present in the soil. In contrast, supercooling does not occur during thawing as thawing is a single step process (Kozlowski 2009). Due to this, it would be more ideal to estimate the SWCC from the thawing SFCC. However, the processes of freezing and thawing (and wetting and drying) are hysteretic and will vary. As a result, it is important that similar processes are matched up when estimating the SWCC from the SFCC. This means that the freezing SFCC should be used to estimate the drying SWCC and the thawing SFCC should be used to estimate the wetting SWCC. The freezing SFCC was used to estimate the SWCC for the purposes of this research for the following reasons:

1. It is easier to compute the drying SWCC in the laboratory compared to the wetting SWCC. As a result, the freezing SFCC needs to be used for comparison to these tests.
2. The tested materials have high initial water contents. As a result, the TDR and RTD probes move substantially during the thawing process and a lot of water may be released resulting in the presence of a zone of water at the top of the sample. Both of these factors influence the position, shape, and correctness of the thawing SFCC. As a result, the freezing SFCC is considered more reliable than the thawing SFCC despite the impacts of supercooling.

6.7 Estimating the SWCC from the GSD Curve

The SWCC can be estimated from the GSD curve using a physico-empirical type model (Fredlund 2006). A commonly used model to estimate the SWCC from the GSD is the method proposed by Fredlund (2000), which involves a combination of parametric study information and a physico-

empirical model. This method relies on the assumption that the GSD provides a physical description of the soil that can be used as a basis to estimate the SWCC (Fredlund et al. 2012). It should be noted that there are limitations associated with this method as the GSD does not provide information on the fabric of the soil or the in situ density or porosity of the soil. The methodology of the Fredlund (2000) method relies on three key theorems, as described by Fredlund et al. 2012:

> *Theorem 1 – A soil composed entirely of uniform, homogeneous particle sizes has a unique drying (or desorption) SWCC*
>
> *Theorem 2 – The capillary model can satisfactorily estimate the air-entry value of each collection of uniform, homogeneous particle sizes.*
>
> *Theorem 3 – The SWCC for soils composed of more than one particle size can be represented as the summation of the SWCCs for each of the individual particles sizes.* (page 257)

Overall, this model uses a pedo-transfer function (PTF) to estimate the SWCC from the GSD of the soil. SoilVision can be used to estimate the SWCC from the GSD using the method proposed by Fredlund (2000). This method requires a packing porosity to be specified for the soil. In theory, it is likely that a different packing porosity exists for each uniform particle size that is dependent on the particle diameter (Fredlund et al. 2012). However, the method assumes that the packing porosity is the same for each successive particle fraction. This method is highly dependent on the value specified for the packing porosity, but no distinct guidelines are provided for the specification of the packing porosity.

In theory, this method offers a great alternative to performing a traditional laboratory SWCC as it relies on the GSD, which is simple and fast to attain. It should be noted that this method does not perform well for the following categories of soil:

- Soils with a large amount of clay-sized particles;
- Soils with a large amount of coarse particles mixed with fines;

- Soils with a bimodal behavior; and,
- Man-made soils (mine tailings and waste rock).

Due to these limitations, the applicability of estimating the S-SWCC from the GSD was investigated for Devon silt, copper tailings, gold tailings, and the centrifuge cake. For all materials, the GSD was fit with a unimodal fit. The estimated SWCCs were fit with Fredlund and Xing's (1994) equation. Comparisons between the S-SWCCs estimated from the GSD and the SWCCs presented for the Devon silt, copper tailings, gold tailings, and centrifuge cake are provided in Figure 6-9 to Figure 6-12. Shrinkage properties were not applied to the SWCCs estimated using the GSD to simulate the easiest possible method for estimating the SWCC. The estimated S-SWCCs fit poorly with the measured S-SWCCs for the Devon silt, copper tailings, and gold tailings. In the case of the Devon silt, this is attributed to the large degree of clay-sized particles present in the material and the bimodal behaviour of the material. In the case of the copper tailings and the gold tailings, the poor fit is attributed to the mixture of coarse and fine particles and that these materials are man-made. Overall, a much better fit was obtained between the S-SWCC estimated from the GSD and the S-SWCC measured using traditional methods for the centrifuge cake. Interestingly, this fit was substantially better than the fit obtained between the S-SWCC estimated from the SFCC and the S-SWCC measured using traditional methods. It is unknown if similar observations would be made with different types of oil sands tailings. Overall, it does not appear that estimating the SWCC from the GSD can be used as a reliable method to replace determining the SWCC using a traditional laboratory test. For the Devon silt, copper tailings, and gold tailings, a better fit was observed by estimating the S-SWCC from the SFCC.

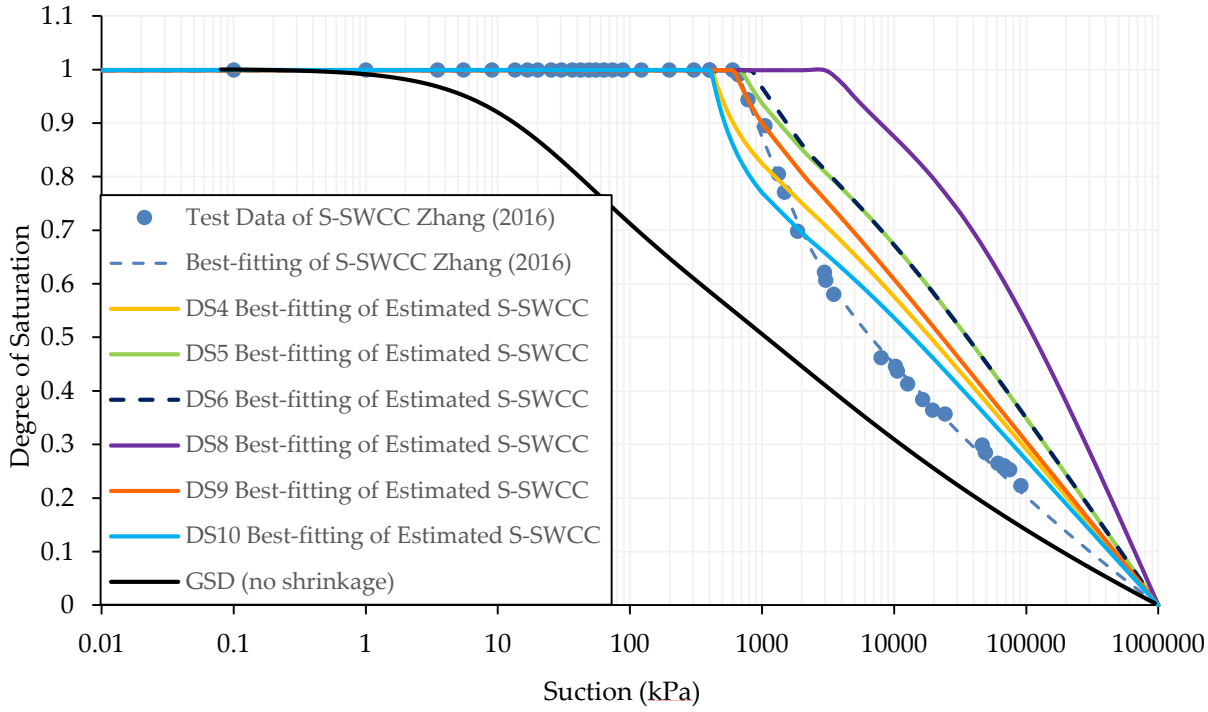

Figure 6-9: Comparison of SWCC Estimated from GSD with SWCC Determined using Traditional Methods and SWCC Estimated from the SFCC for Devon Silt

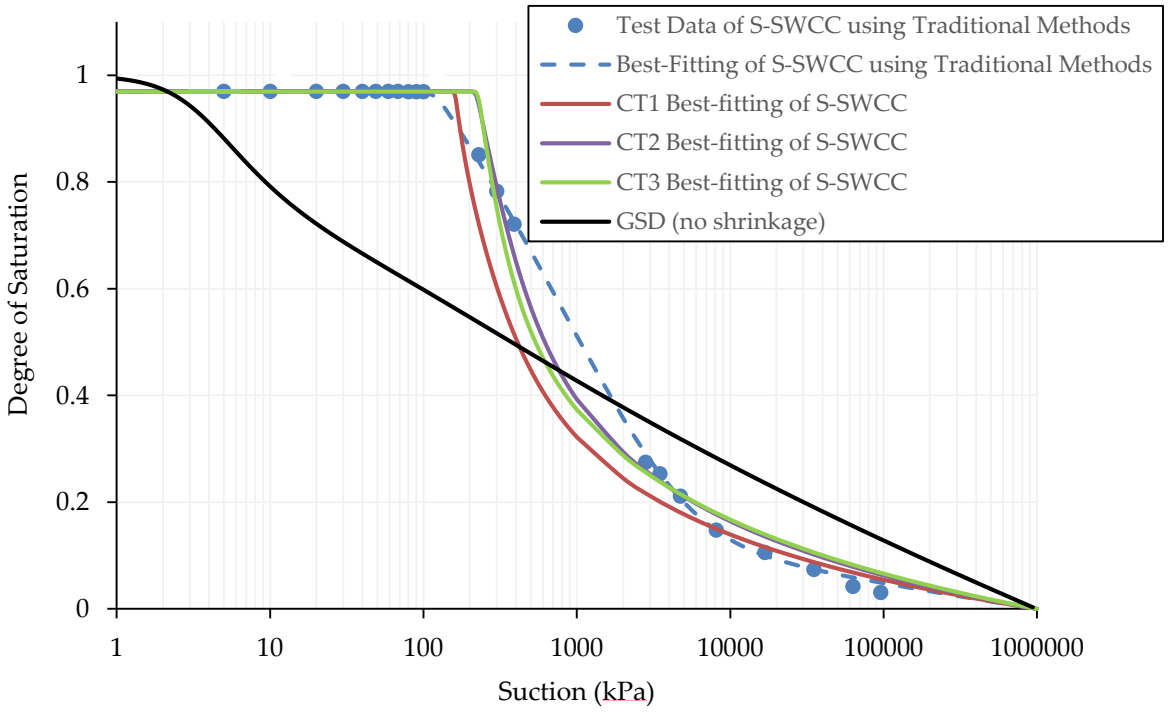

Figure 6-10: Comparison of SWCC Estimated from GSD with SWCC Determined using Traditional Methods and SWCC Estimated from the SFCC for Copper Tailings

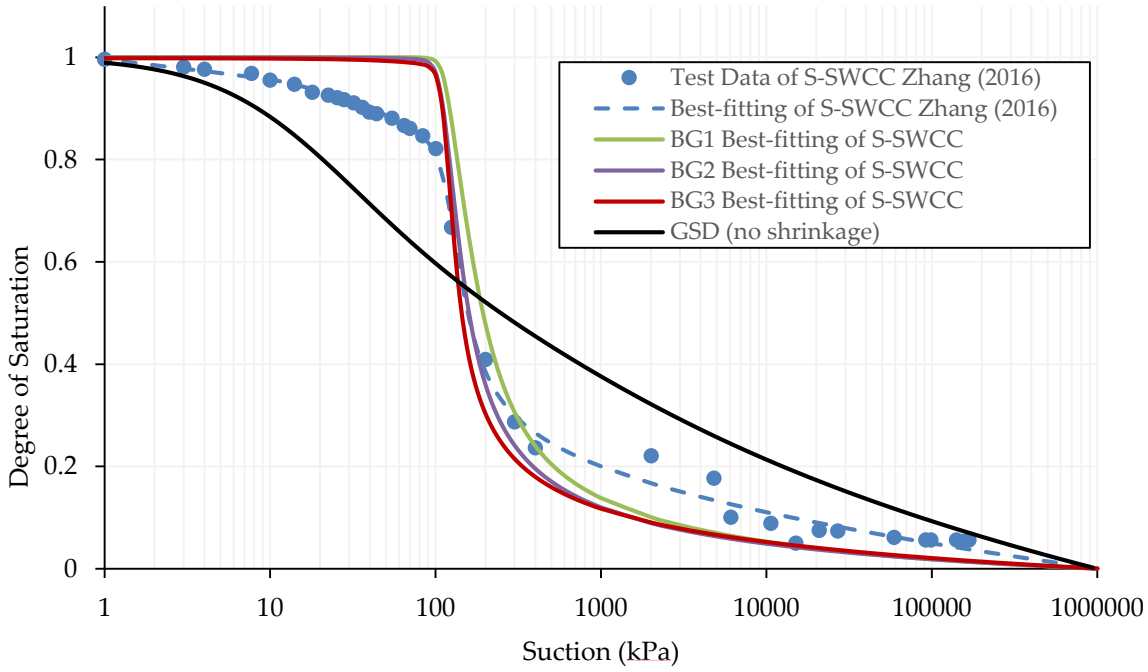

Figure 6-11: Comparison of SWCC Estimated from GSD with SWCC Determined using Traditional Methods and SWCC Estimated from the SFCC for Gold Tailings

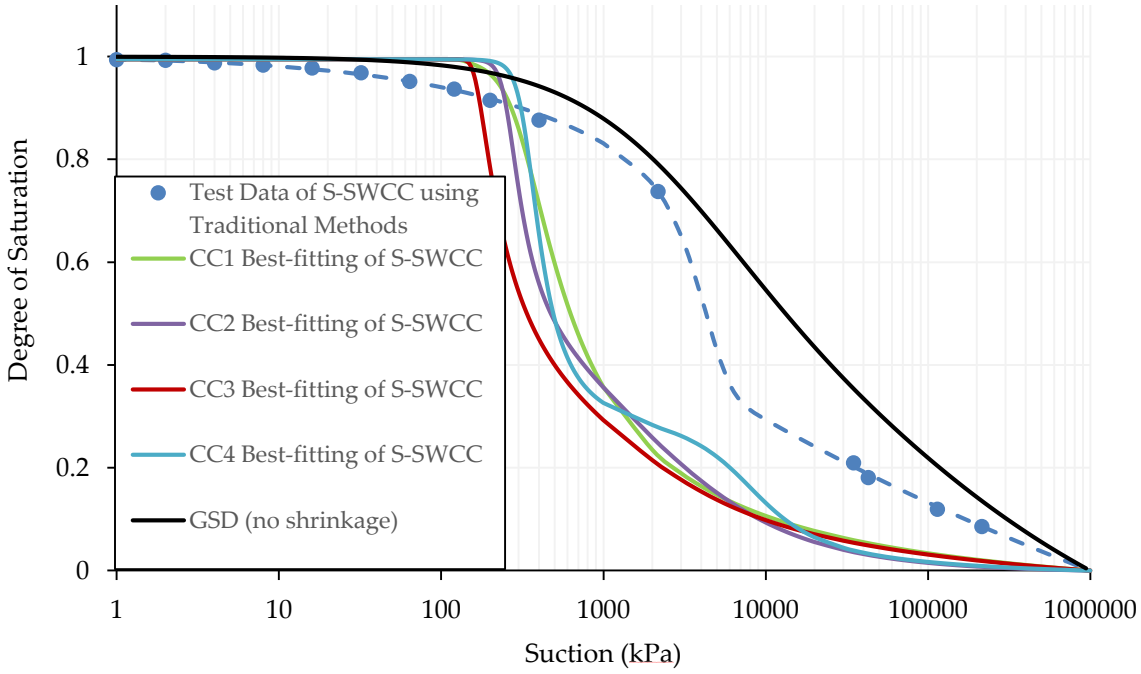

Figure 6-12: Comparison of SWCC Estimated from GSD with SWCC Determined using Traditional Methods and SWCC Estimated from the SFCC for Centrifuge Cake

6.8 Estimating the Shrinkage Curve

A limitation of estimating the SWCC from the SFCC for a high volume change material is the need for the shrinkage curve of the material. While this test is relatively simple to perform, it can take a couple of weeks. As a result, it would be ideal if the shrinkage curve could be estimated to eliminate the need for this test and increase the simplicity of estimating the SWCC from the SFCC.

The shrinkage curve can be estimated by estimating the shrinkage limit of a soil based on the Atterberg limits. The shrinkage limit of the soil can be estimated based on the Casagrande plasticity chart as discussed by Holtz and Kovacs (1981). Holtz and Kovacs (1981) suggest that the shrinkage limit will be approximately 20 when the Atterberg limits of a soil plot near the A-line. If the Atterberg limits plot above the A-line, then the shrinkage limit will be less than 20 by an amount that is dependent on the distance from the A-line (Holtz and Kovacs 1981). Similarly, if the limits plot below the A-line, then the shrinkage limit will be greater than 20 by an amount that is dependent on the distance from the A-line (Holtz and Kovacs 1981). Using this principle, Equation 6-2 and 6-3 can be used to estimate the shrinkage limit.

$$SL_s = 20 \pm (PI_s - PI_A) \quad \textbf{6-2}$$

$$PI_A = 0.73(LL_S - 20) \quad \textbf{6-3}$$

Where SL_s is the shrinkage limit of the soil in percent, PI_s is the plasticity index (difference between the liquid limit and the plastic limit) of the soil in percent, PI_A is the plasticity index on the A-line in percent, and LL_s is the liquid limit of the soil in percent.

As discussed in Section 2.4.3, the shrinkage curve can be described by a hyperbolic curve (Equation 2-6) with three variables: a_{sh}, b_{sh}, and c_{sh}. The a_{sh} variable describes the minimum void ratio of the soil. If the initial saturation of the soil is assumed to 100 percent, then a_{sh} can be estimated using the relationship $Se = wG_s$ where the water content is assumed to be equivalent to the shrinkage limit of the soil as shown in Equation 6-4. The b_{sh} variable can then be calculated

as shown in Equation 6-5 using the initial degree of saturation, specific gravity, and the a_{sh} variable.

$$a_{sh} = SL_s * G_s \quad \textbf{6-4}$$

$$b_{sh} = \frac{a_{sh} S_o}{G_s} \quad \textbf{6-5}$$

The c_{sh} variable describes the curvature of the shrinkage curve. According to Fredlund et al. (2012), the average c_{sh} value is 25.3 with a standard variation of ±25.4 variable for a soil sample that was initially a slurry. A high c_{sh} value (i.e. greater than 50) will result in a horizontal line from the minimum void ratio to the initial saturation line at which point the curve will follow the path along the initial saturation line (Fredlund 2000). An example of this would be the shrinkage curve for the Devon silt as shown in Figure 3-10. In contrast, a low c_{sh} value (i.e. less than 1.5) will result in a very gradual curve that starts from the minimum void ratio and progressively curves towards saturation (Fredlund 2000).

As shown by Fredlund (2000), the shrinkage estimation method works well for approximating the shape of the shrinkage curve, but may perform poorly for determining the minimum void ratio. This is an important limitation as the minimum void ratio is the most critical parameter in the estimation of the shrinkage curve. As a result, Fredlund (2000) recommended that the minimum void ratio be determined experimentally.

The a_{sh}, b_{sh}, and c_{sh} were estimated for the Devon silt, copper tailings and centrifuge cake and compared to the measured values. The shrinkage curve variables were not estimated for the gold tailings as it is non-plastic. The estimated and measured values are provided in Table 6-1. The estimated and measured shrinkage curves for Devon silt are provided in Figure 6-13. The estimated shrinkage curve was used to estimate the S-SWCC using the test data from the traditional SWCC testing for the Devon silt as shown in Figure 6-14. The estimated and measured shrinkage curves for the copper tailings are provided in Figure 6-15. The estimated shrinkage curve was used to estimate the S-SWCC using the test data from the traditional SWCC testing

copper tailings as shown in Figure 6-16. The estimated and measured shrinkage curves for the centrifuge cake are provided in Figure 6-17. The estimated shrinkage curve was used to estimate the S-SWCC using the test data from the traditional SWCC testing centrifuge cake as shown in Figure 6-18. The S-SWCCs determined using the estimated shrinkage curves for the Devon silt, copper tailings, and centrifuge cake provided a good fit to the S-SWCCs determined using the measured shrinkage curves.

Table 6-1: Estimated and Measured Shrinkage Curve Variables

Soil	Estimated			Measured		
	a_{sh}	b_{sh}	c_{sh}	a_{sh}	b_{sh}	c_{sh}
Devon Silt	0.42	0.16	5.0	0.432	0.162	214
Copper Tailings	0.37	0.14	10.0	0.44	0.161	75
Centrifuge Cake	0.36	0.16	5.0	0.47	0.209	3.5

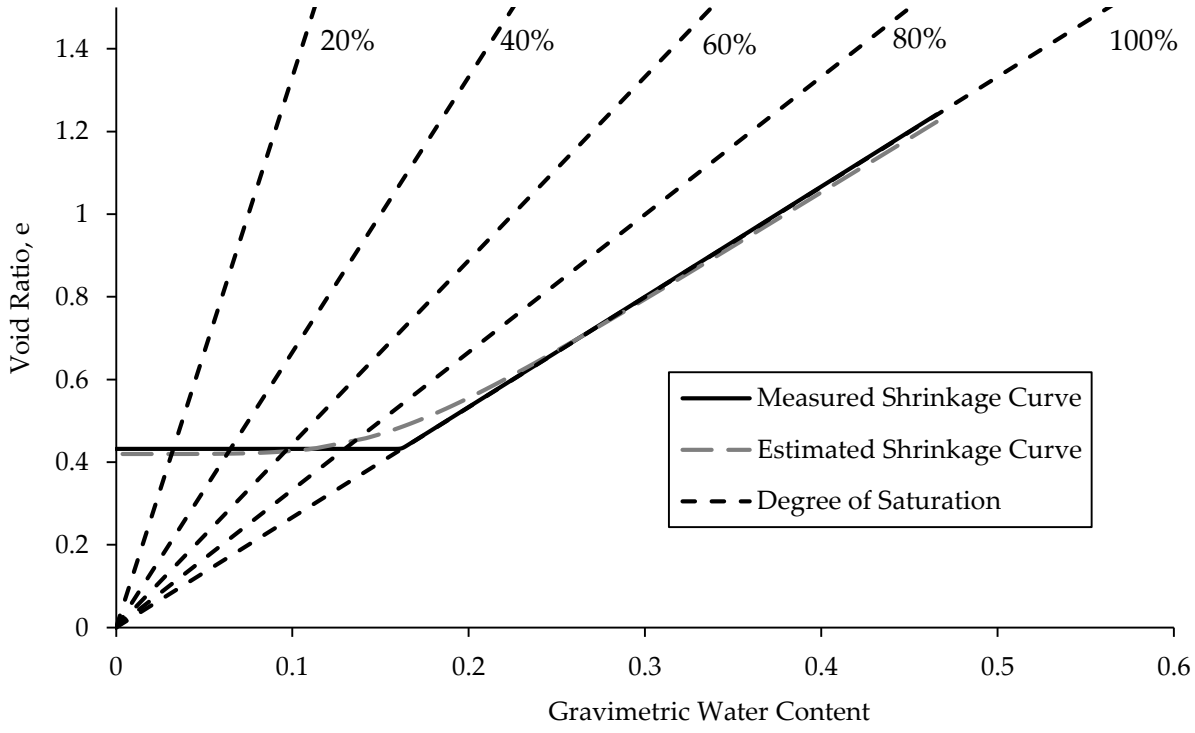

Figure 6-13: Estimated and Measured Shrinkage Curve for Devon Silt

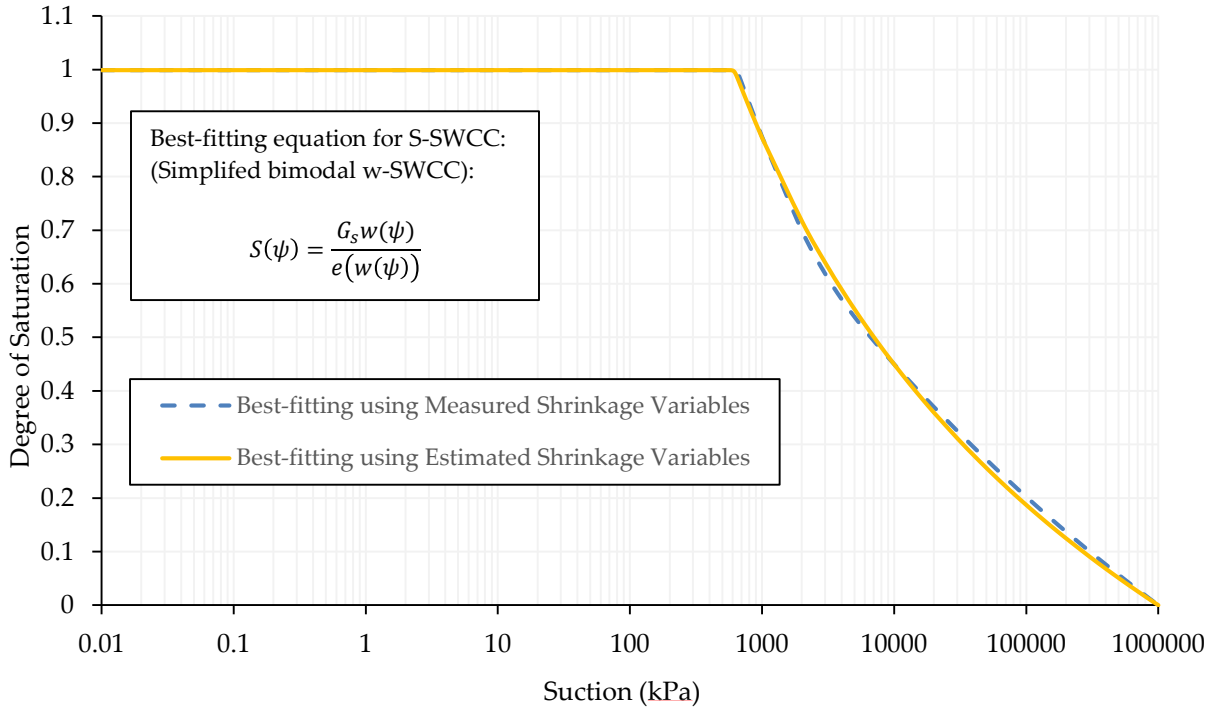

Figure 6-14: Comparison of S-SWCCs Determined using Measured and Estimated Shrinkage Curve Variables for Devon Silt

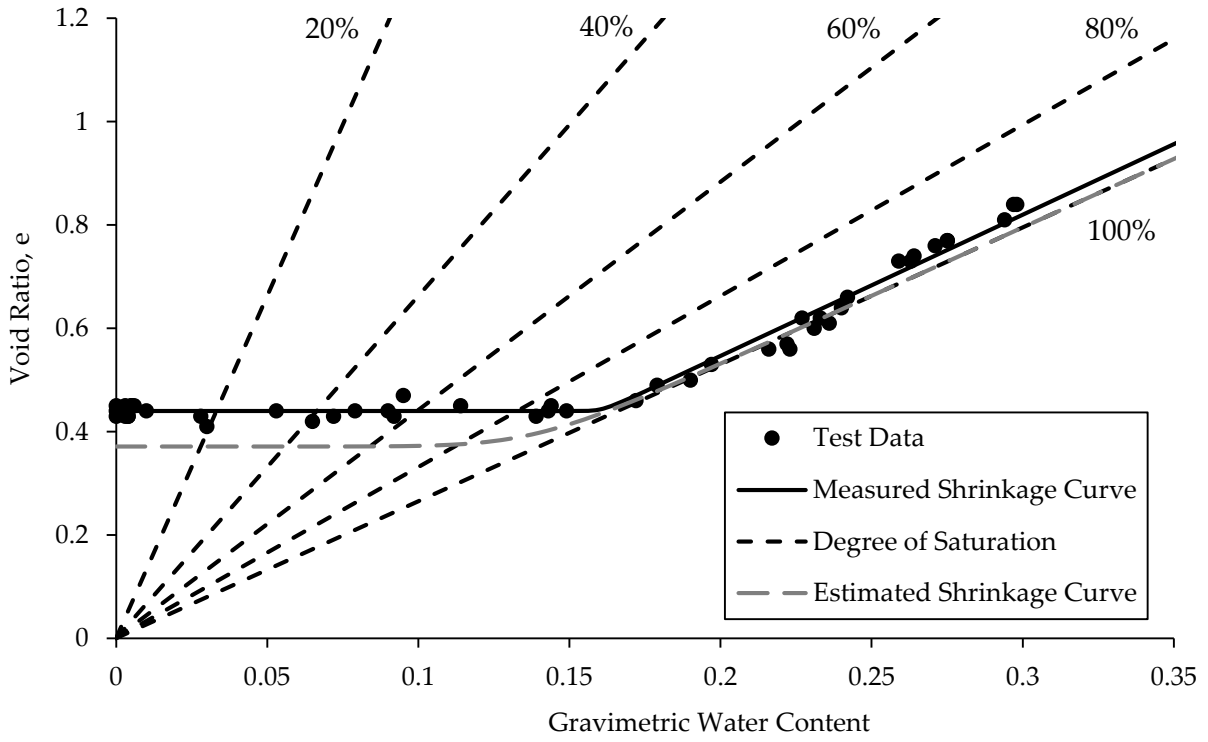

Figure 6-15: Estimated and Measured Shrinkage Curve for Copper Tailings

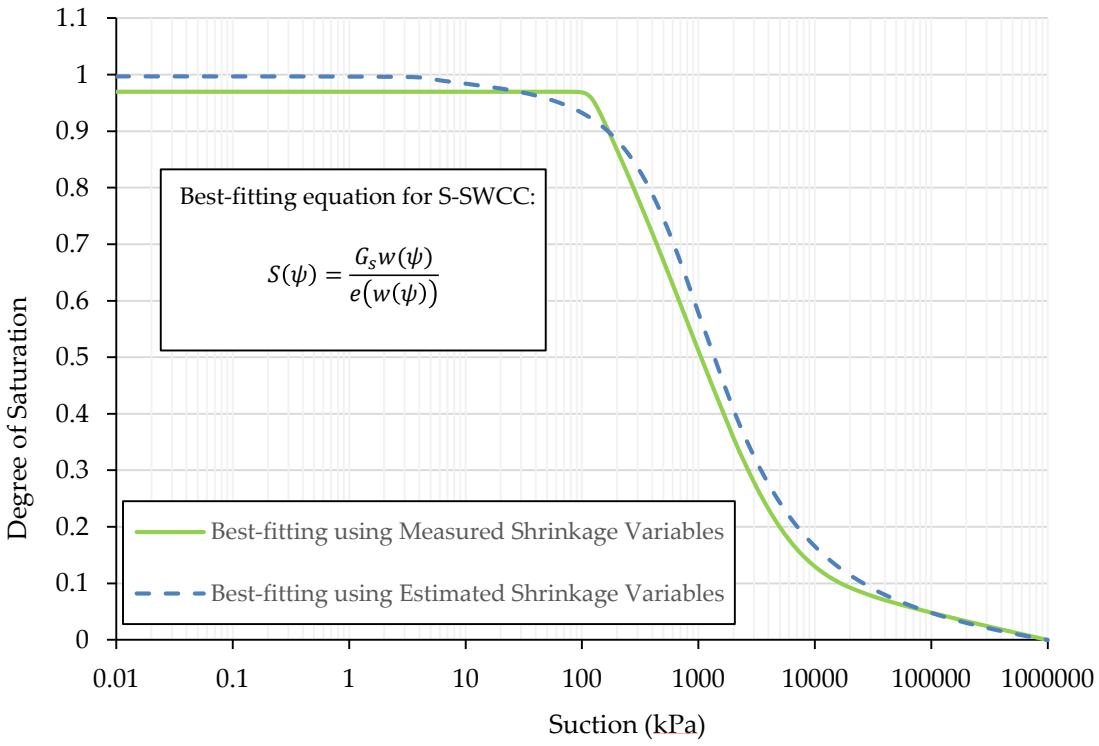

Figure 6-16: Comparison of S-SWCCs Determined using Measured and Estimated Shrinkage Curve Variables for Copper Tailings

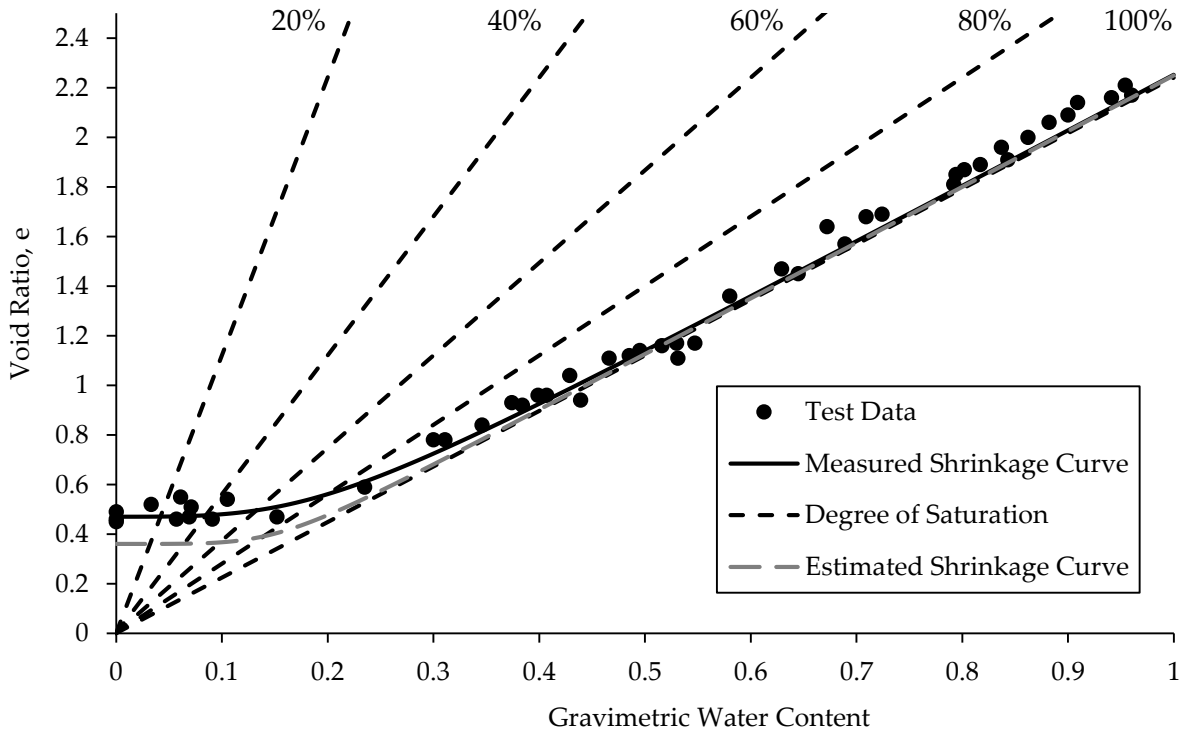

Figure 6-17: Estimated and Measured Shrinkage Curve for Centrifuge Cake

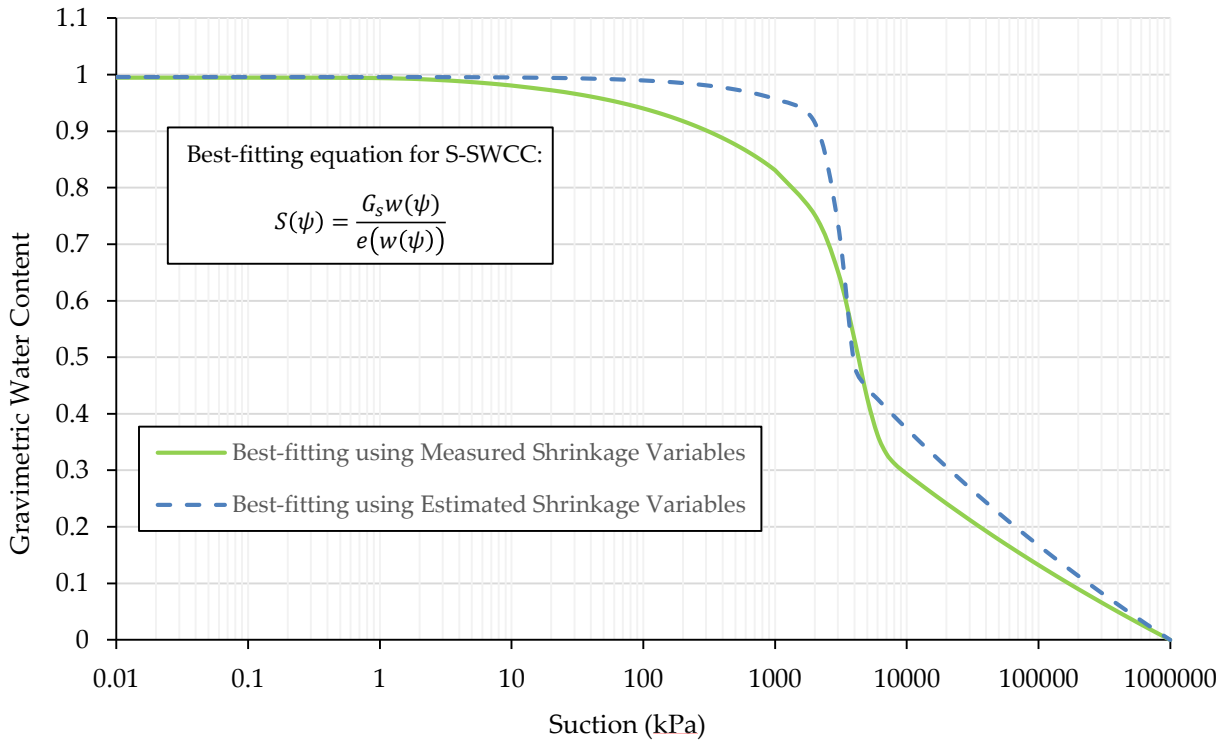

Figure 6-18: Comparison of S-SWCCs Determined using Measured and Estimated Shrinkage Curve Variables for Centrifuge Cake

7 CONCLUSIONS AND RECOMMENDATIONS

7.1 Conclusion

The objective of this research was to investigate the feasibility of using the SFCC to estimate the SWCC in mine waste tailings. An experimental method and apparatus was developed to measure the SFCC. The experimental method involved using a RTD to measure the temperature and a TDR to determine the unfrozen water content of the soil. A soil specific calibration was conducted (where applicable) at unfrozen conditions to determine the volumetric water content from the apparent dielectric constant. The soil specific calibration was then applied to freezing conditions to determine the unfrozen volumetric water content of the soil. SFCC testing was performed on a variety of materials with different GSDs, including Devon silt, copper tailings, sand tailings, gold tailings, and oil sands tailings. The SFCC was used to estimate the SWCC using the following steps:

1. The suction is determined from the temperature measurements using the Clapeyron equation (Equation 2-16).
2. If the soil is non-colloidal, a soil dependent constant of 2.2 is used to estimate the SWCC from the SFCC based on Koopmans and Miller (1966). If the soil is colloidal, a soil dependent constant of 1.0 is used to estimate the SWCC from the SFCC based on Koopmans and Miller (1966).
3. The w_u and the θ_u are assumed to be equivalent to the gravimetric water content and the volumetric water content during drying, respectively. This yields an estimated θ-SWCC and a w-SWCC.
4. High volume change property functions are applied to attain the θ_i-SWCC and the S-SWCC based on Section 2.4.3.

The estimated SWCCs were compared to SWCCs measured using traditional methods. Based on the results of the testing, the following conclusions can be made:

- The method appears to be applicable to metal tailings that have large quantities of sand sized particles with some degree of fines. In general, it is recommended that a shrinkage

test be conducted in conjunction with the SFCC testing so that a S-SWCC can be attained for determination of the AEV. Alternatively, the shrinkage curve can be estimated using the method described by Holtz and Kovacs (1981).

- In some cases, it may be difficult to classify the tailings as purely colloidal or non-colloidal which can make it difficult to select a soil dependent constant, as with the copper tailings. Regardless, this method is useful as a screening tool as it can be used to rapidly test a large number of tailings to decide which materials should have detailed traditional SWCCs conducted.
- At the current time, it does not appear that this method can be used to estimate the SWCC from the SFCC for oil sands tailings. This is attributed to the high clay content (and associated adsorbed water) and water content of the tailings. Based on the results of the testing, it does not appear that the salinity of the centrifuge cake is responsible for the mismatch between the SWCC estimated from the SFCC and the SWCC measured using traditional methods.
- Materials consisting of entirely sand (i.e. sand tailings from the oil sands industry) tend to have very low AEV (less than 10 kPa). This generally coincides with a freezing point just below zero. As a result, the instrument used for measuring temperature must be capable of reliably measuring to 0.001°C in order to test these materials.
- It is recommended that the TDR calibration be conducted using two methods (i.e. NMR and TDR) under freezing conditions. Conducting a soil specific calibration under unfrozen conditions and applying it to frozen conditions resulted in a large degree of uncertainty with respect to the low water content range. This is concerning as this may correspond with desaturation of the material, which is a critical portion of the estimated SWCC. Requiring two methods for TDR calibration may limit the adoption of estimating the SWCC from the SFCC as NMR and other methods are expensive and complex to use compared to TDR alone. In these cases, it may be easier to conduct a traditional SWCC.
- Estimating the SWCC from the SFCC for metal tailings is much more accurate than estimating it from the GSD. The SFCC is performed directly on the soil. This is a huge

advantage over estimating the SWCC from the GSD, especially since this method generally is not recommended for man made materials.

7.2 Contributions of Thesis

The main contributions of this research are:

- An experimental method was developed to measure the SFCC for slurries using TDR and RTDs. The experimental method was shown to produce reliable and repeatable results.
- The results of the research showed that the SWCC could be estimated from the SFCC for tailings from metal mines (gold tailings, copper tailings) with a high portion of sand and a small amount of clay. The SWCC is time-consuming and challenging to determine using traditional laboratory techniques and may take weeks to months to measure. In contrast, the SFCC takes days to measure. This is a huge advantage when determining the unsaturated soil properties of a tailings deposit. Ultimately, this method is very useful as a screening tool to rapidly test a wide variety of tailings to determine which should have detailed traditional SWCC testing.
- The current methodology has not proven to be successful for estimating the SWCC from the SFCC for oil sands tailings. This is attributed to the high clay content and high water content of the tailings.

7.3 Recommendations for Future Research

The following are recommendations for further research regarding estimating the SFCC from the SWCC for mine waste tailings:

- All additional testing should proceed using two methods to conduct a TDR calibration (i.e. NMR and TDR) under frozen conditions. Alternatively, a dielectric mixing model should be used to determine the unfrozen water content from apparent dielectric constant. A dielectric mixing model was not applied in this research program as there was not a way to determine the amount of adsorbed water or the amount of ice present near the probe.

- Further testing should be conducted to determine the range of materials over which this method is applicable. Testing should be conducted using process water from the mine. This will allow the impacts of salinity in the pore fluid on the testing method to be assessed. This was not possible in the current study.
- Further testing should be conducted on oil sands tailings where the TDR calibration is conducted under frozen conditions using two methods to confirm if this method is applicable to oil sands tailings or if the poor fit was a function of the TDR calibration.

References

AER. 2009. Directive 074: Tailings Performance Criteria and Requirements for Oil Sands Mining Schemes, Alberta Energy Regulator, Calgary, Alberta.

AER. 2016a. Alberta's Energy Reserves 2015 & Supply/Demand Outlook 2016-2025 (ST98-2016), Alberta Energy Regulator, Calgary, Alberta.

AER. 2016b. Directive 085: Fluid Tailings Management for Oil Sands Mining Projects, Alberta Energy Regulator, Calgary, Alberta.

Andersland, O.B. and Ladanyi, B. 2004. Frozen Ground Engineering: Second Edition. John Wiley & Sons, Hoboken, New Jersey.

Anderson, D.M. and Tice, A.R. 1972. Predicting unfrozen water contents in frozen soils from surface area measurements. 393, Highway Research Record.

Anderson, D.M. and Morgenstern, N.R. 1973. Physics, chemistry, and mechanics of frozen ground: a review. *In* Proceedings of the 2nd International Conference in Permafrost, Yakutsk, Siberia, 13-28 July 1973, pp. 257-288.

Azmatch, T.F., Sego, D.C., Arenson, L.U. and Biggar, K.W. 2012b. Soil Freezing Characteristic Curve of Devon Silt. *In* David C. Sego Symposium, University of Alberta, Edmonton, Alberta, Canada, 26-27 April 2012.

Azmatch, T.F., Sego, D.C., Arenson, L.U., and Biggar, K.W. 2012a. Using soil freezing characteristic curve to estimate the hydraulic conductivity function of partially frozen soils. Cold Regions Science & Technology, **83-84**: 103-109.

Baker, J.M., and Lascano, R.J. 1989. The Spatial Sensitivity of Time-Domain Reflectometry. Soil Science, **147**(5): 378-384.

Banin, A., and Anderson, D.M. 1974. Effects of salt concentration changes during freezing on the unfrozen water content of porous materials. Water Resources Research, **10**(1): 124-127.

Beier, N.A. 2006. Freeze Separation of Saline Oil Sands Mine Waste Water. M.Sc. thesis, University of Alberta, Edmonton, Alberta.

Beier, N.A. 2015. Development of a tailings management simulation and technology evaluation tool. Ph.D. thesis, University of Alberta, Edmonton, Alberta.

Benson, C.H., and Bosscher, P.J. 1999. Time-Domain Reflectometry (TDR) in Geotechnics: A Review. ASTM Special Technical Publication, **1350**: 113-136.

Biggar, K., and Sego, D. 1993. The strength and deformation behaviour of model adfreeze and grouted piles in saline frozen soils. Canadian Geotechnical Journal, **30**(2): 319-337.

Bing, H., and Ma, W. 2011. Laboratory investigation of the freezing point of saline soil. Cold Regions Science and Technology, **67**(1): 79-88.

Birn, K. and Khanna, P. 2010. A discussion paper on the oil sands: challenges and opportunities, Natural Resources Canada, Ottawa, Canada.

Black, P.B. and Tice, A.R. 1989. Comparison of soil freezing curve and soil water curve data for Windsor sandy loam. CRREL Report 88-16, US Army Corps of Engineers Cold Regions Research and Engineering Laboratory, Hanover, New Hampshire.

Bouksila, F., Persson, M., Berndtsson, R., and Bahri, A. 2008. Soil water content and salinity determination using different dielectric methods in saline gypsiferous soil. Hydrological Sciences Journal, **53**(1): 253-265.

Cary, J.W., and Mayland, H.F. 1972. Salt and Water Movement in Unsaturated Frozen Soil. Soil Science Society of America Proceedings, **36**(4): 549-555.

Chalaturnyk, R.J., Don Scott, J., and Özüm, B. 2002. Management of oil sands tailings. Petroleum Science and Technology, **20**(9-10): 1025-1046.

Cheung, C.H. 1979. Influence of salt on the unfrozen water in frozen clays. Ph.D. thesis, McGill University, Montreal, Quebec.

CTMC. 2012. Oil Sands Tailings Technology Deployment Roadmaps - Volume 1 - Project Summary Report, Consortium of Tailings Management Consultants, Report prepared for AI-EES and the Oil Sands Tailings Consortium (OSTC). June 29, 2012.

Dash, J.G., Fu, H., Wettlaufer, J.S., and Fu, H.Y. 1995. The premelting of ice and its environmental consequences. Reports on Progress in Physics, **58**(1): 115-167.

Dompierre, K.A., Lindsay, M.B., Cruz-Hernández, P., and Halferdahl, G.M. 2016. Initial geochemical characteristics of fluid fine tailings in an oil sands end pit lake. Science of the Total Environment, **556**: 196-206.

Drnevich, V.P., Ashmawy, A.K., Yu, X., and Sallam, A.M. 2005. Time domain reflectometry for water content and density of soils: study of soil-dependent calibration constants. Canadian Geotechnical Journal, **42**(4): 1053-1065.

Drotz, S.H., Tilston, E.L., Sparrman, T., Schleucher, J., Nilsson, M., and Öquist, M.G. 2009. Contributions of matric and osmotic potentials to the unfrozen water content of frozen soils. Geoderma, **148**(3): 392-398.

Flerchinger, G.N., Hardegree, S.P., and Seyfried, M.S. 2006. Using Soil Freezing Characteristics to Model Multi-Season Soil Water Dynamics. Vadose Zone Journal, **5**(4): 1143-1153.

Fredlund, D.G. and Rahardjo, H. 1993. Soil mechanics for unsaturated soils. John Wiley & Sons, Hoboken, New Jersey.

Fredlund, D.G. 2006. Unsaturated soil mechanics in engineering practice. Journal of Geotechnical and Geoenvironmental Engineering, **132**(3): 286-321.

Fredlund, D.G., Rahardjo, H. and Fredlund, M.D. 2012. Unsaturated soil mechanics in engineering practice. John Wiley & Sons, Hoboken, New Jersey.

Fredlund, D., Stone, J., Stianson, J. and Sedgwick, A. 2011. Obtaining unsaturated soil properties for high volume change oil sands material. *In* Proceedings of the 5th Asia Pacific Conference on Unsaturated Soils, Pattaya, Thailand, 14-16 November 2011, pp. 415-420.

Fredlund, M. 2004. SoilVision Theory Manual, SoilVision Systems Ltd., Saskatoon, Saskatchewan.

Fredlund, M.D. 2000. The role of unsaturated soil property functions in the practice of unsaturated soil mechanics. Ph.D. thesis, University of Saskatchewan, Saskatoon, Saskatchewan.

Fredlund, D.G., and Xing, A. 1994. Equations for the soil-water characteristic curve. Canadian Geotechnical Journal, **31**(4): 521-532.

Government of Alberta. 2015. Lower Athabasca Region - Tailings Management Framework for the Mineable Athabasca Oil Sands, Government of Alberta, Edmonton, Alberta.

Government of Alberta 2017b. Oil Sands Information Portal [online]. Available from http://osip.alberta.ca/map/ [accessed 13 June 2017].

Government of Alberta. 2017a. About Oil Sands: Facts and Statistics [online]. Available from http://www.energy.alberta.ca/OilSands/791.asp [accessed 13 June 2017].

Herkelrath, W.N., Hamburg, S.P., and Murphy, F. 1991. Automatic, real-time monitoring of soil moisture in a remote field area with time domain reflectometry. Water Resources Research, **27**(5; 5): 857-864.

Hivon, E.G. 1991. Behaviour of saline frozen soils. Ph.D. thesis, University of Alberta, Edmonton, Alberta.

Holden, A., Donahue, R., and Ulrich, A. 2011. Geochemical interactions between process-affected water from oil sands tailings ponds and North Alberta surficial sediments. Journal of Contaminant Hydrology, **119**(1): 55-68.

Holtz, R.D. and Kovacs, W.D. 1981. An introduction to geotechnical engineering. Prentice-Hall, Englewood Cliffs, New Jersey.

Jacobsen, O.H., and Schjonning, P. 1993. A laboratory calibration of time domain reflectometry for soil water measurement including effects of bulk density and texture. Journal of Hydrology, **151**(2): 147-157.

Jeeravipoolvarn, S. 2010. Geotechnical behavior of in-line thickened oil sands tailings. Ph.D. thesis, University of Alberta, Edmonton, Alberta.

Kabwe, L.K., Scott, J.D., Wilson, G.W. and Sorta, A.R. 2014. From fluid to solid: Oil sands fluid fine tailings. *In* 7th International Congress on Environmental Geotechnics, Melbourne, Australia, 10-14 November 2014.

Kahimba, F.C., and Sri Ranjan, R. 2007. Soil temperature correction of field TDR readings obtained under near freezing conditions. Canadian Biosystems Engineering, **49**: 1.19-1.26.

Kasperski, K.L., and Mikula, R.J. 2011. Waste streams of mined oil sands: characteristics and remediation. Elements, **7**(6): 387-392.

Knight, J.H. 1992. Sensitivity of time domain reflectometry measurements to lateral variations in soil water content. Water Resources Research, **28**(9): 2345-2352.

Konrad, J.M. 1994. Sixteenth Canadian Geotechnical Colloquium: Frost heave in soils: concepts and engineering. Canadian Geotechnical Journal, **31**(2): 223-245.

Koopmans, R.W.R., and Miller, R.D. 1966. Soil Freezing and Soil Water Characteristic Curves. Soil Science Society of America Journal, **30**(6): 680-685.

Kozlowski, T. 2009. Some factors affecting supercooling and the equilibrium freezing point in soil–water systems. Cold Regions Science and Technology, **59**(1): 25-33.

Leong, E.C., and Rahardjo, H. 1997. Review of soil-water characteristic curve equations. Journal of Geotechnical & Geoenvironmental Engineering, **123**(12): 1106-1117.

Liu, Z., Zhang, B., Yu, X., Zhang, B., and Tao, J. 2012. A New Method for Soil Water Characteristic Curve Measurement Based on Similarities Between Soil Freezing and Drying. Geotechnical Testing Journal, **35**(1): 2-10.

Ma, T., Wei, C., Xia, X., Zhou, J., and Chen, P. 2015a. Soil Freezing and Soil Water Retention Characteristics: Connection and Solute Effects. Journal of Performance of Constructed Facilities,: D4015001.

Ma, W., Zhang, L., and Yang, C. 2015b. Discussion of the applicability of the generalized Clausius–Clapeyron equation and the frozen fringe process. Earth-Science Reviews, **142**: 47-59.

Masliyah, J., Zhou, Z.J., Xu, Z., Czarnecki, J., and Hamza, H. 2004. Understanding water-based bitumen extraction from Athabasca oil sands. The Canadian Journal of Chemical Engineering, **82**(4): 628-654.

McKenna, G., Mooder, B., Burton, B. and Jamieson, A. 2016. Shear strength and density of oil sands fine tailings for reclamation to a boreal forest landscape. *In* Proceedings of the 5th International Oil Sands Tailings Conference, Lake Louise, Alberta, 4-7 December 2016.

McLaws, I.J. 1980. Silica sands in the Fort McMurray area, Alberta. Economic Geology Report 6, Alberta Research Council, Edmonton, Alberta.

Mossop, G.D. 1980. Geology of the Athabasca Oil Sands. Science, **207**(4427): 145-152.

Nagare, R., Schincariol, R., Quinton, W., and Hayashi, M. 2011. Laboratory calibration of time domain reflectometry to determine moisture content in undisturbed peat samples. European Journal of Soil Science, **62**(4): 505-515.

Newman, G.P., and Wilson, G.W. 1997. Heat and mass transfer in unsaturated soils during freezing. Canadian Geotechnical Journal, **34**(1): 63-70.

Newson, T.A., and Fahey, M. 2003. Measurement of evaporation from saline tailings storages. Engineering Geology, **70**: 217-233.

OSTC. 2012. Technical guide for fluid fine tailings, Oil Sands Tailings Consortium (OSTC), Calgary, Alberta, 30 August 2012. Available from http://www.cosia.ca/uploads/files/Projects/Tailings/Tech_Guide_Fluid_Tailings_Mgmt_30%20Aug%202012_COSIA.pdf [cited 18 August 2016].

Patterson, D.E., and Smith, M.W. 1980. The use of time domain reflectometry for the measurement of unfrozen water content in frozen soils. Cold Regions Science and Technology, **3**(2–3): 205-210.

Patterson, D.E., and Smith, M.W. 1981. The measurement of unfrozen water content by time domain reflectometry: results from laboratory tests. Canadian Geotechnical Journal, **18**(1): 131-144.

Patterson, D.E., and Smith, M.W. 1985. Unfrozen water content in saline soils: results using time-domain reflectometry. Canadian Geotechnical Journal, **22**(1): 95-101.

Patterson, D.E. and Smith, M.W. 1983. Measurement of unfrozen water content in saline permafrost using time domain reflectometry. *In* Proceedings of the 4th International Conference on Permafrost, Fairbanks, Alaska, 17-22 July 1983, pp. 968-972.

Ponizovsky, A.A., Pachepsky, Y.A., and Chudinova, S.M. 1999. Performance of TDR calibration models as affected by soil texture. Journal of Hydrology, **218**(1): 35-43.

Proskin, S., Sego, D., and Alostaz, M. 2012. Oil sands MFT properties and freeze-thaw effects. Journal of Cold Regions Engineering, **26**(2): 29-54.

Proskin, S.A. 1998. A geotechnical investigation of freeze-thaw dewatering of oil sands fine tailings. Ph.D. thesis, University of Alberta, Edmonton, Alberta.

Qiu, Y., and Sego, D.C. 2006. Optimum deposition for sub-aerial tailings disposal: concepts and theories. International Journal of Mining, Reclamation & Environment, **20**(4): 272-285.

Qiu, Y. 2000. Optimum deposition for sub-aerial tailings disposal. Ph.D. thesis, University of Alberta, Edmonton, Alberta.

Scott, J., Kabwe, L., Wilson, G., Sorta, A. and Jeeravipoolvarn, S. 2013. Properties which affect the consolidation behaviour of mature fine tailings. *In* Proceedings of the 17th International Conference on Tailings and Mine Waste, Banff, Alberta, 3-6 November 2013.

Seyfried, M.S., and Murdock, M.D. 1996. Calibration of time domain reflectometry for measurement of liquid water in frozen soils. Soil Science, **161**(2): 87-98.

Silva, M.J. 1999. Plant dewatering and strengthening of mine waste tailings. Ph.D. thesis, University of Alberta, Edmonton, Alberta.

Simms, P.H. and Grabinsky, M.W. 2004. A simple method for estimating rates of drying and desaturation of paste tailings during surface deposition. *In* Proceedings of the Eleventh Tailings and Mine Waste Conference, Vail, Colorado, 10-13 October 2004, pp. 287-292.

Smith, M.W. and Tice, A.R. 1988. Measurement of the unfrozen water content of soils: Comparison of NMR and TDR methods. CRREL Report 88-18, U.S. Army Cold Regions Research and Engineering Laboratory, Hanover, New Hampshire.

Sorta, A.R., Sego, D.C., and Wilson, W. 2012. Effect of thixotropy and segregation on centrifuge modelling. International Journal of Physical Modelling in Geotechnics, **12**(4): 143-161.

Sorta, A.R., Sego, D.C., and Wilson, G.W. 2013. Time domain reflectometry measurements of oil sands tailings water content: A study of influencing parameters. Canadian Institute of Mining Metallurgy and Petroleum Journal, **4**(2): 109-119.

Spaans, E.J., and Baker, J.M. 1995. Examining the use of time domain reflectometry for measuring liquid water content in frozen soil. Water Resources Research, **31**(12): 2917-2925.

Spaans, E.J.A., and Baker, J.M. 1996. The soil freezing characteristic: its measurement and similarity to the soil moisture characteristic. Soil Science Society of America Journal, **60**(1): 13-19.

Spaans, E.J.A. 1994. The soil freezing characteristic: Its measurement and similarity to the soil moisture characteristic. Ph.D. thesis, University of Minnesota, Minneapolis, Minnesota.

Spence, J., Bara, B., Lorentz, J. and Mikula, R. 2015. Development of the Centrifuge Process for Fluid Fine Tailings Treatment at Syncrude Canada Ltd. *In* World Heavy Oil Congress 2015, Edmonton, Alberta, 24-26 March 2015.

Suzuki, S. 2004. Dependence of unfrozen water content in unsaturated frozen clay soil on initial soil moisture content. Soil Science and Plant Nutrition, **50**(4): 603-606.

Topp, G.C., Davis, J.L., and Annan, A.P. 1980. Electromagnetic determination of soil water content; measurements in coaxial transmission lines. Water Resources Research, **16**(3): 574-582.

Topp, G.C., and Davis, J.L. 1985. Time-domain reflectometry (TDR) and its application to irrigation scheduling. Advances in Irrigation, **3**: 107-127.

Vanapalli, S., Sillers, W. and Fredlund, M. 1998. The meaning and relevance of residual state to unsaturated soils. *In* Proceedings of the 51st Canadian Geotechnical Conference, Edmonton, Alberta, 4-7 October 1998.

Vardon, P.J., Nijssen, T., Yao, Y. and Van Tol, A.F. 2014. Numerical simulation of fine oil sand tailings drying in test cells. *In* Proceedings of the 4th International Oil Sands Tailings Conference, Lake Louise, Canada, 7-10 December 2014.

Watanabe, K., and Wake, T. 2009. Measurement of unfrozen water content and relative permittivity of frozen unsaturated soil using NMR and TDR. Cold Regions Science and Technology, **59**(1): 34-41.

Watanabe, K., and Mizoguchi, M. 2002. Amount of unfrozen water in frozen porous media saturated with solution. Cold Regions Science and Technology, **34**(2): 103-110.

Wen, Z., Ma, W., Feng, W., Deng, Y., Wang, D., Fan, Z., and Zhou, C. 2012. Experimental study on unfrozen water content and soil matric potential of Qinghai-Tibetan silty clay. Environmental Earth Sciences, **66**(5): 1467-1476.

Williams, P.J. 1964. Unfrozen water content of frozen soils and soil moisture suction. Geotechnique, **14**(3): 231-246.

Wu, M., Tan, X., Huang, J., Wu, J., and Jansson, P. 2015. Solute and water effects on soil freezing characteristics based on laboratory experiments. Cold Regions Science and Technology, **115**: 22-29.

Xu, X., Wang, J. and Zhang, L. 2001. Frozen soil physics. Science Press, Beijing, China.

Zhang, F. 2016. Unsaturated Soil Property Functions for High Volume Change Materials. Ph.D. thesis, University of Alberta, Edmonton, Alberta.

Zhang, L., and Chen, Q. 2005. Predicting bimodal soil–water characteristic curves. Journal of Geotechnical and Geoenvironmental Engineering, **131**(5): 666-670.

Zhou, X., Zhou, J., Kinzelbach, W., and Stauffer, F. 2014. Simultaneous measurement of unfrozen water content and ice content in frozen soil using gamma ray attenuation and TDR. Water Resources Research, **50**(12): 9630-9655.

Appendix 1: Development of SFCC Methodology

The experimental methodology and apparatus was developed and validated by determining the SFCC for Devon Silt and comparing the results to those presented by Azmatch et al. (2012a, 2012b). SFCC testing was then performed on Devon Silt and compared to the results from Azmatch et al. (2012a, 2012b) to validate the experimental apparatus and methodology.

Previous Testing on Devon Silt

In 2012, Azmatch et al. conducted SFCC testing on Devon Silt and compared the SWCC derived from the SFCC with the SWCC measured using traditional methods. The Devon Silt was mixed to a water content of 60 percent and then consolidated to various pressures to assess the impact of the initial void ratio on the SFCC. Testing was performed on samples consolidated to 50 kPa, 100 kPa, and 400 kPa. Samples were trimmed to 76.2 mm by 76.2 mm by 304.8 mm and placed in a freezing cell. An RTD and a TDR were inserted into the sample to measure the temperature and the dielectric constant in the soil, respectively. The temperature in the freezing cell was controlled by flowing glycol through brass coils from an external temperature control bath. The samples were subjected to a one step freezing technique where the samples were frozen to -4.0°C over a period of approximately 16 hrs. The unfrozen water content was determined from the dielectric constant using Topp et al.'s (1980) equation (Equation 2-29). The soil suction in the sample was determined according to the relation provided by Konrad (1994), which indicates that the suction increases linearly with decreasing temperature at the rate of 1250 kPa/°C. The Devon Silt was assumed to be colloidal and a soil dependent constant of 1.0 was used to relate the SFCC to the SWCC. The θ-SWCCs estimated from the SFCC are presented in Figure A1- 1.

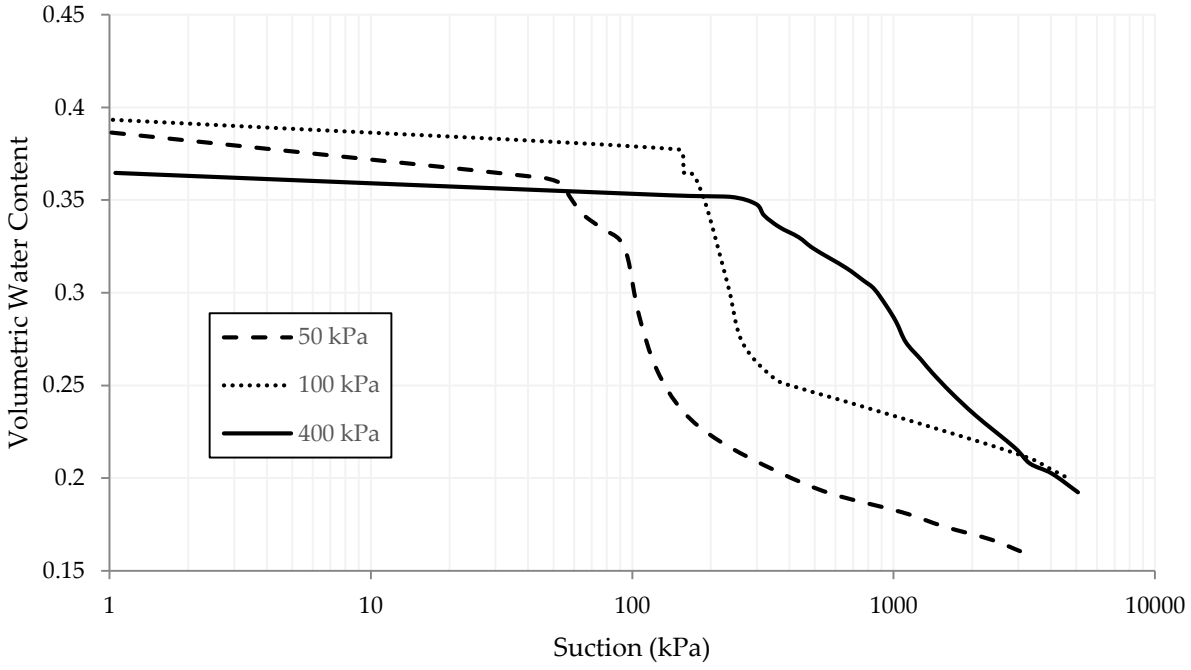

Figure A1- 1: θ-SWCC Estimated from SFCC for Devon Silt (after Azmatch et al. 2012a)
Reprinted from Cold Regions Science and Technology, 83, Azmatch T.F., Sego, D.C., Arenson, L.U., Biggar, K.W., Using soil freezing characteristics curve to estimate the hydraulic conductivity function of partially frozen soils, 103-109, Copyright (2012), with permission from Elsevier.

The data points were fit with Equation 2-4 presented in Section 2.4.1 using SoilVision (Fredlund 2004). This curve was then compared to the SWCC measured using traditional methods. The θ-SWCC estimated from the SFCC, the Fredlund and Xing (1994) fit for the estimated θ-SWCC data, and the SWCC measured using traditional methods are shown in Figure A1- 2 for a sample consolidated to 100 kPa.

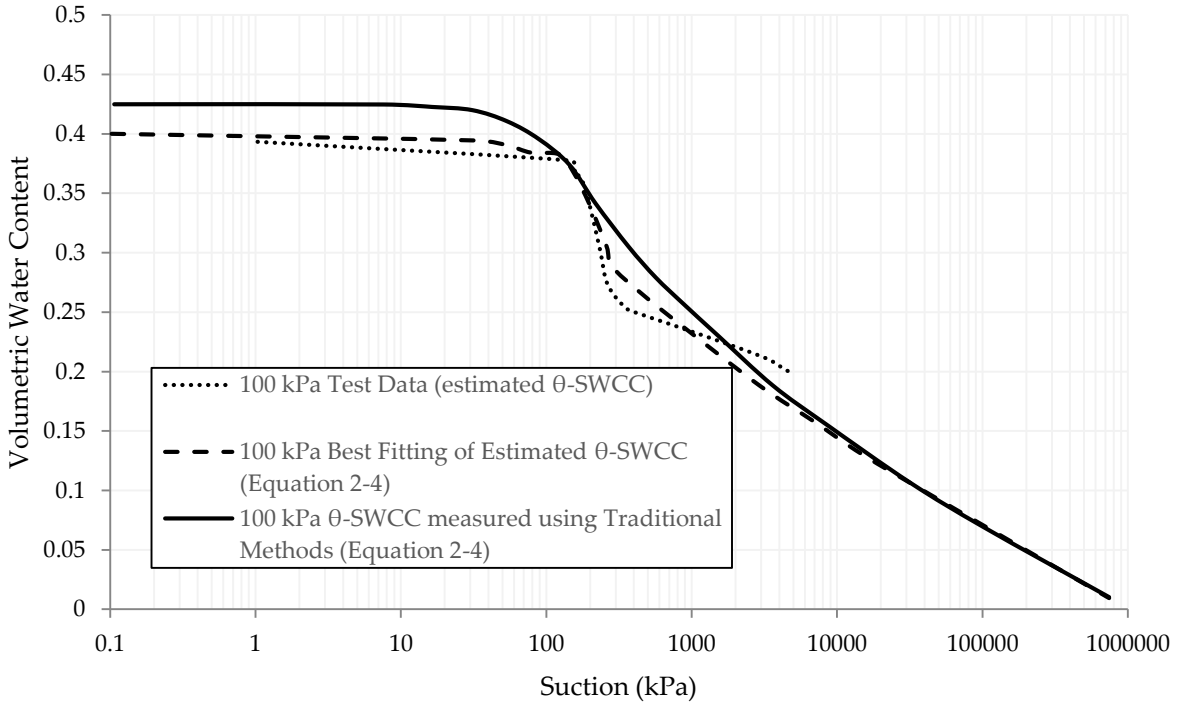

Figure A1- 2: Comparison of the θ-SWCC estimated from the SFCC and the θ-SWCC estimated using traditional methods (Equation 2-4 Fredlund and Xing (1994)) (after Azmatch et al. 2012a)

Azmatch et al. (2012b) also investigated the influence of temperatures on the SFCC by varying the freezing temperature for samples consolidated to 50 kPa. The freezing temperatures were -4°C, -10°C, and -18°C for the first, second, and third samples, respectively. The results from this testing demonstrated that the results are dependent on the freezing temperature and thus the cooling rate.

Validation of Experimental Methodology

SFCC testing was performed on Devon Silt and compared to the results presented by Azmatch et al. (2012a, 2012b). The objective of this was to validate the experimental methodology and apparatus. A sample was mixed using an electric mixer to a gravimetric water content of 60 percent to match the procedure performed by Azmatch et al. (2012a, 2012b). The sample was then consolidated to a pressure of about 50 kPa in a cell using an air bellofram with a height of 250 mm and a diameter of 300 mm as shown in Figure A1- 3. It was difficult to extrude the sample

due to the size of the sample. After extrusion, the sample was not able to retain its shape as shown in Figure A1- 4. The final water content of the sample after consolidation was about 40 percent, which is well above the Devon Silt's liquid limit and much higher than expected. It was discovered that a correction for the difference in diameter between the air bellofram and cell diameter was not used. As a result, it is suspected that this sample was only consolidated to a pressure of 15 kPa. Consequently, three smaller samples (Samples DS1, DS2, and DS3) were cut from the large extruded sample and were tested to determine what improvements should be made to the apparatus and method. The samples were 150 mm by 75 mm by 75 mm. The results from these SFCC tests were not used for comparison to the results presented by Azmatch et al. (2012a, 2012b) due to the uncertainty in the consolidation process, but are presented to demonstrate the improvements that needed to be made to the apparatus and method. The correct bellofram loading was used to consolidate subsequent samples (Samples DS4, DS5, DS6, DS8, DS9, and DS10).

Figure A1- 3: Devon Silt Consolidation Using a Large Cell

Figure A1- 4: Extruded Devon Sample

The initial freezing cell is shown in Figure A1- 5, which consisted of a temperature control bath and an insulated box. Glycol is circulated into the box using brass coils. The sample is placed on a small lift table in the center of the brass coils to promote isotropic freezing. A fan is placed in the corner of the box to circulate air and two RTDs are placed in the box to monitor the air temperature in the box. The freezing cell is placed in a temperature controlled room to reduce the impacts of the ambient room temperature on the freezing process. One RTD and one TDR are inserted into the sample to monitor the temperature and the dielectric constant, respectively, during testing. The volumetric unfrozen water content (θ_u) was determined from the dielectric constant using Topp et al.'s (1980) equation in accordance with the procedure followed by Azmatch et al. (2012a, 2012b) used. The suction was calculated using Konrad's (1994) relationship in the same manner as Azmatch et al. (2012a, 2012b). The Clapeyron Equation (Equation 2-16) was also used to determine the suction and yielded very similar results to the method used by Azmatch et al. (2012a, 2012b). The presented results for Devon silt use Konrad's (1994) relationship for comparison. The gravimetric unfrozen water content (w_u) was computed using Equation 2-3. To estimate the SWCC from the SFCC, the following was performed:

1. The Devon silt was assumed to be colloidal and a soil dependent constant of about 1.0 was used to estimate the SWCC from the SFCC based on Koopmans and Miller (1966)
2. The w_u and the θ_u were assumed to be equal to the gravimetric water content and the volumetric water content during drying, respectively. This yields an estimated θ-SWCC and a w-SWCC.

3. High volume change property functions are applied if applicable to attain the θ_i-SWCC and the S-SWCC based on Section 2.4.3.

The remainder of this section provides estimated θ-SWCCs assuming no volume change.

Figure A1- 5: Initial Freezing Cell

The results from the first sample tested, DS1, are provided in Figure A1- 6. The test was performed using a step freezing process where the temperature was slowly decreased from 0°C to -2.7°C over a period of one week. Minor amounts of supercooling were observed during the testing. Overall, the results suggested that the SFCC test may be quite robust as the estimated θ-SWCCs closely matched the 100 kPa test data from Azmatch et al. (2012a) and was relatively close to the 50 kPa estimated θ-SWCC data despite a number of encountered problems, including:

- Extensive air bubbles were observed in the samples. This is assumed to be a result of the mixing method, which used an electric mixer.
- The RTD and TDR probes moved after insertion. This could potentially have introduced air voids in between the probes and the soil which is undesirable.
- The temperature in the sample and in the box fluctuated substantially in response to the external room temperature.

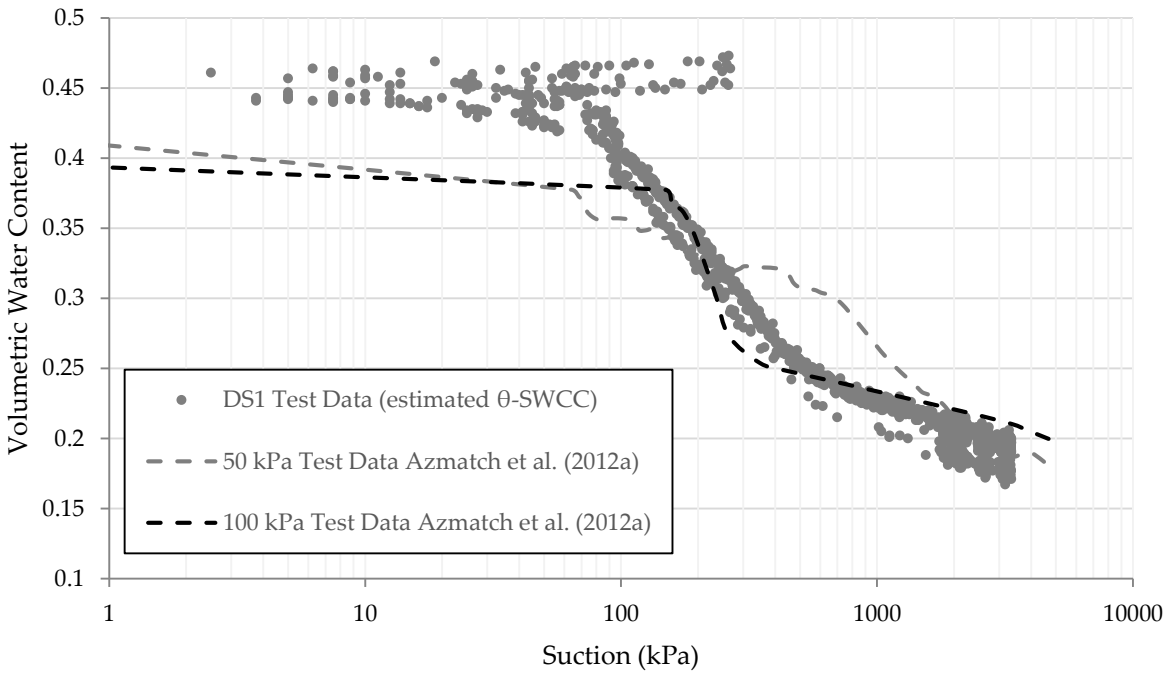

Figure A1- 6: Sample DS1 θ-SWCC Estimated from the SFCC

The following changes were made to help rectify the issues encountered when testing sample DS1:

1. A clamping system was introduced to stabilize the cables of the probes that are inserted into the sample to prevent movement and the introduction of air voids between the probes and the soil.
2. The box was double insulated to dampen the impact of room temperature fluctuations on the temperature in the box and in the sample.

A one step freezing method was used for the following two samples, DS2 and DS3. The internal temperature of sample DS2 was approximately 8°C when it was placed in the freezing cell that was set at -4°C. To reduce the temperature gradient, sample DS3 was brought to a temperature of approximately 1°C before it was put in the freezing cell that was set at -4°C. The laboratory SFCC data is provided in Figure A1- 7. The shape of the estimated SWCC changes dramatically as the temperature gradient changes. This behaviour is expected based on the investigation

conducted by Azmatch et al. (2012b). Based on this behavior, a step freezing method was used moving forward and is discussed below.

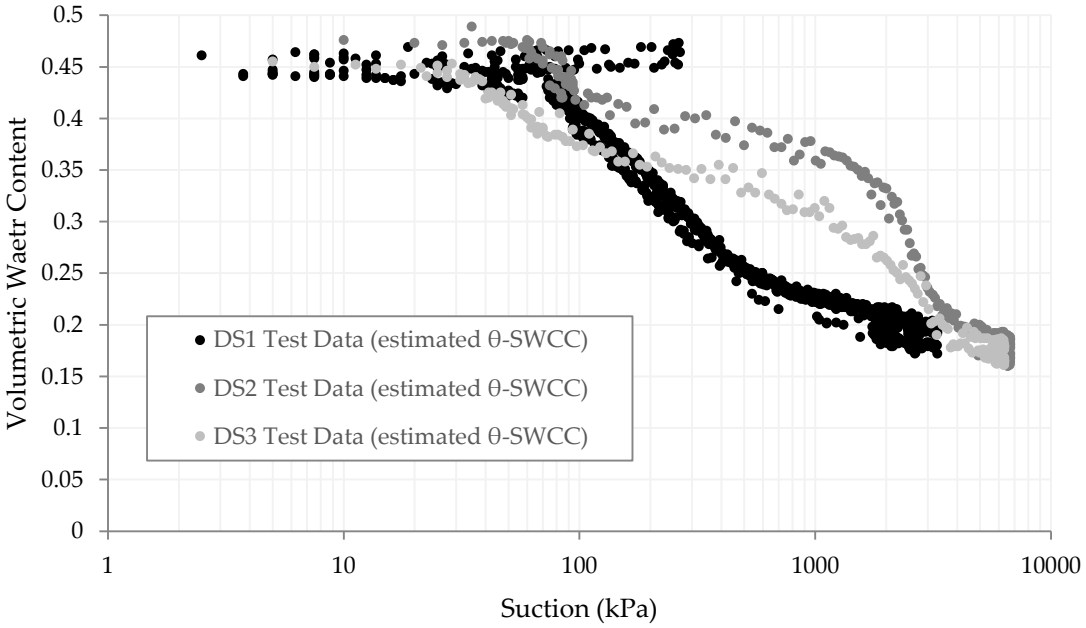

Figure A1- 7: Sample DS1 to DS3 Estimated θ-SWCC from the SFCC

Temperature Plots

Two RTDs were placed in the experimental apparatus to monitor the temperature fluctuations and one RTD was placed in the room that the apparatus was set up in. Temperature plots showing the room temperature, apparatus temperature, and sample temperature are shown in Figure A1- 8 to Figure A1- 13 for the Devon silt. The temperature in the room fluctuated greatly. The temperature in the apparatus fluctuated a minor amount due to the room temperature changes. The temperature in the sample fluctuated a negligible amount in response to the exterior temperature fluctuations.

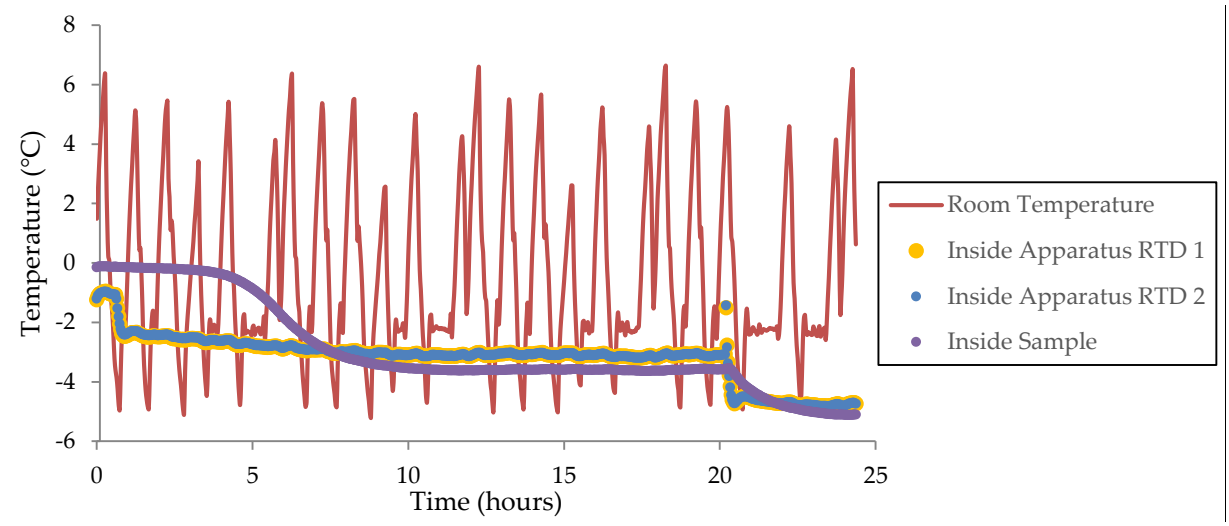

Figure A1- 8: Temperature Plot for Sample DS4

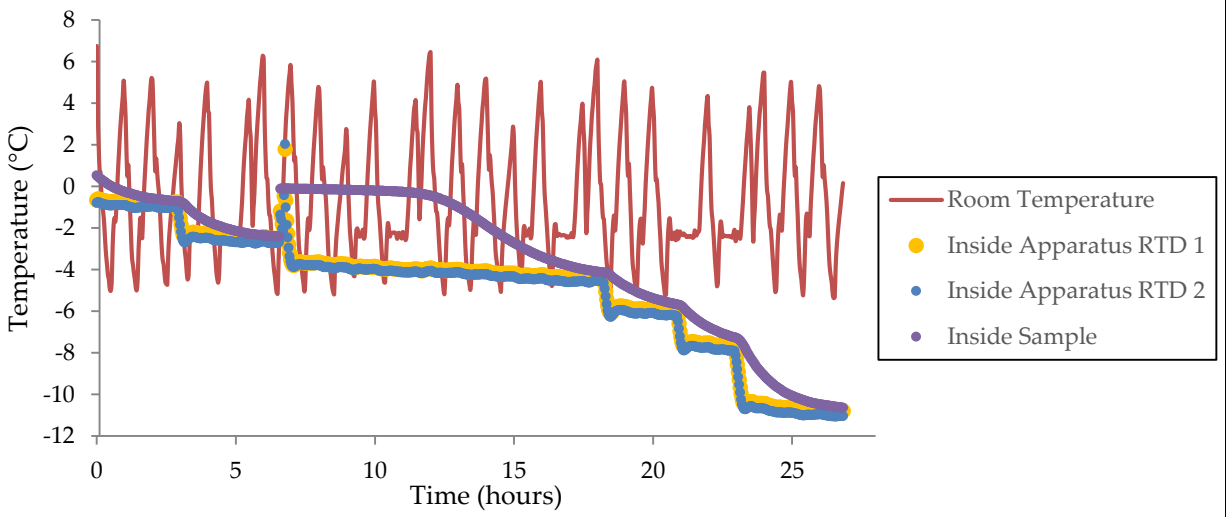

Figure A1- 9: Temperature Plot for Sample DS5

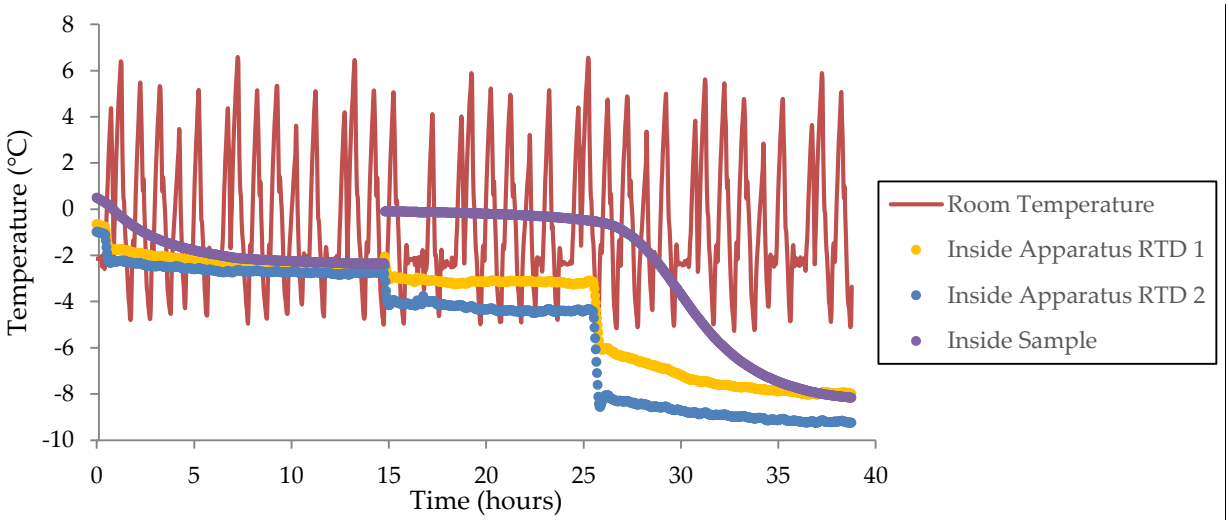

Figure A1- 10: Temperature Plot for Sample DS6

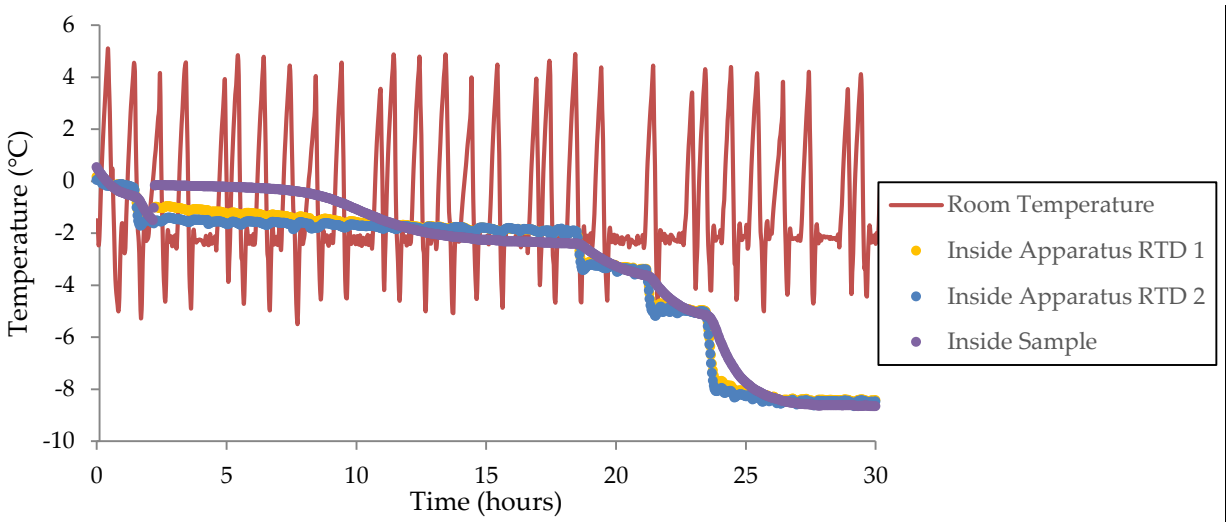

Figure A1- 11: Temperature Plot for Sample DS8

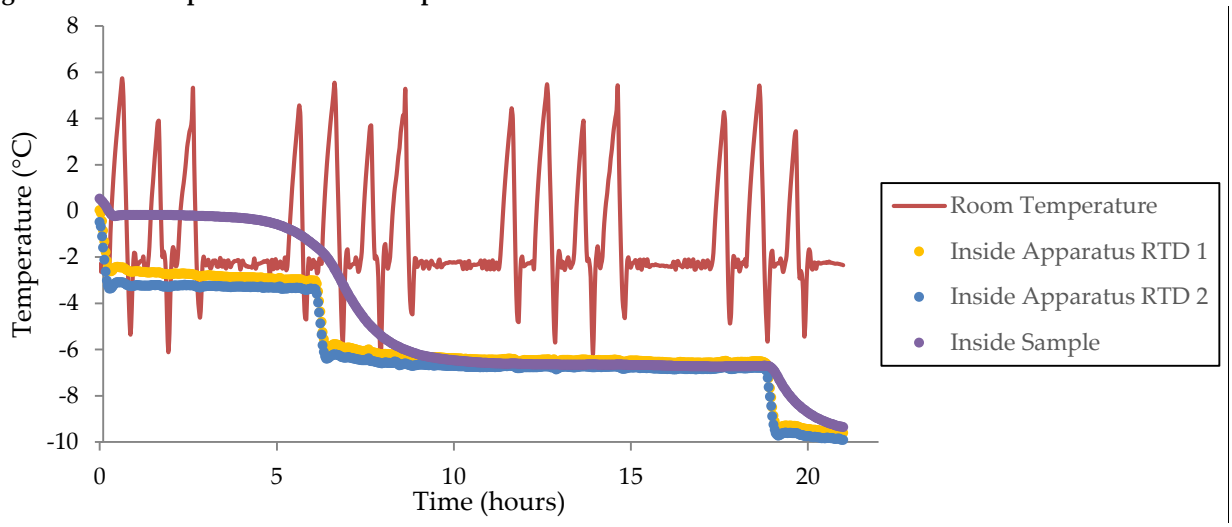

Figure A1- 12: Temperature Plot for Sample DS9

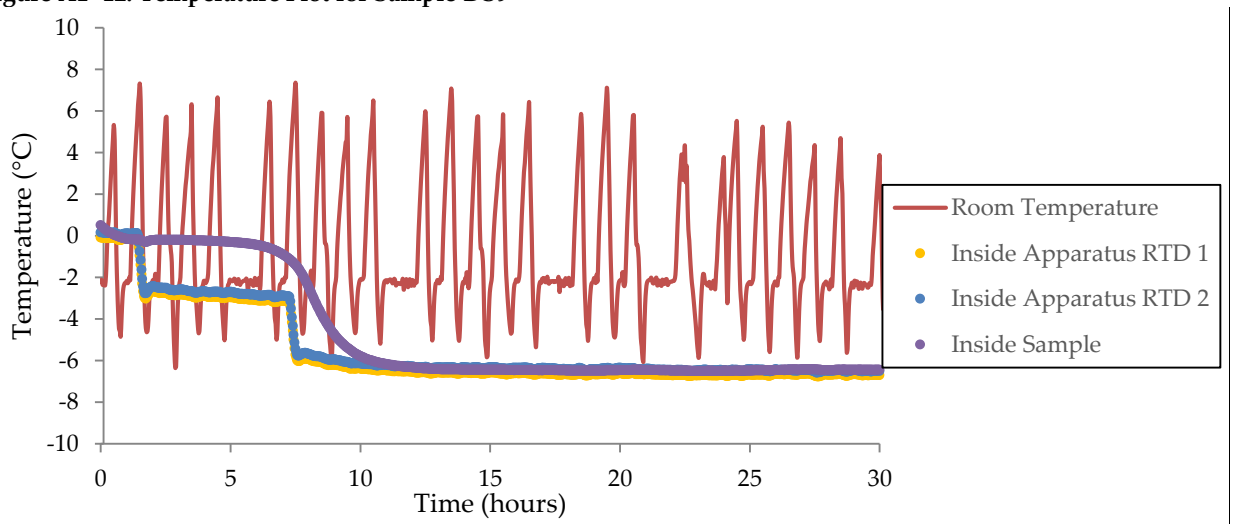

Figure A1- 13: Temperature Plot for Sample DS10